UNIVERSITY OF CRETE

SCHOOL OF MEDICINE

FOUNDATION FOR RESEARCH AND TECHNOLOGY-HELLAS

INSTITUTE OF MOLECULAR BIOLOGY AND BIOTECHNOLOGY

PhD THESIS

ΛΕΙΤΟΥΡΓΙΚΟΣ ΧΑΡΑΚΤΗΡΙΣΜΟΣ ΤΩΝ ΓΟΝΙΔΙΩΝ ΜΕΛΩΝ ΤΗΣ ΟΙΚΟΓΕΝΕΙΑΣ ΤΩΝ EPITHELIAL SODIUM CHANNELS / DEGENERINS (ENaC/DEG) ΚΑΙ ΠΡΟΣΔΙΟΡΙΣΜΟΣ ΤΟΥ ΡΟΛΟΥ ΤΟΥΣ ΣΤΗΝ ΑΠΟΚΡΙΣΗ ΣΤΟ ΣΤΡΕΣ ΣΤΟΝ ΟΡΓΑΝΙΣΜΟ *C. ELEGANS*

FUNCTIONAL CHARACTERIZATION OF EPITHELIAL SODIUM CHANNELS / DEGENERINS (ENaC/DEG) FAMILY MEMBERS AND DETERMINATION OF THEIR ROLE IN ORGANISMAL STRESS RESPONSES IN *C. ELEGANS*

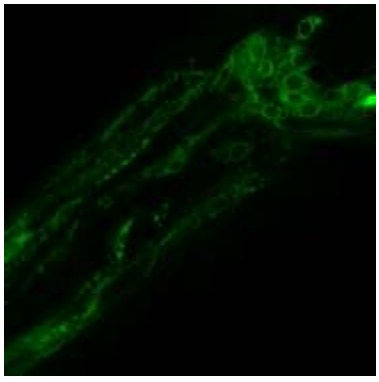

Dionysia Petratou

Heraklion 2023

Three-member advisory committee:

Principal Supervisor:

Nektarios Tavernarakis, Research director, professor of Molecular Systems Biology at the Medical School of the University of Crete

Co-Supervisors:

George Mavrothalassitis, professor of Medical Chemistry at the Medical School of the University of Crete

Achilleas Gravanis, professor of Pharmacology at the Medical School of the University of Crete

Seven-member examining committee:

Nektarios Tavernarakis, Research director, professor of Molecular Systems Biology at the Medical School of the University of Crete

George Mavrothalassitis, professor of Medical Chemistry at the Medical School of the University of Crete

Achilleas Gravanis, professor of Pharmacology at the Medical School of the University of Crete

Domna Karagogeos, professor of Molecular Biology and Developmental Neurobiology at the Medical School of the University of Crete

Despina Alexandraki, professor at the Biology Department of the University of Crete

Christos Delidakis, professor at the Biology Department of the University of Crete

Daphne Bazopoulou, assistant professor at the Biology Department of the University of Crete

The present PhD thesis was partially supported by the European Research Council under the grant agreement “ERC-GA695190-MANNA” to N.T.

This project was also co-financed by the European Union ((European Social Fund - ESF) and Greek national funds through the following operational programs:

Όσα βουνά κι αν ανεβείτε,
απ' τις κορφές τους θ' αγναντεύτε άλλες κορφές
ψηλότερες, μιαν άλλη πλάση ξελογιάστρα·
και στην κορφή σα φτάστε την κατάψηλη,
πάλε θα καταλάβετε πως βρίσκεστε
σαν πρώτα κάτω απ' όλα τ' άστρα.

«Ο Δωδεκάλογος του γύφτου» Κωστής Παλαμάς

To my daughter Christina who
brought joy into my life…

I. Acknowledgements

The present doctoral dissertation was carried out in the laboratory of Neuro-genetics and Aging of the Institute of Molecular Biology and Biotechnology at the Foundation for Research and Technology in Heraklion, Crete.

It gives me enormous pleasure to convey my gratitude to all those whose help and suggestions were valuable in completing my Ph.D. thesis. I am pleased to express my deep appreciation to my supervisor, Dr. Nektarios Tavernarakis, for the immense opportunity to conduct my disquisition in his lab, the provision of precious scientific knowledge, and the economic support of my Ph.D. study.

Besides my supervisor, I would like to thank the members of my three-member committee, Professor Achilleas Gravanis and Professor George Mavrothalassitis, for their insightful comments, constructive remarks, scientific advice, and encouragement. I would also like to thank Professor Domna Karagogeos, Professor Despina Alexandraki, Professor Christos Delidakis, and Professor Daphne Bazopoulou for being part of my seven-member committee.

I am grateful to Eva Kaulich and her principal investigator, Professor William Schafer, for the fruitful collaboration. I am particularly highly indebted to Eva for insisting on and developing our collaboration, for her kind comments, her patience, for sharing her data and, for always being present to answer my questions.

I would also like to thank the members of my lab for the inspiring conversations, the technical support and advice and for sharing the same everyday challenges and worries. I especially thank my fellow labmates Eirini Lionaki, Martha Gjikolaj, Ioanna Daskalaki, Ilias Gkikas and Thanos Metaxakis for the stimulating discussions, the valuable personal and scientific support, the joyful moments, and the fun we had over the last ten years in and out of the lab.

Words cannot express how grateful I am to Eirini Lionaki, a postdoc of excellent scientific knowledge, for the support, scientific guidance, and words of advice. Her supportiveness and belief in the project and my abilities helped me overcome many personal and scientific obstacles. I must express my profound appreciation to her, not only for her motivation, ideas, excellent example as a scientist, immense knowledge, and patience, but for her belief and trust in me. Her morals and integrity serve as a glorious example to follow.

Special thanks to Martha for her valuable assistance, innovative scientific ideas, friendship, and company, and for helping me believe in my project.

Next, I would like to thank Ezgi Gultekin and Myrto Ziogas, who visited the lab as trainees. As long they were under my supervision gave me the opportunity to teach and be reciprocally taught by them.

Nobody was more important to me in completing this project than my family members. This accomplishment would not have been possible without them. I thank my parents and sister for all their help and support through this challenging work. I am full of gratitude to my parents, Panagis and Evangelia, for all the sacrifices they made on my behalf, the unceasing support, and everlasting encouragement throughout all the years of my studies. I disclose my profound appreciation to my partner Manos for being patient and loving and for all his comfort and understanding amid difficult times during my PhD thesis. Last but not least, I would like to thank my daughter, Christina, who revealed to me the true meaning of life.

II. Table of Contents

III. List of Figures, and Tables

a. Introduction

b. Results

c. Appendix

IV. Abstract

Integration of sensory stimuli to appropriately modulate behavioral responses to environmental signals is critical for organismal survival. The nervous system initiates and modulates systemic stress responses ensuing physiological stress. Dopamine signaling is involved in several forms of behavioral plasticity. At the cellular level, ion homeostasis is of utmost importance for neuronal function, both for the maintenance of resting membrane potential and for the creation and propagation of action potentials. Imbalance in neuronal sodium homeostasis is associated with many nervous system pathologies. However, the effect of stress on neuronal sodium homeostasis, excitability, and survival is not explicit. In this study we focus on the ENaC/DEG family of sodium channels, specifically the Degenerins subfamily of *Caenorhabditis elegans*. Degenerins are expressed mainly in the nervous system and are implicated in several sensory modalities. Degenerins form transmembrane proteins that span twice the cytoplasmic membrane and assemble in homo-tetramers or hetero-tetramers to generate sodium channels. By implementing advanced imaging techniques, we found that DEL-2, DEL-3, and DEL-4 degenerins are expressed in dopaminergic, serotonergic, sensory, or motor neurons. We report that the ENaC/DEG family member DEL-4 assembles into a proton-inactivated, amiloride-sensitive, homomeric sodium channel. Distinct types of stress regulate this channel, which then triggers appropriate motor adaptations and organismal stress responses. DEL-4 operates at the neuronal cell membrane to modulate *Caenorhabditis elegans* locomotory behaviour. In *Caenorhabtitis elegans* the functionality of the dopamine pathway can be easily assessed by monitoring the locomotory response to environmental food availability cues, a behavior termed basal slowing. We showed that these ion channel proteins induce basal slowing response. They act through DOP-2 and DOP-3 dopamine receptors and affect the signaling at the neuromuscular junction. Limitation of DEL-4 reduces dopamine signaling and cholinergic neurotransmission at the neuromuscular junction. Concurrently, GABAergic signaling enhances at the neuromuscular junction.

Heat stress and starvation reduce DEL-4 expression, which in turn adjusts the expression and activity of key stress response transcription factors, such as HSF-1, DAF-16, and SKN-1. Notably, comparable to heat stress and starvation, DEL-4 deficiency induces hyperpolarization of dopaminergic neurons to impact neurotransmission. DELs respond to gustatory stimuli and participate in proton and serotonin perception. Utilizing two humanized models of Parkinson's and Alzheimer's disease in *C. elegans*, we demonstrate that DEL-4 promotes neuronal survival in the context of these proteinopathies.

DEL-4 deficiency enhances the degeneration of dopaminergic neurons in aged adults, upon control conditions, and in Parkinson's and Alzheimer's disease models. Our findings provide insight into the molecular mechanisms via which sodium channels uphold neuronal function and promote adaptation under stress.

V. Περίληψη

Ο συνδυασμός αισθητικών ερεθισμάτων για την τροποποίηση της συμπεριφοράς ενός οργανισμού ανάλογα με τα περιβαλλοντικά ερεθίσματα είναι απαραίτητος για την επιβίωσή του. Το νευρικό σύστημα συμμετέχει στην έναρξη και τη ρύθμιση των συστημικών αποκρίσεων που προκύπτουν από διάφορους τύπους περιβαλλοντικού στρες. Η ντοπαμινεργική σηματοδότηση εμπλέκεται σε διάφορες μορφές συμπεριφορικής πλαστικότητας. Σε κυτταρικό επίπεδο, η ομοιόσταση ιόντων είναι υψίστης σημασίας για τη νευρωνική λειτουργία, τόσο για τη διατήρηση του δυναμικού ηρεμίας της μεμβράνης όσο και για τη δημιουργία και τη διάδοση δυναμικών δράσης. Η ανισορροπία στη νευρωνική ομοιόσταση νατρίου σχετίζεται με πολλές παθολογίες του νευρικού συστήματος. Ωστόσο, οι επιπτώσεις του στρες στην ομοιόσταση του νατρίου των νευρώνων, τη διεγερσιμότητα και τη νευρωνική επιβίωση δεν είναι σαφείς. Σε αυτή τη μελέτη, εστιάζουμε στην οικογένειες καναλιών νατρίου ENaC/DEG, και συγκεκριμένα στην υποοικογένεια Degenerins του οργανισμού μοντέλου *Caenorhabditis elegans*. Οι Degenerins εκφράζονται κυρίως στο νευρικό σύστημα και εμπλέκονται σε ποικίλες αισθητικές λειτουργίες. Οι Degenerins σχηματίζουν διαμεμβρανικές πρωτεΐνες που διαπερνούν δύο φορές την κυτταροπλασματική μεμβράνη και αλληλεπιδρούν σε ομοτετραμερή ή ετεροτετραμερή διάταξη για να σχηματίσουν διαύλους νατρίου. Με την εφαρμογή προηγμένων τεχνικών απεικόνισης, διαπιστώσαμε ότι οι Degenerins DEL-2, DEL-3 και DEL-4 εκφράζονται σε ντοπαμινεργικούς, σεροτονινεργικούς, αισθητικούς και κινητικούς νευρώνες. Αναφέρουμε ότι η DEL-4 σχηματίζει ομομερή κανάλια νατρίου, που μπλοκάρονται από πρωτόνια και είναι ευαίσθητα στην αμιλορίδη. Συγκεκριμένοι τύποι στρες ρυθμίζουν αυτό το κανάλι, το οποίο στη συνέχεια ενεργοποιεί κατάλληλες κινητικές προσαρμογές και αντιδράσεις του οργανισμού στο στρες. Το κανάλι DEL-4 λειτουργεί στη νευρωνική μεμβράνη και στη σύναψη για να ρυθμίζει τα χαρακτηριστικά της κινητικής συμπεριφοράς του *Caenorhabditis elegans*. Στο C. elegans η η λειτουργικότητα του ντοπαμινεργικού μονοπατιού μπορεί εύκολα να αξιολογηθεί παρακολουθώντας την κινητική απόκριση σε στη διαθεσιμότητα τροφής, μία συμπεριφορά που ονομάζεται βασική επιβράδυνση. Δείξαμε ότι αυτοί οι δίαυλοι ιόντων νατρίου ενισχύουν τη βασική επιβράδυνση. Δρουν μέσω των υποδοχέων της ντοπαμίνης DOP-2 και DOP-3, και επηρεάζουν τη σηματοδότηση στη νευρομυϊκή σύναψη. Ταυτόχρονα, η GABAεργική σηματοδότηση ενισχύεται στη νευρομυϊκή σύναψη.

Το θερμικό στρες και η ασιτία μεταβάλλουν τα επίπεδα έκφρασης του DEL-4. Η αφθονία του DEL-4 με τη σειρά της προσαρμόζει την έκφραση και τη δραστηριότητα βασικών μεταγραφικών

παραγόντων απόκρισης στο στρες, όπως ο HSF-1, ο DAF-16, και ο SKN-1. Συγκεκριμένα, συγκρίσιμη με το θερμικό στρες και την πείνα, η ανεπάρκεια του DEL-4 προκαλεί υπερπόλωση των ντοπαμινεργικών νευρώνων και επηρεάζει τη νευροδιαβίβαση στους ντοπαμινεργικούς και κινητικούς νευρώνες. Χρησιμοποιώντας δύο εξανθρωπισμένα μοντέλα της νόσου του Πάρκινσον και της νόσου Αλτσχάιμερ στο *C. elegans*, αποδεικνύουμε ότι το DEL-4 προάγει την επιβίωση των νευρώνων στο πλαίσιο αυτών των πρωτεϊνοπαθειών. Η μείωση των επιπέδων της DEL-4 ενισχύει τον εκφυλισμό των ντοπαμινεργικών νευρώνων στο νηματώδη, τόσο υπό φυσιολογικές συνθήκες όσο και σε νηματώδεις μοντέλα για τη νόσο του Αλτζχάιμερ και του Πάρκινσον. Τα ευρήματά μας παρέχουν μια εικόνα για τους μοριακούς μηχανισμούς μέσω των οποίων τα κανάλια νατρίου υποστηρίζουν τη νευρωνική λειτουργία και προάγουν την προσαρμογή υπό στρες.

VI. Introduction

1. *Caenorhabditis elegans* as a model organism

In 1900, Èmile Maupas isolated *Caenorhabditis elegans* from the soil in Algeria and described the nematode for the first time (1). In 1963, Sydney Brenner proposed the employment of the roundworm as a model organism to overcome scientific obstacles in studying developmental biology and neurobiology. Sydney Brenner introduced *C. elegans* with his first publication in 1974 and established the roundworm as a model system (2). Thenceforth, the *C. elegans* research has been upraised and extended in diverse fields of biology.

Caenorhabditis elegans shares several advantages, rendering it an outstanding experimental system. It is a microscopic transparent organism with a rapid life cycle and a large brood size. This tiny roundworm is a self-fertilizing hermaphrodite of 1mm length when adult. Hermaphrodites, when self-fertilized lay around 300, which are all isogenic. Thus, a large population of the same genotype may be exploited for experiments, reducing the statistical error. Embryos hatch and pass through four larval stages to develop into an adult. When reared at 25^{o}C, they grow, in three days, from an egg to an egg-laying adult. Its short lifecycle makes it ideal for lifespan experiments. Recovery of a large population from the same stage for better statistics is feasible. The two techniques employed are egg laying for a few hours or treating gravid adults with a bleach solution to which only eggs are resistant. Temperature is important for *C. elegans* development since low temperature delays while high temperature accelerates the animal's growth. Temperatures, that are permissive for the animal growth, range between 12^{o}C and 25^{o}C. *C. elegans* is a hermaphrodite animal, but a spontaneous male generation emerges by chance at a ratio of 1/1000. This ratio may increase with incubation at 30^{o}C for 4hrs at the l4 stage, enabling genetic crosses.

In nature, *C. elegans* colonizes the soil or the rotting matter, where ample bacterial food is present. For laboratory maintenance, *C. elegans* nourishes on agar plates covered with a bacterial lawn of the Op50 *Escherichia coli* bacterial strain. In food absence, newly hatched larvae arrest at the l1 stage and may survive for several months. Furthermore, arrested l1 larvae display increased resilience and we can freeze them, preserve them at -80^{o}C for years, and recover them when needed with thawing. Thus, *C. elegans* maintenance is easy and inexpensive.

Between 1987 and 1983, Sulston, Horvitz, Kimble and Hirsh resolved the developmental cell lineage of the *C. elegans* somatic cells (3-5). By 1998, the *C. elegans* sequencing consortium published

the animal's complete genome sequence (6). Therefore, *C. elegans* exhibits notable genetic tractability since it is efficiently manipulated with forward or reverse genetics. In addition, *C. elegans* transparency allows in vivo imaging without the need for cross-sectioning or fixation. Moreover, *C. elegans* bears an extensively characterized nervous system and displays significant conservation with mammals.

2. The nervous system of *C. elegans*

The *C. elegans* nervous system has been extensively described, rendering this nematode an ideal model for studying neurobiological functions. In 1986, White et al. reconstructed the structure of the adult hermaphrodite nervous system from electron micrographs and identified 302 neurons that are organized in an invariant arrangement (7). They mainly observed simple neurons with few branches, that establish synapses en passant without employing terminal branches with boutons. The synaptic connections comprise chemical synapses, neuromuscular junctions, and gap junctions (7). In 2012, Jarrell et al. described the posterior mating circuit of the adult male reconstructed again from serial electron micrographs (8). The adult male obtains a total of 383 neurons. These discoveries rendered *C. elegans* the first animal model with the most complete wiring diagram of its nervous system. The invariant cell lineage, the neuroanatomy, and the elementary neuronal morphology of *C. elegans* enabled the determination of behavioral and developmental disorders through genetic screens.

The hermaphrodite neuronal cells constitute almost one-third of the adult animal's body cells (959 cells). Among the 302 neurons, 282 are somatic, and 20 are pharyngeal. The somatic neurons are organized in a few ganglia. Most of them are located in the head around the pharynx, while the rest are disposed at the tail or along the ventral cord. *C. elegans* neurons divide into sensory, motor, and interneurons.

The sensory neurons of the head compose a big part of the head ganglia and project their dendrites to the tip of the nose (9). Apart from the sensory dendrites, most neurites send and receive input from other neurons, making it difficult to distinguish them as axons or dendrites. Neurites mainly synapse at the nerve ring, the ventral and dorsal neural cord, and the tail's neuropil. Sensory axons connect with interneurons in the nerve ring, a tight axon bundle regarded as the worm's brain. Several of these interneurons extend long axons into the ventral cord. There, command interneurons synapse with motor neurons that innervate muscle cells. Unlike vertebrates, nematode muscle cells, and not the motor neurons, send cellular projections to motor neurons to generate synapses. Most *C. elegans* neurons develop in pairs and localize symmetrically on the left and right sides of the animal. Nevertheless,

handedness is not a rule for the nematode's nervous system. *C. elegans'* neuronal cells coincide with 56 glial cells that mainly interact with sensory neurons and are essential for nervous system development and function (10, 11). Neurotransmitters and neuropeptides mediate neuronal signalling in *C. elegans*. The neurotransmitters identified in *C. elegans* are the following: acetylcholine, glutamate, γ-amino butyric acid (GABA), tyramine, octopamine, dopamine, and serotonin. The *C. elegans* neuropeptides belong to three families; the insulin-like, the FLP, and the NLP families (12).

3. The *C. elegans'* neuronal functions and molecular identity

a. The motor neurons

The *C. elegans* neuronal functions and molecular content are extremely characterized. *C. elegans* bears 113 neuronal cells identified as motor neurons that innervate muscle cells. Seventy-five of the 113 neurons synapse with the body wall muscles posterior to the head and reside in the following eight categories: AS, DA, DB, DD, VA, VB, VC, and VD. Body motor neurons spread evenly along the ventral nerve cord. V-named neurons project to ventral muscles, while D-named neurons and AS project to dorsal muscle cells. The A and B classes belong to cholinergic excitatory motor neurons. The D-type neurons are GABAergic inhibitory and always lie post-synaptic to other motor neurons. VC neurons project to the vulva muscles and secrete acetylcholine and serotonin (7, 13). These motor neurons are responsible for animal locomotory behavior, namely crawling or swimming, and for the movements of the alimentary and reproductive systems. Specifically, they are necessary for the sinusoidal movement of the animal when crawling and the C-shaped movement when swimming (14, 15). They also regulate the forward movement on a solid surface, the emergence of reversals and turns during exploratory behavior, and the animal's posture (16-18).

The rest of the motor neurons fall into eleven classes. Some of them innervate the head and neck muscles and generate lateral and dorsoventral head movements not observed in the body. The others project to the gut and the reproductive system, where they trigger defecation and egg-laying behaviours (19).

b. The sensory neurons

C. elegans, through its sensory neurons, detects numerous soluble and volatile chemicals, gases, pheromones, tactile stimuli, humidity, temperature, electric field, osmolarity, and light. Therefore, it

displays several elaborate behaviours, such as sex-specific behaviours like mating and egg-laying, attraction or repulsion to odours, pheromones, gustatory cues, chemicals, oxygen/CO2, temperature, light, and sound. Additionally, the nematode learns and memorizes substantial aspects of its environment and makes associations mainly between the presence of food and different substances. Consequently, *C. elegans* exhibits taxis behaviours, like chemotaxis, thermotaxis, aerotaxis, and galvanotaxis or electrotaxis. This way, the animal travels towards favourable habitats or escapes from harmful stimuli, eliciting attraction or avoidance behaviours. Specific cues generate experience-dependent behavioural plasticity in *C. elegans*. In chemotaxis behaviour, a particular compound, such as water-soluble substances and volatile organic odorants, attracts the animal when combined with food presence (20). On the contrary, elevated concentrations of the same compounds generate an avoidance behaviour in *C. elegans*, termed osmosensation (20, 21). In thermotaxis, the animal associates the presence of gustatory cues with ambient temperature, displaying a preference for the cultivation temperature when migrating on a thermal gradient (22). Aerotaxis refers to navigation in O_2 gradients (23), while in galvanotaxis, the animal navigates toward the negative pole of a static electric field with a fixed direction and magnitude.

The *C. elegans* sensory neurons are 68 and organize into 24 sensillar organs that consist of one or more sensory neurons and two types of glial cells, the socket and sheath cells. However, few sensory neurons are isolated and do not develop into sensilla. Twelve sensory neurons, one sheath, and a socket cell in the head of the animal compose the amphid, the main chemosensory organ of *C. elegans*. Amphid is a bilateral organ whose neuronal cell bodies are located anteriorly to the pharyngeal bulb and their axons connect with the nerve ring. Amphid dendrites project to the tip of the nose. The dendrites of each neuron establish distinct ciliated structures when they reach the anterior end of the head. One sheath cell protects each amphid cilia and a socket cell shapes a channel through which the cilia pass to eventually expose to the extrinsic environment. The neurons that constitute the amphid are ASE, ASG, ASH, ASI, ASJ, ASK, ADF, ADL, AFD, AWA, AWB, and AWC. Among them, AWA, AWB, AWC, and AFD neuronal cilia cease within the sheath cell and do not reach the external environment (24).

Similar to the amphid sensory organ is the phasmid that locates posterior to the anus of *C. elegans* and consists of PHA, PHB, and PQR neurons, one sheath, and two socket cells. PHA and PHB phasmids' cilia are exposed to the external environment, while PQR's cilia terminate within the phasmid socket cell (25). Phasmid neurons' cell bodies are located in the lumbar ganglia of the tail. Their axons project along the posterior ventral nerve cord.

i. Mechanosensation

Mechanosensation refers to the transduction of mechanical forces into electrochemical neural signals. Mechanical stimuli for *C. elegans* constitute the gentle or harsh touch on the nose, the tail, or along the body, the tapping of the animals' cultivation plate, the texture of the surface on which it navigates, and proprioception signals from body stretch. Mechanosensory neurons sense mechanical cues through mechanically-gated ion channels, which give rise to touch- or stretch-evoked currents. These channels belong to two protein superfamilies, the TRP (Transient Receptor Potential) and the DEG/ENaC (Degenerin/ Epithelial Sodium Channels) channels (26). The TRP channels are non-selective cationic channels. They assemble into homo- or hetero-tetramers and span the cytoplasmic membrane with six helices leaving the N- and C-terminus intracellularly. The DEG/ENaC channels are mainly permeable to sodium and, in some cases, to calcium and are predominantly heterotrimeric. Six touch receptor neurons mediate gentle body touch, the ALML, ALMR, AVM, PVM, PLML, and PLMR (27). IL1, ASH, OLQ, and FLP sense nose touch (28, 29). PVD interneurons mediate the harsh touch sensation of the body (30), while PVCs sense the tail's harsh touch (31). Dopaminergic CEP, ADE, and PDE neurons participate in texture sensation (32). Apart from dopaminergic neurons, the rest sensory neurons implicated in mechanosensation are glutamatergic.

ii. Nociception

Nociception is the sensation of noxious environmental stimuli that trigger avoidance behaviours. For *C. elegans*, aversive cues comprise the mechanical stimuli of gentle and harsh body touch, specific odorants and virulent chemicals, some otherwise attractive odorants or chemicals that become repulsive in high concentrations, high osmotic stress, pH of acidic values, extremes of heat and cold, and specific light wavelengths (21, 33).

ASH amphids are the main *C. elegans* nociceptors. ASH neurons are polymodal in the sense that mediate aversion to multiple stimuli, such as nose touch, high osmotic strength of salts and sugars, bitter substances (quinine, 6-n-propyl-2-thiouracil, denatonium), heavy metals (cooper) and, aversive odours (2-octanone, octanol, benzaldehyde) (21, 33). ASHs belong to the amphid neurons with ciliated dendrites exposed to the environment. In the presence of aversive stimuli, these neurons trigger a reversal and turning behaviour to enable rapid escape from the cue (34-36). The TRPV (Transient

Receptor Potential channels of the Vanilloid subtype) channels OSM-9 and OCR-2 mediate the responses of the ASH neuron to all types of noxious stimuli (33). Discrimination of the diverse nociceptive cues arises at the level of the excitation pattern, with divergent amplitudes and patterns of glutamate release (37). In addition, discrete adverse stimuli generate distinct signalling pathways in ASH. The G alpha protein ODR-3 is necessary for osmotic and mechanical avoidance, whereas the Gα protein GPA-3 is responsible for copper and quinine avoidance through ASH (38-40). The novel cytosolic protein OSM-10, expressed in ASH, ASI, PHA, and PHB sensory neurons, is essential for osmosensation but not for avoiding nose touch stimuli or volatile repellents (36).

Other amphid neurons also participate in the perception of nociceptive stimuli. ADL set of sensory neurons engage in the avoidance to octanol, cooper and cadmium. ASK mediate aversion to SDS, ASE to cadmium, and cooper (41, 42), and AWB to aversive odorants such as 2-nonanone and 1-octanol (35).

iii. Chemosensation

There is a wide range of water-soluble gustatory substances that *C. elegans* recognize and distinguish, like anions, cations, cyclic nucleotides, biotin, and amino acids. ASE set of amphid neurons constitute the main *C. elegans* gustatory sensors and emerge as necessary and sufficient for water-soluble chemotaxis. Concurrent ablation of all amphid and phasmid neurons apart from ASE spares chemotaxis (43). Stepwise shifts of NaCl concentration trigger ASE responses, with Na^+ predominantly activating the ASEL while Cl^- and K^+ the ASER neuron (43-45). The two ASE neurons display opposing functions. Elevating NaCl concentration excites ASEL, which acts as an ON-cell. Contrariwise, increasing the concentration of NaCl ceases the otherwise tonically active at baseline ASER. Thus, ASER acts as an OFF-cell (46). ASEL activation promotes forward locomotion (runs), while excitation of ASER augments reversals and changes in direction (turns) (46, 47). Two *C. elegans* subunits of a cyclic nucleotide-gated channel, the TAX-2 and TAX-4 proteins, are necessary for ASE chemosensation (48).

Ablation of ASE neurons renders a limited residual chemotactic response. Five pairs of amphid neurons carry out this response, the ADF, ASG, ASI, ASK, and ASJ neurons (43). ADF participates in chemotaxis to cAMP, biotin, Cl^-, and Na^+, ASG, and ASI to cAMP, biotin, Cl^-, Na^+, and lysine and ASK in chemotaxis to lysine (45). In addition, hypoxia also activates ADF and ASG to evoke a chemotaxis response (49).

iv. Odorsensation

Odorsensation refers to the ability of *C. elegans* to detect and distinguish a sizeable range of volatile organic odorants. At least 50 substances out of 120 tested in an extensive screening emerged as attractive, among them esters, aldehydes, ketones, amines, alcohols, sulfhydryls, organic acids, pyrazines, thiazoles, heterocyclic and aromatic compounds (50). The majority of them constitute natural products of bacterial metabolism. The neurons that sense attractive volatile odours are AWCL/R and AWAL/R sensory amphids. AWC set of neurons distinguishes at least the following five compounds isoamyl alcohol, benzaldehyde, butanone, 2,3-pentanedione, 2,4,5-trimethylthiazole. AWA responds at least to the three odours pyrazine, diacetyl, and 2,4,5-trimethylthiazole (50). Similar to the ASE set of neurons, AWCL and AWCR detect different combinations of odours. AWCL detects butanone, benzaldehyde and isoamyl alcohol, while AWCR detects 2,3-pentanedione, benzaldehyde, and isoamyl alcohol (51). The increased concentration of only a few volatile odours becomes repellent for *C. elegans*. Repulsive odours, such as 2-nonanone and 1-octanol, mainly trigger AWB neurons (35). AWA olfactory neurons respond to increases in odours with regenerative all-or-none action potentials (52, 53), while AWB neurons respond to decreases in odour concentration (54). On the contrary, odour removal triggers AWC neurons, which operate as odour-OFF neurons (55).

The glutamatergic AWC neurons mediate plastic behavioural responses through NLP-1 neuropeptide release (56). A second receptor guanylate cyclase, the ODR-1, generates olfactory responses through the AWB and AWC amphids. ODR-10, a G protein-coupled receptor found particularly in AWA neurons, is necessary and sufficient for detecting diacetyl. Ectopic expression of ODR-10 in AWB neurons renders diacetyl repulsive for *C. elegans* (51). Another gene identified to intercede responses by AWA, AWB, AWC, and ASH neurons is the Gi-like gene *odr-3* (40).

v. Thermosensation

Animals identify their cultivation temperature (Tc) and exhibit preference over it as they associate it with food-existence. In the presence of a thermal gradient, they migrate towards Tc. When they track it, the animals move isothermally along this temperature. This memory is plastic since Tc reestablishment through cultivation at a different temperature within the tolerance range of *C. elegans* redefines this memory (57). The AFD amphid neurons constitute the major thermosensors of *C. elegans*.

Laser ablation of both AFD neurons renders animals athermotactic or cryophilic (22). Memory formation of Tc and temperature sensation result from the coordinated activity of AFD, AWC, and ASI neurons (58-60). The combined action of these three sets of neurons promotes negative thermotaxis. In this case, when animals encounter higher temperatures than Tc in a thermal gradient, their turning frequency raises, and move towards colder temperatures (60). Serendipitous tracking of isothermal suppresses turns and reversals (61).

Thermal signals higher than Tc trigger the AFD neurons, and calcium enters the cells through the TAX-2/TAX-4 cation channel, a cyclic nucleotide-gated ion channel (CNG channel). The guanylyl cyclases that produce cGMP in AFD upon sensing ambient temperature are GCY-23, GCY-8, and GCY-18 (62). The calcium signal of AFD is continuous, graded, and highly reproducible (63, 64). AWC neurons respond to higher and lower temperatures than Tc, while near Tc remain almost inactive. Upon AWC activation by a higher temperature than Tc, the ODR-1 receptor-type guanylyl cyclase produces cGMP that activates the cGMP-dependent TAX-4 cation channel (59). The calcium changes of AWC neurons by temperatures above or below Tc are stochastic and stimulus-correlated (60). The G-protein-coupled receptor SRTX-1 localizes in both AFD and AWC neurons and is necessary for the proper activity of the neurons and normal isothermal tracking (60). ASI neurons display stochastic calcium currents in a specific operating range. Peptidergic neuromodulation of ASI by AFD determines this range (58).

The AFDs, along with FLP neurons in the head and PHC neurons in the tail, also mediate thermonociception. Noxious temperatures above the viable range for *C. elegans* (~35-38 ^{o}C) induce an avoidance reaction. Again, the TAX-2/TAX-4 cation channel in AFD is necessary for this reaction, but the guanylyl cyclase that produces cGMP under this condition is the GCY-12. The cation channels that permit calcium entry in the FLP and PHC neurons are the heat- and capsaicin-sensitive transient receptor potential vanilloid (TRPV) channels, OCR-2 and OSM-9 (62).

vi. Oxygen and carbon dioxide sensation

C. elegans is an aerobic animal that recognizes, in its environment, fluctuations of gases such as oxygen and carbon dioxide. During aerotaxis in a linear oxygen gradient, it avoids low (<4%) and high (>12%) oxygen levels and favours the intermediate one (65, 66). The most crucial neurons implicated in oxygen sensation are the URX, AQR, and PQR (23, 66, 67). AQR and URX cell somas locate at the head of *C. elegans* and PQR at the tail. AQR and PQR project ciliated sensory endings, while URX

projects unciliated dendrites to the tip of the nose. The sensory endings of AQR and PQR are exposed to the animal's coelomic fluid (68). Through the combined function of the formerly mentioned neurons, *C. elegans* may sense both environmental and internal oxygen levels. The neuron ADF also participates in oxygen sensation through mediating avoidance to hyperoxia. In the absence of food, ADF triggers aerotaxis through serotonin production (67).

The URX, AQR, and PQR neurons coexpress the guanylate cyclases GCY-35 and GCY-36, which are essential for aerotaxis behaviour (66, 69). The GCY-35 comprises a heme-binding domain that binds molecular oxygen, rendering it the primary receptor for oxygen aerotaxis (66).

Perception of CO_2 materializes primarily through the AFD, BAG, and ASE neurons, while the oxygen-sensing neurons are also weak CO2 sensors. The elevation of CO2 activates both ASEL and ASER neurons (70).

vii. Light sensation

C. elegans senses light ranging between 350 and 470 nm. A flash of light pointed at the head of the animal ceases the forward movement and initiates reversals. The combined function of ASJ, AWB, ASK, and ASH ciliary neurons induces light avoidance. Only concurrent laser ablation of all four neurons abolishes this response. In-situ whole-cell recording from ASJ neurons evoked an inward current following light illumination. The animal's response to light depends on the intensity of the stimulus. The cyclic nucleotide-gated CNG channel TAX-2 found in ASJ, ASK, and AWB mediates the phototactic response (71).

viii. Electrosensation

The major sensory neurons implicated in electrosensory navigation are the ASJ and ASH, while ASK, AWB, and AWC are minor contributors. Glutamatergic signalling of amphid neurons participates in controlling the animal's speed and orientation (72).

ix. Hygrosensation/Hydrosensation

The sensation of humidity in *C. elegans* involves the combined integration of mechanical and thermal stimuli. The coordinated functions of the mechanosensory FLP and the thermosensory AFD neurons accomplish hygrosensation (73). The FLP neurons are polydendritic and cover most of the head

and neck area. They have ciliated ends not exposed to the outside. They do not constitute a sensillum but rather surround the socket cell of IL neurons and terminate close to the lip cuticle (7, 9, 34). Humidity levels affect the stretching of the subcuticular nerve endings of FLP, conveying mechanical stimuli. The AFD amphid neurons process additional information for hygrosensation, referring to the cooling that arises due to humidity evaporation. Hygrotaxis in a humidity gradient emerges only upon association of humidity with starvation and is a plastic response. The degenerins MEC-6, MEC-10, and ASIC-1, which assemble into the DEG/ENaC ion channels, mediate hygrosensation through the FLP neurons. In the AFD neurons, the TAX-4 cGMP-gated channel is essential for sensing humidity (73).

Similar to hygrosensation, hydrosensation refers to the sensation of water content in the environment apart from the air. *C. elegans* senses water gradient and avoids the wetter regions of an agar plate and the hypo-osmotic water droplets. Hydrosensation involves the DAF-11 guanylate cyclase and the downstream cGMP-gated TAX-2/TAX-4 channel. The ASJ, ASK, and ASI neurons participate in this response. ASJ and ASK respond to air-water switches, while ASI neurons respond to water removal (74).

x. Pheromone sensation

A combination of ascarosides, derivatives of the dideoxysugar ascarylose, constitutes the pheromone of *C. elegans*. ASK is one set of neurons responsible for pheromone sensation, also involved in sexual and social attraction (75-77). ADF, ASI, ASG, ASJ, and ASK neurons control the entry to the dauer stage (45, 78-80). Dauer diapause is a distinct third larval stage in which L1 larvae enter when they confront a harsh environment. Simultaneous laser ablation of ADF, ASI and ASG neurons induces constant entry of the animal to dauer diapause, independently of the environmental conditions (45). ASI neurons secrete the DAF-7 TGF-beta-related peptide, which inhibits dauer formation in a neuroendocrine fashion (80, 81). Upon starvation and high population density, DAF-7 levels are reduced. ADF and ASG neurons express insulin-related ligands of the insulin receptor DAF-2, activation of which inhibits dauer formation (44, 82). Secreted serotonin by ADF also mildly prevents dauer formation (83). Laser ablation of ASJ alone induces permanent arrest at the dauer stage (45). ASJs express another insulin-related peptide that interacts with DAF-2, the DAF-28 (82). G proteins also participate in dauer formation, among them *gpa-2*, *gpa-3*, and *gpa-6* (84, 85).

c. The interneurons

The interneurons comprise the biggest neuronal category in *C. elegans*. The characteristic of interneurons is that they both receive and send information to other nerve cells. Their function is to integrate the received input from one or more neuronal cells of the same or different classes, and to convey the processed information to other neurons. Thus, they modulate decision-making and affect motor output. The interneurons that lie downstream to sensory neurons constitute the first-layer interneurons. Command interneurons are presynaptic to motor neurons and second-layer interneurons are presynaptic to command interneurons.

Specific command interneurons regulate forward or backward movement (86-88). The five interneurons AVB, PVC, AVA, AVD, and AVE integrate responses to mechanical stimuli and control locomotion (7, 31, 86). AIY interneurons integrate gustatory cues and promote forward movement and gradual turnings during chemotaxis (89). AIA, AIB and AIZ mediate attraction and avoidance to water-soluble compounds (90-92). The combined function of AIY, AIZ, AIB, AIA and RIA modulate responses to thermal stimuli (22). AIY and AIB interneurons mediate decisions concerning olfactory and osmotic inputs (55). In gas sensation, AIY and RIA regulate the response to CO_2, while RMG interneurons integrate oxygen inputs (93). RIM and AVA process inputs and affect navigation during galvanotaxis (72).

d. Polymodal neurons

Some *C. elegans* neurons are polymodal, which means that they display at least two distinct circuitry functions, specifically motor and sensory, interneuron, and motor or sensory and interneuron (7). The NSM pharyngeal neurons are neurosecretory, motor, and possibly proprioceptive (94). The M3 neurons of the pharynx arise both motor and sensory. The ventral nerve cord A and B-type motor neurons further behave as proprioceptives. IL1 head neurons are mechanosensory, motor, and interneurons. OLQ neurons of the head are mechanosensory and interneurons. The head neurons RIM, SMB, SMD, RMD, RMH, and RMF function as both motor and interneurons. The AVL head motor neuron also exhibits interneuron-type synapses. The DVA tail interneuron displays stretch sensitivity, also acting as a sensory neuron. The DVB tail motor neuron, which innervates enteric muscles, acts additionally as an interneuron (95).

Furthermore, polymodality characterizes some *C. elegans* sensory neurons. These neurons respond to various sensory cues and thus participate in the sensation of distinct stimuli. The most

common sensory polymodal neurons of *C. elegans* (as also previously mentioned) are the ASH, which function as mechanosensory, osmosensory, odorsensory, and nociceptive. Another example constitutes the ADL neurons, which are chemosensory, odorsensory, pheromone-sensory, and nociceptive (95).

4. Learning and memory in *C. elegans*

C. elegans displays numerous types of behavioural plasticity, such as associative and non-associative learning, long and short-term memory, and imprinting.

a. Non-associative learning

i. Habituation/dishabituation

A type of non-associative learning observed in *C. elegans* is habituation. During habituation, repeated exposure to a stimulus diminishes the animal's response. For example, *C. elegans* exhibits mechanosensory habituation to repeated tapping of the cultivation plate. The mechanical stimuli that emerge from tapping induce backward locomotion termed tap-withdrawal reflex, which ceases following repeated tapping. Additionally, presenting a new stimulus, such as a brief electric shock, evokes dishabituation (96). Depending on the training procedure, the animal may develop short or long-term memory of the habituation (97). The mechanosensory neurons ALM, AVM, PLM, and PVD and the interneurons AVD, AVA, AVB, PVC, and DVA mediate this response (96).

ii. Sensitization

Sensitization is the progressive enhancement of a reflexive response to a stimulus due to repeated presentation or following an adverse stimulus without pairing the two stimuli. Utilizing again the tap withdrawal reflex, Rankin et al. (96) displayed enhancement of *C. elegans* withdrawal upon a noxious mechanosensory stimulus. Specifically, first, they applied two taps to the cultivation plate with an interval of two minutes. Two minutes later, they applied a series of taps that constituted the noxious stimulus followed, by the test taps in which the animal exhibited enhanced response (96).

b. Associative learning

C. elegans exhibits an incredible ability to memorize the environmental conditions that signal the presence or absence of food or the presence of adverse cues. Consequently, the animal performs taxis behaviour in an attempt to approach the favoured environment.

i. Classical conditioning

In classical conditioning, the animal associates the response to an unconditioned stimulus with an irrelevant temporally paired conditioned stimulus. *C. elegans* chemotax on a NaCl gradient towards the NaCl concentration of cultivation. Thus, it associates the specific concentration of NaCl with the presence of food (98). This is an ASE-mediated response. Cultivation of animals at the same NaCl concentration but in the absence of food results in the association of NaCl with starvation and avoidance of the specific concentration (99). In another example of classical conditioning in *C. elegans*, the animals associate the cultivation temperature (Tc) with the presence of food. Therefore, when confronting a thermal gradient, they thermotax towards Tc if it was paired with the presence of food or avoid Tc if it was paired with starvation (57). The AFD sensory neuron and the interneurons AIY, AIZ, and RIA mediate this thermotaxis behaviour (22).

ii. Imprinting

Imprinting is a rapid type of learning that appears at a specific developmental stage and generates long-term memories. Exposure of *C. elegans* to attractive odorants of specific concentration after hatching creates an olfactory imprint. Re-exposure to the same odorants during adulthood induces enhancement of attraction and egg-laying. The presence of food is necessary for imprint formation. AWC odour-sensory neurons and AIY interneurons mediate this response (100).

5. Neural conduction in *C. elegans*

Early studies have indicated that neural conduction in the nematode *Caenorhabditis elegans* differs from that in vertebrates (101). Research on the neuronal electrical properties of *C. elegans* revealed that several neurons generate only graded responses. This notion prevailed as a dogma for all *C. elegans* neurons until the recent discovery that specific sensory neurons may fire action potentials (53). However, potassium and calcium currents generate both graded and action potentials in *C. elegans*. Classical voltage-gated sodium channels and sodium-dependent potentials have not been identified (102). Despite the lack of voltage-dependent sodium channels, many clues support that Na^+ current contributes to neuronal firing in *C. elegans*. Patch-clamp recordings revealed that the absence of extracellular Na^+ abolishes action potentials (103).

6. The Epithelial Sodium Channels/Degenerins (ENaCs/DEGs) Family

a. ENaC/DEG subfamilies

Epithelial Sodium Channels / Degenerins (ENaCs/ DEGs) constitute an enormous protein family with divergent characteristics. ENaCs/DEGs are present only in metazoa, in organisms as divergent as the nematode *Caenorhabditis elegans* and *Homo sapiens*. Their common feature is that they form amiloride-sensitive voltage-insensitive sodium channels expressed mainly in the nervous system and epithelial tissues (Hanukoglu and Hanukoglu, 2016). The ENaC/DEG family is divided into 7 subfamilies, depending on the organism or the tissue they are expressed (Figure 1). The mammalian members constitute three subfamilies, the ENaCs, the ASICs, and the INaCs. The mammalian ENaCs form channels that conduct Na^+ across tight epithelia. They are constitutively active, and their activity is upregulated by aldosterone and vasopressin (104, 105), while proteolytic events seem to enhance the open probability of the channel (106). Moreover, insulin regulates Epithelial Sodium Channels density on the cells of A6 epithelia (107).

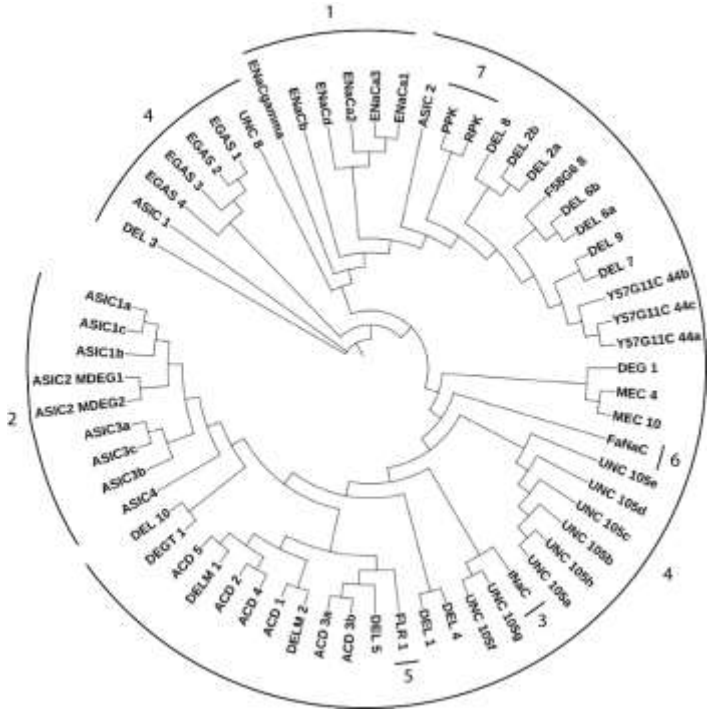

Figure 1. Organization of the ENaC/DEG family in seven subfamilies of related sequences. Human, mollusk, fly, and worm ENaC/DEG family members are organized in an unrooted phylogenetic tree. Human members are separated into three subfamilies ENaCs (1), ASICs (2), and INaCs (3). Other subfamilies are the *C. elegans* DEGs (4) apart from FLR-1 (7), which constitutes a subfamily on its own. *Drosophila* members (5) and mollusk members (6) form two more subfamilies.

ENaCs are expressed in diverse tissues like the kidney, lungs, gastrointestinal tract, skin, sweat glands, pancreas, and even the cochlea, the retina, and osteoblasts (108-116). ASICs are abundantly expressed in the central and peripheral nervous system, knee joint afferents, and fibroblast-like synoviocytes. They participate in nociception, pain perception, associative learning and memory, and hippocampal LTP (117-123). They are gated by protons and are capable of sensing the acidic

environment, like that resulting from ischemia or injury (124). INaCs, like BLINaC (Brain Liver Intestine Sodium Channel) and hINaC (human INaC), are distinct from other ENaCs in the amino acid sequence identity and expression pattern (125-127).

The Drosophila members of this family, like Pickpocket (PPK) and Ripped Pocket (RPK), form another subfamily. RPK is present in fly ovaries and testis, while PPK in sensory neurons of late embryos and is implicated in mechanotransduction and mating behaviour (128, 129). FaNaCs found in the mollusk *Helix aspersa*, the snail *Helisoma trivolvis*, as well as in *Aplysia* are members of this family that form one more subfamily. These channels are gated by the peptide FMRFamide and localize in the nervous system (130-133).

Among the *C. elegans* members, FLR-1 forms a subfamily on its own. FLR-1 encodes an ion channel expressed in the intestine implicated in defecation rhythm, growth rate, and dauer formation (134, 135). Finally, the Degenerins subfamily occupies a large part of the family. Degenerins are the amiloride-sensitive sodium channels expressed in *C. elegans*, mainly in the nervous system. They took their name from the first identified members *deg-1* and *mec-4*, whose mutations lead to the degeneration of the neurons they are expressed (136). Another degenerins characteristic is that some members are activated by mechanical stimuli and are important in touch sensation and proprioception (137).

b. The ENaC/DEG structure

Despite their divergent functions, all the family members share some conserved regions (138, 139). ENaC/DEGs span the cytoplasmic membrane twice, leaving more than half of their polypeptide chain extracellularly, forming a big loop. Intracellularly, the N-terminus is supposed to participate in the regulation of channel gating through an HG (His-Gly) motif. ENaCs contain a motif at the N-terminus that signals the endocytosis of the channel. The cytoplasmic C-terminus is involved in interactions with other proteins, such as phosphorylases, phosphatases, or cytoskeletal components. A proline-rich motif at the C-terminus, unique to the ENaC subfamily, is recognized by an E3 ubiquitin-protein ligase.

The two transmembrane domains, M1 and M2, are located close to the N- and C-terminus respectively, and close to a post-M1 segment (FPxxTxC) and a pre-M2 domain. M1 partakes in the stabilization of the channel in the cytoplasmic membrane and the activity and selectivity of the channel. In the M2 region there are motifs involved in the recognition by amiloride and again in the ion selectivity of the pore. Specifically, in the M2 region of degenerins, there is the DEG motif. Substitution of its residues with larger ones increases the open probability of the channel and causes degeneration of

the neuronal cell it is expressed. A conserved residue in the pre-M2 domain is involved in the opening and closing of the channel pore.

Proteases probably recognize the extracellular loop and activate the channel subunits. This part of the channel is subjected to glycosylation events, which appear in the mammalian members of the family. Other domains located in the extracellular matrix are the Cysteine-Rich Domains CRDII and CRDIII, which probably participate in the formation of disulfide bonds to maintain the tertiary structure of the large extracellular loop. Close to CRDIII, there is the neurotoxin-recognized domain (NTD) (140). The extracellular loop of ASIC1 resembles an extended hand holding a ball and divides into five domains (141). The domains palm and β ball lie close to the membrane and are formed by β strands and loops. More peripherally are located the domains thumb, knuckle and finger, which are consisted of α helices and loops and are less conserved among the ENaC/DEG family members. The thumb domain may assist with the desensitization of the channel to an acidic environment (142). Finally, there are two more motifs located at the extracellular loop find exclusively within the degenerins. It is the CRDI motif followed by an Extracellular Regulatory Domain (ERD) possibly involved in the regulation of the channel gating (136).

ENaC/DEGs adopt a heteromultimeric subunit organization, likely tetrameric (143). At least three homologous subunits come in contact to form homo- or hetero-tetramers that constitute the channel (138, 144). The four subunits assemble around the channel pore. The crystal structure of the chicken ASIC1, which is a homo-trimer with a chalice-like shape, implies a possible trimeric structure (141). The ions that permeate ENaC/DEG pores are mostly monovalent small cations such as Na^+, Li^+ or H^+ (145). Nevertheless, ASICs exhibit also permeability to Ca^{2+} (146, 147).

7. Implication of ENaC/DEG members in human pathologies

Several human disorders have been associated with mutations in these channels, revealing how important they are for an organism's physiology. ENaCs are implicated in diseases where the balance of sodium homeostasis has been disrupted. Mutations altering the splicing of beta and gamma subunits of epithelial sodium channels are linked with hypertension and Liddle's syndrome (148-150). Similarly, mutations of ENaCs alpha and beta subunits are implicated in the autosomal recessive pseudohypoaldosteronism type I, a disease characterized by hyperkalemia, metabolic acidosis, and unresponsiveness to mineralocorticoid hormones (151). Dysregulation of epithelial sodium channels may contribute to the emergence of pulmonary pathologies, such as asthma or cystic fibrosis (152, 153).

ASICs are involved in pathologies of the Central and Peripheral Nervous Systems. Increasing evidence implicate them in several neurodegenerative diseases, such as multiple sclerosis, Parkinson's disease, and Huntington's disease (154-156). ASICs during toxic acidosis, which appears in several neurological dysfunctions, seem to increase their number and participate in intracellular Ca^{2+} raise. In general, in the previously mentioned pathologies blocking of ASICs acts in a neuroprotective fashion (157). ASICs are also associated with panic disorder, anxiety, seizures, migraine concerning the CNS, or diabetic neuropathy and peripheral pain concerning the PNS (158-161). Finally, acid-sensing sodium channels have been correlated with arthritis (123, 162).

8. Stress perception

Physiological stress, perceived by the sensory system, induces cellular stress responses that trigger organismal adaptation. Organisms have adapted to overcome different types of stress that emerge throughout their life. Organismal homeostasis, behaviour, and survival alter upon environmental stress such as heat, starvation, hypoxia, or oxidative stress (163-165). The nervous system constitutes the essential sensor of environmental changes (166). Stress perception and decision-making for specific behavioural responses arise through adjustments in neuronal activity, plasticity, or signal transduction (164). Neurons modify their properties or excitation pattern via structural and functional plasticity to convey stressful messages. Functional neuronal plasticity upon stress is contingent on regulating neurotransmitter receptors, transporters, or ion channels. Several studies in mammals demonstrated the effects of diverse stress types on neurotransmitters or receptor levels. Gamma-Aminobutyric Acid (GABA), glutamate, acetylcholine, corticoid, serotonin, and dopamine receptors compose indicative signalling initiators whose expression levels depend on distinct types of stress (167-171).

Nevertheless, how stressful stimuli are perceived and what molecular modifications eventuate to modulate the intrinsic neuronal properties and excitation pattern remains obscure. Recent studies have revealed that stress modifies ion channel abundance or activation. In mammals, acute and chronic types of stress differentially coordinate the expression levels of voltage-gated potassium channels (172, 173). Activation of AMP-activated protein kinase (AMPK) potentially mediates the effects of acute stress on potassium-conducting channels (173). In *Drosophila melanogaster*, starvation suppresses KCNQ potassium channel activity through the sodium/solute co-transporter-like 5A11 *(SLC5A11)* (174). Oxidative stress adjusts the expression of calcium-conducting channels (175, 176). Likewise, reactive species activate the TRP ankyrin1 channel, which acts as an oxidative and nitrative stress sensor (177).

Yet, the regulation of sodium channels of neuronal cells and their participation in signalling transduction in response to stress is not enlightened (178).

9. ENaC/DEG channels and stress

ENaC/DEG members conduce to several human pathologies comprising respiratory syndromes and vascular, cardiac, and neurodegenerative diseases (179). Only the following studies pinpoint their implication in stress responses. In vertebrates, pharmacological inhibition of Acid Sensing Sodium Channels (ASICs) declines stress-associated reactions in behavioural models and exhibits anti-depressant-like effects (180, 181). Oxidative stress inhibits the expression of α-ENaC (182, 183) and regulates the activation of ASICs (184, 185). SGK1, a Ser-Thr kinase induced by the corticosteroid signalling pathway, modulates the abundance of ENaC and ASIC1 on the plasma membrane (186-188). Corticosterone, elevated by acute stress, causes a protein kinase C (PKC)-dependent increase of ASICs' current in cultured hippocampal neurons (189, 190). In *C. elegans*, laminar shear stress activates the MEC-4/MEC-10 channel implicated in mechanosensation (191).

VII. Aim of thesis

This thesis aimed to get a deeper insight into the sensory perception of stress. We used *C. elegans* as a model organism for its extensively characterized nervous system, exceptional genetic tractability, and significant conservation with mammalian systems. We decided to turn to sodium channels in the sensory system. Sodium channels participate in the regulation of ion balance across the cytoplasmic membrane. A much-expanded family of sodium channels in the nervous system – and not only – is the ENaC/DEG family. Even though it is not very well studied, members of it have been implicated in various diseases.

In the present study, we sought to delineate the participation of ENaC/DEG family members in stress perception and subsequent integration to modify behavioural responses in animals. We focus on three yet unexplored members of the Degenerin family, the degenerin-like (DEL) proteins DEL-2, DEL-3, and DEL-4. We display that these three degenerins localize in chemosensory and dopaminergic neurons. In addition, DEL-3 and DEL-4 localize in serotonergic, with DEL-4 further specified in cholinergic motor neurons. The dopamine-mediated basal slowing (BS) response revealed that these three degenerins affect dopaminergic signalling and mediate gustatory stimuli. Intriguingly, we exhibit that DEL-4 composes a proton-blocked homomeric amiloride-sensitive sodium channel. Utilizing reverse genetics, pharmacological analysis, and imaging techniques, we provide evidence that specific types of stress regulate DEL-4. In turn, DEL-4 contributes to the adaptation of neuronal signalling and the eventual modification of animals' locomotory rate. Analysis of neurodegenerative disease models revealed the neuroprotective properties of DEL-4. Discerning the neuronal mechanisms that drive the effects of stress on sensory integration and neuronal cohesion will add valuable insight into how stress advances the progression of neurodegenerative diseases and may provide new pharmaceutical targets.

VIII. Materials and Methods

EXPERIMENTAL MODELS

Caenorhabditis elegans

Nematodes were maintained following standard procedures, as previously described (2). Stocks were maintained on 5cm NGM plates seeded with OP50 (Table 7). Animal rearing temperature was kept at 20^{o}C unless otherwise noted. The OP50 *E. coli* strain was preferably used as a food source except for RNAi experiments, where NGM plates were seeded with HT115 (DE3) bacteria (Table 7), carrying the desired RNAi plasmid construct. HB101 *E. coli* bacteria (Table 7) were used to form a thin bacterial lawn for the basal and the enhanced slowing response assays.

Isogenic hermaphrodite populations of the same developmental stage were used in all experiments. *C. elegans* has a lifespan of approximately 20 days at 20^{o}C, during which it passes through four larval stages (l1-l4) before reaching adulthood. All experiments were performed during adulthood, with the only exception being the starvation survival assay that monitors animals from the l1 stage until adulthood. Imaging after heat stress and starvation was conducted on day two of adulthood. Animals grown on RNAi plates were imaged on day three or four of adulthood. Animals from the rest of the experiments were imaged on day one of adulthood.

Males emerge spontaneously in a population (frequency ~0.02%). A larger male population was obtained following a mild heat sock (3-4 hrs at 35^{o}C or 2hrs at 37^{o}C) of late l4 stage animals (192). Males were maintained through mating with hermaphrodites. In this study, males were used only for genetic crossing.

Variations *tm717* and *tm5642* were verified by polymerase chain reaction (PCR) using the primers 5′-AAAAGTGTGGACCCGGATAT-3′ and 5′-ACCAAGAGAGGAAGCAGTTCC-3′, 5′-ATGTGGCTCCGAGGACTTTTC-3′ and 5′- GCAATCAGACACCACACCCAGTA-3′ (Table 2). The strains used in this study are listed in Table 1. Strains *unc-119(ed3);*Ex[p_{del-2}DEL-2_{1-27}::DsRed; *unc-119*(+)], *unc-119(ed3);*Ex[p_{del-3}DEL-3_{1-45}::DsRed; *unc-119*(+)] and *unc-119(ed3)*;Ex[p_{del-4}DEL-4_{1-36}::mCherry; *unc-119*(+)] are referred in the text as p_{del-2}DsRed, p_{del-3}DsRed and p_{del-4}mCherry, respectively (Table 1).

Xenopus Oocytes

Electrophysiology experiments were performed with *Xenopus laevis* oocytes. *Xenopus* oocytes were obtained from EcoCyte Bioscience (Dortmund, Germany) (Table 7). They were maintained at 16^{o}C in 1X ND96 solution (96mM NaCl, 2mM $MgCl_2$, 2mM KCl, 1.8mM $CaCl_2$, pH 7.4).

METHOD DETAILS

Generation of *C. elegans* transgenic lines

Genetic transformation with microinjection

For the generation of transgenic animals, plasmid DNAs were mixed, at a concentration of 50 ng/ml of the plasmid of interest with 50 ng/ml of the pRF4 plasmid bearing the dominant mutation *su1006* of the *rol-6* gene (193). The dominant mutation *su1006* causes the roller phenotype. The DNA mixtures were microinjected into the gonads of N2 young adult hermaphrodite animals. F1 transgenic progeny were selected based on the roller phenotype to establish independent lines. Translational reporter fusion lines of *del-4* with the DsRed and ASAP1 were generated by injection. The roller phenotype of the line p_{del-4}DEL-4:: DsRed; *rol-6(su1006)* was used for crosses with the strains BZ555, BZ555;BR5270, and UA44.

Biolistic transformation of *C. elegans*

The second method used to generate transgenic animals was the gold nanoparticle bombardment (biolistic transformation). We used 10 μg of the construct bearing the desired gene and 10μg of the pPK719 rescue plasmid DNA, carrying the coding sequence of the *unc-119* gene (194). Transformed animals bearing the *unc-119* rescue construct exhibit wild-type locomotion. DNAs were bombarded on hermaphrodite *unc-119(ed3)* locomotion defective mutant animals of stage L4 or young adulthood, cultured on 9 cm Na22-seeded plates (Table 7). The remaining constructs, apart from the two generated with microinjection, including another translational reporter of *del-4* with DsRed, were introduced into *C. elegans* with biolistic transformation. The p_{del-4}DEL-4::GFP;p_{del-4}SNB-1::DsRed line was generated by co-bombardment of a DNA mixture containing 7μg p_{del-4}DEL-4::GFP, 7μg p_{del-4}SNB-1::DsRed and 7μg *unc-119* rescue plasmid DNA.

Genetic crosses

Generation of males was achieved with a mild heat sock (3-4hrs at 35^{o}C or 2hrs at 37^{o}C) of late l4 stage

animals (192). For each mating, ~6 hermaphrodites of one genotype were placed in a 3cm OP50-seeded petri plate with ~18 males. Mating was considered successful when an increased number of male progenies was observed in the plate. Selection of transgenic lines was achieved by exploiting the roller phenotype, by using a UV stereoscope (epifluorescence microscope NIKON SMZ800N) to select fluorescent reporters or by isolating genomic DNA (NucleoSpin Tissue, Mini kit for DNA) (Table 7) and performing PCR when selection of genes mutations was needed (see Table 2 for primer sequences).

The following reporters and double mutants were generated by standard genetic crosses (also Tables 1, 2, 6, 7): *unc-119(ed3)*;Ex[p*del-2*DEL-2$_{1-27}$::DsRed; p*flp-8*GFP*;unc-119*(+)], *unc-119(ed3)*;Ex[p*del-2*DEL-2$_{1-27}$::DsRed; OSM-10::GFP*;unc-119*(+)], *unc-119(ed3)*;Ex[p*del-2*DEL-2$_{1-27}$::DsRed; p*dat-1*GFP*;unc-119*(+)], *unc-119(ed3)*;Ex[p*del-3*DEL-3$_{1-45}$::DsRed; p*flp-8*GFP*;unc-119*(+)], *unc-119(ed3)*;Ex[p*del-3*DEL-3$_{1-45}$::DsRed; OSM-10::GFP*;unc-119*(+)], *unc-119(ed3)*;Ex[p*del-3*DEL-3$_{1-45}$::DsRed; p*dat-1*GFP*;unc-119*(+)], *unc-119(ed3)*;Ex[p*del-3*DEL-3$_{1-45}$::DsRed;TPH-1::GFP*;unc-119*(+);*rol-6(su1006)*], *unc-119(ed3)*;Ex[p*del-4*DEL-4$_{1-36}$::mCherry; p*flp-8*GFP*;unc-119*(+)], *unc-119(ed3)*;Ex[p*del-4*DEL-4$_{1-36}$::mCherry; OSM-10::GFP*;unc-119*(+)], *unc119(ed3)*;Ex[p*del4*DEL4$_{1-36}$::mCherry; p*dat1*GFP*;unc-119*(+)], *unc119(ed3)*;Ex[p*del4*DEL4$_{1-36}$::mCherry; TPH1::GFP*;unc-119*(+);*rol-6(su1006)*], *unc-119(ed3)*;Ex[p*del-4*DEL-4$_{1-36}$::mCherry; p*acr-2*GFP*;unc-119*(+)], *del-4(tm717)*; zcls4[p*hsp-4*GFP], *del-4(tm717);* uthls202[aak-2(intron1)::aak-2(aa1-aa321)::Tomato::unc-54 3'UTR ; *rol-6(su1006)], del-4(tm717)*;skn-1b/c::GFP, *del-4(tm717)*; p*asic-1*SNB-1::SEpHluorin; *rol-6(su1006), del-4(tm717)*; [*unc-119(ed3)*; oxSi834[P *unc-47*GFP::SNB-::unc-54 UTR; *unc-119*(+)], *del-4(tm717)*; nuIs183 [p*unc129*NLP-21::Venus; p*myo-2*NLS::GFP], *del-4(tm717);* p*dat-1*ASAP-1; *rol-6(su1006)*], *del-4(tm717)*; egls1[p*dat-1*GFP], p*del-4* DEL-4:: DsRed; egls1 [p*dat-1*GFP]; *rol-6(su1006)*, byIs161 [p*rab-3*F3(delta)K280 + p*myo-2*mCherry]; egIs1 [p*dat-1*GFP], *del-4(tm717)*; byIs161 [p*rab-3*F3(delta)K280 + p*myo-2*mCherry]; egIs1 [p*dat-1*GFP], p*del-4*DEL-4::DsRed; *rol-6(su1006)*; byIs161 [p*rab-3*F3(delta)K280 + p*myo-2*mCherry]; egIs1 [p*dat-1*GFP], *del-4(tm717)*; baIn11[p*dat-1*::a-Synuclein; p*dat-1*GFP], p*del-4*DEL-4:: DsRed; *rol-6(su1006)*]; baIn11[p*dat-1*a-Synuclein; p*dat-1*GFP], *del-4(tm717);dop-1(vs100), del-4(tm717);dop-2(vs105), del-4(tm717);dop-3(vs106), del-4(tm717);pkc-1(ok563), del-4(tm717);pkc-2 (ok328), del-4(tm717);tpa-1 (k501), del-4(tm717);kin-2(ce179), del-4(tm717);unc-43(tm1605), del-4(tm717);* p*hsp-16.2*::GFP, *del-4(tm717);* dvls19 [(pAF15) gst-4p::GFP::NLS)], *del-4(tm717);p**sod-3*::GFP, *del-4(tm717);* P*let-858*GCaMP2.0; *rol-6(su1006)*.

Molecular cloning

All genomic sequences were retrieved from WormBase (www.wormbase.org). To generate a construct for induction of *del-4* RNAi, the *del-4* gene was amplified with PCR from wt genomic DNA isolated from the N2 strain (Nucleospin Tissue kit – see Table 7). Subsequently, the PCR product was inserted into the Topo vector (Table 7) and subcloned in the pL4440 plasmid vector. The amplified region corresponds to exons 1-10 of the *del-4* gene. The resulting construct was transformed into the Ht115 (DE3) *E. coli* strain (Table 7). Ht115 bacteria carrying the empty pL4440 vector were used as a control food in the experiments that use the RNAi technique for gene downregulation. The primers used for the amplification of *del-4* (exons 1-10) were 5′-GATGGGTGTATTTTGGACCG-3′ and 5′-TCAAGACACGATTCTCCTGA-3′ (Table 2).

Conventional cloning procedures were followed for the construction of the translational and transcriptional reporters expressed in *C. elegans*. The promoter region and the first exon of each gene were amplified from wt genomic DNA isolated from the N2 strain, for the generation of p_{del-2}DsRed, p_{del-3}DsRed, and p_{del-4}mCherry transcriptional reporters (Table 7). They were inserted in the Topo vector and subcloned in the pPD95.77 plasmid vector (Table 7) in frame and at the amino (N) terminus of a pre-existing DsRed or mCherry fluorescent protein. The promoter regions amplified were 1.3 Kb upstream to the start codon of *del-2*, 2 Kb of *del-3*, and 1.5 Kb of *del-4*. The primers used were 5′-TCTTATGATGCACGGCG-3′ and 5′-GGTACCCGTCCACTATTAGTAAT-3′ for del-2, 5′-GCATGCTTACATTTGAGGGTTTAG-3′ and 5′-ACCGGTGTTTTCGATTCAGTTTT-3′ for del-3, 5′-CTGCAGGTCGACACATCATAAATC-3′ and 5′-ACCGGTCCTCAACCATCGAGCATTT-3′ for *del-4* (Table 2). Excision of DNA sequences from the Topo vector was performed with HindIII/XhoI for *del-2* and *del-3*, and with EcoRI for *del-4*.

To generate the p_{del-2}DEL-2::mCherry (Table 7) translational reporter construct, we amplified from wt genomic DNA the sequence from the fifth until the eleventh exon, without the stop codon. The primers used were 5′-CTGCAGGATTTCTCTGTCAAGTGG-3′ and 5′-ACCGGTCATATTGTCAGGCAAGTT-3′ (Table 2). The PCR product was inserted into the Topo vector, and an AgeI/PstI was subcloned into the pPD95.77 plasmid vector, in frame with the mCherry coding sequence. Exons two to four were then amplified using the 5′-CTGCAGAGTTGATGATGATTAAAGAA-3′ and 5′-CTGCAGTGAAAATGCTCAAACAAA-3′ primers (Table 2) and subcloned into the Topo vector. A PstI/BglI fragment was then ligated upstream to exon five in pPD95.77 carrying *del-2* (exons 5-11) in frame with mCherry. Finally, the promoter and

the first exon of *del-2* were excised from the Topo vector (created previously for the generation of the *del-2* transcriptional reporter) with SphI/PvuII and ligated into pPD95.77 carrying exons 2-11. The translational reporter p_{del-3}DEL-3::DsRed was generated by amplifying the wild-type genomic region from exon two to exon seven, just before the stop codon, using the primers 5′-ACCGGTTGTTCACGATGATCAACTATT-3′ and 5′-ACCGGTGGTGTGTCTCCTGAAGCTA-3′ (Table 2). The amplified region was inserted into the Topo vector and an AgeI fragment was inserted downstream of exon 1 into pPD95.77 carrying the *del-3* promoter region and the first exon fused with DsRed, created during the construction of the *del-3* transcriptional reporter. For the *del-4* translational reporter p_{del-4}DEL-4::GFP, the promoter and the whole coding region were isolated from genomic wild-type DNA, using the primers 5′-ACGCGTCGACACATCATAAATCTCCACCCAC-3′ and 5′-CGGGGTACCCCATCATTAGAATGAGGCTTTGG-3′, and inserted into the Topo vector. The promoter and coding regions were isolated using SalI/KpnI and fused with GFP in the pPD95.77 plasmid vector. To create p_{del-4}DEL-4::DsRed, the promoter and coding region of *del-4* were isolated from the GFP-tagged translational reporter construct using SphI/AgeI and inserted into pPD95.77, in frame with the coding sequence of the DsRed gene.

To monitor synaptic vesicle localization, we generated the construct p_{del-4}SNB-1::DsRed (Table 7). The SNB-1 coding region and *del-4* promoter were amplified, with 5′-CGG GGTACCGAATTCGGACGCTCAAGGAGATGCCGGC-3′ and 5′-CGGGGTACCGAATTCTTTTCCTCCAGCCCATAAAACG-3′, 5′-CTGCAGGTCGACACATCATAAATC-3′ and 5′-GGATCCCATCTGCAATTTTATTTT-3′ (Table 2), and inserted into Topo vectors. A KpnI DNA fragment of *snb-1* was excised from Topo and inserted into the pPD95.77 plasmid vector in frame with the DsRed coding sequence. An SphI/KpnI fragment of the *del-4* promoter was then fused upstream to *snb-1* gene. To estimate the resting membrane potential, we generated the construct p_{dat-1}ASAP-1 (Table 7). Plasmid pcDNA3.1 /Puro - CAG - ASAP1(195) (plasmid #52519) (Table 7) was retrieved from Addgene. We amplified ASAP-1 from plasmid #52519 and the *dat-1* promoter from wt genomic DNA isolated from the N2 strain, with the primers 5′-TAGCCGCCACCATGGAGAC-3′ and 5′-AGATCTTTCATTAGGTTACCACTTCAAG-3′, 5′-CTGCAGATCCATGAAATGGAACTTGA-3′ and 5′-GGATCCGGCTAAAAATTGTTGAG-3′. The PCR products were then inserted in Topo vectors. The *myo-3* promoter of pPD96.52 was replaced with a PstI/BamHI fragment containing the *dat-1* promoter. Next, a BamHI/EcoRV fragment containing ASAP1 was inserted downstream of the *dat-1* promoter into pPD96.52.

To monitor basal slowing response upon downregulation of both *del-2* and *del-3* with RNAi we generated a construct for RNAi bearing both *del-2* and *del-3* genes (also proposed in the reference (196)). To generate this new construct for double *del-2/del-3(RNAi)* we utilized constructs that we had previously generated for this study. Specifically, *del-2* and *del-3* genes were amplified with PCR from wt genomic DNA isolated from the N2 wild-type strain. Amplified regions correspond to exons 2-11 of the *del-2* gene and exons 2-7 of the *del-3* gene. Subsequently, PCR products were inserted in the Topo vector (Table 7), and the *del-3* gene was subcloned in the pL4440 plasmid vector using the restriction enzymes HindIII and XhoI. The *del-2* gene was then excised from the TOPO vector with the restriction enzyme XhoI and inserted downstream to *del-3* in the pL44440 vector. The resulting construct was transformed into the Ht115 (DE3) *E. coli* strain (Table 7). Ht115 bacteria carrying the empty pL4440 vector were used as a control food in the RNAi experiment. The primers used for the amplification of *del-2* (exons 2-11) and *del-3* (exons 2-7) were 5′- CTGCAGAGTTGATGATGATTAAAGAA -3′, 5′-ACCGGTCATATTGTCAGGCAAGTT -3′ and 5′-ACCGGTTGTTCACGATGATCAACTATT-3′, 5′-ACCGGTGGTGTGTCTCCTGAAGCTA-3′, respectively. All genomic sequences were retrieved from the WormBase (www.wormbase.org).

Total RNA isolation and qRT-analysis

Total RNA extraction from synchronized day-1 or day-2 adult animals was performed using the TRIzol reagent (Invitrogen). For cDNA synthesis the iScript™ cDNA Synthesis Kit (Bio-Rad) was used. Quantitative Real-Time PCR (qRT-PCR) was performed in a Bio-Rad CFX96 Real-Time PCR system and was repeated at least three times. Expression of the housekeeping gene pmp-3 was used as an internal control for normalization. The primers used for measuring pmp-3 mRNA levels were 5′-ATGATAAATCAGCGTCCCGAC-3′ and 5′- TTGCAACGAGAGCAACTGAAC -3′.

Protein Blast

Protein BLAST analysis was performed in silico using the protein BLAST tool of the NCBI website (https://blast.ncbi.nlm.nih.gov/Blast.cgi). For this analysis, we retrieved the protein sequences of DEL-2 (isoforms a and b), DEL-3, and DEL-4 from the WORMBASE (https://wormbase.org//#012-34-5).

RNAi treatment

Specific gene downregulation was achieved using the RNA interference technique (RNAi). Animals were fed bacteria expressing double-stranded (ds) RNA, which targets the gene of interest. For the basal slowing assay and *hsf-1* downregulation, animals were synchronized with bleaching solution and eggs were placed on RNAi plates. They were allowed for 2 days at 20^{o}C to grow until the l4 stage. Four to five l4 animals were transferred on new RNAi plates and allowed for 3-4 days to lay progenies. One-day-old adult animals from the second generation grown on RNAi plates were used to measure the basal slowing response. For imaging during *del-4* downregulation, isogenic populations of animals were synchronized with bleaching. Eggs were placed on NGM plates seeded with dsRNA for *del-4* and allowed to hatch and grow until the fourth day of adulthood. Animals were transferred to new RNAi plates every second day. RNAi plates were seeded with 200 μl of O/D culture inoculated with 50μl O/N culture/ml of the O/D and incubated for 3-4hrs shaking at 37^{o}C.

Microscopy

Confocal imaging

Confocal images were acquired using an LSM710 Zeiss confocal microscope (Axio-observer Z1). Image z-stacks were captured, and maximum intensity projections were obtained using ZEN 2.3 software (Carl Zeiss, Jena, Germany). Animals were immobilized on a 5% agarose (in M9 solution) pad with a drop of 10μl Nanobeads (Nanobeads NIST Traceable Particle Size Standard 100nm, Polysciences) (Table 7). The animals used were hermaphrodites on day one of adulthood unless otherwise stated. A 40x lens was used when the images were used for estimating the neuronal pattern of DELs, whereas for the rest of the confocal images, used to estimate colocalization or neurodegeneration, a 63x lens was used.

We followed previously suggested procedures to evaluate dense core and synaptic vesicle release (197, 198). Quantitation of synaptic and dense core vesicle numbers was performed in the dorsal nerve cord, when oriented towards the objective, at the turn of the posterior gonadal arm of young adults (day 1 of adulthood). Maximum intensity projection images were obtained from the dorsal neural cord of $p_{unc-129}$NLP-21::YFP and p_{unc-47}GFP::SNB-1 expressing animals (Table 1). We cross-fertilized *del-4(tm717)* mutants with animals carrying a GFP marker of synaptic vesicles (SVs) expressed under the GABAergic motor neuron-specific, *unc-47* promoter (p_{unc-47}GFP::SNB-1). Genetic tagging of synaptic vesicle-associated proteins or neuropeptides with fluorescent proteins can be used to estimate vesicle and

neuropeptide density at presynaptic sites (199). We quantified SVs at the presynaptic elements of the dorsal nerve cord at the turn of the posterior gonadal arm. We measured the number of puncta per 10 μm and the mean puncta intensity of neurons.

Previous studies assessed the levels of DCVs released via a YFP reporter of NLP-21 neuropeptide expressed under the *unc-129* promoter (Table 7) (198). Using this reporter, we determined the relative amount of DCVs in the dorsal neural cord cholinergic motor neurons. We assessed the release of DCVs by calculating the mean intensity ratio of the axon to coelomocytes, as coelomocytes retrieve the released NLP-21::YFP (198). We crossed the DCVs reporter strain with the *del-4(tm717)* mutant (Table 1) and performed high-magnification confocal microscopy analysis.

Maximum intensity projections were also retrieved for the posterior coelomocytes of the $p_{unc-129}$NLP-21::YFP strain. The images were analyzed using the Volocity Software (Quorum Technologies). We measured the mean fluorescence intensity of cholinergic motor neuron axons from the posterior coelomocytes of NLP-21:: YFP-expressing animals. The number of fluorescent puncta/10 μm was counted, and the ratio of axon to coelomocyte mean fluorescence intensity was calculated. Likewise, the mean fluorescence intensity of puncta and the number of puncta per 10μm were computed in p_{unc-47}GFP::SNB-1 animals.

To monitor neurodegeneration, we cross-fertilized animals overexpressing DEL-4 (p_{del-4}DEL-4::GFP) and *del-4(tm717)* mutants with *C. elegans* Parkinson's and Alzheimer's disease models (Table 1). The UA44 strain was used as the model for Parkinson's disease. It expresses human α-synuclein in dopaminergic neurons, labelled with GFP to monitor degeneration (p_{dat-1}GFP;p_{dat-1}a-synuclein) (200). We assessed neurodegeneration in the Parkinson's disease model at day seven of adulthood. We used the BR5270 strain that pan-neuronally expresses the pro-aggregation F3ΔK280 tau fragment as a tauopathy model (197). To detect dopaminergic neuronal loss, we crossed the BR5270 strain with animals carrying the p_{dat-1}GFP (BZ555) reporter (Table 1). We measured the degenerated neurons in the tauopathy model at day 5 of adulthood.

Neurodegeneration was assessed based on the morphology of the six dopaminergic neurons in the head (4 CEP and 2 ADE) on days 5 and 7 of adulthood. Estimation of dopaminergic neuron degeneration was performed as previously described (201). Neurons were considered degenerated when they exhibited none of the following morphological defects: neuritic blebbing, breaks in neuronal processes or dendrites, absence of neuronal processes, cell body shrinkage, reduced fluorescence, or absence. If one

or more of the above-mentioned phenotypes were observed, then the neuron was considered degenerated. Fifty to sixty animals were examined per biological replicate for each genotype. The number of degenerated neurons per animal is plotted in graphs for each genotype. Scoring was performed by two investigators (DP and MG), and one of them performed it blindly.

Epifluorescence microscopy

Epifluorescence microscopy was performed using a Zeiss Axio Imager Z2 or EVOS™ FV Auto2 Imaging System (Thermo Fisher Scientific). Mounting of animals on slides was achieved with a 13 µl drop of 30 mM Tetramisole (Tetramisole hydrochloride, Sigma-Aldrich) for imaging with a 5x lens or with 2% agarose pads and 15 µl of 30 mM Tetramisole for imaging with the 20x lens (Table 7). Imaging after heat stress and starvation was conducted on day two of adulthood. Animals grown on RNAi plates were imaged on day three or four of adulthood. Animals from the rest of the experiments were imaged on day one of adulthood.

To assess DEL-4 expression levels, we used the DEL-4::GFP translational reporter and measured the intensity of the most brightly fluorescent neuronal cell body in the head of each animal. The HSF-1::GFP expression levels were collected from entire animals and GFP-positive nuclei in the hypodermis. We overlooked the nuclei located above the gut to avoid intestinal autofluorescence. Measurements of SKN-1b/c::GFP were collected from entire animals and ASI neurons. The DAF-16::GFP expression levels were measured from the whole animal and intestinal cells. We measured the intensity levels of DAF-16 in the nuclei and adjacent cytoplasm of gut cells and calculated the nucleus-to-cytoplasm ratio. The intensity of neuronal cell somas in the head of p_{asic-1}SNB-1::SEpHluorin animals was counted to estimate the basal levels of synaptic release from dopaminergic neurons. Super ecliptic phluorin (SEpHluorin) (Tables 1, 5) is a pH-sensitive GFP. When genetically tagged with SNB-1, SEPhluorin is expressed inside synaptic vesicles, where the low pH quenches its fluorescence. Upon vesicle release, SEpHluorin encounters the less acidic environment of the synaptic cleft and recovers its fluorescence, allowing for estimation of synaptic vesicle release. Similarly, the fluorescence intensity from the cell bodies of cholinergic motor neurons was measured in p_{acr-2}SNB-1::SEpHluorin-expressing animals. We acquired visualizations of the ventral cord posterior and anterior to the vulva. To estimate the voltage levels using ASAP1, we counted the intensity from the cell bodies of dopaminergic neurons. Expression levels of phsp-16.2GFP, p_{sod-3}GFP, p_{skn-1}SKN-1::GFP, p_{gst-4}GFP, p_{hsp-4}GFP, $p_{let-858}$GaMP2.0, and p_{aak-}

$_{2}$AAK-2::Tomato were measured from the entire body and expressed as mean pixel intensity in arbitrary units (a.u.).

Imaging with the EVOS™ Imaging System was performed for $p_{acr\text{-}2}$SNB-1::SEpHluorin, the voltage indicator $p_{dat\text{-}1}$ASAP1, and $p_{daf\text{-}16}$DAF-16::GFP in gut nuclei, and the z-stack analysis of the imaging system was used. Analysis of epifluorescence images was performed using Image J 1.48V. For presentation purposes only, the 'straighten' function of ImageJ software was utilized for isolating and straightening animals' heads, bodies, or neuronal processes. The line width in pixels used was 300 for Figures 3, 12A, 7E, 8D, 8E, 9I (gut nuclei), and 12A, 400 for Figure 12D, 80 for Figures 12K and 12L, 220 for 8C, 350 for S6E (gut nuclei), and 600 for S6E (hypodermis nuclei).

Behavioural assays

Basal and enhanced slowing response assays

The procedure followed for the basal slowing response and the enhanced slowing response assays was previously described (32). For the basal slowing response NGM plates were seeded with HB101 (Table 7) in a ring shape, leaving the centre of the plate without food. NGM plates seeded with HB101 bacteria and non-seeded plates were incubated for 16 h (O/N) at 37 °C and allowed to cool to room temperature before use. Synchronized well-fed animals on day 1 of adulthood were washed in a 20 µl drop of M9 solution (3g KH_2PO_4, 6g Na_2HPO_4, 5g NaCl, 1ml 1M $MgSO_4$, H_2O up to 1 litre) twice. Subsequently, the animals were placed in the unseeded region at the centre of the plate with eyelash hair and allowed to recover for 5 min. The bend number of the anterior body region was counted for each active animal during 20sec. The forward and backward movements were included. The procedure was performed in the absence or presence of bacteria. Measurements on the seeded plate were performed only for animals that moved on the bacteria. Ten to fifteen hermaphrodite animals were placed on each assay plate, and 8-15 measurements were taken. Each experiment was repeated at least 3 times. To quantify the locomotory response, we calculated for each experiment the ratio of Δ body bends/20sec. Δ body bends/20sec corresponds to the body bends/20sec of each animal on an unseeded plate minus the body bends/20sec on a plate with food.

We followed the same procedure for the enhanced slowing response, but applied a 30min starvation on an unseeded NGM prior to measuring body bends on the HB101 seeded plates. The same procedure was also followed when HB101 bacteria were replaced with 100µl Sephadex G-200 beads.

Population drop-test assay

We performed the population drop test following the standard protocol described in the WormBook (202) (Table 7), with minor modifications. In brief, 30 animals of each genotype were placed on a 6cm unseeded NGM agar plate and allowed to rest for 5 min. Drops of M13 buffer (30mM Tris-HCl pH 7.0, 100mM NaCl, 10mM KCl) were delivered with a 0.5ml syringe at the animal's tail. Glacial acetic acid was used to prepare M13 solutions with pH values of 6.6, 4.5, and 2.2. Backward movement within 4 seconds of drop delivery was considered a positive avoidance response. Each animal was tested with 2-3 drops with an inter-stimulus interval of at least 2min. We examined well-fed hermaphrodites on day one of adulthood. The avoidance index was calculated as the number of positive responses divided by the total number of trials. An avoidance index of 1 represents complete avoidance to the M13 solution, and an index of 0 represents a total lack of avoidance response.

Chemotaxis to serotonin

We performed chemotaxis to serotonin as previously described with few modifications (203). The POND assay for the sensory systems of C. elegans was applied. In brief, the day before the experiment 9cm assay plates were prepared containing 10ml of the solid phase medium (1M potassium phosphate (pH 6.0), 1mL of 1M CaCl2, 1mL of 1M MgSO4, and 20g agar in 1L of H2O sterilized by autoclaving). The serotonin gradient was formed by placing two agar plugs of 0.5cm diameter excised from a 9cm plate filled with 20ml of the solid phase medium. The two agar plugs were soaked in 5.5µg/ml and placed on each assay plate. The distance between them was 2.5cm and the distance between each plug and the centre of the plate was 3.3cm. On the day of the experiment, plugs were removed and ponds of 0.5cm diameter were formed using a straw. Four ponds were created, two at the site of the plugs and another two at the diametrically opposite site, which constituted the control regions. Ponds were filled with wash buffer solution (25µL of 1M potassium phosphate (pH 6.0), 1mL of 1M CaCl2, 1mL of 1M MgSO4 in 1L of H2O; sterilized by autoclaving). One-day adult animals were collected with wash buffer solution, washed once, and placed at the centre of the plate. Excess of wash buffer was wiped with a paper wipe and the plate was covered with its lead. Plates were sealed with paraffin film (Parafilm; Bemis, IL, USA). Animals were allowed for three hrs at 20^{o}C and ponds were refilled with pond assay buffer every one hr to avoid drying. After the three hrs had passed images were taken and the number of animals in each pond was counted. The chemotaxis index (C.I.) was calculated as follows:

[the number of animals trapped in the ponds at the test side (where the serotonin-soaked plugs were placed)-the number of animals trapped in the ponds on the control side]/the number of animals trapped in all ponds.

Social Behaviour

Social feeding behavior was quantified as described previously, except that 80 animals were used on bacterial lawns of 6cm NGM (204). Bordering and clumping behaviors were quantitated simultaneously. NGM plates containing 2.1% agar were seeded 1 day before the assay with 200µl of *E. coli* OP50 in LB medium. Approximately 80 well-fed adult worms from uncrowded plates were transfered onto freshly seeded NGM and left at 20^{o}C for 3hr. After 3 hr, behavior was measured by calculating the fraction of animals that were in contact with two or more clumping other animals along at least 50% of their body length. At the same time, bordering behavior was measured by calculating the fraction of animals that resided within 2 mm of the edge of the bacterial lawn.

Egg laying assay

L4-stage animals were picked onto 2cm NGM with plentiful food seeded the night before with 70µL of *E. coli* OP50 and grown under standard conditions at 20^{o}C for 24hrs. For each genotype and condition, we assessed three animals. Every 24hrs, worms were transferred to a new 2cm plate, and the number of eggs laid by each animal was counted. The plates after egg-laying were placed at 4^{o}C to avoid hatching. We counted brood size for four days of adulthood. We used Prism 6 (GraphPad) for statistical analysis and to plot data.

Spontaneous food leaving assay on *E. coli* OP50

We assessed food leaving behavior as previously described (205) with few modifications. For measuring food leaving, one-day adults were added on the food lawn of freshly prepared NGM. The number of worms found off the food was recorded after 30 minutes. We then compared mutant and overexpressing nematodes with wild-type animals tested in parallel. The spontaneous food-leaving behaviour was measured upon control conditions and heat stress. We stressed one-day adult animals at 37^{o}C for 35min and then allowed them to recover for 35min at 20^{o}C. On food index was calculated as the number of worms on food minus the number of worms off food divided by the total number of worms. For data

analysis, Two-way ANOVA analysis was performed to compare all mutants with wild-type (N2) control animals.

Radial thermotaxis (Ttx) assay

For the thermotaxis assay, we followed the standard procedure, as previously described (206). Before the assay, remove lids of the Ttx plates and dry the plates for about 30 min at room temperature. Use 9cm NGM plates. Mark the center and a point 1.5 cm from the edge on the bottom of the plate. Take the vials containing frozen glacial acetic acid out of the cold room and leave the vials for 10min at room temperature (25°C) to allow the acetic acid to start to melt. The melting point of glacial acetic acid is 16.7°C. Place the vial at the center of the Ttx plate. Leave the plates for ~10-15min at room temperature to form a stable radial thermal gradient on the surface of the Ttx plate (Figure 17D). The thermal gradient is maintained for 1hr on the plate with the glacial acetic acid vial. Replace the vials when half the glacial acid has melt. Wash the animals twice with M9 and place them at the marked point near the edge of the Ttx plate. Leave the plates for 50-60 min at room temperature for the animals to migrate, and then place the plate at 4^{o}C to immobilize animals until they are measured. Calculate the percent of nematodes in each thermal zone (17^{o}C, 20^{o}C, 25^{o}C). One-day adults were used.

Conditioning to isoamyl alcohol

We followed standard procedures for measuring conditioning to isoamyl alcohol (IA) (207). *Ad libitum*-fed adult Day 1 animals were washed off an NGM plate with 1.5 mL M9 buffer. Animals were washed with M9 at least twice until they were free from bacteria. Then, they were transferred to a conditioning plate using a pipette. Excess buffer was dried with a small piece of Kimwipe under a stereoscope. For naïve plates (no OP50, no IA), plates were sealed with parafilm after transferring the animals. For IA plates (no OP50, plus IA), a drop of pure IA (5 μL) was placed on the internal surface of the IA plate's lid, spread around evenly, and plates were then sealed with parafilm immediately. Animals were incubated at 20°C for 90 min. Chemotaxis assay plates were marked to define the points for A, B, and x (A-B=6.5cm, A-x=B-x=4.5cm), and the designated name of each genotype (Figure 17F). 15min before the assay, sodium azide (100mM, 10μL) was added at both point A and point B. Animals were then collected with M9 from the conditioning plates and transferred to point x on the matched assay plates. Excess buffer was dried using a small piece of Kimwipe. Subsequently, a square piece of parafilm (size of 0.5 × 0.5 cm) was placed on spot A on the agar and 3μL of diluted IA (ratio 1:100 in water) was

added on top of the parafilm. Plates were sealed with parafilm and incubated at 20°C for 2h. After 2.5hrs, the number of worms at each point was counted under the stereoscope. Chemotaxis index was calculated as follows (A-B)/(A+B). One-day adult worms were utilized. 300-500 nematodes were used in each experiment.

Chemorepulsion assay to Cu^{+2}

We performed chemosensation to Cu^{2+} as previously described with few modifications (91). Briefly, 150-200 animals were washed free of bacteria with M9 solution and placed on one side of a Cu^{2+} (~20μl 100mM $CuSO_4$) line barrier on a 9 cm NGM assay plate. Sodium azide (NaN_3) was spotted on the other side to immobilize worms. After 60min, the number of animals on each side was scored. The Cu^{2+} avoidance index represents the fraction of animals that did not cross the Cu^{2+} line minus those that crossed it towards the total number of animals (Figure 17H). Data from at least three independent experiments were used for quantification analysis. We used one-day adults. For induction of oxidative stress, animals were treated for 4hrs prior to the chemorepulsion assay with 8mM Paraquat (see also oxidative stress in Stress assays section). For heat stress induction, animals were incubated on NGM plates at 37ºC for 35min and afterward, they were allowed to recover for 35min at 20ºC, prior to the cooper avoidance assay.

Chemotaxis to NaCl

On day one of adulthood, animals were washed thrice free from bacteria with M9 in 1.5ml tubes. Subsequently, they were transferred on assay plates and excess of M9 was collected with a Kimwipe. For generation of assay plates, two nematode growth mediums were prepared, one with 50mM NaCl concentration, which is the standard cultivation concentration of NaCl. The second medium had a concentration of 1M NaCl, which constitutes a repulsive concentration. Mediums were poured in 9 cm plates. After medium has solidified in the plates, it was cut along the plate's diameter. Assay plates were generated by replacing the one half of 50mM with one half of 1M in the 9cm plate. The gap between the two halves was filled with medium (NaCl concentration 50mM) to avoid animal-losing in the gap. 70-100 animals were used in each experiment.

Conditioning to NaCl

Chemotaxis assays were based on those described by Bargmann and colleagues (45, 50) with some modifications. In brief, 20 gravid adults were transferred to a seeded 6cm plate and allowed to lay eggs

at 20°C for 7hrs. Three days later, the F_1 progeny grew to young one-day adults under well-fed conditions. Plates on which the bacterial lawn had been exhausted at this stage were discarded. The animals were washed off the plates with M9 buffer (3mg/ml KH_2PO_4, 6mg/ml Na_2HPO_4, 1mM $MgSO_4$, 5mg/ml NaCl) and transferred to a 1.5ml tube. The animals were washed three times by allowing the adults to fall through the wash buffer by gravity and replacing the supernatant. For the naive chemotaxis assay, washed animals were placed directly onto chemotaxis plates, and excess fluid was absorbed with a Kimwipe. For conditioning, washed animals were placed on a conditioning unseeded NGM plate, and excess fluid was absorbed with a Kimwipe. After incubation at 20°C for 4hrs under, the animals were collected again with M9 buffer and chemotaxis was assayed. Assay plates contained 5mmol/l potassium phosphate, pH6.0, 1mmol/l $CaCl_2$, 1mmol/l $MgSO_4$ and 20g/l agar. For generating a NaCl inclination, an agar plug was excised from a NaCl plate (made up as above but with the addition of 100mmol/l NaCl) with a cork borer and placed off-centre on the surface of an assay plate, which was then left overnight (14–24hrs). Shortly before the chemotaxis assay, the NaCl plug was removed, and 1µl of 0.5mol/l sodium azide was spotted in the same position to anesthetize the animals at the center of the gradient. As a control, sodium azide was also spotted at a position approximately 4 cm away from the center of the NaCl gradient. Approximately 100 animals (either naive or conditioned) were then placed equidistant (approximately 3cm) from these two spots and left to move freely on the assay plate for 60min at 20°C. The assay plates were then chilled to 4°C, and the number of worms around each spot was counted. The chemotaxis index (CI) was calculated as CI=(A−B)/(A+B), where A is the number of animals within 1.5cm of the centre of the NaCl gradient, and B is the number within 1.5cm of the control spot. Assays were typically performed in triplicate. The number of independent experiments performed is indicated in the figure legends.

Chemotaxis to stable linear gradient of NaCl

The assay was performed as previously described (208) with few modifications. A linear gradient of NaCl was generated on a 25cm x 25cm plate. To generate the gradient, a 25cm x 25cm Petri plate, elevated at one side with a pencil, was half filled with melted agar of 50mM NaCl concentration to create a triangle wedge. Once it solidified, the plate was laid flat and the other half of the plate was filled with melted agar of 0mM NaCl concentration. The generated gradient expands from 0mM until 50mM of NaCl. Behavioural assays were performed 18–32hrs after the gradients were established. In each assay, 250-300 one-day adult worms were washed in NGM buffer (identical ingredients as NGM plates

but without agar) for about 1 min before starting in the NaCl gradient. Animals were placed in the middle of the gradient at ~25mM, excess NGM buffer was removed with a Kimwipe, and were allowed for 1hr at 20^{o}C to chemotax. Animals were cultivated on NGM of 50mM NaCl concentration. For the induction of heat stress prior to the assay animals were incubated for 35 min at 37^{o}C, and then were transferred with NGM buffer on the assay plates. There was not given time for recovery. The excess buffer was removed with a Kimwipe. For the induction of oxidative stress animals were incubated on OP50-seeded NGM with Paraquat applied at a concentration of 10mM for 4.5hrs. Paraquat was applied before the assay and was allowed to dry before adding the animals to the plate. Subsequently, animals were collected with NGM buffer and transferred to the assay plates. Long-term starvation was achieved by transferring with a platinum worm-picker one-day adults on unseeded NGM plates and allowing them to starve for 24hrs. Animals were then transferred to the assay plates with NGM buffer. In this case, nematodes associated starvation with 50mM NaCl.

DEL-4 expression and TEVC on Xenopus oocytes

cDNA generation

C. elegans cDNA was obtained from N2 wild-type and purified using the Invitrogen™ SuperScript™ III First-Strand Synthesis System (Table 7). The cDNA inserts were subcloned into the KSM vector under the control of the T7 promoter containing the 3' and 5' untranslated regions (UTRs) of the Xenopus beta-globin gene and the poly(A) tail.

Primer generation

The forward primer 5′-AGATCTGGTTACCACTAAACCAGCC-3′ and reverse primer 5′-TGCAGGAATTCGATATCAAGCTTATCGATACC-3′ were used to amplify the KSM vector. Based on the sequence on wormbase.org, the forward primer 5′-CTTGATATCGAATTCCTGCAATGGGTGTATTTTGGACCGGC-3′ and the reverse primer 5′-GTTTAGTGGTAACCAGATCTTCAATCATTAGAATGAGGCTTTGGTGGAAC-3′ were used for amplification of the *del-4* cDNA (based on the sequence in wormbase.org). To generate *del-4(tm717)* deletions, we used the NEB Q5® Site-Directed Mutagenesis Kit (Table 7). Plasmids generated were pEK230 (*del-4* cDNA in the KSM vector (209) and pEK238 (*del-4(tm717)* cDNA in the KSM vector). The NEBuilder HiFi DNA Assembly Reaction Protocol was used to assemble the KSM vector and

cDNA inserts using NEBuilder® HiFi DNA Assembly Master Mix (Table 7) and a vector:insert ratio of 1:2.

mRNA synthesis and microinjection

The linear plasmid was used as the template for *in vitro* RNA synthesis from the T7 promoter using the mMessage T7 kit (Ambion #AM1344) (Table 7) to produce 5'-capped RNA (Table 7). Oocytes were injected with 25nl of RNA solution at a total concentration of approximately 500ng/µl using the Roboinject (MultiChannel Systems). Oocytes were kept at 16°C in 1X ND96 prior to TEVC.

Two-electrode voltage clamp (TEVC)

TVEC was performed 1-2 days post-injection at room temperature using the Robocyte2 (MultiChannel Systems) as previously described (209, 210). *Xenopus* oocytes were clamped at −60 mV using ready-to-use Measuring Heads from MultiChannel Systems filled with 3M KCl. All channels were tested using the Robocyte2 (MultiChannel Systems). Since millimolar concentrations of Ca^{2+} and other divalent ions except Mg^{2+} can block ASIC currents (211), Ca^{2+}-free buffers were used for substitution experiments of monovalent cations adapted from a previous protocol (212): 96mM XCl, 1mM $MgCl_2$, 5mM HEPES, pH adjusted to 7.4 with XOH, where X was Na^+, K^+ or Li^+, respectively. We used a previous protocol (213) to test ion permeability for Ca^{2+}, by replacing Na^+ with equimolar Ca^{2+}. If necessary, D-Glucose was used to adjust the osmolarity. Osmolarity was checked and confirmed to be within an error of 210 m(214). To test pH sensitivity, 1X ND96 solution was used; for solutions with a pH of 5 or lower, MES was used instead of HEPES and adjusted with HCl. I-V relationships for ion selectivity and proton conductance were calculated by subtracting the background leak current in the presence of 500µM amiloride from the current observed in the absence of amiloride to get the actual current. Actual current I-V curves for each oocyte were fitted to a linear regression line, and the x-intercept was compared between solutions to calculate an average reversal potential (E_{rev}). The reversal potential shift (ΔE_{rev}) was calculated for each oocyte when shifting between pH solutions or from a NaCl to a KCl, LiCl, or $CaCl_2$ solution. To test the responses to pH, channel-expressing *Xenopus* oocytes were perfused with 1X ND96 (using HEPES for buffering pH above 5.5, and MES for pH below 5). The pH was adjusted with HCl and ranged from pH 7.4 (neutral pH of the ND96 solution) to pH 3.8 or pH 4. Background currents measured at pH 7.4 were subtracted from those measured during the activation of the channels. For

analysis, currents were normalized to maximal currents (I/I_{max}) and best fitted using Hill's equation (variable slope).

DiI staining

To identify the DEL-4 subcellular localization, we labelled amphid and phasmid neurons with the lipophilic carbocyanine tracer DiI (dioctadecyl tetramethylindodicarbocyanine-disulphonic acid, Invitrogen) (Table 7), prepared as described earlier (215). DiI stains the membranes of amphids, phasmids, and chemosensory neurons with nerve endings exposed to the environment. In brief, one-day-old adult hermaphrodite animals were washed twice with 200µl M9 free of bacteria and incubated in 200µl 10µg/ml DiI diluted in M9. Animals were rotated in a 200µl tube with DiI for 2-3 hours, washed twice with M9, and then allowed to recover and de-stain for an hour on an OP50-seeded NGM plate before imaging.

mRFP bacteria feeding assay

In this assay well-fed animals on Day one of adulthood were transferred with a platinum worm-picker on NGM plates seeded with OP50 bacteria expressing Red Fluorescent Protein (RFP). *E. coli* OP50 expressing RFP was provided by the *C. elegans* Ageing Laboratory at the University College London. *E.coli* OP50 was transformed with plasmid *pRZT3::dsRED* to construct RFP-expressing *E. coli* OP50. The plasmid also contains genes for tetracycline resistance. As a result, LB RFP *E. coli* OP50 was grown in LB containing 10µg/ml of tetracycline overnight at 37°C on a shaker. Nematodes were fed with RFP expressing bacteria for 30min, then collected with M9 and washed free from bacteria, placed on a glass slide with 15µl levamisole to become anesthetized, covered with a coverslip and observed under an epifluorescence microscope.

Stress assays

Heat Stress (HS)

To assess DEL-4 expression levels following heat stress, 1-day adult animals expressing DEL-4::GFP were treated for 2 hrs at 37ºC. Animals were allowed to recover O/N at 20ºC on NGM plates seeded with OP50 and then imaged on day 2 of adulthood. To assess the effect of heat stress on the voltage of dopaminergic neurons, which was measured with ASAP1, 2-day adult hermaphrodite animals were stressed for one hour at 37°C on OP50-seeded plates and then imaged immediately. For inducing heat

stress prior to food-leaving and cooper-avoidance assays one-day adult animals were placed for 35min at 37^{o}C and then allowed to recover for 35min at 20^{o}C. For inducing heat stress prior to chemotaxis assay to linear NaCl gradient, one-day adult animals were incubated for 35min at 37^{o}C, then were collected and washed with NGM buffer, and transferred free from bacteria on assay plates, without recovery time.

Long-term Starvation (LTSt)

For the starvation assay, one-day-old adult hermaphrodite animals were placed with a platinum pick on unseeded NGM plates. They were allowed to starve for 24 hrs and then imaged on day two of adulthood. We followed the same treatment for inducing long-term starvation prior to chemotaxis assay. In this case, animals were collected after starvation with NGM buffer and transferred on the assay plates.

Oxidative stress (OS)

To induce oxidative stress, Paraquat (N, N'-dimethyl-4,4'-bipyridinium dichloride, Sigma-Aldrich) (Table 7) was added on top of OP50-seeded NGM. Paraquat was added to a final concentration of 8 mM diluted in water. Water was placed on the control plates. Plates were allowed to absorb the drug, and animals at the L4 stage were placed on plates. Animals were stressed O/N and then imaged on day one of adulthood. For treatment prior to the Cooper-avoidance assay, one-day adults were treated for 4hrs on an NGM with 8mM Paraquat. For inducing oxidative stress before the chemotaxis assay to a linear gradient of NaCl, animals were incubated on seeded NGM with 10mM Paraquat for 4.5hrs. In all cases, before adding Paraquat to the NGM plate, bacteria were UV-killed for 10min.

ER stress (ERS)

To induce ER stress, tunicamycin (Sigma-Aldrich) (Table 7) was plated on OP50-seeded NGM. Tunicamycin was added to a final concentration of 2.5μg/ml in M9. M9 was placed on control plates. Plates were allowed to absorb the drug or M9, and animals at the L4 stage were placed in the assay plates. Animals were stressed O/N and then imaged on day one of adulthood.

Acidic stress (AS)

To elicit low-pH stress, we used an M13 solution adjusted with CH3COOH at the appropriate pH. Before treatment, one washing step was performed in a 20μl drop of M13 pH6.6. For the measurement of DEL-4 expression levels upon acidic stress, one-day adults were incubated for 1 hr within a 20μl M13

drop of pH6.6 (control) or pH3.5 (at low pH stress). To estimate the ASAP1 levels after acidic stress, 2-day adult animals were incubated for 15 min in a 20µl M13 drop of pH 6.6 (control) or pH4.5 (low pH stress). After treatment, the animals were incubated in a 20µl drop of M13 solution pH6.6 to recover GFP fluorescence that quenches due to the pH sensitivity of GFP.

Survival assays

Survival assay after heat shock

For thermotolerance evaluation, 1-day adult animals were placed on OP50-seeded NGM plates and exposed to 37 ºC for 2.5 hours. Animals were allowed to recover overnight at 20ºC, and from the following day, death events were monitored per day. Animals were scored as dead when they failed to respond to prodding with the platinum wire. Animals were transferred to new plates once every two days to avoid mixing with the progeny (216).

Starvation Survival assay

To analyse survival during starvation, we followed the procedure described previously (217), with a few modifications. After synchronization with the bleaching solution, ~3.500 eggs were incubated in 1.5ml BSA-coated tubes filled with sterile M9 solution on a rotating carousel (Stuart Scientific SB1 Blood Test Tube Rotator) at 20ºC. Twenty-four hours after egg preparation and every second or third day, 20µl was collected from each tube, plated on OP50-seeded NGM and, allowed to grow at 20ºC for three days. Three samples (20µl) were collected from each strain, and the average was calculated. We then counted the animals that reached the L4 stage or young adulthood. Day 1 was considered the day after egg preparation and was used as a control and denominator to calculate the percentage of animals that recovered.

Pharmacological assays

Acute aldicarb resistance assay

Aldicarb is a cholinesterase inhibitor that causes paralysis due to acetylcholine (ACh) accumulation at the synaptic cleft. We used aldicarb (100mM stock in 70% ethanol; Sigma-Aldrich) (Table 7), as proposed by Mahoney et al. (218). Animals were collected and washed twice in M9. We differentiated the procedure by placing one-day adult animals in a 15µl drop of 10mM aldicarb in M9 instead of using NGM plates with aldicarb. The animals were monitored to identify the moment at which they stopped

moving. Seven animals were used per condition in each experiment, with a total of six biological replicates.

Levamisole resistance assay

Levamisole is a nicotinic receptor agonist that paralyzes animals through continuous muscle stimulation. For the levamisole assay, we used 400μM concentration in M9. Animals were collected with M9 and washed twice. Subsequently, they were placed in a 20μl drop of 400μM levamisole (Table 7). Locomotion was evaluated by the number of animals not moving in the levamisole drop reported every 5 min until all animals were paralyzed.

Dopamine resistance assay

To monitor dopamine-induced paralysis, 30-40 animals, of the selected genotypes at day one of adulthood, were collected with M9 and washed twice. Subsequently, we placed the animals in a 20μl drop of 40mM dopamine (Dopamine hydrochloride, Sigma-Aldrich) (Table 7), diluted with M9. The number of moving animals was recorded every 5 min of exposure until all animals were paralyzed. We always used freshly prepared dopamine to avoid oxidization.

QUANTIFICATION AND STATISTICAL ANALYSIS

Sample sizes were not predetermined using statistical methods. Statistical analysis and graphical illustrations were performed using the Prism software package (GraphPad Software Inc., San Diego, CA, USA). The results are presented as XY graphs, with error bars representing the standard error of the mean (SEM). Two-way analysis of variance (TWO-WAY ANOVA) was performed for most of the experiments to compare the mean values and evaluate statistical significance. TWO-WAY ANOVA is selected where the mean values of independent biological replicates with pre-calculated SEM are represented in the graph. In the other cases, One-way ANOVA is used. The post-hoc analysis to correct for multiple comparisons was performed using Tukey's multiple comparisons test or the ordinary Two-way ANOVA test for the TWO-WAY ANOVA analysis, while the one-way Tukey's test was used in the One-way ANOVA. For survival analysis, the Log-rank (Mantel-Cox) test was used to evaluate statistical significance. All experiments were repeated at least thrice. The number of biological replicates, the sample sizes, the specific type of ANOVA, and any further statistical information related

to each graph can be found in the Figure legends. The P-values in the graphs are indicated with the following symbols: ns p=0.1234, *p=0.0332, **p=0.0021, ***p=0.0002, ****p<0.0001.

IX. Results

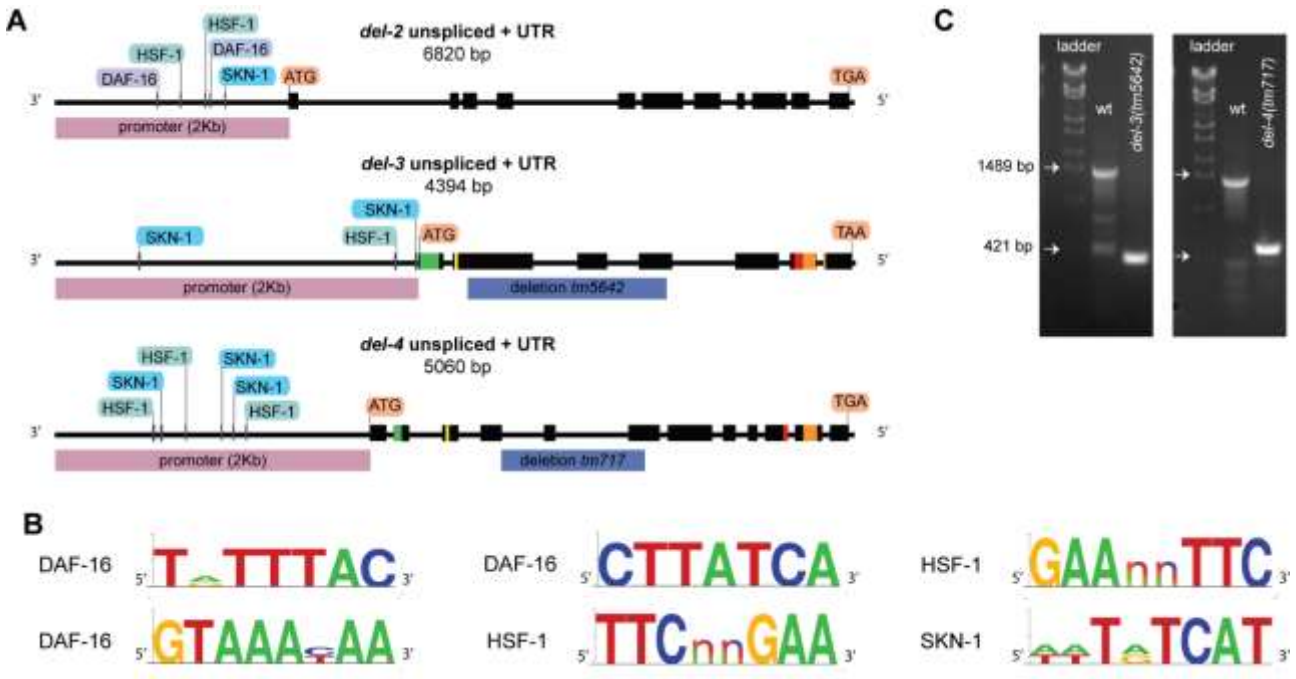

Figure 2. Genomic organization and gene structures of *C. elegans del-2, del-3,* and *del-4* genes.

(A) Intron-exon organization, different isoforms, and regions missing in mutants are annotated. Genetic loci are retrieved from WormBase. Genetic loci of *del-2*, *del-3* and *del-4* genes. Black boxes, starting from ATG until the stop codon, indicate exons. Upstream to ATG are designated 2 Kb of the promoter region (pink box) and binding sites of DAF-16, HSF-1, and SKN-1 transcription factors (cyan and purple boxes). Sites of deletions identified in *del-3(tm5642)* and *del-4(tm717)* mutants are shown in blue boxes below *del-3* and *del-4* open reading frames. Deletion sites of both genes lead to the development of premature stop codons, immediately after the missing sequence. The designation of coding regions that correspond to protein domains is seen in green, yellow, red, and orange. The green region denotes the first transmembrane domain, the yellow box denotes the post-M1 domain, the red region corresponds to the pre-M2 domain and the orange box denotes the second transmembrane domain. DNA sequences and exon/intron annotation are retrieved from WormBase (https://wormbase.org//). Transmembrane domains were estimated with the bioinformatic tool Phobius (https://phobius.sbc.su.se/). The annotation of the *del-2* sequence corresponds to isoform 1. Transcription factor binding sites in the promoter regions correspond only to the forward direction. Editing and annotation of DNA sequences were performed with the software products SnapGene and Vector NTI.

(B) DNA sequences that have been recognized as SKN-1, DAF-16, and HSF-1 binding sites (An and Blackwell, 2003; Murphy et al., 2003; Trinklein et al., 2004). For the generation of DNA sequence logos, the WEBLOGO application was exploited (https://weblogo.berkeley.edu/). Letter n stands for any nucleotide.

Figure 2. Continued.

(C) Images of PCR reactions for *del-3* (left) and *del-4* (right) run on a 1% w/v agarose gel, stained with ethidium bromide. Genomic DNAs were isolated from wild type, *del-3(tm5642)*, and *del-4(tm717)* mutant animals. These DNAs were used as substrates for PCR. Primers flanking DNA regions of *del-3* or *del-4* mutations were utilized for amplification of genomic DNA. Expected band size: (left) wt 1401 bp, *del-3(tm5642)* 368 bp and (right) wt 1404 bp, *del-4(tm717)* 498 bp. The ladder was created from λ phage DNA digested with StyI.

DEL-2, DEL-3 and DEL-4 share a contiguous neuronal expression pattern

The Degenerin ENaC/DEG subfamily of *C. elegans* comprises approximately 30 members. We focused on the three members DEL-2, DEL-3, and DEL-4 (Figure 2A) previously identified in serial analysis of gene expression to localize in ASE neurons, the primary set of gustatory neurons of *C. elegans* (208). Since we sought to investigate stress-regulated channels, we screened the promoter regions of *del-2, del-3,* and *del-4* genes for binding sites of transcription factors implicated in stress

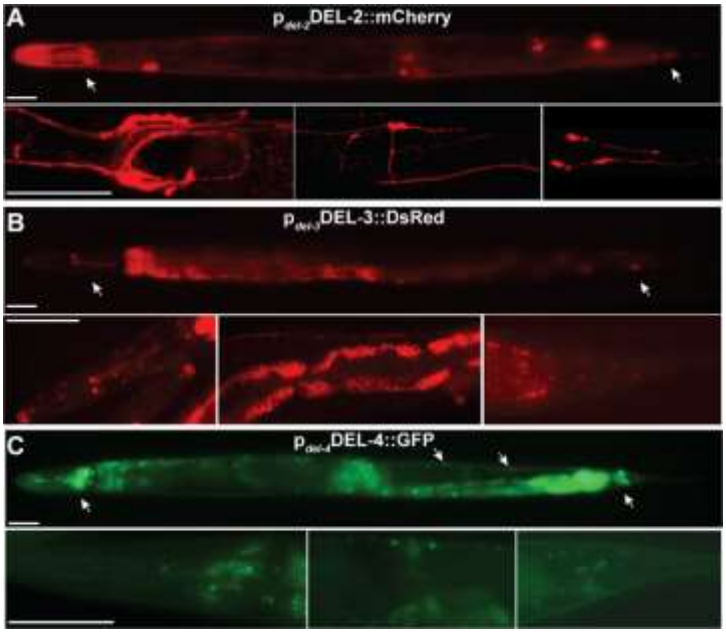

Figure 3. Expression pattern of DEL-2, DEL-3 and DEL-4

All three DELs are expressed in neuronal cells in the head and tail regions of *C. elegans*. DEL-4 is additionally expressed in a series of neurons that extend in a row next to each other along *C. elegans* body. Epifluorescence images of *del-2, del-3* and *del-4* translational reporters. Arrows indicate sites of expression. Lens 20x. Images from the head, midbody and tail region were captured and put together with Adobe Photoshop CS5 to illustrate the entire animal. Left is anterior. Scale bar 50μm. (A) DEL-2 expression pattern. DEL-2 localizes in head (A) tail (B) and midbody (C) neurons. A diffuse pattern is observed in the cell bodies and a more punctuate in the axons and dendrites. The expression pattern was monitored in worms expressing the pdel-2DEL-21-27::DsRED construct. Confocal images. (B) DEL-3 expression pattern. DEL-3 localizes in head (A), tail (B), motor (C) and midbody neurons (D) in pdel-3DEL-3::DsRED worms. Epifluorescence images. (C) DEL-4 expression pattern. DEL-4 localizes in head (1), tail (5) and midbody neurons (2-4) in pdel-4DEL-4::GFP worms. In neuronal processes DEL-4 displays a punctuate pattern. Epifluorescence images.

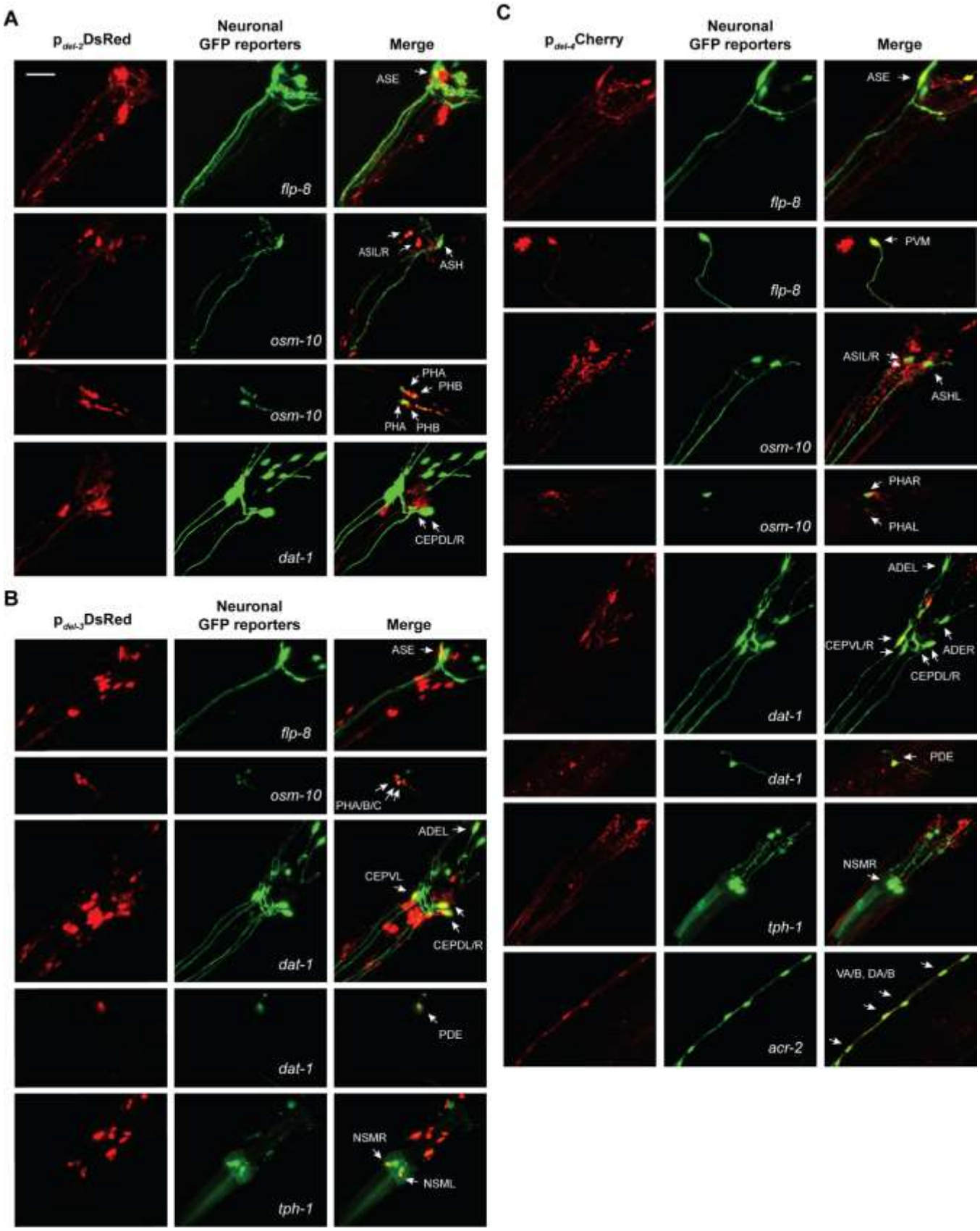
A
p_{dat-2}DsRed
Neuronal GFP reporters
Merge
ASE
flp-8
ASIL/R
ASH
osm-10
PHA
PHB
PHA
PHB
osm-10
CEPDL/R
dat-1
B
p_{dat-3}DsRed
Neuronal GFP reporters
Merge
ASE
flp-8
PHA/B/C
osm-10
ADEL
CEPVL
CEPDL/R
dat-1
PDE
dat-1
NSMR
NSML
tph-1
C
p_{dat-4}Cherry
Neuronal GFP reporters
Merge
ASE
flp-8
PVM
flp-8
ASIL/R
ASHL
osm-10
PHAR
PHAL
osm-10
ADEL
CEPVL/R
ADER
CEPDL/R
dat-1
PDE
dat-1
NSMR
tph-1
VA/B, DA/B
acr-2

Figure 4. Neuronal expression of DEL-2, DEL-3 and DEL-4.

(A) Expression of DEL-2 in chemosensory neurons ASE, ASH, ASI, PHA, and PHB and CEPDL/R set of dopaminergic neurons in the head.

(B) Expression of DEL-3 in chemosensory neurons ASE, PHA, PHB, and PHC, in CEPDL/R, CEPVL, ADEL, and PDE dopaminergic neurons in the head and midbody, and the serotonergic neurons NSMR/L.

(C) Identification of DEL-4 expression in chemosensory neurons ASE, ASI, ASH, and PHA, in the mechanosensory neuron PVM, in all 6 dopaminergic neurons CEPDL/R, CEPVL/R, ADEL/R in the head and PDE in the midbody, in the serotonergic neuron NSMR and cholinergic motor neurons VA/B and DA/B.

(A-C) Confocal images at 40x lens (maximum intensity projections) of strains that came up by crossing *del-2*, *del-3*, or *del-4* transcriptional reporters (seen in red – left column) with the respective neuronal reporters (seen in green – middle column). (left columns) *del-2*, *del-3* and *del-4* promoters drive the expression of mCherry or DsRED in the nervous system. (middle columns) Transcriptional GFP neuronal reporters are seen in green. Promoters of *flp-8* and *osm-10* drive expression in sensory neurons, ASE, URX, PVM, and ASH, ASI, PHA, and PHB, respectively. The promoter of *dat-1* drives expression of GFP in dopaminergic neurons CEPD, CEPV, ADE, PDE, *tph-1* promoter in the serotonergic neurons NSM, ADF and *acr-2* promoter in the cholinergic motor neurons VA/B, DA/B. (right columns) The right column of each panel corresponds to merged images. Merged images of z-stacks were utilized to assess colocalization (see also Figure S2). One-day adult animals**.** Arrows indicate neuronal cell somas where mCherry or DsRED is co-expressed with GFP (left is anterior). Scale bar 20 μM.

responses. We searched for binding sites for DAF-16, SKN-1, and HSF-1, the FOXO, NRF2, and HSF1 mammalian homologues in the two kb region upstream of the start codon of each del gene (Figure 2B) (219-221). We disclosed that the *del-2* promoter region carries DAF-16, SKN-1, and HSF-1 binding sites, whilst the *del-3* and *del-4* promoter regions contain HSF-1 and SKN-1 binding sites (Figure 2A, B). These data suggested the proteins DEL-2, DEL-3, and DEL-4 as potent candidates for studying sensory integration upon stress.

We generated the transcriptional reporters of these three degenerins to determine their expression pattern. All reporters bear the promoter region 2Kb upstream of the coding region and the first exon of the coding sequence tagged with a fluorescent reporter. Epifluorescent imaging revealed that all three DELs localize in the head, midbody, and tail neurons (Figure 3). To specify the neurons that express DEL-2, DEL-3, and DEL-4, we crossed their transcriptional reporters with several neuron-specific fluorescent markers (Tables 1, 4, 5). We employed neuronal reporters for sensory neurons (p_{osm-10}GFP – ASH, ASI, PHA, PHB and p_{flp-8}GFP – ASE, URX, PVM), for dopaminergic neurons (p_{dat-1}GFP - CEPD, CEPV, ADE, PDE), for serotonergic neurons (p_{tph-1}GFP – NSM, ADF) and cholinergic motor neurons (p_{acr-2}GFP - VA/B, DA/B).

We first examined and verified the expression of these three channels in ASE neurons, as previously described (222), exploiting the transcriptional reporter of FLP-8 (Figure 4). Further analysis revealed that DEL-2 localizes in the amphids ASH and ASI (apart from ASE), the phasmids PHA and PHB, and the dopaminergic neurons CEPDL/R (Figure 4A). DEL-3 is present in the chemosensory neurons ASE, PHA, PHB, and PHC, in most dopaminergic neurons (CEPDL/R, CEPVL, ADEL, PDE),

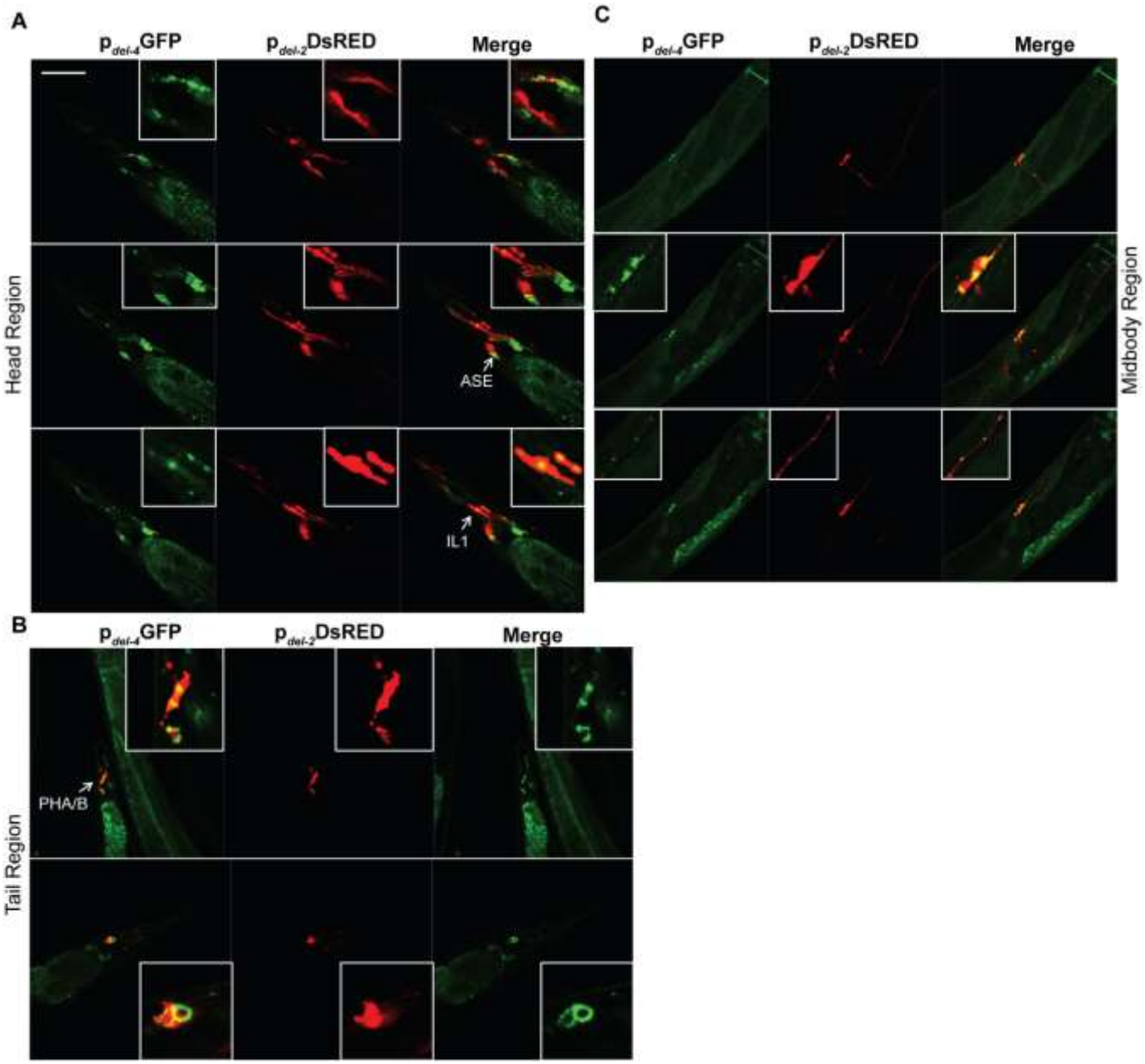

Figure 5. Colocalization experiment of DEL-2 and DEL-4. Confocal images of worms expressing p_{del-2}DEL-21-27::DsRED (seen in red) and p_{del-4}DEL-41-36::GFP (seen in green). DEL-2 and DEL-4 seem to colocalize in six neurons throughout the body.

and the serotonergic neurons NSML/R (Figure 4B). DEL-4 displays a broader expression pattern. It localizes in the chemosensory neurons ASE, ASI, ASH, and PHA, the serotonergic neuron NSMR, and all dopaminergic neurons (CEPDL/R, CEPVL/R, ADEL/R, PDE) (Figure 4C). Moreover, DEL-4 subsists in the cholinergic motor neurons VA/B, DA/B, and the mechanosensory PVM neurons (Figure

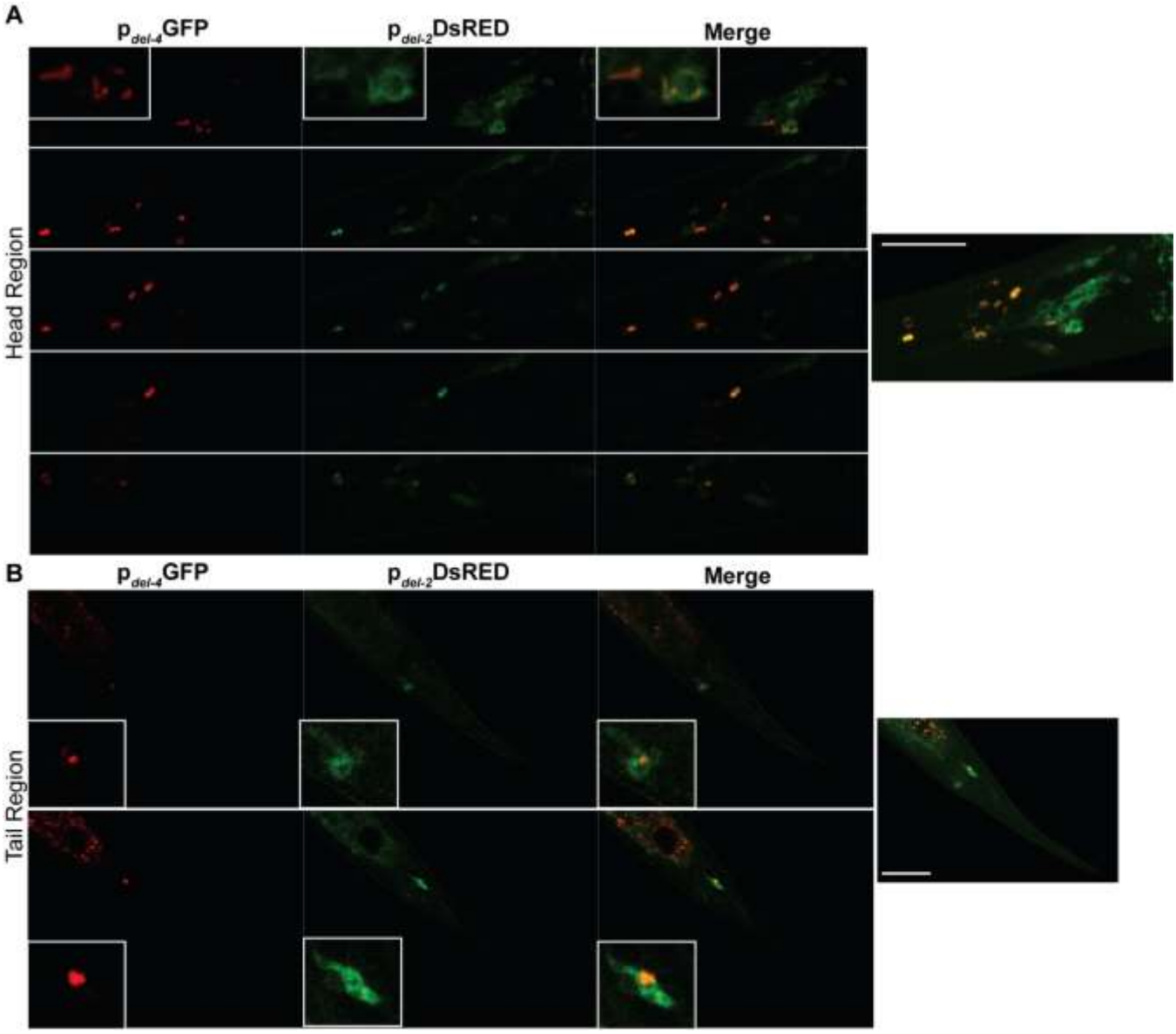

Figure 6. Colocalization experiment of DEL-3 and DEL-4. Confocal images of worms expressing p_{del-3}DEL-3::DsRED (seen in red) and p_{del-4}DEL-4::GFP (seen in green). DEL-3 and DEL-4 seem to colocalize in nine neurons in the head (A) and two in the tail (B).

4C). Therefore, DEL-2, DEL-3, and DEL-4 obtain a neuronal localization pattern, which, in the case of DEL-4, expands from sensory to motor neurons. Subsequently, we co-expressed the transcriptional reporter of DEL-4 with DEL-2 or DEL-3 reporters to verify possible colocalization and speculate on the interaction between those Degenerins. We performed genetic crossing between animals expressing the construct p_{del-4}DEL-4_{1-36}::GFP and others expressing the p_{del-2}DEL-2_{1-27}::DsRED. Nematodes expressing the constructs p_{del-4}DEL-4::GFP and p_{del-3}DEL-3::DsRED were generated by co-bombarting the two transgenes. We identified that the three degenerins colocalize in a few but not all of the neurons in which they are expressed. DEL-4 colocalizes with DEL-2 in two neurons in the head, ASE probably, two neurons in the tail, which could be the PHA or PHB, and a couple of neurons at the midbody close to the vulva (Figure 5). DEL-4 and DEL-3 seem to co-express in around eight neurons in the head and a couple of neurons in the tail (Figure 6). According to the above localization findings, these three degenerins could interact in some neurons to create a sodium channel.

DEL-4 down-regulation simulates a stress-like state

To investigate the possible effects of stress on the DEL-4 ion channel, we measured its expression under various types of stress (Figure 7). We exploited the translational reporter of DEL-4 (p_{del-4}DEL-4::GFP) and counted its expression levels from the neuronal cell somas that displayed the most robust expression in the head. Heat stress and long-term starvation reduced DEL-4 levels (Figure 7A and E). In contrast, oxidative stress, endoplasmic reticulum (ER), and acidic pH stress did not affect them (Figure 7B-E). These findings suggest that heat stress and long-term starvation can modulate DEL-4-mediated signalling.

HSF-1 is the homologue of the mammalian HSF1 and the master regulator of heat shock response (219-221). Heat stress response translocates activated HSF-1 to the nucleus, where it transcribes heat shock proteins (HSPs), chaperones that promote the proper folding of misfolded proteins (223, 224). Interestingly, heat stress in the absence of *hsf-1* further reduces *del-4* expression (Figure 8A). This implies that *del-4* suppression upon HS is not HSF-1-dependent, however, the presence of HSF-1 ameliorates DEL-4 depletion upon HS. Consistently, i*n silico* analysis revealed the presence of HSF-1 binding sites in the *del-4* promoter region (Figure 2A and B) and *del-4* regulation by HSF-1 was verified with RT (Figure 8B). Since heat stress curtailed the abundance of DEL-4 on the

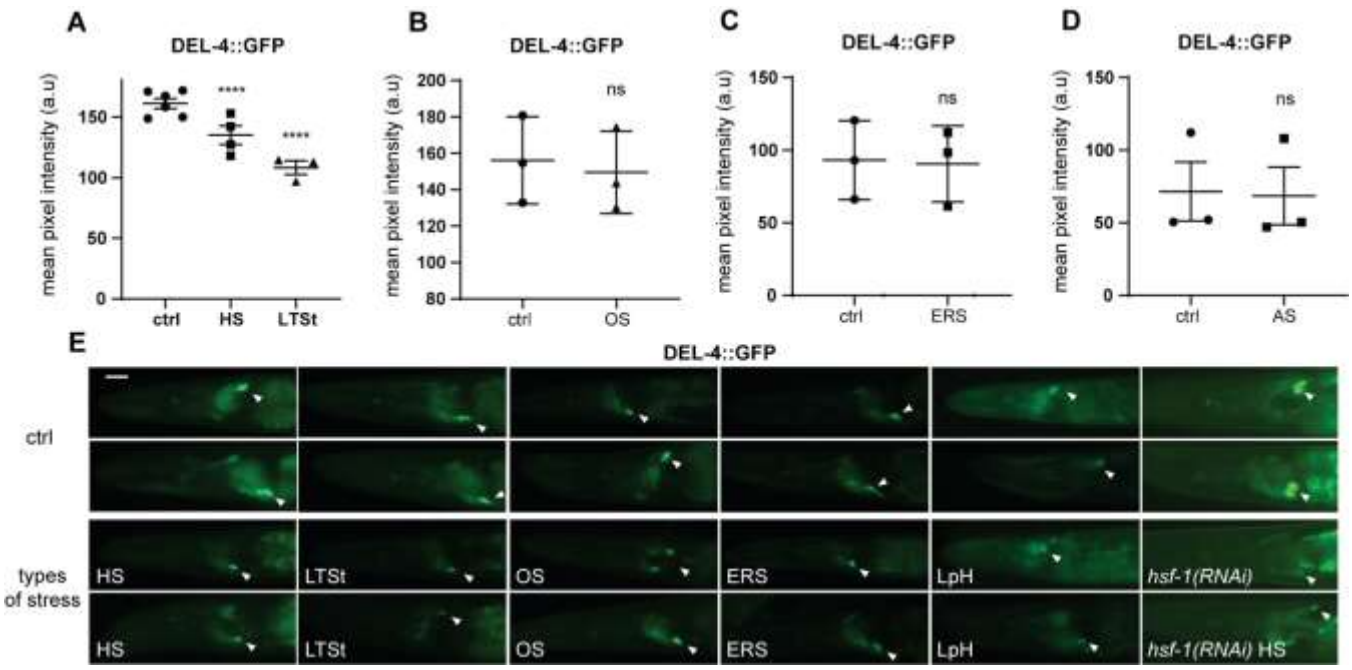

Figure 7. Regulation of DEL-4 expression by specific stress stimuli.

(A) Expression levels of DEL-4 diminish upon heat stress and starvation. Imaging of 2-day adult animals, control or treated for 3 hrs at 37°C and left O/N for recovery or starved for 24 hrs (Star methods).

(B-C) Oxidative stress and ER stress do not alter the expression levels of DEL-4. For **oxidative** stress induction, we placed animals expressing the DEL-4 translational reporter on OP50-seeded NGM treated with Paraquat to a final concentration of 8 mM (Star Methods). We induced ER stress with tunicamycin, plated on OP50-seeded NGM at a final concentration of 2.5 μg/ml. Animals were placed on NGM with Paraquat or tunicamycin at the L4 stage. Imaging was performed on day one of adulthood.

(D) Acidic stress does not affect DEL-4 levels. One-day adult animals were treated for 1 hr in a 15 μl drop with M13 brought to pH3.5 with CH3COOHNa.

(E) Representative epifluorescent images of the head region of DEL-4::GFP-expressing animals under control conditions or upon heat stress, long-term starvation, oxidative stress, ER stress, and low pH stress (Star methods). We measured the intensity only in the neuronal cell body, which exhibited the highest expression level (arrowhead). Left is anterior. Lens 40x. Scale bar 20 μm.

(A-D) Dot plots, dots represent the number of independent biological replicates, error bars represent SEM. Non-significant (ns) p=0.1234, *p=0.0332, **p=0.0021, ***p=0.0002, ****p<0.0001. Two-way ANOVA analysis. n represents number of neuronal cell somas. (A) Control: n=289; HS: n=205; LTSt: n=177. All HS and LTSt experiments were performed separately, except for one of the three repeats, but were plotted together for illustration purposes. (B) ctrl: n= 169, OS: n=161. (C) ctrl: n=97, ERS: n=105. OS and ERS experiments were performed separately but plotted together for illustration purposes. (D) ctrl n= 105 and LpH n=102. (A-E) Control (ctrl), heat stress (HS), long-term starvation (LTSt), low pH stress (LpH), oxidative stress (OS), and ER stress (ERS) (Table 5).

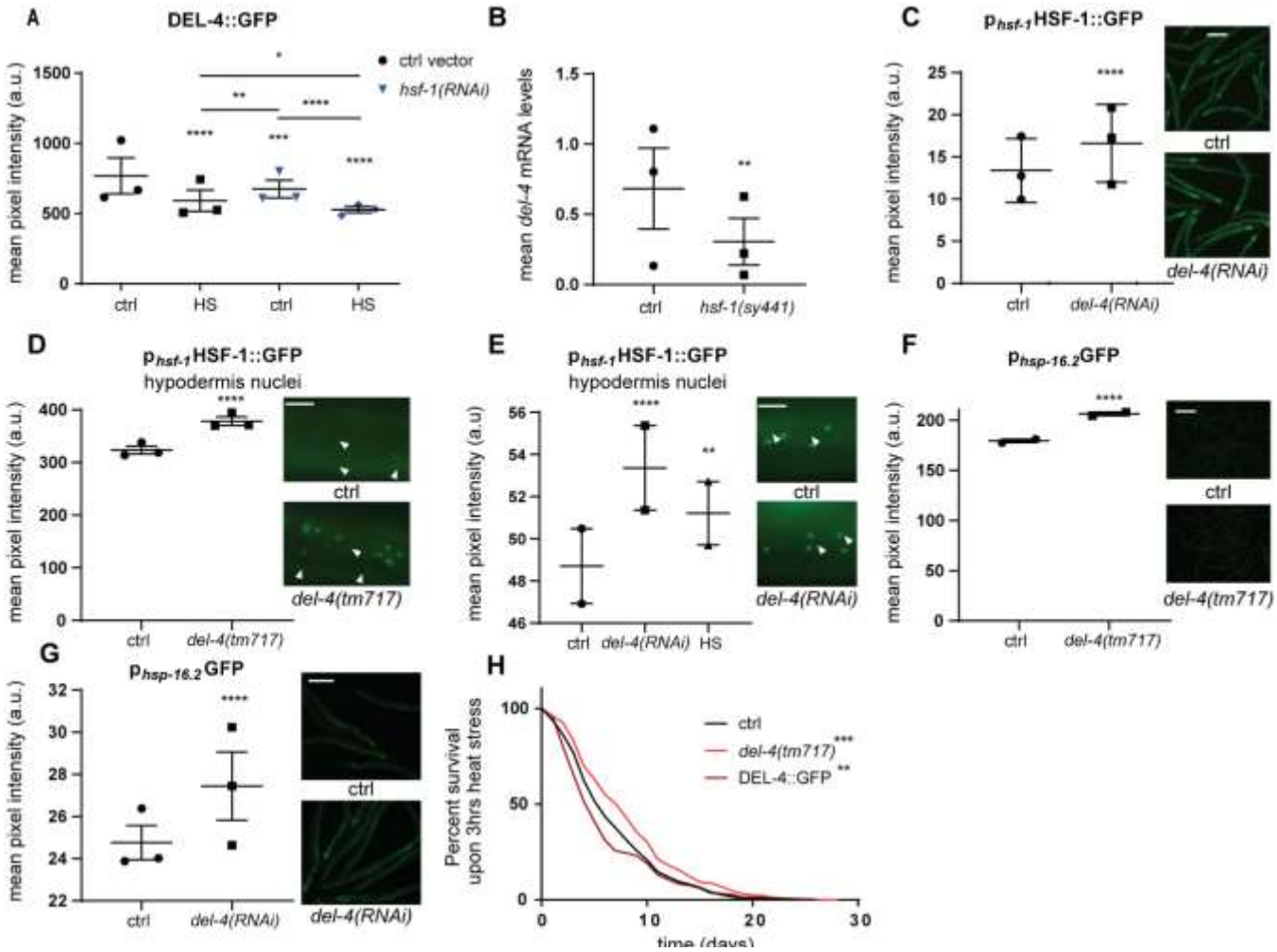

Figure 8. Interplay between DEL-4 and HSF-1.

(A, B) HSF-1 regulates the expression levels of DEL-4. (A) Downregulation of *hsf-1* with RNAi reduces the expression levels of DEL-4::GFP, upon control conditions and HS. Imaging of 2-day adult animals, control or treated for 3 hrs at 37ºC and left O/N for recovery.

(B) Reduced *del-4* mRNA levels in the *hsf-1(sy441)* mutant. We measured, with RT-PCR, the mean *del-4* mRNA levels, using as template cDNA of 3-day adult wt and *hsf-1* mutant animals. We isolated total mRNA from wt and *hsf-1* mutants, reversely transcribed it into complementary DNA (cDNA), and used it as the template for RT-PCR. Dot plot, dots represent the mean *del-4* mRNA levels from independent biological replicates. We performed 3 independent biological replicates and three technical replicates for each biological replicate.

(C-E) *del-4* depletion activates HSF-1.

(C) Increased HSF-1 expression levels upon *del-4*(RNAi). The levels of HSF-1 were measured from the whole body at day 4 of adulthood. 5x lens, scale bar 20 μm.

(D) The *del-4* mutant *(tm717)* displays an increased nucleus to cytoplasm ratio of HSF-1 expression levels. HSF-1 levels in hypodermis nuclei are increased in the *del-4* mutant. We overlooked the nuclei located above the gut to avoid intestinal autofluorescence. 40x lens, scale bar 200 μm.

Figure 8. Continued.

(E) HSF-1 expression levels in hypodermis nuclei increased upon *del-4(RNAi)*. We measured the mean fluorescence intensity of hypodermis nuclei of animals expressing the p_{hsf-1}HSF-1::GFP construct. We overlooked the nuclei located above the gut to avoid intestinal autofluorescence. The expression levels of HSF-1 upon HS treatment served as the positive control.

(F) Absence of DEL-4 increases the expression levels of the HSF-1 target *hsp-16.2*. Measurements from the whole body of one-day adults. 5x lens, scale bar 20 μm.

(G) Depletion of *del-4* with RNAi increases the expression levels of the HSF-1 target HSP-16.2. We used the $p_{hsp-16.2}$GFP transcriptional reporter expressing animals and measured the whole body upon control and *del-4(RNAi)* conditions.

(H) Survival of wt, *del-4(tm717)* mutants and DEL-4 overexpressing animals after 2.5 hrs of heat stress applied on day 1 of adulthood. Death events were measured every second day. Mutants of *del-4* display enhanced resistance, while DEL-4 overexpressing animals exhibit reduced resistance to heat stress. For statistical significance survival curve analysis was performed.

(A-G) Dot plots, dots represent the number of independent biological replicates, error bars represent SEM. Non-significant (ns) p=0.1234, *p=0.0332, **p=0.0021, ***p=0.0002, ****p<0.0001. Two-way ANOVA analysis. (E, G) Four-day adults. (A) ctrl: n=243, HS: n=233, hsf-1(RNAi): n=213, HS and *hsf-1(RNAi)*: n=286. Control (ctrl), heat stress (HS), long-term starvation (LTSt), acidic (AS), oxidative stress (OS), and ER stress (ERS) (Table S1). (C) ctrl n=219, *del-4(RNAi)* n=237, n represents the number of individual animals measured (D) ctrl n=279, HS n=325, n represents the number of nucleuses (E) ctrl n= 257, *del-4(RNAi)* n=291, HS n=392, n = the number of hypodermis nuclei measured. (F) ctrl: n=161, *del-4(tm717*): n=96, n represents number of animals. (G) ctrl n=245, *del-4(RNAi)* n=177. (H) 4 biological replicates, ctrl n=356, *del-4(tm717)* n=396, DEL-4::GFP n=273, n represents number of animals participated in the lifespan assay.

neuronal cell membrane, we hypothesized that the null *del-4* mutant (Figure 2C), where DEL-4 is permanently absent, would experience sustained stress. Indeed, alleviation of DEL-4 resulted in a statistically significant increase of HSF-1 protein levels throughout the body (Figure 8C) and hypodermis nuclei (Figure 8D and E). HSP-16.2 expression levels, directly regulated by HSF-1, are also increased in the *del-4* mutant background (Figure 8F and G). To further verify the activation of HSF-1 in the absence of *del-4*, we tested the thermotolerance of *del-4* mutants and overexpressing animals. As predicted, *del-4* mutants were HS resistant as they survived longer than wt after HS, while DEL-4 overexpressing animals were sensitive to thermal stress (Figure 8H). These findings underline the role of DEL-4 in the regulation of heat shock response.

As mentioned above, long-term starvation depletes DEL-4 protein levels (Figure 7A). DAF-16, the homologue of mammalian FOXO, is a key transcription factor activated in response to starvation.

Upon starvation, DAF-16 translocates to the nucleus to promote metabolic adaptations necessary for stress resistance (225). Nonetheless, long-term starvation reduces DAF-16 expression and triggers its translocation back to the cytoplasm in an AGE-1/PI3K dependent manner (226). We hypothesized that *del-4* down-regulation, also observed after long-term starvation (24 hrs at day 1 of adulthood), would affect DAF-16 levels. Interestingly, long-term starvation (LTSt) in the absence of *daf-16* does not further reduce *del-4* expression (Figure 9A). This implies that *del-4* suppression upon LTSt is DAF-16-dependent. However, as previously mentioned, i*n silico* analysis did not reveal the presence of DAF-16

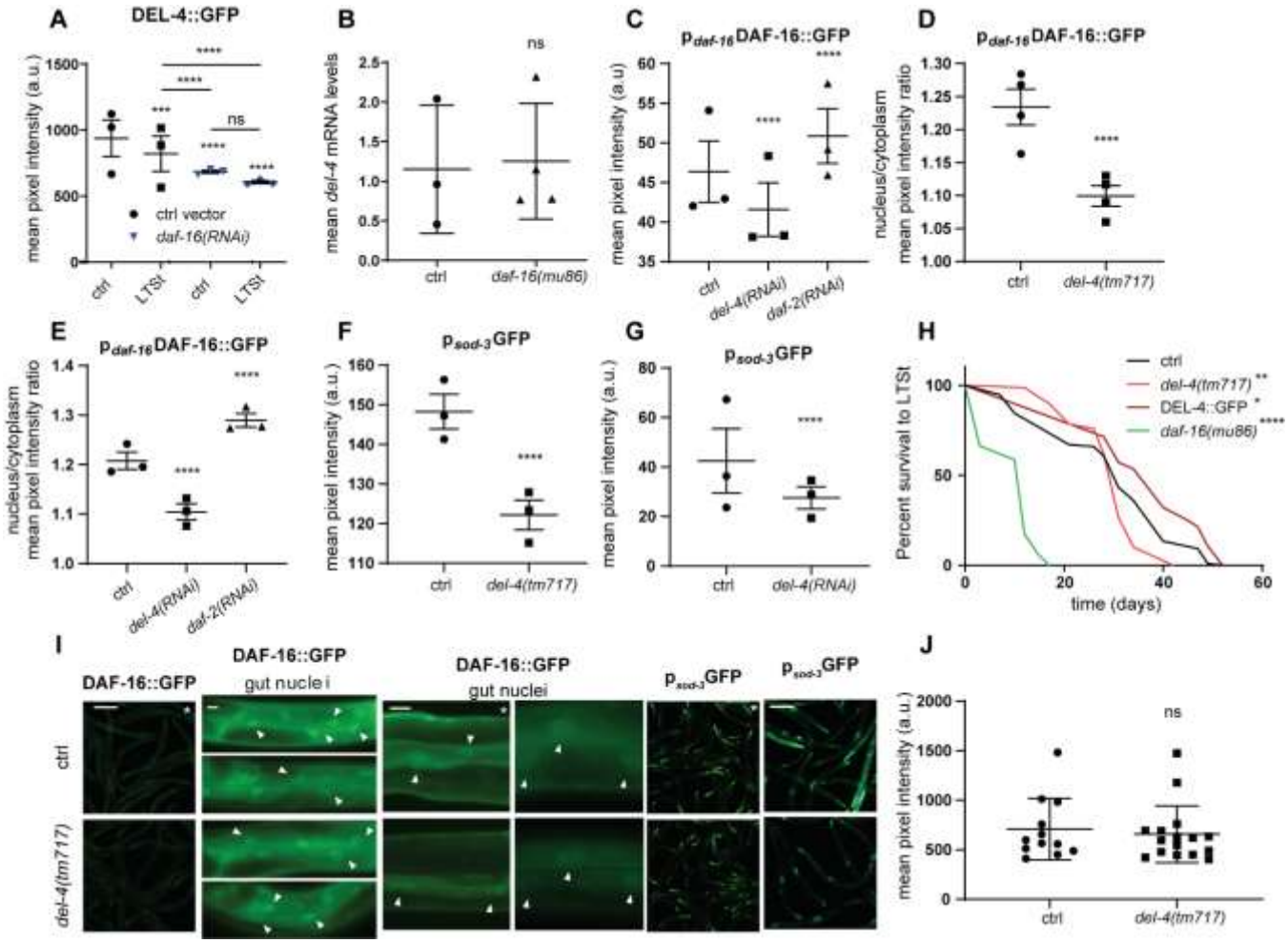

Figure 9. DEL-4 affects DAF-16 activation.

(A) Diminution of *daf-16* with RNAi reduces the expression levels of DEL-4::GFP, upon control conditions, more than Long-term Starvation (LTSt) alone. LTSt in the absence of DAF-16 does not reduce DEL-4 levels any further. Imaging of 2-day adult animals, control or starved for 24 hrs on empty NGM at 20 ºC.

(B) Absence of transcriptional regulation of *del-4* by DAF-16. We measured with RT-PCR the mean *del-4* mRNA levels, using as template cDNA of 3-day adult wt and *daf-16(mu86)* mutant animals. We isolated total mRNA from

Figure 9. Continued.

wt and *daf-16(mu86)* mutants, reversely transcribed it into complementary DNA (cDNA), and used it the as template for RT-PCR. Dot plot, dots represent the mean *del-4* mRNA levels from independent biological replicates. We performed 3 independent biological replicates and for each biological we performed three technical replicates.

(C) Downregulation of *del-4* by RNAi decreases DAF-16 expression levels, measured in the whole body. *daf-2* RNAi was used as a positive control. Four-day adult animals.

(D) The DAF-16 ratio of nucleus to cytoplasm is decreased in the *del-4(tm717)* mutant. We measured the intensity levels of DAF-16 in the nuclei and adjacent cytoplasm of the gut and calculated the ratio. One-day adult animals.

(E) The DAF-16 ratio of the nucleus to the cytoplasm decreased upon *del-4(RNAi)*. *daf-2* RNAi was used as a positive control. We measured the intensity levels of DAF-16 in the nuclei and adjacent cytoplasm of the gut, using a strain expressing the p_{daf-16}DAF-16::GFP translational reporter.

(F) *del-4* elimination lowers the DAF-16 target SOD-3 expression levels. We measured the expression levels of *sod-3* from the whole body of animals expressing the transcriptional reporter p_{sod-3}GFP, under control conditions and in the *del-4(tm717)* mutant.

(G) Elimination of *del-4* with RNAi lowers the expression levels of the DAF-16 target SOD-3. We measured the fluorescence intensity from the whole body of 4-day adult animals expressing the p_{sod-3}GFP transcriptional reporter upon control and *del-4* RNAi conditions.

(H) *del-4(tm717)* mutant animals were sensitive to food deprivation compared to wt, while animals overexpressing DEL-4 were more resistant. We measured the survival of wt, *del-4(tm717)* mutants, DEL-4::GFP-overexpressing animals, and *daf-16(mu86)* mutants during starvation. The *daf-16(mu86)* mutant was used as the positive control. Animals were bleached and placed as eggs in 1.5ml M9. Every second day, 20μl were retrieved from each genotype, put on OP50-seeded NGM as L1 larvae, and allowed three days to grow. We counted the animals that reached the L4 stage or adulthood (Star methods). Survival curve analysis was used for the evaluation of statistical significance.

(I) Representative images of the designated reporters. Asterisks indicate *del-4(RNAi)* instead of the *del-4* mutant. Images illustrating whole animals were retrieved with a 5x lens and the scale bar corresponds to 20μm. Images of p_{daf-16}DAF-16::GFP (gut nuclei) were captured with a 20x lens, and those of p_{skn-1}SKN-$1^{B/C}$::GFP in ASI nuclei with a 40x lens. In this case, the scale bar corresponds to 200μm (left is anterior).

J) DEL-4 mutants do not display altered feeding rhythm compared to control wild-type animals. The amount of feeding is measured using mRFP-expressing bacteria. Mean pixel intensity is measured from one-day adult animals seeded with bacteria expressing mRFP.

(A-C, E-J) Dot plots, dots indicate mean levels of independent biological replicates. Two-way ANOVA. Error bars represent SEM. Non-significant (ns) p=0.1234, *p=0.0332, **p=0.0021, ***p=0.0002, ****p<0.0001. One-way ANOVA.

(A) Ctrl: n= 213, LTSt: n= 164, *daf-16(RNAi)*: n= 207, LTSt and *daf-16(RNAi)*: n= 160. (C) ctrl n=134, *del-4(RNAi)* n=149, *daf-2(RNAi)* n=152, n represents the number of animals. (D) ctrl n=442, *del-4(tm717)* n=375, n represents the

Figure 9. Continued.

number of nuclei. (E)) ctrl n=519, *del-4(RNAi)* n=733, daf-2(RNAi) n=642, n = the number of gut nuclei measured. (F) ctrl n=178, *del-4(tm717)* n=132, n represents number of animals. (G) ctrl n=156, *del-4(RNAi)* n=154. (H) ctrl n=97, *del-4(tm717)* n=79, DEL-4::GFP n=28, *daf-16(mu86)* n=92, n represents number of animals. (J) ctrl: n=20, *del-4(tm717)*: n=30, n= number of animals.

binding sites in the *del-4* promoter region (Figure 2A, B) and RT results also agreed (Figure 9B). Moreover, we performed RNAi for *del-4* and measured the levels of DAF-16 and SOD-3, a superoxide dismutase that is a well-established DAF-16 target (227). We found that downregulation of *del-4* reduced DAF-16 protein levels in the whole body (Figure 9C and I) and decreased the nucleus/cytoplasm ratio of DAF-16 (Figure 9D, E, and I), mimicking the response to long-term starvation. We also observed a reduction in the expression of *sod-3*, upon *del-4* suppression (Figure 9F, G, and I). To further verify the reduced activity of DAF-16 in the absence of DEL-4, we performed a survival assay upon starvation. In this assay, we utilized wt animals, animals lacking or overexpressing DEL-4 and *daf-16(mu86)* mutants that served as a positive control. We allowed the eggs from each strain to hatch in 1,5 ml M9 and counted, every other day, the number of surviving L1 larvae. L1 larvae required DAF-16 activation and nuclear translocation to enter into starvation-induced diapause and endure starvation (226, 228). Since *del-4* downregulation reduced DAF-16 levels and activity, we hypothesized that arrested L1 survival would be reduced in a *del-4* mutant background. In accordance with our hypothesis, we discovered that *del-4* mutants were more sensitive to long-term starvation compared to wt (Figure 9H), whilst DEL-4 overexpressing animals were more resistant corroborating the notion that DEL-4 is required for an intact response to prolonged starvation. The transcription factor DAF-16 as a regulator of the insulin/IGF-1 signalling pathway normally translocates to the nucleus when the food is limited. Therefore, we hypothesized that *del-4* mutation might affect food intake of the animal which, however, was not the case (Figure 9J).

To determine whether DEL-4 deficiency triggers other types of metabolic stress responses, we assessed the activation of the ER unfolded protein response (ER^{UPR}) and oxidative stress response in the *del-4* mutant background. To identify if DEL-4 influences the induction of ER stress, we crossed *del-4*(*tm717)* mutants with animals expressing the transcriptional reporter of HSP-4 (p_{hsp-4}GFP), a well-established target of ER^{UPR} and a homologue of the mammalian BiP. We observed that the depletion of DEL-4 upregulated *hsp-4* expression (Figure 10A, B, and K). Disruption of energy balance, Ca^{2+}

homeostasis, or redox state causes ER stress (229). ER stress triggers cytosolic Ca^{2+} release from the sarco-endoplasmic reticulum which in turn induces Ca^{2+}-calmodulin protein kinase β (CaMKK2)-dependent AMPK activation (230, 231). To determine whether DEL-4 is a mediator of this pathway, we suppressed *del-4* in animals carrying the genetically encoded calcium indicator GCaMP2.0 expressed throughout the body ($p_{let-858}$GCaMP2.0) or an AMPK translational reporter (p_{aak-2}AAK-2::Tomato). In both cases, the reduction or absence of DEL-4 induced a systemic increase in the cytoplasmic calcium and AMPK levels (Figure 10C-F and K).

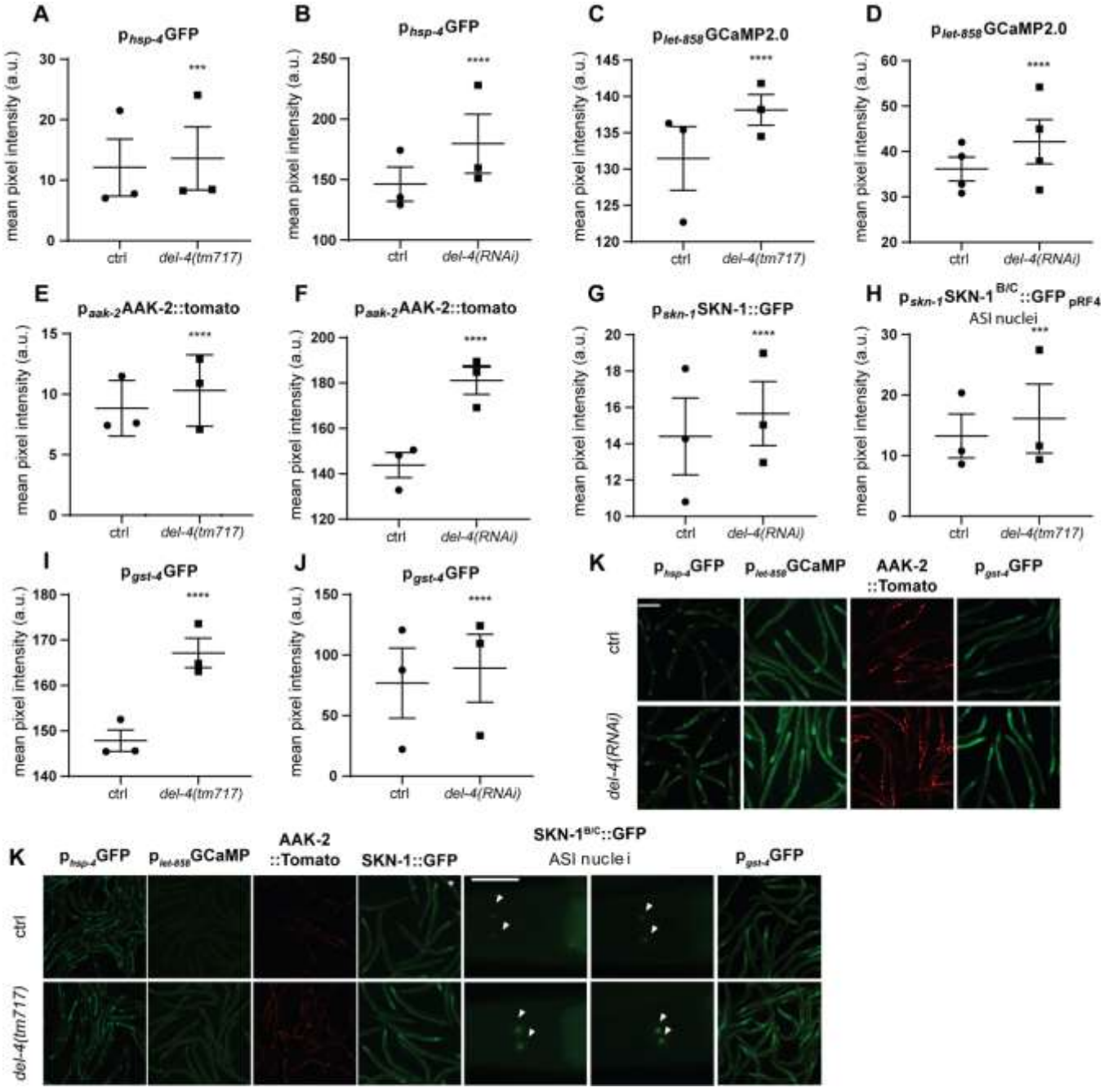

Figure 10. DEL-4 regulates systemic stress responses.

(A) The transcriptional reporter of HSP-4, an ER stress marker, displays elevated fluorescence intensity levels in the *del-4* mutant background compared to the control. One-day adult animals.
(B) Depletion of *del-4* with RNAi also increases the expression levels of HSP-4. We used animals expressing the transcriptional reporter p_{hsp-4}GFP and measured fluorescence intensity from the whole body upon control and *del-4(RNAi)* conditions.
(C) Cytoplasmic Ca^{2+} levels rise upon *del-4* depletion. Measurement of intracellular Ca^{2+} levels using the genetically encoded calcium indicator GCaMP2.0 driven by the *let-858* promoter for systemic expression.
(D) Cytoplasmic Ca^{2+} levels rise upon *del-4(RNAi)*. Measurement of intracellular Ca^{2+} levels using animals expressing the genetically encoded calcium indicator GCaMP2.0 driven by the *let-858* promoter for systemic expression. Measurements were obtained from the whole body.
(E) Increased AAK-2 levels in *del-4(tm717)* mutant animals. We measured the expression levels of AAK-2 from the whole body of animals expressing the translational reporter p_{aak-2}AAK-2::Tomato. (F) Increased AAK-2 expression levels were observed upon *del-4(RNAi)*. We measured the mean fluorescence intensity from the whole body of animals expressing the translational reporter p_{aak-2}AAK-2::Tomato.
(G) DEL-4 downregulation increases systemic expression levels of SKN-1 (four-day adult animals).
(H) SKN-1 expression levels of isoforms B and C are elevated in ASI nuclei in the *del-4* mutant background. One-day adults.
(I) DEL-4 downregulation increases systemic expression levels of SKN-1 target GST-4 (one-day adult animals).
(J) The expression level of the GST-4 SKN-1 target increase upon treatment with *del-4(RNAi)*. The expression levels of animals expressing the transcriptional reporter p_{gst-4}GFP were measured from the whole body.
(K) Representative images of the designated reporters. Asterisks indicate *del-4(RNAi)* instead of the *del-4* mutant. Images illustrating whole animals were retrieved with a 5x lens and the scale bar corresponds to 20μm. Images of p_{skn-1}SKN-$1^{B/C}$::GFP in ASI nuclei were captured with a 40x lens. In this case the scale bar corresponds to 200μm (left is anterior).
(A-J) Dot plots, dots indicate mean levels of independent biological replicates. Two-way ANOVA. Error bars represent SEM. Non-significant (ns) p=0.1234, *p=0.0332, **p=0.0021, ***p=0.0002, ****p<0.0001. One-way ANOVA.
(A) ctrl n=120, *del-4(tm717)* n=112, n represents number of animals. (B) ctrl n=128, *del-4(RNAi)* n=154. (C) ctrl n=155, *del-4(tm717)* n=161, n represents number of animals. (D) ctrl n=207, *del-4(RNAi)* n=217. (E) ctrl n=128, *del-4(tm717)* n=92, n represents number of animals. (F) ctrl n=142, *del-4(RNAi)* n=127, (G) ctrl n=301, *del-4(RNAi)* n=300, n represents number of animals. (H) ctrl n=143, *del-4(tm717)* n=113, n represents number of ASI nuclei. (I) ctrl n=165, *del-4(tm717)* n=162, n represents number of animals. (J) ctrl n=250, *del-4(RNAi)* n=245.

According to late discoveries, ER stress activates SKN-1 in an oxidative stress response-independent manner. SKN-1, the *C. elegans* homologue of mammalian Nrf2, is known for its role in Phase II

detoxification genes transcription, thereby contributing to survival and resistance to oxidative stress (232). Thereupon, SKN-1 promotes proteostasis and possibly exerts a combined action with XBP-1 to induce ER^{UPR} (233). To assess if DEL-4 reduction affects SKN-1 activation, we employed *del-4* feeding RNAi to reporter strains of SKN-1 and a well-characterized SKN-1 target, the *gst-4* (p_{gst-4}GFP). We observed that systemic *del-4* knockdown enhanced the expression levels of *skn-1* and its target gene *gst-4* (Figure 10G-K). Specifically, SKN-1 increased both systemically (Figure 10G and K) and particularly in the ASI nuclei (Figure 10H and K). Collectively, these data indicate that DEL-4, acting in neurons, modulates the activation of several metabolic stress responses throughout the body. The question that rises is how this signal is transmitted from neurons to distal tissues and whether it is translated to behavioural adaptation to environmental stress.

DEL-4 modulates dopaminergic signalling

The expression of all three degenerins DEL-2, DEL-3, and DEL-4 in dopaminergic neurons indicated that they may impact dopaminergic signalling. Dopamine signalling engages in several forms of behavioural plasticity, reward, stress processing, and control of the motor output. Therefore, we reasoned that DELs could integrate stress stimuli through dopaminergic signalling. In *C. elegans*, the functionality of the dopamine pathway can be readily assessed by monitoring a specific locomotory response to environmental food availability cues, termed basal slowing response (BSR) (32), and consists of a decrease in the animal's locomotory rate upon encountering food (32). To assess whether DEL-4 modulates dopaminergic signalling, we tested the ability of animals to elicit a BSR in the presence or absence of DEL-4. Interestingly, null mutant animals *del-3*(*tm5642*) and *del-4*(*tm717*) (Figure 2C) exhibited a strengthened slowing response when encountering food compared to the wild-type (wt) (Figure 11A). In addition, transgenic animals carrying translational reporters for DEL-2, DEL-3, and DEL-4, and thus overexpressing these DELs, displayed a faster locomotory rate on food compared to the wt (Figure 11B). These results suggest the involvement of DELs in the regulation of dopaminergic signalling.

Contemplating the same effect of DEL-2, DEL-3, and DEL-4 on the locomotory rate of *C. elegans* and their common expression pattern, we hypothesized that they might act in the same signalling pathway. In line with the above, we evaluated the basal slowing response upon simultaneous downregulation of two or all three degenerins. RNA interference (RNAi) for *del-2* or *del-3* on *del-4(tm717)* mutant, double RNAi for *del-2* and *del-3* on *del-4(tm717)* mutant (Figure 11C) or single RNAi

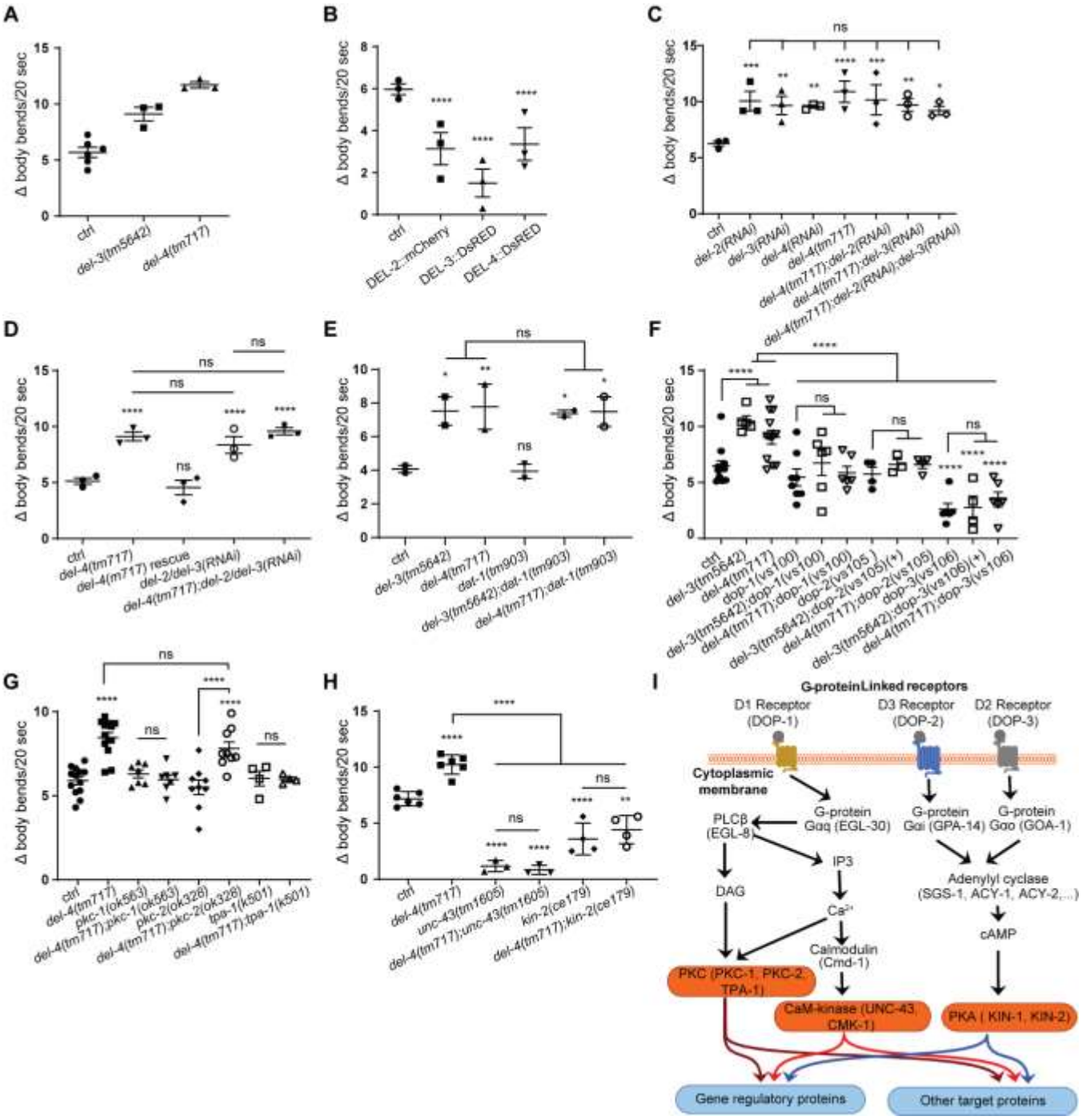

Figure 11. DEL-2, DEL-3, and DEL-4 act in the dopaminergic signalling pathway to modulate *C. elegans* locomotory rate.

(A) Basal slowing response (BSR) of wt, *del-3(tm5642)*, and *del-4(tm717)* mutants. *del-3* and *del-4* mutant animals show strengthened BSR.

(B) BSR of wt and animals overexpressing DEL-2, DEL-3 and DEL-4. Animals overexpressing DELs display reduced BSR and move faster on a plate with food compared with an empty plate.

Figure 11. Continued.

(C) BSR of wt and *del-4(tm717)* mutants after RNAi treatment for *del-2*, *del-3*, or both. Double downregulation of *del-4* and *del-2*, or *del-4* and *del-3*, and triple downregulation of *del-4*, *del-2*, and *del-3* has the same effect on the locomotory rate of *C. elegans* as *del-2*, *del-3*, or *del-4* downregulation alone. Animals were grown on HT115 bacterial strain carrying either the control pL4440 vector or expressing *del-2* and/or *del-3* dsRNA. Single RNAis were diluted with an empty pL4440 vector to be comparable to double RNAi.

(D) Repeat of experiment seen in (C) using a construct bearing both *del-2* and *del-3* loci for RNAi, to avoid dilutions used in double RNAi. we performed RNAi experiments with wild type and *del-4(tm717)* mutant animals. Again, we observed that the double del-2/del-3(RNAi) applied on wild-type animals increased the basal slowing response (BSR) compared to wild-type and similar to the *del-4(tm717)* mutant animals. Additionally, double *del-2/del-3* RNAi applied on *del-4(tm717)* mutants did not result in an additive effect concerning the BSR, implying that all three DELs studied act in the same pathway. We performed three independent biological replicates.

(E) Basal slowing response for single and double mutants of dels and the dopamine transporter DAT-1. Double mutants between dels and the dopamine transporter display the same phenotype in the basal slowing response with the *del-3* and *del-4* single mutants, indicating that the effect of dels on the basal slowing response lies downstream to the dopamine transporter DAT-1.

(F) Dopamine receptors lye downstream to DEL-4. BSR of wt, *del-4(tm717)*, *dop-1(vs100)*, *dop-2(vs105)*, *dop-3(vs106)*, *del-4(tm717);dop-1(vs100)*, *del-4(tm717);dop-2(vs105)*, and *del-4(tm717);dop-3(vs106)* animals. The phenotype of double mutants for *del-4* and *dop-1*, *dop-2*, or *dop-3* is the same as in the single mutants of dopamine receptors.

(G) PKC-1 and TPA-1 lye downstream to DEL-4, while PKC-2 possibly does not participate in the DEL-4 phenotype. BSR of wt, *del-4(tm717)*, *pkc-1(ok563)*, *del-4(tm717);pkc-1(ok563)*, *pkc-2(ok328)*, *del-4(tm717);pkc-2(ok328)*, *tpa-1(k501) and del-4(tm717);tpa-1(k501)*. Double deficient mutants of *del-4(tm717);pkc-1(ok563)* and *del-4(tm717);tpa-1(k501)* have the same phenotype with *pkc-1(ok563)* or *tpa-1(k501)* single mutants, respectively. BSR of *del-4(tm717);pkc-2(ok328)* double mutants have the same response as *del-4(tm717)* single mutant. BSR for homologues of mammalian PKC isoforms.

(H) UNC-43 and KIN-2 lie downstream to DEL-4 at the dopaminergic signalling pathway. BSR of wt, *del-4(tm717)*, *unc-43(tm1605)*, *del-4(tm717);unc-43(tm1605)*, *kin-2(ce179)* and *del-4(tm717);kin-2(ce179)* animals. Double mutants *del-4(tm717);unc-43(tm1605) and del-4(tm717);kin-2(ce179)* have the same phenotype with *unc-43(tm1605)* and *kin-2(ce179)* single mutants, respectively. UNC-43 is an ortholog of human calcium/calmodulin-dependent protein kinase II. KIN-2 is a regulator of KIN-1, which is an ortholog of human cAMP-dependent protein kinase. *kin-2(ce179)* mutant carries a gain of function mutation.

(I) Schematic representation of the dopamine signalling pathway. Dopamine receptors form G-protein coupled receptors, that upon dopamine binding activate downstream G-proteins. D1 Receptors activate the IP3/DAG calcium pathway, and D3 and D2 receptors activate the adenylyl cyclase/cAMP signalling pathway. Inside parenthesis: *C. elegans* homologues.

Figure 11. Continued.

(A-H) Dot plots, dots represent the ratio Δ body bends/20sec of independent biological experiments. Δ body bends/20sec corresponds to body bends/20sec on empty plate minus body bends/20sec on plate with food. In every independent biological replicate of each BSR experiment 8-15 animals were tested. One-day adult animals were used in all experiments**.** Error bars represent SEM. Non-significant (ns) p=0,1234, *p=0,0332, **p=0,0021, ***p=0,0002, ****p<0,0001. Two-way ANOVA.

(A) ctrl n=61, *del-3(tm5642)* n= 37, *del-4(tm717)* n=36, (B) ctrl n=26, DEL-2::mCherry n= 30, DEL-3::DsRED n= 30, DEL-4::DsRED n=28, (C) ctrl n=33, *del-2(RNAi)* n=35, *del-3(RNAi)* n=35, *del-4(RNAi)* n=25, *del-4(tm717)* n= 35, *del-4(tm717);del-2(RNAi)* n=35, *del-4(tm717);del-3(RNAi)* n=35, *del-4(tm717);del-2(RNAi);del-3(RNAi)* n=25, (D) ctrl n=45, *del-4(tm717)* n=45, *del-4(tm717)* rescue n=45, *del-2/del-3(RNAi)* n=41, *del-4(tm717);del-2/del-3(RNAi)* n=45. (E) ctrl n=14, *del-3(tm5642)* n= 14, *del-4(tm717)* n= 15, *dat-1(tm903)* n= 16, *del-3(tm5642);dat-1(tm903)* n= 13, *del-4(tm717);dat-1(tm903)* n= 18, (F) ctrl n=116, *del-3(tm5642)* n= 50, *del-4(tm717)* n=112, *dop-1(vs100)* n=74, *del-3(tm717);dop-1(vs100)* n=55, *del-4(tm717);dop-1(vs100)* n=103, *dop-2(vs105)* n=37, *del-3(tm5642);dop-2(vs105) n= 30, del-4(tm717);dop-2(vs105)* n=36, *dop-3(vs106)* n=59, *del-3(tm5642;dop-3(vs106)* n=40, *del-4(tm717);dop-3(vs106)* n=58, (G) ctrl n=117, *del-4(tm717)* n=117, *pkc-1(ok563)* n=69, *del-4(tm717);pkc-1(ok563)* n=66, *pkc-2(ok328)* n=88, *del-4(tm717);pkc-2(ok328)* n=84, *tpa-1(k501)* n=41, *del-4(tm717); tpa-1(k501)* n=51. (H) ctrl 6 n=60, *del-4(tm717)* n=60, *unc-43(tm1605)* n=30, *del-4(tm717);unc-43(tm1605)* n=30, *kin-2(ce179)* n=40, *del-4(tm717);kin-*

downregulating both *del-2* and *del-3* applied on the *del-4(tm717)* mutant (Figure 11D) drove to the same phenotype as *del-4(tm717)* alone. We did not observe additive phenotype. We conclude that DEL-2, DEL-3, and DEL-4 act through the same signalling pathway to modulate the locomotory rate of *C. elegans*.

Subsequently, we explored the possible epistatic interaction of DEL-4 with the intracellular dopaminergic signalling pathway (Figure 11I). We performed the basal slowing assay for double-mutants of *del-3* or *del-4* and the dopamine transporter *dat-1* or each of the dopamine receptors (*dop-1*, *dop-2*, or *dop-3*) (Figure 11E and F) or *del-4* and the downstream kinases (*pkc-1*, *pkc-2*, *tpa-1*, *unc-43* or *kin-2*) (Figure 11G and H) (Table 1). In most instances, we observed that the basal slowing response of the double-mutants was equivalent to that of the dopamine receptors or the kinases single-mutants. The only exceptions were the *del-4(tm717);dat-1(tm903)* and the *del-4(tm717);pkc-2(ok328)* double-mutants, which share the same phenotype as *del-4(tm717)*. These findings imply that PKC-2 either lies upstream of DEL-4 or does not participate in the *del-4(tm717)* phenotype. Additionally, the above discoveries indicate that DEL-4 acts in the dopaminergic signalling pathway upstream to the dopamine receptors and downstream of the dopamine transporter. Therefore, the locomotion phenotype of the *del-*

4 mutant observed in the basal slowing response is due to its effects on neurons downstream of the dopaminergic.

To corroborate the effects of DEL-4 on dopaminergic signalling, we sought to estimate dopamine levels in the synapse of dopaminergic neurons in the presence or absence of DEL-4. To this end, we used a pH-sensitive version of EGFP, the super ecliptic phluorin (SEpHluorin) (Tables 1, 4, 6), fused to synaptobrevin, and specifically expressed in dopaminergic neurons (p_{asic-1}SNB-1::SEpHl). The fluorescence of SEpHluorin quenches inside vesicles where the pH is low. Synaptic vesicle release exposes SEpHl to the higher pH of the synaptic cleft, and thus it's fluorescence increases (234). We crossed the animals expressing p_{asic-1}SNB-1::SEpHl with the *del-4(tm717)* mutants. We observed reduced basal levels of synaptic release in the absence of DEL-4 (Figure 12A). To further verify our findings, we proceeded with a dopamine resistance assay (Figure 12B and C). Reduced levels of dopamine release in the *del-4(tm717)* mutant should induce slower paralysis compared to wt. Indeed, *del-4(tm717)* mutants were resistant to paralysis in the dopamine resistance assay, further suggesting that the amount of dopamine in the synaptic cleft is reduced in the absence of DEL-4 (Figure 12B and C). These results suggest that DEL-4 affects synaptic vesicle release from dopaminergic neurons.

DEL-4 affects synaptic release at the neuromuscular junction of cholinergic and GABAergic motor neurons

DEL-4 was present in the VA, VB, DA, and DB cholinergic motor neurons of the ventral nerve cord (Figure 3C and 4C). Muscle cells are innervated by cholinergic and GABAergic neurons. Firing through cholinergic neurons promotes muscle contraction, whereas the activation of GABAergic neurons evokes muscle relaxation. Both types of motor neurons express dopamine receptors, which act antagonistically to control *C. elegans* locomotion. The D1-like dopamine receptor, DOP-1, is confined to cholinergic motor neurons, where it stimulates ACh release (Table 5). The D2-like dopamine receptor, DOP-3, localizes primarily in GABAergic neurons and, to a much lesser extent, in cholinergic motor neurons. DOP-3 functions by inhibiting ACh release (235). According to the BSR data (Figure 11F), all three dopamine receptors lie downstream to DEL-4, concerning the effects of DEL-4 on BSR. To study the effect of DEL-4 downregulation on motor output, we estimated the degree of synaptic release initially at the cholinergic and subsequently at the GABAergic neuromuscular junctions (NMJ). We performed *del-4* RNAi on transgenic animals expressing super ecliptic phluorin tagged with SNB-1

under the *acr-2* promoter, driving expression in the cholinergic motor neurons. Interestingly, we saw that DEL-4

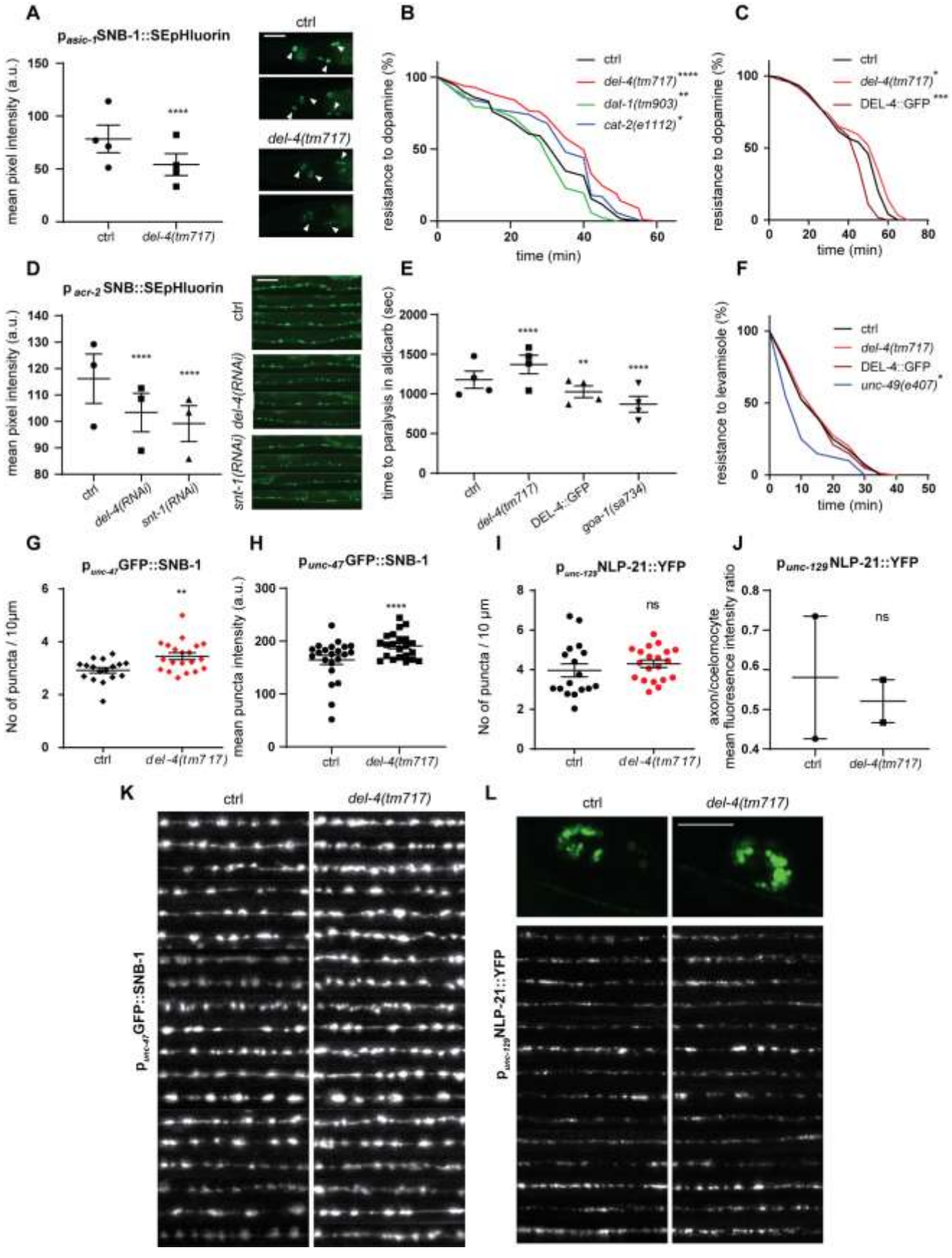

Figure 12. Synaptic vesicle exocytosis of dopaminergic and motor neurons is altered in response to DEL-4 abundance.

(A) Basal levels of synaptic release from dopaminergic neurons are reduced in the *del-4(tm717)* mutant background. Left, measurements of Super Ecliptic pHluorin (Star methods) expressed in synaptic vesicles of dopamine-releasing neurons in controls and *del-4(tm717)* mutants. (Right) Representative images of p_{asic-1}SNB-1::SEpHluorin from control (top) and *del-4(tm717)* mutants (bottom). Some of the illustrated images came up by merging serial stacks using Adobe Photoshop CS5 (Table 7) for illustration purposes only, so that all dopaminergic neurons may be visible in one image. We counted the mean pixel intensity in one-day adults from all cell bodies in the head (indicated with arrowheads). Left is anterior. Lens 40x. Scale bar 20 μM.
(B) Animals lacking DEL-4 are resistant to exogenously applied dopamine. DEL-4 amelioration results in increased resistance to dopamine. We measured the time to paralysis in a 20 μl drop of 40 mM dopamine of ctrl, *del-4(tm717)*, *dat-1(tm903)* and *cat-2(e1112)* animals (Tables 1 and S4). *dat-1(tm903)* and *cat-2(e1112)* animals were used as controls. *dat-1* encodes for the dopamine transporter; thus, in the absence of DAT-1 dopamine is retrieved from the synapse back to the pro-synaptic cell accumulating at the synaptic cleft. Therefore, dat-1 mutants are expected to paralyze faster compared to wt. CAT-2 is involved in dopamine biosynthesis from tyrosine. Therefore, in the absence of CAT-2 reduced amount of dopamine would be released at the synaptic cleft and it would take more time for *cat-2* mutants to paralyze in dopamine compared to wt. We observed that *del-4* and *cat-2* mutant animals are resistant to dopamine, while *dat-1(tm903)* animals are sensitive. Experiments were performed with day-1 adult animals. Survival curve analysis was performed for estimation of significance.
(C) Increased resistance of *del-4(tm717)* mutant animals to dopamine. Time course to paralysis of *del-4* mutant and overexpressing animals. We performed the time course assay with one-day adult animals in a 15 μl drop of 40 mM dopamine diluted with M9. Thirty animals per genotype were used in each experiment. Survival curve analysis was performed to estimate the statistical significance. Biological independent replicates were performed by two experimenters (MG and DP) and by one of them blindly. See also Figure S5.
(D) (Left) Reduced synaptic release from cholinergic motor neurons following *del-4* knockdown. We employed the Super Ecliptic pHluorin tagged with SNB-1 driven by the *acr-2* promoter to measure the basal levels of synaptic release in cholinergic motor neurons. The mean pixel intensity of neuronal somas was calculated. We used *snt-1(RNAi)* as a positive control. (Right) Representative images of cholinergic motor neurons from animals expressing p_{acr-2}SEpHl::SNB-1 , upon control (ctrl) (top), *del-4* (middle) or *snt-1* RNAi conditions. Scale bar 20 μm. Lens 20x. One-day adults.
(E) *del-4(tm717)* downregulation increases the resistance to aldicarb-mediated paralysis. We measured the time to paralysis of indicated genotypes at day one of adulthood in 15 μl of 10 mM aldicarb (Star methods). Positive control *goa-1(sa734)* (Tables 1 and S4) is an aldicarb hypersensitive strain. Survival curve analysis was performed to estimate statistical significance. Biological independent replicates were performed by two experimenters (MG and DP) and by one of them blindly.
(F) Absence or overexpression of DEL-4 causes the same phenotype as wt in the levamisole resistance assay. Time course to paralysis of the indicated genotypes at day one of adulthood in a 15 μl drop of 400 μM levamisole

Figure 12. Contibued.

diluted with M9 (Star methods). We used the *unc-49(e407)* mutant strain (Tables 1 and S4) that exhibited sensitivity to levamisole as a positive control. For statistical analysis, survival curve analysis was performed.
(G, H, K) Synaptobrevin 1 positive puncta accumulate at the presynaptic terminals of dorsal cord GABAergic motor neurons in the *del-4(tm717)* mutant. Measurements were performed at day-one adult animals (Star methods).
(G) Increased number of puncta/10 μm in the *del-4* mutant background. Scatter plot graph of control and *del-4(tm717)* animals showing the number of SNB-1 puncta per 10 μm. We measured the number of puncta per ten μm of GABAergic motor neurons from animals expressing the p_{unc-47}GFP::SNB-1 synaptic vesicle genetic reporter.
(H) Increased intensity of SNB-1 positive puncta in the *del-4(tm717)* mutant. We measured the mean puncta intensity along GABAergic motor neurons of control and *del-4(tm717)* mutants.
(I, J, L) DEL-4 absence does not alter the release of dense core vesicles from the dorsal chord cholinergic motor neurons. Measurements were performed at day-one adult animals.
(I) Scatter plot demonstrating the number of NLP-21::YFP puncta per 10 μm of the dorsal neural chord. Cholinergic expression was achieved with the *unc-129* promoter Star methods). Fluorescence of coelomocytes is a result of NLP-21::YFP endocytosis upon release. Control and *del-4(tm717)* mutant animals display the same phenotype.
(J) Quantification of neuropeptide release from cholinergic motor neurons, expressed as the mean pixel intensity ratio of axons to coelomocytes for control and *del-4* mutants. We measured the mean fluorescence intensity from axons of cholinergic motor neurons from animals expressing the neuropeptide NLP-21. We didn't observe a statistically significant difference between control and *del-4* mutants.
(K) A panel of 19 images of dorsal neural cords expressing SNB-1::GFP in GABAergic motor neurons driven by the *unc-47* promoter. Left, control. Right, *del-4(tm717)*. Axons were straightened using the straightened function of ImageJ[94] (see KRT). The scale bar is the same as that in (L).
(L) Top, shown in green, representative images of the NLP-21::YFP strain indicating cholinergic motor neurons alongside coelomocytes in control (left) and *del-4(tm717)* (right) animals. Bottom, shown in black and white, panel of fragments of 14 straightened dorsal cord cholinergic motor neurons.
(K, L) Scale bar, 10 μm. Confocal images. Lens 63x. Day one of adulthood
(A, D, E, G-J) Dot plots, dots represent the mean values of biologically independent experiments. Error bars represent SEM. ns p=0.1234, *p=0.0332, **p=0.0021, ***p=0.0002, ****p<0.0001. Two-way ANOVA analysis. (A) ctrl n=301, *del-4(tm717)* n=405, n= number of cell bodies, (B) ctrl n=172, *del-4(tm717)* n=170, *dat-1(tm903)* n=170, *cat-2(31112)* n=100. n represents number of animals. (C) ctrl n=120, *del-4(tm717)* n=120, DEL-4::GFP n=120, n= number of animals (D) ctrl n=494, *del-4(RNAi)* n=618, *snt-1(RNAi)* n=594, n=number of neuronal cell somas, (E) ctrl n=21, *del-4(tm717)* n=26, DEL-4::GFP n=22, *goa-1(e407)* n=21, n represents number of animals . (F) ctrl n= 80, *del-4(tm717)* n=80, DEL-4::GFP n=80, *unc-49(3407)* n=20, n= number of animals. (G) ctrl n=30, *del-4(tm717)* n=34, n=number of animals (H) ctrl n=272, *del-4(tm717)* n=322, n=number of GFP::SNB-1 positive puncta counted from 30 ctrl and 34 *del-4(tm717)* animals, (I) ctrl n=482, *del-4(tm717)* n=646, n=number of NLP-21::YFP positive puncta counted from 25 ctrl and 31 *del-4(tm717)* animals, (J) ctrl n=20, *del-4(tm717)* n=35.

depletion results in reduced basal levels of synaptic release at the cholinergic NMJ, compared to wt (Figure 12D). To verify that the decreased cholinergic neurotransmission at the NMJ is due to a presynaptic defect, we used a combination of aldicarb and levamisole resistance assays (218). Aldicarb is a cholinesterase inhibitor that causes paralysis as a result of acetylcholine (ACh) accumulation at the synaptic cleft. Levamisole is a nicotinic receptor agonist that paralyzes animals because of continued muscle stimulation. The levamisole resistance assay specifies whether the site of a defect observed with the aldicarb resistance assay lies within the pre- or postsynaptic cell (218). We practiced the aldicarb resistance assay with one-day adult wt, *del-4(tm717)*, DEL-4 overexpressing (p_{del-4}DEL-4::GFP) animals, and *goa-1(sa734)* aldicarb hypersensitive mutants that served as a positive control. We placed the animals in a 15 μl drop of 10mM aldicarb and measured the time to paralysis. *del-4* mutants were resistant to the paralytic effects of aldicarb whilst animals overexpressing DEL-4 were sensitive, compared to wt (Figure 12E). In the levamisole resistance assay, besides *del-4* mutants and overexpressing animals, we also employed *unc-49(e382)* levamisole hypersensitive mutants as positive control. However, DEL-4 depletion or overexpression did not alter the resistance of animals to levamisole (Figure 12F). These results indicate a presynaptic defect at the NMJ upon DEL-4 downregulation, causing a reduction in ACh synaptic release.

Subsequently, we sought to investigate the effects of DEL-4 depletion on GABAergic neurotransmission. DEL-4 is not expressed in GABAergic motor neurons. Therefore, we anticipated that alterations in GABAergic neurotransmission would rely solely on dopaminergic signalling. We cross-fertilized *del-4(tm717)* mutants with animals carrying a GFP marker of synaptic vesicles (SVs) expressed under the specific for GABAergic motor neurons *unc-47* promoter (p_{unc-47}GFP::SNB-1). Fluorescent tagging of synaptic vesicle-associated proteins can accommodate the estimation of vesicle density at presynaptic sites (199). We quantified SVs at presynaptic elements of the dorsal nerve cord at the turn of the posterior gonadal arm. We measured the number of puncta per 10μm and the mean puncta intensity of the neuron. Notably, *del-4* mutants exhibit increased SV density in GABAergic motor neurons compared to the control (Figure 12G, H, and K). This result indicates a dopamine-dependent increase in GABAergic motor neuron signalling upon DEL-4 downregulation or an accumulation of GABA at the presynaptic site. The activation of inhibitory motor neurons combined with the reduced cholinergic motor signalling explain the moderate locomotor activity of the *del-4* strain in the BSR.

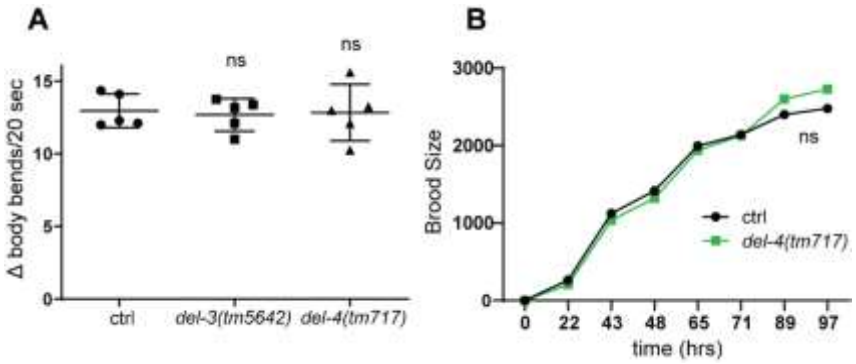

Figure 13. Degenerins DEL-3 and DEL-4 do not mediate serotonergic signalling.

(A) Enhanced slowing response of wt, *del-3(tm5642)* and *del-4(tm717)* mutants. *del-3* and *del-4* mutant animals display the same phenotype as the control nematodes. Dot plot, dots represent the ratio Δ body bends/20sec of independent biological experiments. Δ body bends/20sec corresponds to body bends/20sec on an empty plate minus body bends/20sec on a plate with food. In every independent biological replicate of each BSR experiment, 9-14 animals were tested. One-day adult animals were used in all experiments**.** Error bars represent SD.

(B) The mutant *del-4(tm717)* displays physiological brood size. The number of eggs laid by control wild-type N2 animals and *del-4(tm717)* mutants was counted. The measurements were obtained for the first four days after adulthood. Animals were placed on 2cm OP50-seeded NGM plates (one animal/plate) and were transferred to a new NGM every day. Plates were placed at 4ºC to avoid hatching and then the number of eggs laid per day for each genotype was counted. Plotted is the mean number of eggs laid by each genotype.

(A, B) Non-significant (ns) p=0,1234, *p=0,0332, **p=0,0021, ***p=0,0002, ****p<0,0001. Two-way ANOVA.

(A) ctrl n=57, *del-3(tm5642)* n= 56, *del-4(tm717)* n=56, n represents the number of animals, dots represent the number of biological replicates.

(B) ctrl n=1, *del-4(tm717)* n=1, n= number of worms, brood size corresponds to number of eggs.

Apart from neurotransmitters, neurons release neuropeptides packed into dense core vesicles (DCVs) throughout the neuronal cell soma, axons, and dendrites. Former studies described the evaluation of released DCVs levels via a YFP reporter of NLP-21 neuropeptide expressed under *unc-129* promoter (198). Applying this reporter, we studied the levels of DCVs alongside cholinergic motor neurons of the dorsal neural cord. We assessed DCVs release by calculating the mean intensity ratio of the axon to coelomocytes since coelomocytes retrieve released NLP-21::YFP (198). We cross-fertilized the DCVs reporter with *del-4(tm717)* strain and performed high magnification confocal imaging. We determined the number of DCVs in the dorsal neural cord cholinergic motor neurons and did not observe any difference between *del-4* and control animals (Figure 12I, J, and L). We measured the puncta

dorsally close to the turn of the posterior gonadal arm. These results suggest that DEL-4 specifically affects signalling through SVs but not through DCVs.

Collectively, the aforementioned findings support the notion that DEL-4 depletion decreases dopaminergic signalling, with an ultimate impact on downstream motor neuron neurotransmission and locomotory behaviour.

DEL-4 does not participate in serotonergic signalling

Having in mind the expression of DEL-3 and DEL-4 in the NSM serotonergic neurons (Figure 4B and C), we decided to utilize the enhanced slowing response assay (ESR), an assay similar to the basal slowing response with the difference that it requires 30min starvation before the assay. Sawin et al. (32) presented that when nematodes encounter food reduce their locomotory rate (BSR). Starvation for 30min on an empty unseeded NGM plate enhances this slowing reaction and produces the enhanced slowing response (ESR). ESR necessitates proper serotonin biosynthesis levels and constitutes an assay for estimating the functionality of the serotonergic signalling pathway. We measured the ESR of wild-type and mutant animals for the *del-3* and *del-4* genes (*del-3(tm5642)* and *del-4(tm717)*) and observed no statistically significant difference between the three genotypes (Figure 13A). To further verify this result, we estimated the egg-laying behaviour of *del-4* mutant animals and measured their brood size. Serotonergic signalling mediates egg-laying through a neuronal circuit that consists of the two serotonergic HSN neurons, found in the animal's midbody, and six cholinergic ventral C neurons that synapse with vulval muscle cells (236-238). In accordance with the previous result, *del-4(tm717)* mutants display the same brood size as wild-type animals (Figure13B). Therefore, DEL-3 and DEL-4 do not mediate serotonergic signalling. To shed light on the mechanism through which DEL-4 modulates neuronal function we subsequently investigated the physiological characteristics of a putative DEL-4 channel.

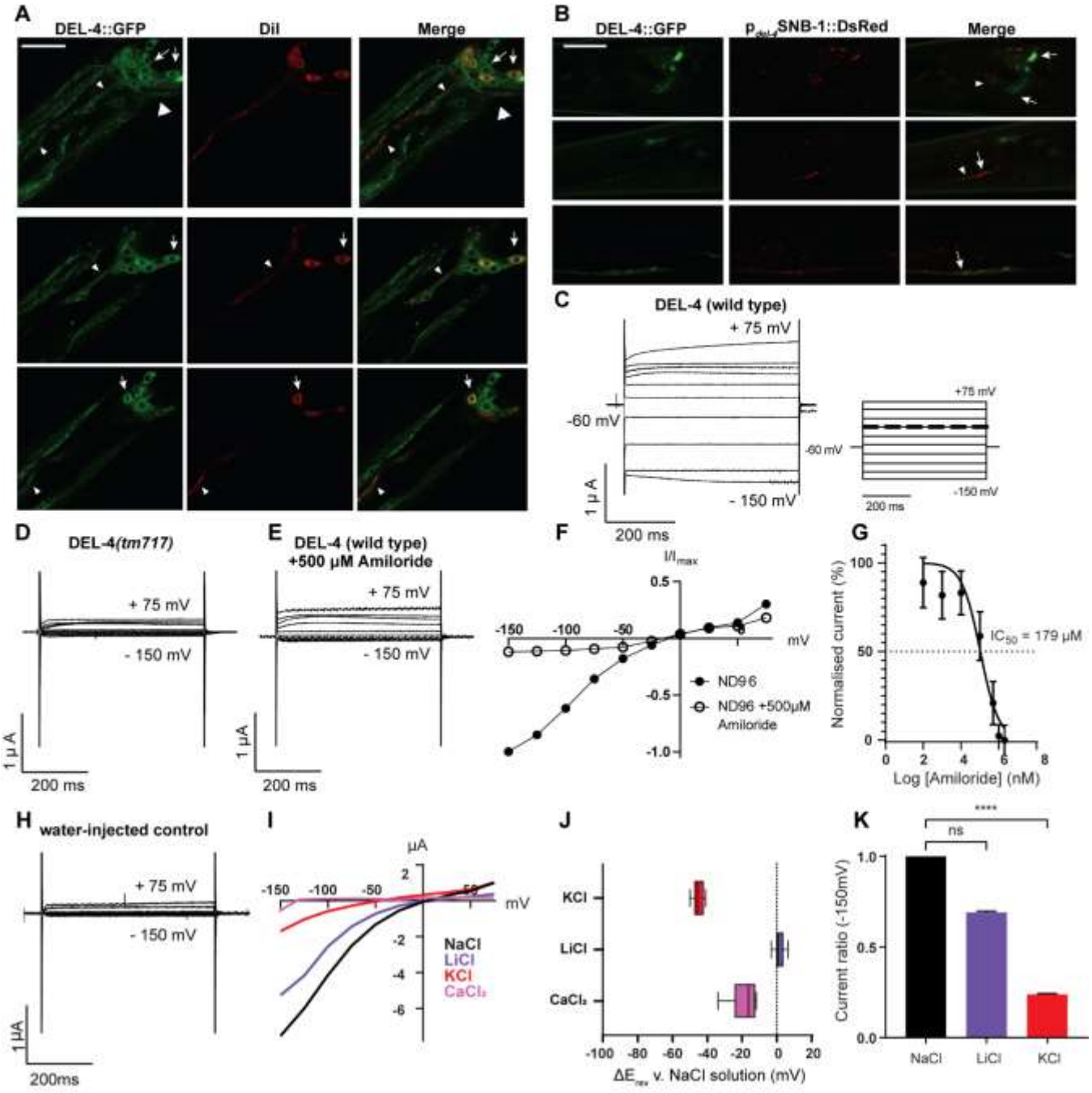

Figure 14. Subcellular localization, ion selectivity, and amiloride sensitivity of the homomeric DEL-4 channel.

(A) Membranous localization of DEL-4 on neuronal cells. DEL-4 localizes to the cytoplasmic membrane of neuronal cells. The DEL-4 translational reporter colocalizes with DiI staining (KRT) on the surface of neuronal cell bodies and processes. Left: the *del-4* promoter drives the expression of DEL-4 tagged with GFP. Middle: DiI staining is seen in red. Right: merged images. We utilized the merged images of z-stacks (2nd and 3rd row) to assess colocalization. The images in the 1st row constitute maximum intensity projections. Neuronal cell bodies

Figure 14. Contibued.

(arrows), dendrites (small arrowheads), and axons (large arrowhead) are indicated. Left is anterior. One-day adult animals. Left is anterior. Scale bar 20 μM. Confocal images with a 63x lens.

(B) Co-expression of DEL-4::GFP and SNB-1::DsRed driven by the same promoter (*del-4* promoter) revealed only random cases of colocalization. Left, expression of DEL-4 tagged with GFP in neurons driven by the *del-4* promoter ($p_{del\text{-}4}$DEL-4::GFP). Middle, *del-4* promoter drives the expression of *snb-1* (seen in red) in neurons ($p_{del\text{-}4}$SNB-1::DsRed. Right, merged images. Confocal images (Z-stacks). Lens 63x. Arrows indicate random cases of colocalization. Arrowheads indicate sites where DEL-4 and SNB-1 do not colocalize. We utilized merged z-stack images to assess colocalization. Left is anterior. Scale bar 20 μm.

(C) DEL-4 subunits assemble into a constitutively open homomeric channel at neutral pH 7.4 that conduct current.

(D) Oocytes injected with the DEL-4 protein product of the mutant *del-4(tm717)* do not exhibit transient currents at neutral pH when perfused with sodium rich solution.

(E) DEL-4 currents at neutral pH are blocked by 500 μM amiloride (Star methods).

(F) Amiloride inhibits the DEL-4 channel. Current-voltage (I-V) relationships for *Xenopus* oocytes injected with *del-4* cRNA, following perfusion of oocytes with a physiological NaCl solution (1X ND96) (black circles), and in the presence of 500 μM of the DEG/ENaC channel blocker amiloride (open circles) (n = 10). Voltage steps were from – 150 mV to +75 mV, from a holding potential of -60 mV.

(G) Blocking of the DEL-4 homomeric channel by amiloride is dose-dependent. The normalized (I/Imax) current of the amiloride dose-response curves for the DEL-4 homomer revealed a half-maximal inhibitory concentration (IC_{50}) of 179 μM (LogIC50 = 4.61) (n = 5), as denoted by the dashed line. Currents were recorded at a holding potential of -60mV, normalized to maximal currents, and best fitted with Hill's equation (nonlinear fit log (inhibitor) vs. normalized response – variable slope) in GraphPad Prism.

(H) Water-injected oocytes used as negative controls do not exhibit transient currents at neutral pH when perfused with sodium-rich solution.

(C-E,H) Representative transient currents in a *Xenopus* oocyte injected with *del-4* cRNA or *del-4(tm717)* cRNA or nuclease-free water and perfused with a physiological NaCl solution (ND96) at pH 7.4, in the absence (C, D, H) or presence (E) of 500 μM amiloride. The voltage steps applied were from -150 mV to +75 mV from a holding potential of -60 mV.

(I, J) Representative normalized current-voltage (IV) relationships for *Xenopus* oocytes expressing DEL-4. The raw current for each oocyte and the leak current were subtracted at pH 7.4. We calculated the average ΔE_{rev} of 9 oocytes for each construct when shifting from a NaCl solution to a KCl, LiCl, or $CaCl_2$ solution. The interpolated curves displayed a shift in the reversal potential ΔE_{rev}. Replacement of NaCl with equimolar LiCl did not shift the reversal potential ($E_{rev(Na/Li)}$= -1.18 ± 0.93 mV), but replacement with equimolar KCl resulted in a reversal potential shift ($E_{rev(Na/K)}$= 43.45 ± 1.86 mV) $E_{rev(Na/Ca)}$ 31.24 ± 7.77 mV (N=10). A negative shift in E_{rev} indicates a preference for Na^+ over the respective ion, and a positive shift indicates a preference for the respective ion over Na^+. Data are presented as median and interquartile range (IQD), calculated using the Tukey method.

(K) The DEL-4 channel is permeable to monovalent cations (Na^+, Li^+), as established by determining the ratio of the current at -150 mV when perfusing oocytes with NaCl, LiCl, or KCl solutions (n = 10).

DEL-4 is a proton-gated sodium channel on neuronal cell membrane

To assess whether the subcellular localization of DEL-4 fits the known pattern of transmembrane channels, we labelled animals expressing the DEL-4::GFP with the lipophilic dye DiI. DiI stains the membranes of amphids, phasmids, and chemosensory neurons with nerve endings exposed to the environment (Table 4). Confocal imaging at high magnification revealed the colocalization of DEL-4 with DiI and its membranous localization (Figure 14A). To further examine the DEL-4 site of action on neuronal membrane, we co-expressed DEL-4::GFP with SNB-1::DsRed, a synaptic vesicle marker, under the control of the *del-4* promoter. Despite their partial colocalization, the two reporters showed distinct expression patterns (Figure 14B). DEL-4 has a broader expression pattern, expands throughout cell somas and neuronal processes, and does not exhibit a punctate distribution similar to SNB-1. Therefore, we conclude that DEL-4 is not exclusively located in synaptic regions.

Channels of the diverse DEG/ENaC family consist of three subunits. In mammals, ENaCs form heterotrimeric channels, whereas ASICs are both heterotrimeric and homotrimeric (139, 239). As indicated above (figures 5 and 6) DEL-2, DEL-3, and DEL-4 colocalize in some neurons but are not co-expressed in every neuron they localize. The subunit composition modifies the biophysical properties of the channel (240). ENaCs are highly selective for Na^+ and Li^+ ions (144). ASICs exhibit a weak preference for Na^+ and Li^+, but are also permeable for K^+ and in some cases Ca^{2+} ions (241). We have previously shown that DEL-4 is a constitutively open channel mediating inward Na^+ current at neutral pH (209). To further characterize DEL-4 channels' physiological properties, we implemented a two-electrode voltage clamp (TEVC) in *Xenopus laevis* oocytes, ectopically expressing either the wild-type protein DEL-4 or the protein product of the *del-4* mutant and nuclease-free water-injected oocytes as negative control (Figure 14C, D, H, and 15A). The truncated protein, that emerges from the *del-4* mutant, was translated in frame from the N' terminus up to a small part of the extracellular loop, comprising the first cytoplasmic domain at the N' terminus, the first transmembrane domain, and the whole post-M1 domain (Figure 2A). We perfused oocytes with a sodium-rich solution (1XNDN96, see Methods) and recorded the currents produced by stepping the membrane voltage from -150 mV to +75 mV, from a holding potential of -60 mV (Figure 14C). Amiloride, a common blocker of DEG/ENaC channels, abolished these currents in a dose-dependent manner, with an IC_{50} of 179 μM (Figure 14E-G). The truncated DEL-4 product did not elicit currents similar to the nuclease-free water-injected control (Figure 14D, H). The latter suggests that the missing parts of the protein are either responsible for the Na^+ currents or the trafficking of the protein to the plasma membrane. Next, we investigated ion

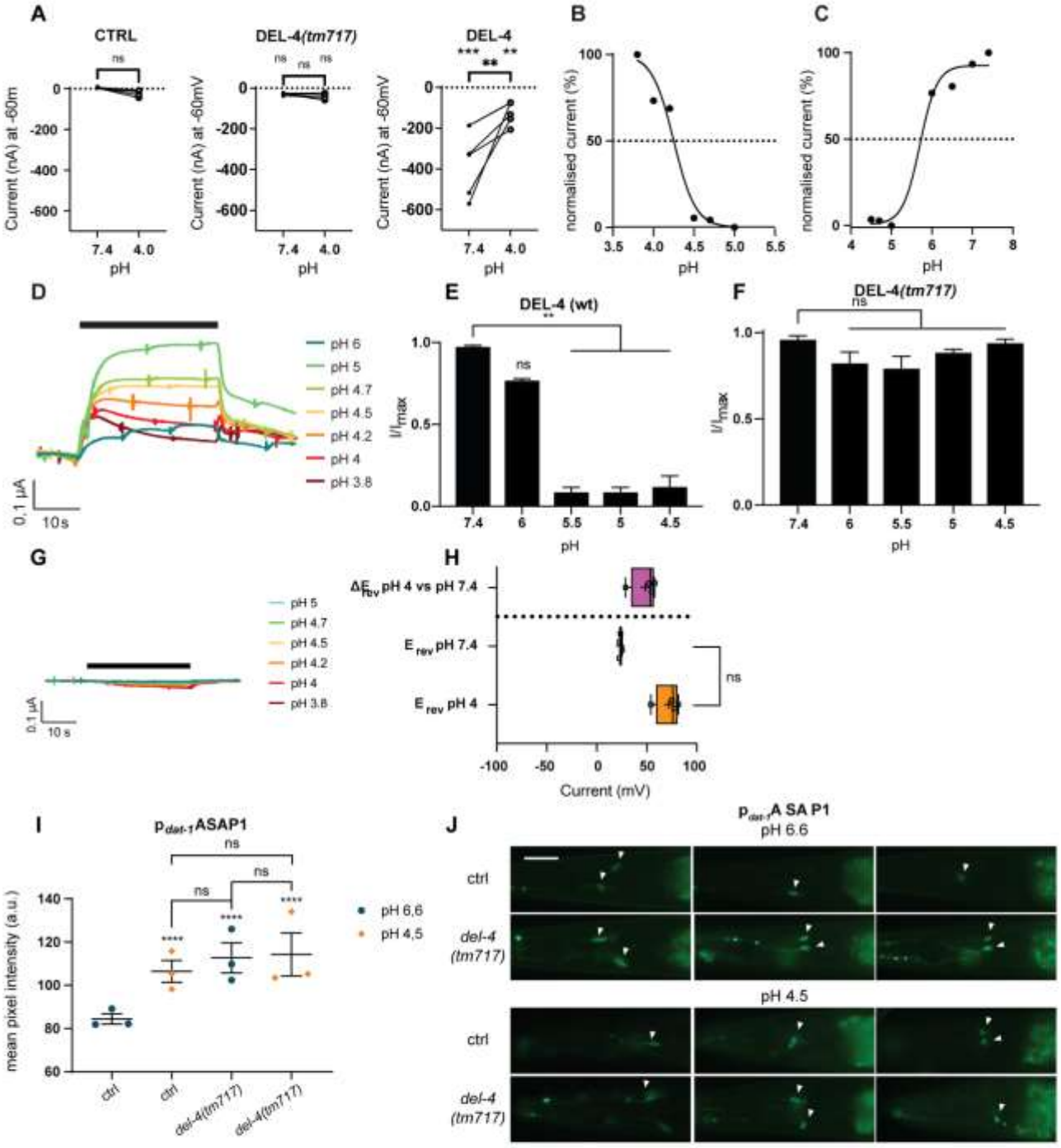

Figure 15. Acidic pH blocks the homomeric DEL-4 channel and hyperpolarizes dopaminergic neurons, similar to DEL-4 depletion

(A) DEL-4 currents at neutral pH are inhibited at pH 4. Currents of the nuclease-free water-injected controls and the truncated DEL-4(tm717) mutant currents are not blocked by acidic pH 4. Graphs show raw current upon perfusion with either pH 7.4 (filled circle) or pH 4 (open circle), as indicated for *Xenopus* oocytes injected with

Figure 15. Continued.

the DEL-4 *wild-type* or *tm717* mutant or water-injected controls. Lines connect data from individual oocytes. (n = (from left to right) 5, 5, 6) Currents were recorded at a holding potential of -60mV.

(B, C) Extracellular protons inhibit the DEL-4 homomeric channel. Current to pH relationships of heterologously expressed DEL-4 homomeric channel, when perfused with solutions of increasing pH starting from 3.8 until 7.5 (n = 5). The channel is fully open at 100% current and closed at 0% current. Amount of total DEL-4 cRNA (500 ng/µl) injected. Only the mean values are presented. The voltage steps were from -150 mV to +75 mV from a holding potential of -60 mV. Currents were recorded at a holding potential of -60mV, normalized to maximal currents, and best fitted with Hill's equation in GraphPad Prism.

(D) Representative traces of DEL-4 expressing *Xenopus* oocytes when perfused with ND96 solution at various proton concentrations from a neutral baseline (pH 7.4). Currents were recorded at a holding potential of -60mV, and traces were baseline-subtracted and drift-corrected using Roboocyte2+ (Multichannels) software.

(E, F) Low pH in the range of 4.5-5.5 blocks the DEL-4 homomeric channel. Heterologously expressed DEL-4 channel, perfused with solutions of increasing pH starting from pH 4.5 to 7.5 (n = 5). Currents were recorded at a holding potential of -60mV, normalized to maximal currents (I/I_{max}), Kruskal-Wallis test and post-hoc Dunnett's multiple comparisons test found no significant difference in current ratio for the DEL-4(*tm717*) mutant controls, but DEL-4 wild-type currents were significantly blocked at low pH (n = 5 each). Amount of total cRNA (500 ng/µl) injected for each construct. Error bars represent Mean and SEM.

(G) Representative traces of water-injected *Xenopus* oocytes used as controls of DEL-4 expressing oocytes when perfused with ND96 solution at various proton concentrations from a neutral baseline (pH 7.4). Currents were recorded at a holding potential of -60mV, and traces were baseline-subtracted and drift-corrected using Roboocyte2+ (Multichannels) software.

(H) DEL-4 is not permeable for protons. Summary of reversal potential E_{rev} of DEL-4 expressing oocytes and controls (DEL-4(tm717) mutant and water-injected oocytes) when perfused with basal pH 7.4 (cyan) and acidic pH 4 (orange) (top to bottom, n= 6, 8, 3). Low pH did not statistically significantly change the E_{rev} as assessed by a paired Wilcoxon test (top to bottom, p=0.094, ns; p=0.844, ns; p =0.750, ns). DEL-4(tm7171) and water-injected controls have significantly lower currents which might contribute to higher variability. Data are presented as boxplots with median (dash), mean (cross), and min and max error bars. E_{rev} was calculated as described in the methods.

(I) Low pH enhances the intensity of ASAP1 in dopamine-releasing neurons. Quantification of resting membrane potential using a line expressing the genetic voltage indicator ASAP1 in dopaminergic neurons using the dat-1promoter. Control and *del-4(tm717)* mutant animals were imaged on day 2 of adulthood under control conditions and after acidic stress. Absence of DEL-4 and acidification increase ASAP1 fluorescence intensity, thus hyperpolarizing dopaminergic neurons. Mean pixel intensity was measured from cell bodies of dopaminergic neurons. Fluorescence intensity measurements of ASAP1 after 15 min incubation in M13 solution of pH 6.6 (ctrl) or pH 4.5, generated with $CH_3COOHNa$ (pH). The incubation time was followed by a recovery time of 10 min in

Figure 15. Continued.

M13 pH 6.6, to recover GFP fluorescence that quenched due to the pH sensitivity of GFP. Error bars represent the SEM. ns p=0.1234, *p=0.0332, **p=0.0021, ***p=0.0002, ****p<0.0001. Two-way ANOVA analysis. Dot plot, dots represent the mean fluorescence of biological replicates. ctrl pH 6.6 n=263, ctrl pH 4.5 n=216, *del-4(tm717)* pH 6.6 n=307, *del-4(tm717)* pH 4.5n=317. n= number of dopaminergic neuron cell somas.
(J) Representative images of dopaminergic neurons expressing ASAP1 ($p_{dat\text{-}1}$ASAP1) in control and *del-4(tm717)* mutant animals under control or acidic stress conditions. Top, pH 6.6, bottom, pH 4.5. Scale bar 20 μm. Lens 20x. Left is anterior. See also Figure S6.

selectivity by carrying out ion substitution experiments. DEL-4 homomeric channel is permeable to monovalent cations, preferentially to Na^+ (selectivity sequence: Na^+=Li^+>K^+>Ca^{2+}) but appears to be Ca^{2+} impermeable, at least in the *Xenopus* oocytes expression system (Figure 14I-K). These results revealed that DEL-4 subunits can form a homomeric channel in *Xenopus* oocytes. This channel localizes on the plasma membrane of neuronal cells, is blocked by amiloride in a dose-dependent manner, and is highly permeable to Na^+ and Li^+.

DEG/ENaC family members create sodium channels that are either constantly activated or gated by mechanical stimuli, peptides, or protons (242). DEL-4 was previously shown to be a constitutively open channel at neutral pH and significantly inhibited by extracellular acidity (209) (Figure 15A). To further determine the DEL-4 homomeric channel's properties, we perfused DEL-4 expressing *Xenopus* oocytes with solutions of gradually reduced pH, starting from a baseline of pH7.4. DEL-4 expressing oocytes showed a maximal current at around pH5 that was inhibited by both high and lower pH, with pH_{50S} of 5.78 and 4.25 (Figure 15B-E). The truncated control and the water-injected control oocytes do not show this inhibition with decreased pH (Figure 15A, F, G). DEL-4 was not permeable to protons, as the ΔE_{rev} did not show a statistically significant shift when extracellular proton concentration was increased from neutral pH to pH4 (Figure 15H). It is likely that the pH_{50S} reflects the physiological range similar to what has been described for all the DEG/ENaC members, such as the nematode ACD-5 or the human ENaCs. Their pH responses presumably reflect the environmental contexts meaning the intestinal luminal membrane or epithelia, respectively, where they are expressed (209, 243). Therefore, inhibition of the DEL-4 homomeric channel by protons emerges in the limited range of pH 4.5-5.5, and this function is lost in the *del-4* mutant, which is incompetent to conduct current in *Xenopus oocytes*.

Blocking a sodium channel in neurons may disrupt ion balance along the plasma membrane since Na^+ stops entering the cytoplasm. Thus, the cytoplasmic membrane becomes more negatively charged,

reducing the likelihood of an action potential. To verify this hypothesis, we used the genetically encoded voltage-indicator, ASAP1 (Table 5), expressed in dopaminergic neurons. Changes in the membrane potential cause conformational changes in ASAP1, which lead to an increase in fluorescence upon hyperpolarization and a decrease in depolarization events (195). As shown previously, DEL-4 is inhibited by extracellular low pH (Figure 15A-E). Interestingly, treatment of ASAP1 reporter animals with low pH buffer leads to neuronal hyperpolarization in the presence of DEL-4 (Figure 15I, J). Similarly, *del-4* mutant animals displayed elevated levels of ASAP1 fluorescence compared to control animals under neutral pH conditions, whilst acidification did not affect the membrane potential of *del-4* mutants (Figure 15I, J). Therefore, both extracellular acidification and DEL-4 channel deficiency hyperpolarizes the dopaminergic neurons *in vivo*, following our *in vitro* data.

DEL-4 participates in low pH sensory detection and modulates behavioural responses to stress

Given DEL-4's ability to block Na^+ currents upon extracellular acidification, we wanted to test the behavioural response of control and *del-4* mutant animals upon encountering a low pH environment. To this end, we performed a drop test assay, where the backward movement of animals upon contact with a drop of acidic buffer was monitored and quantified. This behavioural response is considered as avoidance to low pH stimulus. We challenged the animals with solutions of pH 2.2, 4.5, or 6.6. We observed that animals lacking DEL-4 were insensitive to pH 4.5 but not 2.2 or 6.6. By contrast, wt animals and animals that overexpress DEL-4 responded to all different buffers (Figure 16A). This finding indicates that the closure of DEL-4 mediates the behavioural response to low pH stimuli.

Having established that DEL-4's ability to conduct current is affected by pH (Figure 15A-E) and that blocking of Na^+ influx through DEL-4 leads to neuronal hyperpolarization (Figure 15I, J), we sought to identify whether heat shock (HS) and long-term starvation (LTSt) could affect neuronal membrane potential in the presence or absence of DEL-4. Towards this direction, we utilized the reporter animals expressing ASAP1 in dopaminergic neurons and subjected them to prolonged starvation, thermal stress, or acidic stress (Figure 16B-D). We found that all tested types of stress lead to hyperpolarization of dopaminergic neurons when DEL-4 is present. Interestingly, in the absence of DEL-4, neuronal membrane potential is not altered any further, than the state of the unstressed mutant, an effect that is also obvious upon DEL-4 depletion alone (Figure 16B-D). Since starvation and heat stress limit the expression of DEL-4 (Figure 7A, E), whilst acidic stress blocks the channel's pore (Figure 15A-E), we propose that different types of stress may hyperpolarize dopaminergic neurons by

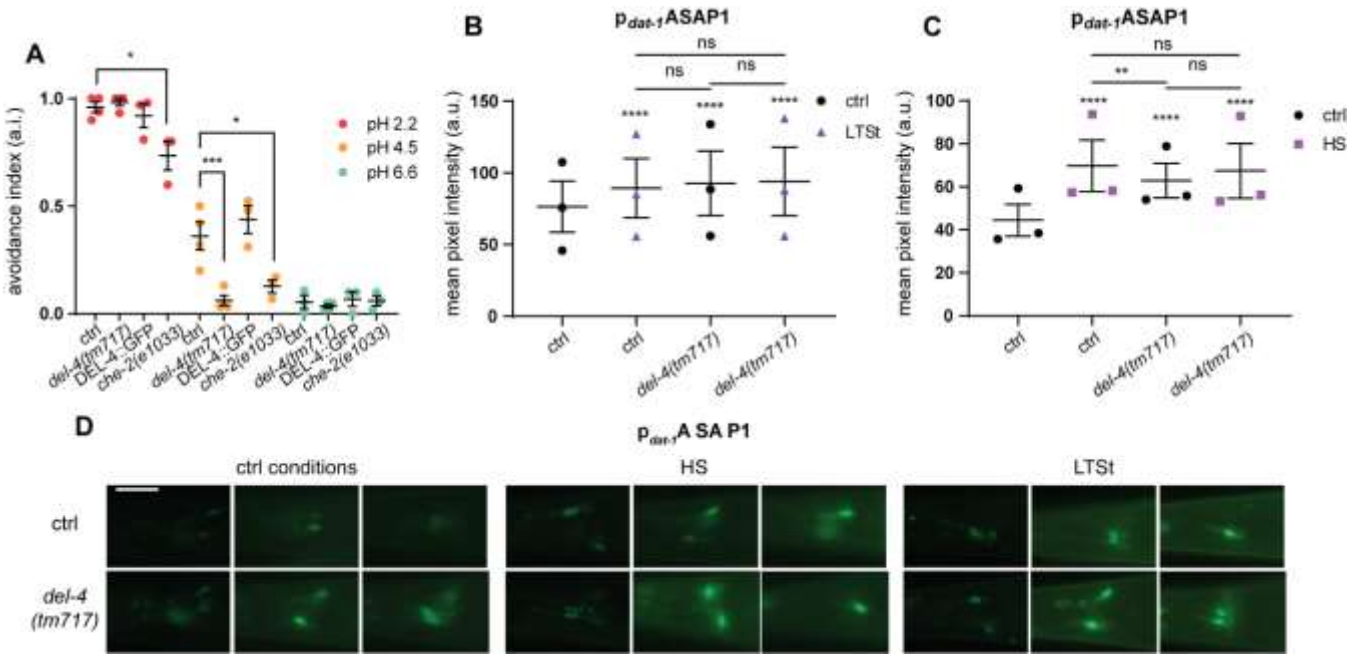

Figure 16. Dopaminergic neurons hyperpolarize upon heat stress and starvation.

(A) Graph of avoidance index to M13 solutions of diverse pH values. We measured the responses of wt, *del-4(tm717)*, DEL-4::GFP, and *che-2(e1033)* (Tables 1 and S4) animals in the drop test assay. A drop of M13 buffer was applied with a syringe at the tail of each animal and a backward movement was accounted as avoidance. An avoidance index of 1 represents complete avoidance to the M13 solution, and 0 represents a total lack of avoidance response. The *che-2(e1033)* strain was used as a positive control. Animals were tested on day one of adulthood.

(B, C) Quantification of resting membrane potential using the line expressing ASAP1 in dopaminergic neurons. The voltage indicator ASAP1 was expressed under the *dat-1* promoter. Control and *del-4(tm717)* mutant animals were imaged on day 2 of adulthood under control conditions or after stress (Star methods). The absence of DEL-4, LTSt, and HS increase ASAP1 levels, thus hyperpolarizing dopaminergic neurons. The mean pixel intensity was measured from the neuronal cell bodies.

(B) Long-term starvation (LTSt) hyperpolarizes dopaminergic neurons, similar to the *del-4(tm717)* mutant. We estimated the intensity levels of ASAP1 in control and *del-4(tm717)* animals after long-term starvation for 24 hrs on unseeded NGM.

(C) The fluorescence of ASAP1 in dopaminergic neurons increases in the *del-4(tm717)* mutant and upon heat stress (HS). We calculated the intensity levels of ASAP1 in dopaminergic neuronal somas from control and *del-4(tm717)* animals after thermal stress for 1 hr at 37ºC.

(D) Representative images of dopaminergic neurons expressing ASAP1 in control and *del-4(tm717)* mutant animals under control or stress conditions. Scale bar 20 μm. Lens 20x. Left is anterior.

Error bars represent SEM. ns p=0.1234, *p=0.0332, **p=0.0021, ***p=0.0002, ****p<0.0001. Two-way ANOVA analysis. Dot plots, dots represent the mean of independent biological experiments (A) ctrl pH 2.2 n=79, ctrl pH 4.2 n=118, ctrl pH 6.6 n=104, *del-4(tm717)* pH 2.2 n=107, *del-4(tm717)* pH 4.5 n=125, *del-4(tm717)* pH 6.6 n=113, DEL-4::GFP pH 2.2 n=106,, DEL-4::GFP pH 4.5 n=80, DEL-4::GFP pH 6.6 n=123, *che-2(e1033)*

Figure 16. Contibued.

pH 2.2 n=108, *che-2(e1033)* pH 4.5 n=93, *che-2(e1033)* pH 6.6 n=104. n represents the total number of responses (positive and negative) counted in all experimental repeats. (B) ctrl ctrl n=197, ctrl LTSt n=212, del-4(tm717) ctrl n=189, and del-4(tm717) LTSt n=260. (C) Three trials, ctrl ctrl n=177, ctrl HS n=180, *del-4(tm717)* ctrl n=213, and *del-4(tm717)* HS n=186. (B, C) n represents number of dopaminergic neuron cell somas.

either reducing DEL-4 levels or by inhibiting conductance of current through DEL-4 channel. These findings put DEL-4 at the epicentre of stress stimuli sensation and integration.

DEL-4 mediates gustatory stimuli

To further investigate the sensory role of degenerins DEL-2, DEL-3, and DEL-4, we performed several behavioural assays regulated by specific neurons and screened for defects in common *C. elegans* behaviours such as egg laying and social feeding. By exploiting these assays, we tried to estimate DELs participation in the functionality of the neurons they are expressed, through affecting behaviours regulated by these neurons. In search of stimuli that DELs may convey, we assessed their role in BS locomotory behaviour. The basal slowing response has been formerly described to be mediated by mechanical stimuli (32). To identify whether the strengthened basal slowing response of del mutants is due to gustatory or mechanical stimuli, emerging from the bacteria, we replaced bacteria with sterile Sephadex G-200 beads. Sephadex beads create a three-dimensional matrix that resembles the bacterial lawn but lacks its gustatory cues. In the presence of beads, wild-type animals exhibit normal basal slowing response (32). Similarly, *del-3(tm5642)* and *del-4(tm717)* mutant animals exerted regular basal slowing compared to wt (Figure 17A) on the matrix generated by the beads. According to this result, gustatory stimuli are responsible for the augmented slowing, in the presence of food, of the del mutants. This implies that it is not the basal slowing response per se that is affected in del mutants. Instead, DEL proteins affect *C. elegans* locomotion, also mediated by dopamine but due to gustatory stimuli. Therefore, we searched for behaviours controlled by the presence of food or other gustatory stimuli that implicate DEL-expressing neurons.

Social feeding is a well-characterized behaviour regulated by sensory neurons such as the nociceptive neurons ASH and ADL. ASH and ADL are necessary for social feeding versus solitary (244). The two phenotypes that emerge, the social and the solitary, depend on the genetic variation of neurotransmitter receptor genes. Solitary-feeding worms move swiftly throughout the bacterial lawn

while social move slowly and aggregate at the thick tip of the bacterial lawn. Solitary and social feeding constitute two opposite behaviours found in nature physically. A natural genetic variation only in one residue of NPR-1, a neuropeptide Y receptor homolog, results in this behavioural variation (204). Other identified polymorphisms to contribute to this behaviour involve the genetic loci of the GABA neurotransmitter receptor EXP-1 and the neuroglobin GLB-5 (294). Mutant *del-4* worms display solitary behaviour similar to the wild-type laboratory strain Bristol (N2) (Figure 17B).

The types of food and food perception regulate food leaving rates and navigational strategies (245-247). In general, wild-type hermaphrodites when on a food source remain on it. ASE sensory neurons promote food-leaving behaviour (92, 248). This behaviour depends on the detection of environmental cues such as oxygen, odours, or metabolites and is therefore influenced by a variety of sensory neurons (205, 246, 247, 249-251). We performed the food leaving assay to measure the percent of animals staying on food (Figure 17C). We used wild-type hermaphrodites, *del-3* and *del-4* mutant animals, *DEL-2, DEL-3, and DEL-4* overexpressing animals. In all cases, the food leaving behaviour was the same as that of the control.

C. elegans senses ambient temperature and generates temperature preferences when associates it with favorable conditions. AFD, AWC, and ASI amphid neurons are necessary for temperature perception (252). We performed a thermotaxis assay. To create a radial thermal gradient, we used glass vials filled with frozen glacial acetic acid, allocated at the centre of an NGM plate (figure 17D). Nematodes were placed at approximately 20^{o}C and were expected to migrate towards the temperature they were cultivated with food abundance, in this case, the 25^{o}C. We observed that *del-3(tm5642)* and *del-4(tm717)* mutants could discriminate and move towards the desired temperature relative to wild-type (figure 17E).

Subsequently, we carried out chemotaxis to isoamyl alcohol (207). Isoamyl alcohol is a volatile odorant sensed by AWC neurons at low attractive concentrations (295). Dopamine signalling is necessary upon conditioning with starvation (253). In the chemotaxis assay the nematodes choose between a spot of attractive isoamyl alcohol with anesthetic placed diametrically of a spot of anesthetic alone (figure 17F). Animals overexpressing DEL-4 and mutants for *del-3* and *del-4* could recognize the attractive odour (figure 17G, naive). Additionally, animals from all genotypes tested avoided isoamyl alcohol upon pairing with starvation, similar to controls (Figure 17G, conditioned).

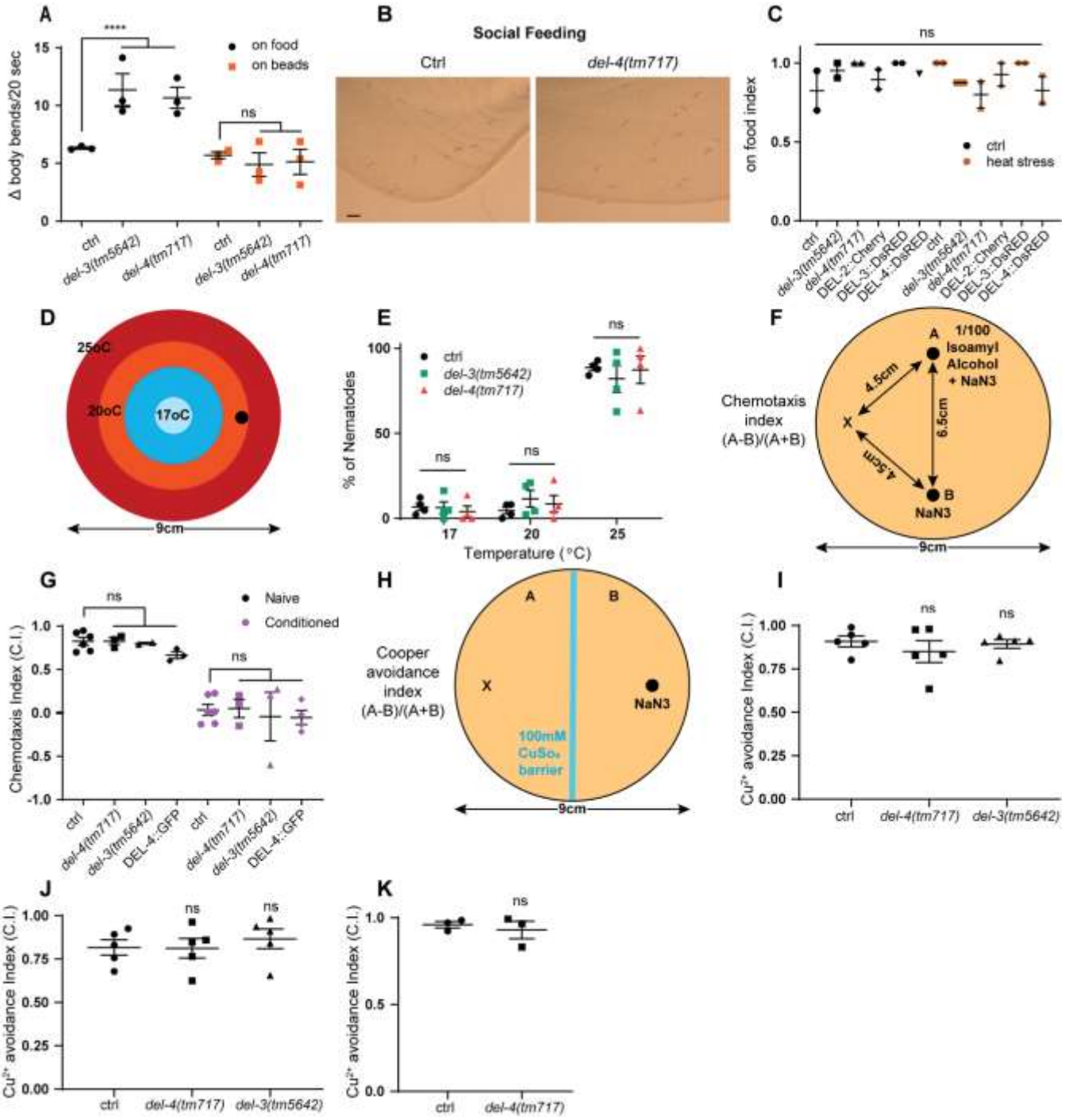

Figure 17. DELs respond to gustatory stimuli.

(A) The effect of DEL-3 and DEL-4 on the basal slowing response depends on gustatory stimuli. BSR of *del-3(tm5642)* and *del-4(tm717)* on NGM plates seeded with HB101 bacteria (on food – black dots) or spread with Sephadex beads (on beads – orange dots). Mutant animals for *del-3* or *del-4* present regular BSR on Sephadex beads compared to wt. Δ body bends/20sec corresponds to body bends/20sec on an empty plate minus body bends/20sec on a plate with food. In every trial of each BSR experiment, 8-15 animals were tested.

Figure 17. Contibued.

(B) DEL-4 mutant animals are solitary, similar to the wild-type. We observed the social behaviour of control and *del-4(tm717)* animals on the bacterial lawn of OP50-seeded plates. In both cases, bordering and clumping behaviours were very close to zero and not statistically different between the two. Scale bar corresponds to 1mm.
(C) DELs do not affect spontaneous food-leaving behaviour upon control and heat stress conditions. Animals overexpressing DEL-2 (DEL-2::Cherry), DEL-3 (DEL-3::DsRED) and DEL-4(DEL-4::DsRED) display the same food leaving behaviour as *del-3(tm5642)*, *del-4(tm717)* mutants and wild type animals. Animals were allowed to move on food for 30min before calculate the food-index. The experiment was repeated upon control conditions and heat stress for 35min at 37ºC. Heat stress (HS) was followed by 30min recovery time. On food index corresponds to the ratio of the number of worms on food minus the number of worms off food by the total number of worms (on and off food).
(D) Schematic of the radial thermotaxis assay plate. A radial thermotaxis is performed on a 9cm assay plate. A radial thermal gradient is formed by placing a glass vial filled with frozen glacial acetic acid at the center of the plate. The melting point of glacial acetic acid is 16.7°C. Therefore, a thermal inclination is formed, starting from 17ºC at the center of the plate and reaching 25ºC at the plate's periphery. The black dot indicates the start point where nematodes are placed.
(E) DELs do not participate in thermosensation or food-temperature association. Mutant animals for *del-3* and *del-4* display the same thermotaxis index as the wild type. *C. elegans* cultivated at a particular temperature with food migrates to the cultivation temperature on thermal gradients. Animals were cultivated at 25ºC and started thermotaxing at ~20ºC. The percent of nematodes in each part of the plate (as indicated with blue, orange, and red in D) was calculated.
(F) Schematic of conditioning to isoamyl alcohol assay plate. Conditioning was performed on 9cm assay plates. The start point of the assay where nematodes are introduced is shown with X. Diluted 1/100 isoamyl alcohol and NaN3 are placed at points A and B, equidistant to point X. After 2.5hrs, the number of worms at each point was counted and chemotaxis index is calculated as (A-B)/(A+B).
(G) DELs do not participate in conditioning to isoamyl alcohol. Mutant animals *del-3(tm5642)* and *del-4(tm717)* and animals expressing DEL-4::GFP display non-significant differences in conditioning isoamyl alcohol with starvation. All naïve animals demonstrate attraction to isoamyl alcohol (IA), and conditioned nematodes associated starvation with the presence of IA and developed an avoidance response to it. Conditioned animals were starved for 90min. The chemotaxis index corresponds to the number of worms around point A minus the number of worms around point B divided by the number of worms in A and B.
(H) Schematic of Cooper avoidance assay plate. Nematodes avoid passing the cooper barrier formed by 20μl 100mM $CuSO_4$ along the diameter of the plate. Worms are placed at one side of the barrier (point X) and are allowed to navigate freely for 1hr. The copper avoidance index is calculated as the fraction of animals that did not cross the Cu^{2+} line minus those that crossed it towards the total number of animals.
(I, J, K) Copper avoidance assay of del mutants upon control conditions (I), oxidative stress (J), and heat stress (K). DELs do not participate in avoidance behavior towards cooper in control conditions or upon stress.

Figure 17. Continued.

(J) To induce oxidative stress, animals were treated for 4hrs before the assay with 8mM Paraquat, spread on OP50-seeded NGM.

(K) For heat stress induction, animals were incubated on OP50-seeded NGM plates at 37ºC for 35 min. Afterward, they were allowed to recover for 35min at 20ºC, before the cooper avoidance assay.

(A, C, E, G, I-K) One-day adult animals were used in all experiments**.** Dot plots, dots represent the mean values of biologically independent experiments. Error bars represent the SEM. n=number of animals. Non-significant (ns) p=0,1234, *p=0,0332, **p=0,0021, ***p=0,0002, ****p<0,0001. (A, C, G, I, J) Ordinary one-way ANOVA analysis. (E) Two-way ANOVA analysis. (K) Unpaired t-test. (A) On food: ctrl n=30, *del-3(tm5642)* n=30, *del-4(tm717)* n=30, On beads: ctrl n=30, *del-3(tm5642)* n=30, *del-4(tm717)* n=30. (C) Ctrl ctrl n=80, ctrl *del-3(tm5642)* n=84, ctrl *del-4(tm717)* n=84, ctrl DEL-2::Cherry n=96, ctrl DEL-3::DsRED n=60, ctrl DEL-4::DsRED n=29, HS ctrl n=80, HS *del-3(tm5642)* n=32, HS *del-4(tm717)* n=70, HS DEL-2::Cherry n=82, HS DEL-3::DsRED n=80, HS DEL-4::DsRED n=46. (E) ctrl n=190, *del-3(tm5642)* n=222, *del-4(tm717)* n=170. (G) Naïve: ctrl n=1202, *del-3(tm5642)* n=499, *del-4(tm717)* n=676, DEL-4::GFP n=301, Conditioned: ctrl n=1893, *del-3(tm5642)* n=198, *del-4(tm717)* n=1013, DEL-4::GFP n=475. (I) ctrl n=837, *del-3(tm5642)* n=787, *del-4(tm717)* n=904. (J) ctrl n=658, *del-3(tm5642)* n=776, *del-4(tm717)* n=741. (K) ctrl n=807, *del-4(tm717)* n=856.

Since it is confirmed that DEL-2, DEL-3, and DEL-4 are found in ASE pair of neurons, we decided to carry out ASE-specific behavioural assays. ASE neurons participate in chemotaxis to water-soluble gustatory stimuli, either attractive like Na^+, Cl^-, cAMP, biotin, lysine or repulsive like Cd^{2+} or Cu^{2+} (45). In addition, ASE neurons are involved in adaptive food-leaving behaviour and sensation of CO_2 (70, 248). We tested *del-3* and *del-4* mutants for chemorepulsion to $CuSO_4$. In the chemorepulsion assay, a cooper barrier (20µl of 100mM $CuSO_4$) is formed along the diameter of a nine-centimeter plate. Worms are placed on the one side of the barrier. Sodium azide (NaN_3) is used as an anesthetic on the other side to retain the worms that pass the barrier (Figure 17H). A chemotaxis index is calculated as the ratio of the worms that have not passed the barrier minus those that have passed it toward the total number of worms used. In this assay, *del-3* and *del-4* mutants perform similarly to the wild-type (Figure 17I).

To test for a possible role of degenerins upon stresses, we performed the copper barrier assay upon heat and oxidative stress (Figure 17J, K). Thirty-five min heat stress at 37ºC followed by 35min recovery at 20ºC or 8mM of Paraquat (N,N′-dimethyl-4,4′-bipyridinium dichloride) supplied on the food for 4hr were applied before the behavioural assay. Worms on each position were counted one hour after placing them on the assay plate. Four-day adult worms were used in this assay. Again, there were not

observed significant differences between the mutants and the wild-type worms at the repulsion assay upon stresses (Figure 17J, K).

Subsequently, we tested for chemoattraction to NaCl. Most amphid and phasmid neurons are chemosensory. In chemotaxis to NaCl one-day adult worms are placed in the middle of a plate containing nematode growth medium separated in two different concentrations of NaCl, one attractive (50mM) and one repelling (1M). Attractive concentration for the nematodes is the one in which they have grown with plentiful food. The percent of the worms in each concentration was calculated 15min after placing them on the assay plate. Wild-type worms migrate towards the attractive concentration. *del-3 and, del-4* mutants were capable of distinguishing between the two concentrations, just like wild-type (Figure 18A). Having established that DELs recognize abrupt changes in NaCl concentration, we performed a conditioning assay to NaClby pairing NaCl with starvation. Again, all animals could discriminate and move towards the preferred NaCl concentration (Figure 18B, naïve) and could associate starvation with NaCl (Figure 18B, conditioned).

Afterward, we tested *del-4* mutants for the recognition of stepwise concentration changes of NaCl in an ASE-specific behavioural assay (Figure 18C-H). Luo et al. showed that animals subjected to genetic or laser ablation of ASE neurons could not perform chemotaxis to NaCl gradient (208). To test for a possible role of degenerins upon stresses, we performed this assay upon control conditions, heat stress, oxidative stress, and starvation. In this assay, the gradient formed extends from 0mM to 50mM of NaCl. Two-day adult worms were initially placed at the 25mM, while the preferred concentration was the 50mM. One hour after placing the worms on the assay plate, we calculated the percent of the worms on the different NaCl concentrations of the gradient. In the case of heat stress and starvation, they were also counted after 2hr on the assay plate since there was no recovery time. Upon control condition and oxidative stress, *del-4* mutant nematodes performed similarly to the wild-type (Figure 18C, D). In contrast, heat stress and starvation caused significant differences between the two genotypes in chemotaxis performance (Figure 18E-H). In both cases, there were more *del-4(tm717)* animals at the preferred concentrations. The differences following heat stress were observed after one hour on the assay plate (Figure 18E) and were strengthened after two hours (Figure 18F). Upon starvation, we observed statistically significant differences at the one-hour measurement (Figure 18G) that were abolished at the 2hrs count (Figure 18H). Thus, *del-4* mutants can discriminate absolute and stepwise changes in NaCl concentration and can associate NaCl concentration with food availability. However, in the absence of DEL-4, we observe a rushing behaviour towards preferred concentrations upon heat

stress and starvation. This behaviour may result from the already activated stress response pathways observed in the *del-4* mutant.

In search of a gustatory que that might be recognized by DELs, apart from protons, we performed a chemotaxis assay to serotonin, another attractive gustatory stimulus (45). We observed limited attraction of *del-4(tm717)* to serotonin, similar to the positive control *che-2(e1033)*. By contrast, DEL-4 overexpressing nematodes and *del-4(tm717)* animals rescued for the *del-4* gene were normally attracted to serotonin (Figure 18I).

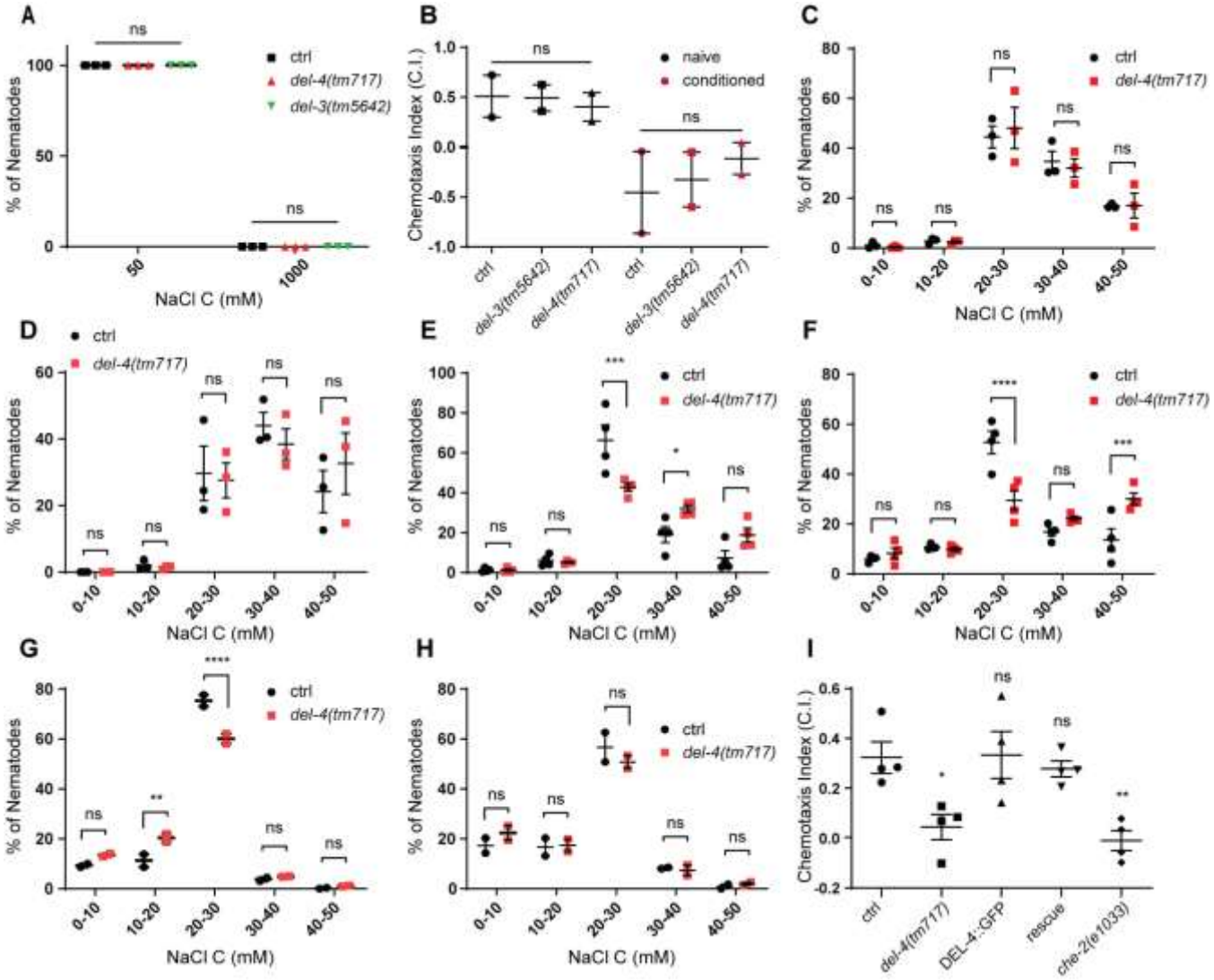

Figure 18. DEL-4 participates in attraction to serotonin and affects NaCl attraction upon heat stress and starvation.

(A) DELs do not participate in the recognition of abrupt changes in NaCl concentration.

Wild-type worms, *del-3(tm5642)*, and *del-4(tm717)* mutants were tested for chemotaxis to NaCl. All nematodes preferred the 50mM NaCl concentration. Half of the NGM medium of the assay plates had an attractive 50mM

Figure 18. Continued.

NaCl concentration, while the other half had a repulsive concentration of 1M. The percent of worms in each compartment of the plate with the two different concentrations was calculated. Day one adult worms were placed in the middle of the plate to start chemotaxis.

(B) DEL mutants recognize gradual changes in NaCl concentration and make associations between food and NaCl concentration. (Left-black dots) Mutants for *del-3* and *del-4* display normal compared to wild-type attraction to NaCl. (Right-red dots) Association of 50mM NaCl with starvation reduces the attraction to NaCl to the same extent for control animals and del mutants. The percent of nematodes in each concentration compartment was calculated.

(C-H) Nematodes performance at linear gradient chemotaxis assay. Wild-type worms and *del-4(tm717)* mutants were tested. Chemotaxis assay (C) upon control condition, (D) oxidative stress, (E, F) heat stress, and (G, H) starvation. Worms were grown at 50mM and started at 25mM. Therefore, they were expected to migrate towards the 50mM NaCl concentration, with the only exception when they were starved at 50mM (G, H). Following starvation animals are expected to travel towards lower concentration. The percent of nematodes in each concentration compartment was calculated after 1hr (C, D, D, G) or 2hrs (F, H) incubation on the assay plate.

(C, D) Control and *del-4(tm717)* mutants display non-significant differences in chemotaxis to linear gradient of NaCl upon control conditions (C) and upon 4.5hrs treatment with 10mM Paraquat. They recognize small changes in NaCl concentration and can associate the presence of food with NaCl concentration.

(E, F) Chemotaxis to NaCl of control animals and *del-4(tm717)* mutants upon heat stress for 35min at 37ºC. The percent of nematodes in each compartment of the assay plate carrying different NaCl concentrations was measured after 1hr (E) and 2hrs (F). Mutant animals for *del-4* display faster migration and enhanced attraction towards the preferred NaCl concentration upon heat stress. The effect, observed at the measurement after 1 hr on the assay plate (E), is amplified at the 2hrs measurement (F).

.(G, H) Chemotaxis to NaCl of control animals and *del-4(tm717)* mutants upon long-term starvation for 24hrs. The percent of nematodes in each compartment of the assay plate carrying different NaCl concentrations was measured after 1hr (G) and 2hrs (H). Mutant animals for *del-4* display faster migration and enhanced attraction towards the preferred NaCl concentration upon starvation. The effect, observed at the measurement after 1 hr on the assay plate (E), is lost at the 2hrs measurement (F).

(I) DEL-4 is necessary for the recognition of the gustatory stimulus of serotonin. *del-4* mutants displayed reduced chemotaxis to serotonin, indicating a reduced ability to respond to chemical food-derived cues. We performed two biological and two technical replicates.

(A-I) One-day adult animals were used in all experiments**.** Dot plots, dots represent the mean values of the chemotaxis index from biologically independent experiments. Error bars represent the SEM. n=number of animals. Non-significant (ns) p=0,1234, *p=0,0332, **p=0,0021, ***p=0,0002, ****p<0,0001. (A, C-H) Two-way ANOVA analysis. (B, I) Ordinary one-way ANOVA analysis. (A) ctrl n=240, *del-3(tm5642)* n=260, *del-4(tm717)* n=250. (B) Naïve: ctrl n=174, *del-3(tm5642)* n=587, *del-4(tm717)* n=1169, Conditioned: ctrl n=247, *del-3(tm5642)* n=703, *del-4(tm717)* n=761. (C) ctrl n=780, *del-4(tm717)* n=691. (D) ctrl n=686, *del-4(tm717)* n=704. (E) ctrl

Figure 18. Continued.

n=969, *del-4(tm717)* n=1036. (F) ctrl n=908, *del-4(tm717)* n=897. (G) ctrl n=547, *del-4(tm717)* n=467. (H) ctrl n=519, *del-4(tm717)* n=447. (I) ctrl n=306, del-4(tm717) n=513, DEL-4::GFP n= 399, *del-4(tm717)* rescue n=418, *che-2(e1033)* n=341.

DEL-4 displays neuroprotective effects on neurodegenerative human disease models in *C. elegans*

Several studies have shown that dysregulated dopaminergic signalling has a causative effect on the initiation and progression of neurodegenerative diseases, including Parkinson's disease (PD) and Alzheimer's disease (AD) (254, 255). Both pathologies are complex disorders that depend on environmental and genetic factors. Data from gene expression profiling revealed the deregulation of neurotransmitters and ion channel receptors expression in PD (256). Low levels of ach and dopamine in the brain characterize AD and PD, respectively (257). Moreover, chronic stress exacerbates AD and PD pathology (258, 259). In line with the effects of DEL-4 on neurotransmission and locomotion and the regulation of DEL-4 by stress, we hypothesized that downregulation of DEL-4 would aggravate the phenotype of these two neurodegenerative diseases. We utilized two *C. elegans* disease models, the

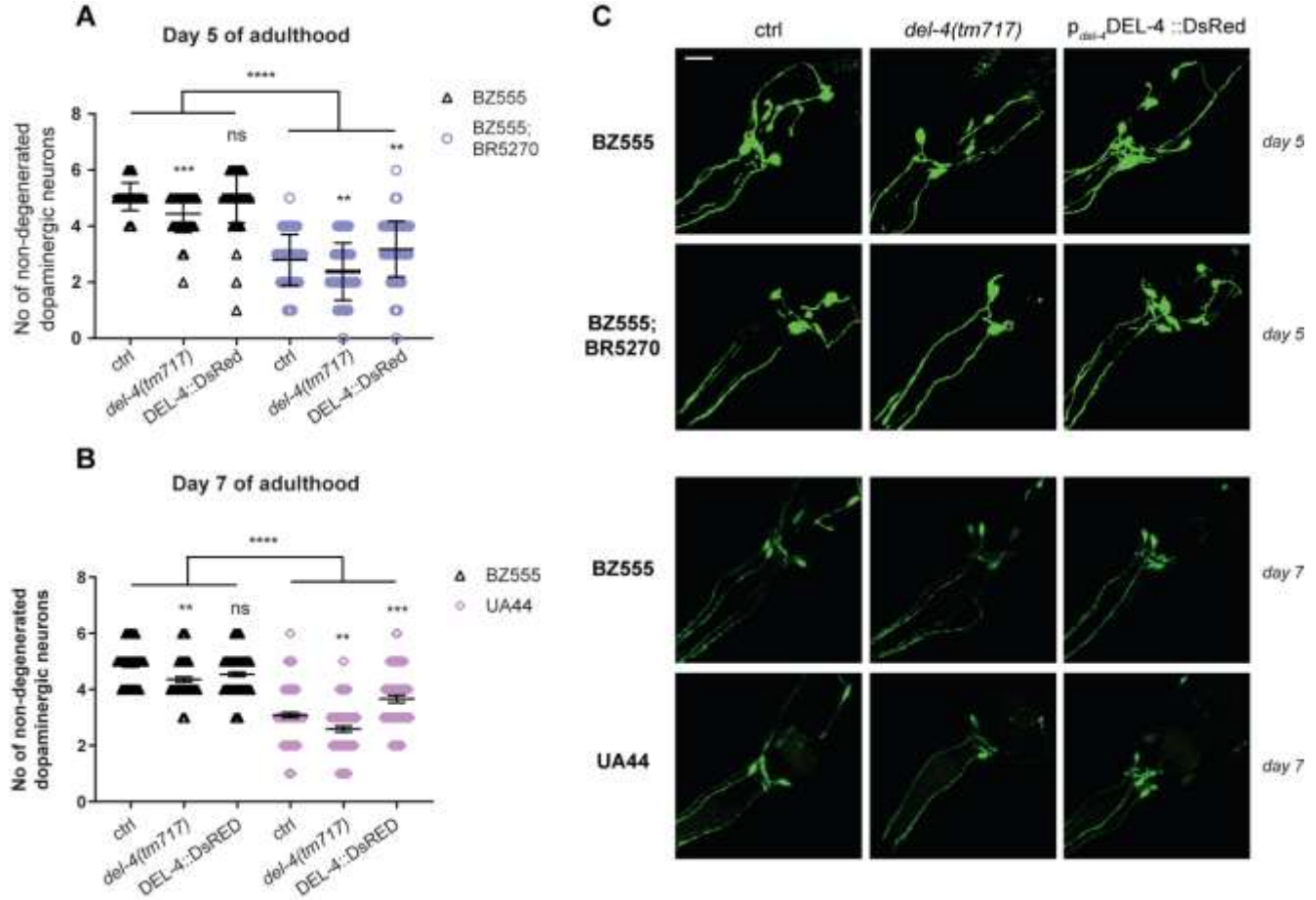

Figure 19. DEL-4 protects against neurodegeneration.

(A) Overexpression of DEL-4 promotes survival of dopamine-releasing neurons in the head of *C. elegans* in an Alzheimer's disease model. The graph indicates the number of surviving dopaminergic neurons in the head of control and *del-4(tm717)* mutant animals in control (BZ555) and disease conditions (BR5270) (Tables 1 and S4). DEL-4 elimination results in an increased number of degenerated neurons under control conditions and in the tauopathy model. The strain BR5270, which overexpresses the F3 pro-aggregation fragment of the human Tau protein with deleted K280, pan-neuronally, under the rab-3 promoter (p_{rab-3}F3(delta)K280), was used. Measurements were performed on 5-day adult animals.

(B) The *del-4(tm717)* mutant displays increased neurodegeneration under control conditions and in a model of Parkinson's disease at day seven of adulthood. Comparison of surviving neurons of control and *del-4(tm717)* mutants under control conditions (BZ555) and in the UA44 model of Parkinson's disease. DEL-4 overexpressing animals exhibit reduced degeneration compared to control. The UA44 strain (p_{dat-1}GFP; p_{dat-1}a-syn) expresses human α-synuclein and GFP in dopaminergic neurons. We used UA44 as the synucleinopathy model.

(A, B) Error bars represent the SEM. ns p=0.1234, *p=0.0332, **p=0.0021, ***p=0.0002, ****p<0.0001. One-way ANOVA analysis.

(A-D) Dot plots, dots represent the number of non-degenerated neurons counted per animal.

(C) Representative images from the head of control animals (left), *del-4(tm717)* mutants (middle), and DEL-4 overexpressing animals (DEL-4::DsRed) (right). Top, images from the BR5270 strain and the BZ555 control on day five of adulthood. Bottom, images from the UA44 strain and the BZ555 control on day seven of adulthood. Confocal images (maximum intensity projections). Lens 40x. Scale bar 20 μm. Left is anterior.

(A-C) Strain BZ555 expresses GFP in dopaminergic neurons (p_{dat-1}GFP). We utilized BZ555 as a control for disease models. (A) BZ555 n=73, *del-4(tm717)* n=68, DEL-4::DsRed n=88, BR5270 n=158, BR5270;*del-4(tm717)* n=134, BR5270;DEL-4::DsRed n=151. (B) BZ555 n=143, *del-4(tm717)* n=67, DEL-4::DsRed n=92, UA44 n=117, UA44;*del-4(tm717)* n=83, UA44;DEL-4::DsRed n=63.

UA44 as a Parkinson's model and the BR5270 as an Alzheimer's disease model. These models express human α-synuclein in dopaminergic neurons, or the pro-aggregation F3ΔK280 tau fragment pan-neuronally (197, 200). In accordance with our hypothesis, we discovered that in both disease models overexpression of DEL-4 curtailed degeneration, whereas DEL-4 downregulation exacerbated this phenotype (Figure 19). In addition, depletion of DEL-4 induced dopaminergic neurodegeneration on days 5 and 7 of adulthood, even in the absence of aggregation-prone proteins (Figure 19). Consequently, we propose that disruption of neuronal sodium homeostasis exacerbates neurodegeneration in control and disease genetic background.

X. Discussion

Our findings suggest that heat stress and starvation modulate DEL-4 levels. We exhibit that thermal stress and long-term nutrient deprivation reduce the GFP-tagged fluorescence in animals overexpressing DEL-4. Both types of stress increase ASAP1 intensity in dopaminergic neurons, similar to *del-4(tm717)* mutants. In addition, we identified binding sites of HSF-1 and SKN-1 in the *del-4* promoter region. Conversely, we display that DEL-4 elimination activates HSF-1, SKN-1, and ER^{UPR} and decreases DAF-16 activity. Preceding results imply that distinct types of stress differentially tune DEL-4 channel activity.DEL-4 tuning arises through adjusting its levels or gating to impact the induction of stress responses master regulators. Our discoveries are consistent with previous studies indicating that stress regulates mammalian ENaCs and ASICs (182-186, 188). However, our experiments represent the first implemented *in vivo* to illustrate that specific types of stress affect the abundance of a DEG/ENaC channel on the cytoplasmic membrane of neuronal cells.

Our electrophysiology and imaging results exhibit that low pH blocks the DEL-4 homomeric channel and hyperpolarizes dopaminergic neurons. Acidification develops in physiological and pathological conditions such as exercise (260), ischemic stroke (261), cardiac ischemia (262), tumours (263), and inflammation (264). Similarly, in *C. elegans*, oxidative stress and mitochondrial fragmentation lead to cellular acidosis triggered by ROS production (265, 266). Pathogen infection and exercise also induce acidification (266, 267).

Mammalian voltage-dependent sodium channels are sensitive to protons, which block the pore and alter the channel activation properties (268). The site(s) of proton binding for channel opening in the mammalian ASICs are still poorly understood, with several candidate binding sites in the pore-forming and extracellular domains (269). Among the *C. elegans* DEG/ENaCs, two groups of acid-sensitive DEG/ENaCs are characterised by being either inhibited or activated by increasing proton concentrations. Three of these acid-sensitive DEG/ENaCs are activated by acidic pH, making them functionally similar to most the vertebrate ASICs (209). By contrast, DEL-4 is an acid-inhibited member, similarly to the degenerin ACD-1, a proton-inhibited glial sodium channel that participates in sensory perception and affects neuronal function (213). Among mammalian members, low extracellular pH blocks the heteromeric αβ ENaC epithelial channel (270). Although ENaCs mainly localize in epithelial tissues, alpha and beta ENaC subunits are abundantly co-expressed in many brain regions (271). Regarding its in vivo function, our results have shown that *del-4* mutants are insensitive to solution with pH 4.5,

indicating that DEL-4 could be directly involved in acid-sensation. Additionally, DEL-4 may play a more modulatory role during neurotransmission. Consequently, DEL-4 could have dual roles depending on where it is expressed. This is similar to what has been suggested for another *C. elegans* DEG/ENaC, DEG-1, which in chemosensory neurons functions in responses to both attractive and repellent cues (213) but in nose nociceptor neurons is required for mechanoreceptor currents (272). Overall, this work highlights the importance of proton homeostasis in regulating sodium channel gating and possibly in stress perception.

We provide evidence that DEL-4 affects resting membrane potential and subsequent synaptic activity levels by mediating the sodium balance of the plasma membrane. The intensity of ASAP1 increased in the *del-4(tm717)* mutant background and acidic solution. The absence of DEL-4 moderated the release of SVs from dopaminergic and cholinergic motor neurons. In agreement with the previous results, *del-4(tm717)* mutants were resistant to paralysis by dopamine or aldicarb. Additionally, when DEL-4 was missing, GABAergic motor neurons displayed elevated synaptic vesicle content, as disclosed by the SNB-1::GFP reporter. Thus, DEL-4 manipulates neurotransmission from specific neurons to impact the integration of transmitted signals and eventually modify animal locomotion.

We observe altered neuronal signalling of motor neurons in the absence of DEL-4. We propose that in the case of *del-4* mutant, there are two levels of regulation of ach release from cholinergic motor neurons. First, DEL-4 is expressed in cholinergic motor neurons, therefore its absence could alter (similar to its effect on dopaminergic neurons) the resting membrane potential of cholinergic neurons due to defective ion homeostasis. The second level of regulation of cholinergic motor neurons arises from altered dopaminergic signaling in the *del-4* mutant. In *C. elegans* D1-like dopamine receptor, DOP-1, localizes on the cytosolic membrane of cholinergic motor neurons, where it stimulates ACh release. In addition, deregulation of synaptic homeostasis has been observed in neurological diseases (273). In *C. elegans*, released dopamine reaches dopamine receptors found on motor neurons through diffusion. We hypothesize that the DOP-3 receptor expressed on GABAergic motor neurons is less activated in the *del-4* mutant, therefore increasing GABAergic signalling and further reducing Ach release. Overall, we believe that in the *del-4* mutant, there is a defected neuronal ionstasis and homeostasis that settle a new equilibrium concerning neuronal activation and synaptic release.

DEL-4 at steady-state conditions behaves as a permanently open channel. Thus, it may participate in neuronal resting membrane potential generation as a Na^+ leak channel. The subcellular localization pattern of DEL-4 supports this notion. *DEL-4*, contrary to other ASICs, allocates throughout

the plasma membrane and not specifically at the synapse (120, 274). Additionally, synaptic ASICs mainly open in response to low pH, while DEL-4 closes. The regulation of the DEL-4 channel by specific types of stress embodies a mechanism for controlling and altering neuronal excitability in response to environmental stress. DEL-4 modulates transcription factors that affect synaptic activity, neuronal structural maintenance, and survival and may also participate in the effect of DEL-4 on signal transmission (275-279). Vice versa, HSF-1 participates in regulation of DEL-4, thereby mediating stress signal transmission.

The difference between DEL-4 and other ASICs is that it constitutes a sodium leak channel at physiological conditions, contrary to most of mammalian ASICs that open upon acidification. The sodium background channel NALCNis a voltage-independent cation channel and regulates neuronal membrane conductance and excitability (280). Disruption of NALCN results in neuronal hyperpolarization and has been linked with neurodegenerative diseases, such as Alzheimer's disease (281). In view of these findings, the effects of DEL-4 on membrane potential and neurodegeneration are not contrary to a large body of evidence supporting that hyperpolarization is normally protective. In most of these cases, reduced depolarization is mediated by potassium or voltage-gated sodium channels (282, 283).

DEL-4 is essential for neural cell homeostasis and survival. The *del-4(tm717)* mutant has increased neuronal loss with age compared to the control. Contrariwise, heightened DEL-4 levels act in a neuroprotective manner on Parkinson's and Alzheimer's disease models. Conversely, blocking ASICs' current attenuates accumulation of a-synuclein and protects neurons from degeneration (284). In the *del-4* mutant context, we observed increased intracellular Ca^{2+}, AMPK levels, and ER stress response activation. Previous studies correlated neurodegeneration with elevated Ca^{2+} and metabolic stress (285). Also, prolonged ER^{UPR} activation accompanies the pathogenesis of neurodegenerative diseases (286). Several studies bridge chronic stress with the progression of Alzheimer's (AD) and Parkinson's (PD) diseases. In mammalian AD models, long-term adverse stress worsens cognitive functions and accelerates Aβ deposits (259). Chronic stress in rodents reduces dopaminergic signalling in distinct brain regions and confines locomotory activity (287). Research in animal models and humans with PD reveals that stress worsens mental health and locomotion defects (258). Mammalian ASICs have also been involved in brain ischemia. Inhibition of ASIC1a attenuates intracellular Ca^{2+} elevation due to cerebral ischemia (288). Interestingly, acidity has been implicated in the onset and progression of several features of amyotrophic lateral sclerosis (289, 290). ASIC2 and ASIC3 are up-regulated in motor neurons of

ALS patients (291). Our results, concerning the proton-inhibition and the attenuated locomotory rate observed upon DEL-4 downregulation, corroborate the findings that ASICs are implicated in a variety of neurodegenerative diseases in which acidification is observed.

Several studies have linked chronic stress with the progression of Alzheimer's disease (AD) and Parkinson's disease (PD). In mammalian AD models, long-term adverse stress worsens cognitive functions and accelerates Aβ deposition (259). Chronic stress in rodents reduces dopaminergic signalling in distinct brain regions and confines locomotory activity (287). Research in animal models and humans with PD has revealed that stress worsens mental health and causes locomotion defects (258). Our findings provide new insights into the molecular mechanisms underlying chronic stress that affects the onset and accelerates the progression of neurodegenerative diseases.

Our electrophysiological analysis indicates that DEL-4 forms a proton-gated homomeric channel. We have not explored possible interactions of DEL-4 with other degenerin ion channels that could result in the formation of heteromeric sodium channels with distinct electrophysiological properties. We note that DEL-4 shows extensive sequence similarity with human ENaC1b and ASIC1b. Therefore, it could potentially form either homomeric or heteromeric channels *in vivo*. Whether the heteromeric channels will share the same electrophysiological properties as the DEL-4 homomeric channel remains to be elucidated. Nevertheless, depletion of DEL-4 is expected to affect all types of DEL-4-containing channels *in vivo*.

XI. Conclusions

In this study, we characterized the contribution of a proton-inhibited DEG/ENaC channel to the perception and sensorimotor integration of specific types of stress. We observed that heat stress and starvation reduced the expression levels of DEL-4, which localizes to the plasma membrane of sensory, dopaminergic, serotonergic, and motor neurons whilst, vice versa DEL-4 affects the activation of cellular stress responses throughout the body. Mechanistically, DEL-4 modifies the neuronal excitability pattern and alters synaptic vesicle release from dopaminergic and motor neurons to adjust the locomotory rate of the animal. Finally, we demonstrated that DEL-4 modulation affects the integrity and viability of dopaminergic neurons. Our data highlight the significance of a DEG/ENaC member in neuronal sodium homeostasis and stabilization of resting membrane potential and provide valuable

insight into DEG/ENaC sodium channel regulation upon stress. Our findings are consistent with those of previous studies, indicating that stress regulates mammalian ENaCs and ASICs (182-186, 188). However, our experiments represent the first *in vivo* study to illustrate that specific types of stress affect the abundance of a DEG/ENaC channel on the cytoplasmic membrane of neuronal cells.

We propose a model in which specific types of stress or acidity reduce or inhibit the DEL-4 channel, inducing hyperpolarization of dopamine neurons and the subsequent perturbation of synaptic release. Concomitantly, cell-non-autonomous modulation of several stress responses affects the excitation patterns of cholinergic and GABAergic motor neurons. This regulation adjusts the motor output of animals to elicit proper behaviour in response to stress. Thus, neuronal ionstasis fine-tunes stress response mechanisms and neuroendocrine signalling to control physiological processes, such as locomotion (Figure 20).

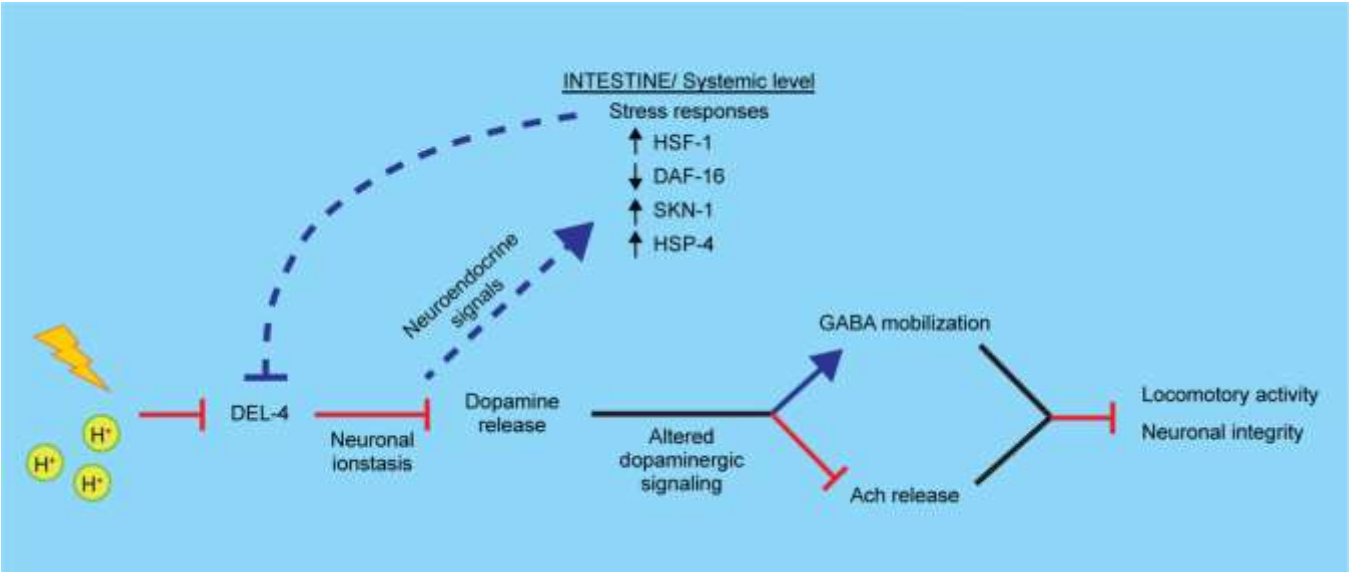

Figure 20. Proposed model.

According to our results, we propose that several types of stress regulate the expression or the gating of the DEL-4 channel, which acts in mediating stress perception. Consequently, modulation of DEL-4 by stress alters the downstream neuronal signalling through dopaminergic and motor neurons for the animal to adapt its behavioural response. Additionally, the altered neuronal signalling triggers the activation of stress response transcription factors that act through a feedback loop on the DEL-4 channel, to further modulate the stress response.

XII. Bibliography

1. Maupas E. Modes et formes de reproduction des nématodes. Archives de Zoologie Expérimentale et Générale. 1900;8:463–624.
2. Brenner S. The genetics of Caenorhabditis elegans. Genetics. 1974;77(1):71-94.
3. Sulston JE, Horvitz HR. Post-embryonic cell lineages of the nematode, Caenorhabditis elegans. Developmental biology. 1977;56(1):110-56. Epub 1977/03/01.
4. Kimble J, Hirsh D. The postembryonic cell lineages of the hermaphrodite and male gonads in Caenorhabditis elegans. Developmental biology. 1979;70(2):396-417. Epub 1979/06/01.
5. Sulston JE, Schierenberg E, White JG, Thomson JN. The embryonic cell lineage of the nematode Caenorhabditis elegans. Developmental biology. 1983;100(1):64-119. Epub 1983/11/01.
6. Genome sequence of the nematode C. elegans: a platform for investigating biology. Science. 1998;282(5396):2012-8. Epub 1998/12/16.
7. White JG, Southgate E, Thomson JN, Brenner S. The structure of the nervous system of the nematode Caenorhabditis elegans. Philosophical transactions of the Royal Society of London Series B, Biological sciences. 1986;314(1165):1-340. Epub 1986/11/12.
8. Jarrell TA, Wang Y, Bloniarz AE, Brittin CA, Xu M, Thomson JN, et al. The connectome of a decision-making neural network. Science. 2012;337(6093):437-44. Epub 2012/07/28.
9. Ward S, Thomson N, White JG, Brenner S. Electron microscopical reconstruction of the anterior sensory anatomy of the nematode Caenorhabditis elegans.?2UU. The Journal of comparative neurology. 1975;160(3):313-37. Epub 1975/04/01.
10. Oikonomou G, Shaham S. The glia of Caenorhabditis elegans. Glia. 2011;59(9):1253-63. Epub 2011/07/07.
11. Shaham S. Glial development and function in the nervous system of Caenorhabditis elegans. Cold Spring Harbor perspectives in biology. 2015;7(4):a020578. Epub 2015/01/13.
12. Li C, Kim K. Neuropeptides. WormBook : the online review of C elegans biology. 2008:1-36. Epub 2008/09/27.
13. White JG, Southgate E, Thomson JN, Brenner S. The structure of the ventral nerve cord of Caenorhabditis elegans. Philosophical transactions of the Royal Society of London Series B, Biological sciences. 1976;275(938):327-48. Epub 1976/08/10.
14. Croll N. Components and patterns in the behavior of the nematode Caenorhabditis elegans. Journal of Zoology. 2009;176:159-76.
15. Faumont S, Miller AC, Lockery SR. Chemosensory behavior of semi-restrained Caenorhabditis elegans. Journal of neurobiology. 2005;65(2):171-8. Epub 2005/08/23.
16. Jorgensen EM, Nonet ML. Neuromuscular junctions in the nematode C. elegans. Seminars in Developmental Biology. 1995;6(3):207-20.
17. Jorgensen EM. Gaba. WormBook : the online review of C elegans biology. 2005:1-13. Epub 2007/12/01.
18. Gray JM, Hill JJ, Bargmann CI. A circuit for navigation in Caenorhabditis elegans. Proceedings of the National Academy of Sciences of the United States of America. 2005;102(9):3184-91. Epub 2005/02/04.
19. Hall ZFAaDH. Nervous system, general description. WormAtlas Hermaphrodite Handbook. 2011.
20. Kunitomo H, Sato H, Iwata R, Satoh Y, Ohno H, Yamada K, et al. Concentration memory-dependent synaptic plasticity of a taste circuit regulates salt concentration chemotaxis in Caenorhabditis elegans. Nature communications. 2013;4:2210. Epub 2013/07/28.
21. Culotti JG, Russell RL. Osmotic avoidance defective mutants of the nematode Caenorhabditis elegans. Genetics. 1978;90(2):243-56. Epub 1978/10/01.
22. Mori I, Ohshima Y. Neural regulation of thermotaxis in Caenorhabditis elegans. Nature. 1995;376(6538):344-8. Epub 1995/07/27.

23. Cheung BH, Cohen M, Rogers C, Albayram O, de Bono M. Experience-dependent modulation of C. elegans behavior by ambient oxygen. Current biology : CB. 2005;15(10):905-17. Epub 2005/05/27.
24. Inglis PN, Ou G, Leroux MR, Scholey JM. The sensory cilia of Caenorhabditis elegans. WormBook : the online review of C elegans biology. 2007:1-22. Epub 2007/12/01.
25. Hall DH, Russell RL. The posterior nervous system of the nematode Caenorhabditis elegans: serial reconstruction of identified neurons and complete pattern of synaptic interactions. The Journal of neuroscience : the official journal of the Society for Neuroscience. 1991;11(1):1-22. Epub 1991/01/01.
26. Arnadottir J, Chalfie M. Eukaryotic mechanosensitive channels. Annual review of biophysics. 2010;39:111-37. Epub 2010/03/03.
27. Chalfie M, Sulston J. Developmental genetics of the mechanosensory neurons of Caenorhabditis elegans. Developmental biology. 1981;82(2):358-70. Epub 1981/03/01.
28. Hart AC, Sims S, Kaplan JM. Synaptic code for sensory modalities revealed by C. elegans GLR-1 glutamate receptor. Nature. 1995;378(6552):82-5. Epub 1995/11/02.
29. Chatzigeorgiou M, Schafer WR. Lateral facilitation between primary mechanosensory neurons controls nose touch perception in C. elegans. Neuron. 2011;70(2):299-309. Epub 2011/04/28.
30. Way JC, Chalfie M. The mec-3 gene of Caenorhabditis elegans requires its own product for maintained expression and is expressed in three neuronal cell types. Genes & development. 1989;3(12A):1823-33. Epub 1989/12/01.
31. Chalfie M, Sulston JE, White JG, Southgate E, Thomson JN, Brenner S. The neural circuit for touch sensitivity in Caenorhabditis elegans. The Journal of neuroscience : the official journal of the Society for Neuroscience. 1985;5(4):956-64. Epub 1985/04/01.
32. Sawin ER, Ranganathan R, Horvitz HR. C. elegans locomotory rate is modulated by the environment through a dopaminergic pathway and by experience through a serotonergic pathway. Neuron. 2000;26(3):619-31. Epub 2000/07/15.
33. Tobin DM, Bargmann CI. Invertebrate nociception: behaviors, neurons and molecules. Journal of neurobiology. 2004;61(1):161-74. Epub 2004/09/14.
34. Perkins LA, Hedgecock EM, Thomson JN, Culotti JG. Mutant sensory cilia in the nematode Caenorhabditis elegans. Developmental biology. 1986;117(2):456-87. Epub 1986/10/01.
35. Troemel ER, Kimmel BE, Bargmann CI. Reprogramming chemotaxis responses: sensory neurons define olfactory preferences in C. elegans. Cell. 1997;91(2):161-9. Epub 1997/11/05.
36. Hart AC, Kass J, Shapiro JE, Kaplan JM. Distinct signaling pathways mediate touch and osmosensory responses in a polymodal sensory neuron. The Journal of neuroscience : the official journal of the Society for Neuroscience. 1999;19(6):1952-8. Epub 1999/03/05.
37. Mellem JE, Brockie PJ, Zheng Y, Madsen DM, Maricq AV. Decoding of polymodal sensory stimuli by postsynaptic glutamate receptors in C. elegans. Neuron. 2002;36(5):933-44. Epub 2002/12/07.
38. Hilliard MA, Bergamasco C, Arbucci S, Plasterk RH, Bazzicalupo P. Worms taste bitter: ASH neurons, QUI-1, GPA-3 and ODR-3 mediate quinine avoidance in Caenorhabditis elegans. The EMBO journal. 2004;23(5):1101-11. Epub 2004/02/28.
39. Lans H, Rademakers S, Jansen G. A network of stimulatory and inhibitory Galpha-subunits regulates olfaction in Caenorhabditis elegans. Genetics. 2004;167(4):1677-87. Epub 2004/09/03.
40. Roayaie K, Crump JG, Sagasti A, Bargmann CI. The G alpha protein ODR-3 mediates olfactory and nociceptive function and controls cilium morphogenesis in C. elegans olfactory neurons. Neuron. 1998;20(1):55-67. Epub 1998/02/12.
41. Sambongi Y, Nagae T, Liu Y, Yoshimizu T, Takeda K, Wada Y, et al. Sensing of cadmium and copper ions by externally exposed ADL, ASE, and ASH neurons elicits avoidance response in Caenorhabditis elegans. Neuroreport. 1999;10(4):753-7. Epub 1999/04/20.
42. Hilliard MA, Bargmann CI, Bazzicalupo P. C. elegans responds to chemical repellents by integrating sensory inputs from the head and the tail. Current biology : CB. 2002;12(9):730-4. Epub 2002/05/15.

43. Bargmann CI. Chemosensation in C. elegans. In: Community TCeR, editor. WormBook : the online review of C elegans biology: WormBook; 2006.
44. Pierce-Shimomura JT, Faumont S, Gaston MR, Pearson BJ, Lockery SR. The homeobox gene lim-6 is required for distinct chemosensory representations in C. elegans. Nature. 2001;410(6829):694-8. Epub 2001/04/05.
45. Bargmann CI, Horvitz HR. Chemosensory neurons with overlapping functions direct chemotaxis to multiple chemicals in C. elegans. Neuron. 1991;7(5):729-42.
46. Suzuki H, Thiele TR, Faumont S, Ezcurra M, Lockery SR, Schafer WR. Functional asymmetry in Caenorhabditis elegans taste neurons and its computational role in chemotaxis. Nature. 2008;454(7200):114-7. Epub 2008/07/04.
47. Appleby PA. A model of chemotaxis and associative learning in C. elegans. Biological cybernetics. 2012;106(6-7):373-87. Epub 2012/07/25.
48. Jansen G, Thijssen KL, Werner P, van der Horst M, Hazendonk E, Plasterk RH. The complete family of genes encoding G proteins of Caenorhabditis elegans. Nature genetics. 1999;21(4):414-9. Epub 1999/04/07.
49. Pocock R, Hobert O. Hypoxia activates a latent circuit for processing gustatory information in C. elegans. Nature neuroscience. 2010;13(5):610-4. Epub 2010/04/20.
50. Bargmann CI, Hartwieg E, Horvitz HR. Odorant-selective genes and neurons mediate olfaction in C. elegans. Cell. 1993;74(3):515-27. Epub 1993/08/13.
51. Wes PD, Bargmann CI. C. elegans odour discrimination requires asymmetric diversity in olfactory neurons. Nature. 2001;410(6829):698-701. Epub 2001/04/05.
52. Larsch J, Flavell SW, Liu Q, Gordus A, Albrecht DR, Bargmann CI. A Circuit for Gradient Climbing in C. elegans Chemotaxis. Cell reports. 2015;12(11):1748-60. Epub 2015/09/15.
53. Liu Q, Kidd PB, Dobosiewicz M, Bargmann CI. C. elegans AWA Olfactory Neurons Fire Calcium-Mediated All-or-None Action Potentials. Cell. 2018;175(1):57-70 e17. Epub 2018/09/18.
54. Tanimoto Y, Yamazoe-Umemoto A, Fujita K, Kawazoe Y, Miyanishi Y, Yamazaki SJ, et al. Calcium dynamics regulating the timing of decision-making in C. elegans. eLife. 2017;6. Epub 2017/05/24.
55. Chalasani SH, Chronis N, Tsunozaki M, Gray JM, Ramot D, Goodman MB, et al. Dissecting a circuit for olfactory behaviour in Caenorhabditis elegans. Nature. 2007;450(7166):63-70. Epub 2007/11/02.
56. Chalasani SH, Kato S, Albrecht DR, Nakagawa T, Abbott LF, Bargmann CI. Neuropeptide feedback modifies odor-evoked dynamics in Caenorhabditis elegans olfactory neurons. Nature neuroscience. 2010;13(5):615-21. Epub 2010/04/07.
57. Hedgecock EM, Russell RL. Normal and mutant thermotaxis in the nematode Caenorhabditis elegans. Proceedings of the National Academy of Sciences of the United States of America. 1975;72(10):4061-5. Epub 1975/10/01.
58. Beverly M, Anbil S, Sengupta P. Degeneracy and neuromodulation among thermosensory neurons contribute to robust thermosensory behaviors in Caenorhabditis elegans. The Journal of neuroscience : the official journal of the Society for Neuroscience. 2011;31(32):11718-27. Epub 2011/08/13.
59. Kuhara A, Okumura M, Kimata T, Tanizawa Y, Takano R, Kimura KD, et al. Temperature sensing by an olfactory neuron in a circuit controlling behavior of C. elegans. Science. 2008;320(5877):803-7. Epub 2008/04/12.
60. Biron D, Wasserman S, Thomas JH, Samuel AD, Sengupta P. An olfactory neuron responds stochastically to temperature and modulates Caenorhabditis elegans thermotactic behavior. Proceedings of the National Academy of Sciences of the United States of America. 2008;105(31):11002-7. Epub 2008/08/01.
61. Luo L, Clark DA, Biron D, Mahadevan L, Samuel AD. Sensorimotor control during isothermal tracking in Caenorhabditis elegans. The Journal of experimental biology. 2006;209(Pt 23):4652-62. Epub 2006/11/23.
62. Liu S, Schulze E, Baumeister R. Temperature- and touch-sensitive neurons couple CNG and TRPV channel activities to control heat avoidance in Caenorhabditis elegans. PloS one. 2012;7(3):e32360. Epub 2012/03/27.

63. Coburn CM, Bargmann CI. A putative cyclic nucleotide-gated channel is required for sensory development and function in C. elegans. Neuron. 1996;17(4):695-706. Epub 1996/10/01.
64. Komatsu H, Mori I, Rhee JS, Akaike N, Ohshima Y. Mutations in a cyclic nucleotide-gated channel lead to abnormal thermosensation and chemosensation in C. elegans. Neuron. 1996;17(4):707-18. Epub 1996/10/01.
65. Dusenbery DB. Appetitive response of the nematodeCaenorhabditis elegans to oxygen. Journal of comparative physiology. 1980;136(4):333-6.
66. Gray JM, Karow DS, Lu H, Chang AJ, Chang JS, Ellis RE, et al. Oxygen sensation and social feeding mediated by a C. elegans guanylate cyclase homologue. Nature. 2004;430(6997):317-22. Epub 2004/06/29.
67. Chang AJ, Chronis N, Karow DS, Marletta MA, Bargmann CI. A distributed chemosensory circuit for oxygen preference in C. elegans. PLoS biology. 2006;4(9):e274. Epub 2006/08/15.
68. Coates JC, de Bono M. Antagonistic pathways in neurons exposed to body fluid regulate social feeding in Caenorhabditis elegans. Nature. 2002;419(6910):925-9. Epub 2002/11/01.
69. Cheung BH, Arellano-Carbajal F, Rybicki I, de Bono M. Soluble guanylate cyclases act in neurons exposed to the body fluid to promote C. elegans aggregation behavior. Current biology : CB. 2004;14(12):1105-11. Epub 2004/06/19.
70. Bretscher AJ, Kodama-Namba E, Busch KE, Murphy RJ, Soltesz Z, Laurent P, et al. Temperature, oxygen, and salt-sensing neurons in C. elegans are carbon dioxide sensors that control avoidance behavior. Neuron. 2011;69(6):1099-113.
71. Ward A, Liu J, Feng Z, Xu XZ. Light-sensitive neurons and channels mediate phototaxis in C. elegans. Nature neuroscience. 2008;11(8):916-22. Epub 2008/07/08.
72. Gabel CV, Gabel H, Pavlichin D, Kao A, Clark DA, Samuel AD. Neural circuits mediate electrosensory behavior in Caenorhabditis elegans. The Journal of neuroscience : the official journal of the Society for Neuroscience. 2007;27(28):7586-96. Epub 2007/07/13.
73. Russell J, Vidal-Gadea AG, Makay A, Lanam C, Pierce-Shimomura JT. Humidity sensation requires both mechanosensory and thermosensory pathways in Caenorhabditis elegans. Proceedings of the National Academy of Sciences of the United States of America. 2014;111(22):8269-74. Epub 2014/05/21.
74. Wang W, Qin LW, Wu TH, Ge CL, Wu YQ, Zhang Q, et al. cGMP Signalling Mediates Water Sensation (Hydrosensation) and Hydrotaxis in Caenorhabditis elegans. Scientific reports. 2016;6:19779. Epub 2016/02/20.
75. Jang H, Kim K, Neal SJ, Macosko E, Kim D, Butcher RA, et al. Neuromodulatory state and sex specify alternative behaviors through antagonistic synaptic pathways in C. elegans. Neuron. 2012;75(4):585-92. Epub 2012/08/28.
76. Lockery SR. Neuroscience: A social hub for worms. Nature. 2009;458(7242):1124-5. Epub 2009/05/02.
77. Macosko EZ, Pokala N, Feinberg EH, Chalasani SH, Butcher RA, Clardy J, et al. A hub-and-spoke circuit drives pheromone attraction and social behaviour in C. elegans. Nature. 2009;458(7242):1171-5. Epub 2009/04/08.
78. Kim K, Sato K, Shibuya M, Zeiger DM, Butcher RA, Ragains JR, et al. Two chemoreceptors mediate developmental effects of dauer pheromone in C. elegans. Science. 2009;326(5955):994-8. Epub 2009/10/03.
79. Ouellet J, Li S, Roy R. Notch signalling is required for both dauer maintenance and recovery in C. elegans. Development. 2008;135(15):2583-92. Epub 2008/07/05.
80. Schackwitz WS, Inoue T, Thomas JH. Chemosensory neurons function in parallel to mediate a pheromone response in C. elegans. Neuron. 1996;17(4):719-28. Epub 1996/10/01.
81. Ren P, Lim CS, Johnsen R, Albert PS, Pilgrim D, Riddle DL. Control of C. elegans larval development by neuronal expression of a TGF-beta homolog. Science. 1996;274(5291):1389-91. Epub 1996/11/22.
82. Li W, Kennedy SG, Ruvkun G. daf-28 encodes a C. elegans insulin superfamily member that is regulated by environmental cues and acts in the DAF-2 signaling pathway. Genes & development. 2003;17(7):844-58. Epub 2003/03/26.
83. Sze JY, Victor M, Loer C, Shi Y, Ruvkun G. Food and metabolic signalling defects in a Caenorhabditis elegans serotonin-synthesis mutant. Nature. 2000;403(6769):560-4. Epub 2000/02/17.

84. Zwaal RR, Mendel JE, Sternberg PW, Plasterk RH. Two neuronal G proteins are involved in chemosensation of the Caenorhabditis elegans Dauer-inducing pheromone. Genetics. 1997;145(3):715-27. Epub 1997/03/01.
85. Chute CD, DiLoreto EM, Zhang YK, Reilly DK, Rayes D, Coyle VL, et al. Co-option of neurotransmitter signaling for inter-organismal communication in C. elegans. Nature communications. 2019;10(1):3186. Epub 2019/07/20.
86. White MCaJ. The Nervous System. Cold Spring Harbor Monograph Archive. 1988;17:337-91.
87. Driscoll M, Kaplan J. Mechanotransduction. In: Riddle DL, Blumenthal T, Meyer BJ, Priess JR, editors. C elegans II. 2nd ed. Cold Spring Harbor (NY)1997.
88. Von Stetina SE, Treinin M, Miller DM, 3rd. The motor circuit. International review of neurobiology. 2006;69:125-67. Epub 2006/02/24.
89. Kocabas A, Shen CH, Guo ZV, Ramanathan S. Controlling interneuron activity in Caenorhabditis elegans to evoke chemotactic behaviour. Nature. 2012;490(7419):273-7. Epub 2012/09/25.
90. Iino Y, Yoshida K. Parallel use of two behavioral mechanisms for chemotaxis in Caenorhabditis elegans. The Journal of neuroscience : the official journal of the Society for Neuroscience. 2009;29(17):5370-80. Epub 2009/05/01.
91. Ishihara T, Iino Y, Mohri A, Mori I, Gengyo-Ando K, Mitani S, et al. HEN-1, a secretory protein with an LDL receptor motif, regulates sensory integration and learning in Caenorhabditis elegans. Cell. 2002;109(5):639-49. Epub 2002/06/14.
92. Tomioka M, Adachi T, Suzuki H, Kunitomo H, Schafer WR, Iino Y. The insulin/PI 3-kinase pathway regulates salt chemotaxis learning in Caenorhabditis elegans. Neuron. 2006;51(5):613-25. Epub 2006/09/05.
93. Chen C, Itakura E, Nelson GM, Sheng M, Laurent P, Fenk LA, et al. IL-17 is a neuromodulator of Caenorhabditis elegans sensory responses. Nature. 2017;542(7639):43-8. Epub 2017/01/19.
94. Albertson DG, Thomson JN. The pharynx of Caenorhabditis elegans. Philosophical transactions of the Royal Society of London Series B, Biological sciences. 1976;275(938):299-325. Epub 1976/08/10.
95. Z. F. Altun LAH, C. A. Wolkow, C. Crocker, R. Lints, and D. H. Hall. WormAtlas. 2002-2023.
96. Rankin CH, Beck CD, Chiba CM. Caenorhabditis elegans: a new model system for the study of learning and memory. Behavioural brain research. 1990;37(1):89-92. Epub 1990/02/12.
97. Beck CDO, Rankin CH. Long-term habituation is produced by distributed training at long ISIs and not by massed training or short ISIs inCaenorhabditis elegans. Animal Learning & Behavior. 1997;25(4):446-57.
98. Wen JY, Kumar N, Morrison G, Rambaldini G, Runciman S, Rousseau J, et al. Mutations that prevent associative learning in C. elegans. Behavioral neuroscience. 1997;111(2):354-68. Epub 1997/04/01.
99. Saeki S, Yamamoto M, Iino Y. Plasticity of chemotaxis revealed by paired presentation of a chemoattractant and starvation in the nematode Caenorhabditis elegans. The Journal of experimental biology. 2001;204(Pt 10):1757-64. Epub 2001/04/24.
100. Remy JJ, Hobert O. An interneuronal chemoreceptor required for olfactory imprinting in C. elegans. Science. 2005;309(5735):787-90. Epub 2005/07/30.
101. Goodman MB, Hall DH, Avery L, Lockery SR. Active currents regulate sensitivity and dynamic range in C. elegans neurons. Neuron. 1998;20(4):763-72. Epub 1998/05/15.
102. Bargmann CI, Kaplan JM. Signal transduction in the Caenorhabditis elegans nervous system. Annual review of neuroscience. 1998;21:279-308. Epub 1998/04/08.
103. Lockery SR, Goodman MB. The quest for action potentials in C. elegans neurons hits a plateau. Nature neuroscience. 2009;12(4):377-8. Epub 2009/03/27.
104. Barbry P, Hofman P. Molecular biology of Na+ absorption. The American journal of physiology. 1997;273(3 Pt 1):G571-85. Epub 1997/10/08.
105. Bankir L, Bichet DG, Bouby N. Vasopressin V2 receptors, ENaC, and sodium reabsorption: a risk factor for hypertension? American journal of physiology Renal physiology. 2010;299(5):F917-28. Epub 2010/09/10.

106. Chraibi A, Vallet V, Firsov D, Hess SK, Horisberger JD. Protease modulation of the activity of the epithelial sodium channel expressed in Xenopus oocytes. The Journal of general physiology. 1998;111(1):127-38. Epub 1998/02/14.
107. Blazer-Yost BL, Liu X, Helman SI. Hormonal regulation of ENaCs: insulin and aldosterone. The American journal of physiology. 1998;274(5):C1373-9. Epub 1998/06/05.
108. Ecelbarger CA, Kim GH, Terris J, Masilamani S, Mitchell C, Reyes I, et al. Vasopressin-mediated regulation of epithelial sodium channel abundance in rat kidney. American journal of physiology Renal physiology. 2000;279(1):F46-53. Epub 2000/07/15.
109. Hummler E, Barker P, Gatzy J, Beermann F, Verdumo C, Schmidt A, et al. Early death due to defective neonatal lung liquid clearance in alpha-ENaC-deficient mice. Nature genetics. 1996;12(3):325-8. Epub 1996/03/01.
110. DeSimone JA, Lyall V. Taste receptors in the gastrointestinal tract III. Salty and sour taste: sensing of sodium and protons by the tongue. American journal of physiology Gastrointestinal and liver physiology. 2006;291(6):G1005-10. Epub 2006/07/01.
111. Roudier-Pujol C, Rochat A, Escoubet B, Eugene E, Barrandon Y, Bonvalet JP, et al. Differential expression of epithelial sodium channel subunit mRNAs in rat skin. Journal of cell science. 1996;109 (Pt 2):379-85. Epub 1996/02/01.
112. Waldmann R, Champigny G, Bassilana F, Voilley N, Lazdunski M. Molecular cloning and functional expression of a novel amiloride-sensitive Na+ channel. The Journal of biological chemistry. 1995;270(46):27411-4. Epub 1995/11/17.
113. Killick R, Richardson G. Isolation of chicken alpha ENaC splice variants from a cochlear cDNA library. Biochimica et biophysica acta. 1997;1350(1):33-7. Epub 1997/01/03.
114. Mirshahi M, Nicolas C, Mirshahi S, Golestaneh N, d'Hermies F, Agarwal MK. Immunochemical analysis of the sodium channel in rodent and human eye. Experimental eye research. 1999;69(1):21-32. Epub 1999/06/22.
115. Lu L, Wu L, Jia H, Li Y, Chen J, Xu D, et al. The epithelial sodium channel is involved in dexamethasone-induced osteoblast differentiation and mineralization. Cell biology and toxicology. 2012;28(5):279-89. Epub 2012/07/04.
116. Wang RY, Yang SH, Xu WH. Role of Epithelium Sodium Channel in Bone Formation. Chinese medical journal. 2016;129(5):594-600. Epub 2016/02/26.
117. Deval E, Lingueglia E. Acid-Sensing Ion Channels and nociception in the peripheral and central nervous systems. Neuropharmacology. 2015;94:49-57. Epub 2015/03/01.
118. Dube GR, Elagoz A, Mangat H. Acid sensing ion channels and acid nociception. Current pharmaceutical design. 2009;15(15):1750-66. Epub 2009/05/16.
119. Lingueglia E. Acid-sensing ion channels in sensory perception. The Journal of biological chemistry. 2007;282(24):17325-9. Epub 2007/04/14.
120. Voglis G, Tavernarakis N. A synaptic DEG/ENaC ion channel mediates learning in C. elegans by facilitating dopamine signalling. The EMBO journal. 2008;27(24):3288-99. Epub 2008/11/28.
121. Liu TT, Qu ZW, Ren C, Gan X, Qiu CY, Hu WP. Prolactin potentiates the activity of acid-sensing ion channels in female rat primary sensory neurons. Neuropharmacology. 2016;103:174-82. Epub 2015/07/19.
122. Gong W, Kolker SJ, Usachev Y, Walder RY, Boyle DL, Firestein GS, et al. Acid-sensing ion channel 3 decreases phosphorylation of extracellular signal-regulated kinases and induces synoviocyte cell death by increasing intracellular calcium. Arthritis research & therapy. 2014;16(3):R121. Epub 2014/06/14.
123. Ikeuchi M, Kolker SJ, Sluka KA. Acid-sensing ion channel 3 expression in mouse knee joint afferents and effects of carrageenan-induced arthritis. The journal of pain. 2009;10(3):336-42. Epub 2009/02/03.
124. Johnson MB, Jin K, Minami M, Chen D, Simon RP. Global ischemia induces expression of acid-sensing ion channel 2a in rat brain. Journal of cerebral blood flow and metabolism : official journal of the International Society of Cerebral Blood Flow and Metabolism. 2001;21(6):734-40. Epub 2001/08/08.

125. Schaefer L, Sakai H, Mattei M, Lazdunski M, Lingueglia E. Molecular cloning, functional expression and chromosomal localization of an amiloride-sensitive Na(+) channel from human small intestine. FEBS letters. 2000;471(2-3):205-10. Epub 2000/04/18.
126. Wiemuth D, Sahin H, Falkenburger BH, Lefevre CM, Wasmuth HE, Grunder S. BASIC--a bile acid-sensitive ion channel highly expressed in bile ducts. FASEB journal : official publication of the Federation of American Societies for Experimental Biology. 2012;26(10):4122-30. Epub 2012/06/28.
127. Wiemuth D, Grunder S. The pharmacological profile of brain liver intestine Na+ channel: inhibition by diarylamidines and activation by fenamates. Molecular pharmacology. 2011;80(5):911-9. Epub 2011/08/11.
128. Adams CM, Anderson MG, Motto DG, Price MP, Johnson WA, Welsh MJ. Ripped pocket and pickpocket, novel Drosophila DEG/ENaC subunits expressed in early development and in mechanosensory neurons. The Journal of cell biology. 1998;140(1):143-52. Epub 1998/02/14.
129. Liu L, Johnson WA, Welsh MJ. Drosophila DEG/ENaC pickpocket genes are expressed in the tracheal system, where they may be involved in liquid clearance. Proceedings of the National Academy of Sciences of the United States of America. 2003;100(4):2128-33. Epub 2003/02/07.
130. Furukawa Y, Miyawaki Y, Abe G. Molecular cloning and functional characterization of the Aplysia FMRFamide-gated Na+ channel. Pflugers Archiv : European journal of physiology. 2006;451(5):646-56. Epub 2005/09/01.
131. Lingueglia E, Champigny G, Lazdunski M, Barbry P. Cloning of the amiloride-sensitive FMRFamide peptide-gated sodium channel. Nature. 1995;378(6558):730-3. Epub 1995/12/14.
132. Jeziorski MC, Green KA, Sommerville J, Cottrell GA. Cloning and expression of a FMRFamide-gated Na(+) channel from Helisoma trivolvis and comparison with the native neuronal channel. The Journal of physiology. 2000;526 Pt 1(Pt 1):13-25. Epub 2000/07/06.
133. Perry SJ, Straub VA, Schofield MG, Burke JF, Benjamin PR. Neuronal expression of an FMRFamide-gated Na+ channel and its modulation by acid pH. The Journal of neuroscience : the official journal of the Society for Neuroscience. 2001;21(15):5559-67. Epub 2001/07/24.
134. Take-Uchi M, Kawakami M, Ishihara T, Amano T, Kondo K, Katsura I. An ion channel of the degenerin/epithelial sodium channel superfamily controls the defecation rhythm in Caenorhabditis elegans. Proceedings of the National Academy of Sciences of the United States of America. 1998;95(20):11775-80. Epub 1998/09/30.
135. Kobayashi Y, Kimura KD, Katsura I. Ultradian rhythm in the intestine of Caenorhabditis elegans is controlled by the C-terminal region of the FLR-1 ion channel and the hydrophobic domain of the FLR-4 protein kinase. Genes to cells : devoted to molecular & cellular mechanisms. 2011;16(5):565-75. Epub 2011/04/27.
136. Garcia-Anoveros J, Ma C, Chalfie M. Regulation of Caenorhabditis elegans degenerin proteins by a putative extracellular domain. Current biology : CB. 1995;5(4):441-8. Epub 1995/04/01.
137. Tavernarakis N, Driscoll M. Mechanotransduction in Caenorhabditis elegans: the role of DEG/ENaC ion channels. Cell biochemistry and biophysics. 2001;35(1):1-18. Epub 2002/03/20.
138. Kellenberger S, Schild L. Epithelial sodium channel/degenerin family of ion channels: a variety of functions for a shared structure. Physiological reviews. 2002;82(3):735-67. Epub 2002/06/28.
139. Hanukoglu I, Hanukoglu A. Epithelial sodium channel (ENaC) family: Phylogeny, structure-function, tissue distribution, and associated inherited diseases. Gene. 2016;579(2):95-132. Epub 2016/01/17.
140. Tavernarakis N, Driscoll M. Caenorhabditis elegans degenerins and vertebrate ENaC ion channels contain an extracellular domain related to venom neurotoxins. Journal of neurogenetics. 2000;13(4):257-64. Epub 2000/06/20.
141. Jasti J, Furukawa H, Gonzales EB, Gouaux E. Structure of acid-sensing ion channel 1 at 1.9 A resolution and low pH. Nature. 2007;449(7160):316-23. Epub 2007/09/21.
142. Krauson AJ, Carattino MD. The Thumb Domain Mediates Acid-sensing Ion Channel Desensitization. The Journal of biological chemistry. 2016;291(21):11407-19. Epub 2016/03/27.

143. Firsov D, Gautschi I, Merillat AM, Rossier BC, Schild L. The heterotetrameric architecture of the epithelial sodium channel (ENaC). The EMBO journal. 1998;17(2):344-52. Epub 1998/02/28.
144. Canessa CM, Schild L, Buell G, Thorens B, Gautschi I, Horisberger JD, et al. Amiloride-sensitive epithelial Na+ channel is made of three homologous subunits. Nature. 1994;367(6462):463-7. Epub 1994/02/03.
145. Palmer LG. Epithelial Na channels: the nature of the conducting pore. Renal physiology and biochemistry. 1990;13(1-2):51-8. Epub 1990/01/01.
146. Hoagland EN, Sherwood TW, Lee KG, Walker CJ, Askwith CC. Identification of a calcium permeable human acid-sensing ion channel 1 transcript variant. The Journal of biological chemistry. 2010;285(53):41852-62. Epub 2010/11/03.
147. Jiang N, Rau KK, Johnson RD, Cooper BY. Proton sensitivity Ca2+ permeability and molecular basis of acid-sensing ion channels expressed in glabrous and hairy skin afferents. Journal of neurophysiology. 2006;95(4):2466-78. Epub 2006/01/13.
148. Shimkets RA, Warnock DG, Bositis CM, Nelson-Williams C, Hansson JH, Schambelan M, et al. Liddle's syndrome: heritable human hypertension caused by mutations in the beta subunit of the epithelial sodium channel. Cell. 1994;79(3):407-14. Epub 1994/11/04.
149. Hansson JH, Schild L, Lu Y, Wilson TA, Gautschi I, Shimkets R, et al. A de novo missense mutation of the beta subunit of the epithelial sodium channel causes hypertension and Liddle syndrome, identifying a proline-rich segment critical for regulation of channel activity. Proceedings of the National Academy of Sciences of the United States of America. 1995;92(25):11495-9. Epub 1995/12/05.
150. Rossier BC, Pradervand S, Schild L, Hummler E. Epithelial sodium channel and the control of sodium balance: interaction between genetic and environmental factors. Annual review of physiology. 2002;64:877-97. Epub 2002/02/05.
151. Chang SS, Grunder S, Hanukoglu A, Rosler A, Mathew PM, Hanukoglu I, et al. Mutations in subunits of the epithelial sodium channel cause salt wasting with hyperkalaemic acidosis, pseudohypoaldosteronism type 1. Nature genetics. 1996;12(3):248-53. Epub 1996/03/01.
152. Thibodeau PH, Butterworth MB. Proteases, cystic fibrosis and the epithelial sodium channel (ENaC). Cell and tissue research. 2013;351(2):309-23. Epub 2012/06/26.
153. Wang W, Ji HL. Epithelial Sodium and Chloride Channels and Asthma. Chinese medical journal. 2015;128(16):2242-9. Epub 2015/08/13.
154. Vergo S, Craner MJ, Etzensperger R, Attfield K, Friese MA, Newcombe J, et al. Acid-sensing ion channel 1 is involved in both axonal injury and demyelination in multiple sclerosis and its animal model. Brain : a journal of neurology. 2011;134(Pt 2):571-84. Epub 2011/01/15.
155. Arias RL, Sung ML, Vasylyev D, Zhang MY, Albinson K, Kubek K, et al. Amiloride is neuroprotective in an MPTP model of Parkinson's disease. Neurobiology of disease. 2008;31(3):334-41. Epub 2008/07/09.
156. Wong HK, Bauer PO, Kurosawa M, Goswami A, Washizu C, Machida Y, et al. Blocking acid-sensing ion channel 1 alleviates Huntington's disease pathology via an ubiquitin-proteasome system-dependent mechanism. Human molecular genetics. 2008;17(20):3223-35. Epub 2008/07/29.
157. Arun T, Tomassini V, Sbardella E, de Ruiter MB, Matthews L, Leite MI, et al. Targeting ASIC1 in primary progressive multiple sclerosis: evidence of neuroprotection with amiloride. Brain : a journal of neurology. 2013;136(Pt 1):106-15. Epub 2013/02/01.
158. Gregersen N, Dahl HA, Buttenschon HN, Nyegaard M, Hedemand A, Als TD, et al. A genome-wide study of panic disorder suggests the amiloride-sensitive cation channel 1 as a candidate gene. European journal of human genetics : EJHG. 2012;20(1):84-90. Epub 2011/08/04.
159. Ziemann AE, Schnizler MK, Albert GW, Severson MA, Howard MA, 3rd, Welsh MJ, et al. Seizure termination by acidosis depends on ASIC1a. Nature neuroscience. 2008;11(7):816-22. Epub 2008/06/10.
160. Ziemann AE, Allen JE, Dahdaleh NS, Drebot, II, Coryell MW, Wunsch AM, et al. The amygdala is a chemosensor that detects carbon dioxide and acidosis to elicit fear behavior. Cell. 2009;139(5):1012-21. Epub 2009/12/01.

161. Gugliandolo A, Gangemi C, Caccamo D, Curro M, Pandolfo G, Quattrone D, et al. The RS685012 Polymorphism of ACCN2, the Human Ortholog of Murine Acid-Sensing Ion Channel (ASIC1) Gene, is Highly Represented in Patients with Panic Disorder. Neuromolecular medicine. 2016;18(1):91-8. Epub 2015/11/22.
162. Sluka KA, Rasmussen LA, Edgar MM, O'Donnell JM, Walder RY, Kolker SJ, et al. Acid-sensing ion channel 3 deficiency increases inflammation but decreases pain behavior in murine arthritis. Arthritis and rheumatism. 2013;65(5):1194-202. Epub 2013/01/22.
163. Jang W, Lee S, Choi SI, Chae HS, Han J, Jo H, et al. Impairment of proprioceptive movement and mechanical nociception in Drosophila melanogaster larvae lacking Ppk30, a Drosophila member of the Degenerin/Epithelial Sodium Channel family. Genes, brain, and behavior. 2019;18(5):e12545. Epub 2019/01/25.
164. Prahlad V, Morimoto RI. Integrating the stress response: lessons for neurodegenerative diseases from C. elegans. Trends in cell biology. 2009;19(2):52-61. Epub 2008/12/30.
165. Kim KW, Jin Y. Neuronal responses to stress and injury in C. elegans. FEBS letters. 2015;589(14):1644-52. Epub 2015/05/17.
166. Kagias K, Nehammer C, Pocock R. Neuronal responses to physiological stress. Frontiers in genetics. 2012;3:222. Epub 2012/11/01.
167. Cattaneo A, Riva MA. Stress-induced mechanisms in mental illness: A role for glucocorticoid signalling. The Journal of steroid biochemistry and molecular biology. 2016;160:169-74. Epub 2015/08/05.
168. Fogaca MV, Duman RS. Cortical GABAergic Dysfunction in Stress and Depression: New Insights for Therapeutic Interventions. Frontiers in cellular neuroscience. 2019;13:87. Epub 2019/03/28.
169. Guan ZZ. Cross-talk between oxidative stress and modifications of cholinergic and glutaminergic receptors in the pathogenesis of Alzheimer's disease. Acta pharmacologica Sinica. 2008;29(7):773-80. Epub 2008/06/21.
170. Juarez Olguin H, Calderon Guzman D, Hernandez Garcia E, Barragan Mejia G. The Role of Dopamine and Its Dysfunction as a Consequence of Oxidative Stress. Oxidative medicine and cellular longevity. 2016;2016:9730467. Epub 2016/01/16.
171. Murnane KS. Serotonin 2A receptors are a stress response system: implications for post-traumatic stress disorder. Behavioural pharmacology. 2019;30(2 and 3-Spec Issue):151-62. Epub 2019/01/12.
172. Chen C, Wang L, Rong X, Wang W, Wang X. Effects of fluoxetine on protein expression of potassium ion channels in the brain of chronic mild stress rats. Acta pharmaceutica Sinica B. 2015;5(1):55-61. Epub 2015/11/19.
173. Zhou JJ, Gao Y, Kosten TA, Zhao Z, Li DP. Acute stress diminishes M-current contributing to elevated activity of hypothalamic-pituitary-adrenal axis. Neuropharmacology. 2017;114:67-76. Epub 2016/12/03.
174. Park JY, Dus M, Kim S, Abu F, Kanai MI, Rudy B, et al. Drosophila SLC5A11 Mediates Hunger by Regulating K(+) Channel Activity. Current biology : CB. 2016;26(18):2550. Epub 2016/09/28.
175. Nunez-Villena F, Becerra A, Echeverria C, Briceno N, Porras O, Armisen R, et al. Increased expression of the transient receptor potential melastatin 7 channel is critically involved in lipopolysaccharide-induced reactive oxygen species-mediated neuronal death. Antioxidants & redox signaling. 2011;15(9):2425-38. Epub 2011/05/05.
176. Roedding AS, Tong SY, Au-Yeung W, Li PP, Warsh JJ. Chronic oxidative stress modulates TRPC3 and TRPM2 channel expression and function in rat primary cortical neurons: relevance to the pathophysiology of bipolar disorder. Brain research. 2013;1517:16-27. Epub 2013/04/23.
177. Benemei S, Fusi C, Trevisan G, Geppetti P. The TRPA1 channel in migraine mechanism and treatment. British journal of pharmacology. 2014;171(10):2552-67. Epub 2013/11/12.
178. Wang S, Yuan F, Li DP. M channels and stress response. Oncotarget. 2017;8(21):34026-7. Epub 2017/04/20.
179. Qadri YJ, Rooj AK, Fuller CM. ENaCs and ASICs as therapeutic targets. American journal of physiology Cell physiology. 2012;302(7):C943-65. Epub 2012/01/27.

180. Dwyer JM, Rizzo SJ, Neal SJ, Lin Q, Jow F, Arias RL, et al. Acid sensing ion channel (ASIC) inhibitors exhibit anxiolytic-like activity in preclinical pharmacological models. Psychopharmacology. 2009;203(1):41-52. Epub 2008/10/25.
181. Zhou W, Ye S, Luo R, Wu LM, Wang W. Inhibition of acid-sensing ion channels reduces the hypothalamus-pituitary-adrenal axis activity and ameliorates depression-like behavior in rats. RSC advances. 2019;9(16):8707-13. Epub 2019/03/15.
182. Ilatovskaya DV, Pavlov TS, Levchenko V, Staruschenko A. ROS production as a common mechanism of ENaC regulation by EGF, insulin, and IGF-1. American journal of physiology Cell physiology. 2013;304(1):C102-11. Epub 2012/11/09.
183. Xu H, Chu S. ENaC alpha-subunit variants are expressed in lung epithelial cells and are suppressed by oxidative stress. American journal of physiology Lung cellular and molecular physiology. 2007;293(6):L1454-62. Epub 2007/10/02.
184. Andrey F, Tsintsadze T, Volkova T, Lozovaya N, Krishtal O. Acid sensing ionic channels: modulation by redox reagents. Biochimica et biophysica acta. 2005;1745(1):1-6. Epub 2005/08/09.
185. Cadiou H, Studer M, Jones NG, Smith ES, Ballard A, McMahon SB, et al. Modulation of acid-sensing ion channel activity by nitric oxide. The Journal of neuroscience : the official journal of the Society for Neuroscience. 2007;27(48):13251-60. Epub 2007/11/30.
186. Arteaga MF, Coric T, Straub C, Canessa CM. A brain-specific SGK1 splice isoform regulates expression of ASIC1 in neurons. Proceedings of the National Academy of Sciences of the United States of America. 2008;105(11):4459-64. Epub 2008/03/13.
187. Liu W, Yuen EY, Yan Z. The stress hormone corticosterone increases synaptic alpha-amino-3-hydroxy-5-methyl-4-isoxazolepropionic acid (AMPA) receptors via serum- and glucocorticoid-inducible kinase (SGK) regulation of the GDI-Rab4 complex. The Journal of biological chemistry. 2010;285(9):6101-8. Epub 2010/01/07.
188. Pearce D. SGK1 regulation of epithelial sodium transport. Cellular physiology and biochemistry : international journal of experimental cellular physiology, biochemistry, and pharmacology. 2003;13(1):13-20. Epub 2003/03/22.
189. Xiong Z, Liu Y, Hu L, Ma B, Ai Y, Xiong C. A rapid facilitation of acid-sensing ion channels current by corticosterone in cultured hippocampal neurons. Neurochemical research. 2013;38(7):1446-53. Epub 2013/05/04.
190. Ye S, Yang R, Xiong Q, Yang Y, Zhou L, Gong Y, et al. Acute stress enhances learning and memory by activating acid-sensing ion channels in rats. Biochemical and biophysical research communications. 2018;498(4):1078-84. Epub 2018/03/21.
191. Shi S, Luke CJ, Miedel MT, Silverman GA, Kleyman TR. Activation of the Caenorhabditis elegans Degenerin Channel by Shear Stress Requires the MEC-10 Subunit. The Journal of biological chemistry. 2016;291(27):14012-22. Epub 2016/05/18.
192. Fay DS. Classical genetic methods. WormBook : the online review of C elegans biology. 2013:1-58.
193. Mello CC, Kramer JM, Stinchcomb D, Ambros V. Efficient gene transfer in C.elegans: extrachromosomal maintenance and integration of transforming sequences. The EMBO journal. 1991;10(12):3959-70.
194. Praitis V, Casey E, Collar D, Austin J. Creation of low-copy integrated transgenic lines in Caenorhabditis elegans. Genetics. 2001;157(3):1217-26.
195. St-Pierre F, Marshall JD, Yang Y, Gong Y, Schnitzer MJ, Lin MZ. High-fidelity optical reporting of neuronal electrical activity with an ultrafast fluorescent voltage sensor. Nature neuroscience. 2014;17(6):884-9. Epub 2014/04/24.
196. Min K, Kang J, Lee J. A modified feeding RNAi method for simultaneous knock-down of more than one gene in Caenorhabditis elegans. BioTechniques. 2010;48(3):229-32. Epub 2010/04/03.
197. Fatouros C, Pir GJ, Biernat J, Koushika SP, Mandelkow E, Mandelkow EM, et al. Inhibition of tau aggregation in a novel Caenorhabditis elegans model of tauopathy mitigates proteotoxicity. Human molecular genetics. 2012;21(16):3587-603. Epub 2012/05/23.

198. Sieburth D, Madison JM, Kaplan JM. PKC-1 regulates secretion of neuropeptides. Nature neuroscience. 2007;10(1):49-57. Epub 2006/11/28.
199. Dittman JS, Kaplan JM. Factors regulating the abundance and localization of synaptobrevin in the plasma membrane. Proceedings of the National Academy of Sciences of the United States of America. 2006;103(30):11399-404. Epub 2006/07/18.
200. Cao S, Gelwix CC, Caldwell KA, Caldwell GA. Torsin-mediated protection from cellular stress in the dopaminergic neurons of Caenorhabditis elegans. The Journal of neuroscience : the official journal of the Society for Neuroscience. 2005;25(15):3801-12.
201. Sanjiib Guha GC, Pankaj Kapahi. Morphological analysis of dopaminergic neurons with age using Caenorhabditis elegans GFP reporter strains. bio-protocol. 2018.
202. Hart (ed.) AC. Behavior. In: Community TCeR, editor. WormBook : the online review of C elegans biology: WormBook.
203. Suzuki M, Hattori Y, Saito T, Harada Y. Pond Assay for the Sensory Systems of Caenorhabditis elegans: A Novel Anesthesia-Free Method Enabling Detection of Responses to Extremely Low Chemical Concentrations. Biology. 2022;11(2). Epub 2022/02/26.
204. de Bono M, Bargmann CI. Natural variation in a neuropeptide Y receptor homolog modifies social behavior and food response in C. elegans. Cell. 1998;94(5):679-89. Epub 1998/09/19.
205. Wolf T, Perez A, Harris G. Glutamatergic transmission regulates locomotory behavior on a food patch in C. elegans. microPublication biology. 2020;2020. Epub 2020/12/05.
206. Goodman MB, Klein M, Lasse S, Luo L, Mori I, Samuel A, et al. Thermotaxis navigation behavior. WormBook : the online review of C elegans biology. 2014:1-10. Epub 2014/02/25.
207. Cao SQ, Wang HL, Palikaras K, Tavernarakis N, Fang EF. Chemotaxis assay for evaluation of memory-like behavior in wild-type and Alzheimer's-disease-like C. elegans models. STAR protocols. 2023;4(2):102250. Epub 2023/04/27.
208. Luo L, Wen Q, Ren J, Hendricks M, Gershow M, Qin Y, et al. Dynamic encoding of perception, memory, and movement in a C. elegans chemotaxis circuit. Neuron. 2014;82(5):1115-28. Epub 2014/06/09.
209. Kaulich E, McCubbin PTN, Schafer WR, Walker DS. Physiological insight into the conserved properties of Caenorhabditis elegans acid-sensing degenerin/epithelial sodium channels. The Journal of physiology. 2022.
210. Kaulich E, Carroll T, Ackley BD, Tang YQ, Hardege I, Nehrke K, et al. Distinct roles for two Caenorhabditis elegans acid-sensing ion channels in an ultradian clock. eLife. 2022;11.
211. Paukert M, Babini E, Pusch M, Grunder S. Identification of the Ca2+ blocking site of acid-sensing ion channel (ASIC) 1: implications for channel gating. The Journal of general physiology. 2004;124(4):383-94. Epub 2004/09/29.
212. Hardege I, Xu S, Gordon RD, Thompson AJ, Figg N, Stowasser M, et al. Novel Insertion Mutation in KCNJ5 Channel Produces Constitutive Aldosterone Release From H295R Cells. Mol Endocrinol. 2015;29(10):1522-30. Epub 2015/09/05.
213. Wang Y, Apicella A, Jr., Lee SK, Ezcurra M, Slone RD, Goldmit M, et al. A glial DEG/ENaC channel functions with neuronal channel DEG-1 to mediate specific sensory functions in C. elegans. The EMBO journal. 2008;27(18):2388-99.
214. Awayda MS, Subramanyam M. Regulation of the epithelial Na+ channel by membrane tension. The Journal of general physiology. 1998;112(2):97-111. Epub 1998/08/05.
215. Hedgecock EM, Culotti JG, Thomson JN, Perkins LA. Axonal guidance mutants of Caenorhabditis elegans identified by filling sensory neurons with fluorescein dyes. Developmental biology. 1985;111(1):158-70.
216. Morley JF, Morimoto RI. Regulation of longevity in Caenorhabditis elegans by heat shock factor and molecular chaperones. Molecular biology of the cell. 2004;15(2):657-64.
217. You YJ, Kim J, Cobb M, Avery L. Starvation activates MAP kinase through the muscarinic acetylcholine pathway in Caenorhabditis elegans pharynx. Cell metabolism. 2006;3(4):237-45.

218. Mahoney TR, Luo S, Nonet ML. Analysis of synaptic transmission in Caenorhabditis elegans using an aldicarb-sensitivity assay. Nature protocols. 2006;1(4):1772-7.
219. An JH, Blackwell TK. SKN-1 links C. elegans mesendodermal specification to a conserved oxidative stress response. Genes & development. 2003;17(15):1882-93. Epub 2003/07/19.
220. Trinklein ND, Murray JI, Hartman SJ, Botstein D, Myers RM. The role of heat shock transcription factor 1 in the genome-wide regulation of the mammalian heat shock response. Molecular biology of the cell. 2004;15(3):1254-61.
221. Murphy CT, McCarroll SA, Bargmann CI, Fraser A, Kamath RS, Ahringer J, et al. Genes that act downstream of DAF-16 to influence the lifespan of Caenorhabditis elegans. Nature. 2003;424(6946):277-83. Epub 2003/07/08.
222. Etchberger JF, Lorch A, Sleumer MC, Zapf R, Jones SJ, Marra MA, et al. The molecular signature and cis-regulatory architecture of a C. elegans gustatory neuron. Genes & development. 2007;21(13):1653-74. Epub 2007/07/04.
223. Morimoto RI. Regulation of the heat shock transcriptional response: cross talk between a family of heat shock factors, molecular chaperones, and negative regulators. Genes & development. 1998;12(24):3788-96. Epub 1998/12/31.
224. Morton EA, Lamitina T. Caenorhabditis elegans HSF-1 is an essential nuclear protein that forms stress granule-like structures following heat shock. Aging cell. 2013;12(1):112-20. Epub 2012/10/31.
225. Hibshman JD, Doan AE, Moore BT, Kaplan RE, Hung A, Webster AK, et al. daf-16/FoxO promotes gluconeogenesis and trehalose synthesis during starvation to support survival. eLife. 2017;6. Epub 2017/10/25.
226. Weinkove D, Halstead JR, Gems D, Divecha N. Long-term starvation and ageing induce AGE-1/PI 3-kinase-dependent translocation of DAF-16/FOXO to the cytoplasm. BMC biology. 2006;4:1. Epub 2006/02/07.
227. Henderson ST, Bonafe M, Johnson TE. daf-16 protects the nematode Caenorhabditis elegans during food deprivation. The journals of gerontology Series A, Biological sciences and medical sciences. 2006;61(5):444-60. Epub 2006/05/25.
228. Kaplan RE, Baugh LR. L1 arrest, daf-16/FoxO and nonautonomous control of post-embryonic development. Worm. 2016;5(2):e1175196.
229. Bahar E, Kim H, Yoon H. ER Stress-Mediated Signaling: Action Potential and Ca(2+) as Key Players. International journal of molecular sciences. 2016;17(9). Epub 2016/09/21.
230. Hardie DG. Keeping the home fires burning: AMP-activated protein kinase. Journal of the Royal Society, Interface. 2018;15(138). Epub 2018/01/19.
231. Arias-Del-Val J, Santo-Domingo J, Garcia-Casas P, Alvarez-Illera P, Nunez Galindo A, Wiederkehr A, et al. Regulation of inositol 1,4,5-trisphosphate-induced Ca(2+) release from the endoplasmic reticulum by AMP-activated kinase modulators. Cell calcium. 2019;77:68-76. Epub 2018/12/18.
232. An JH, Vranas K, Lucke M, Inoue H, Hisamoto N, Matsumoto K, et al. Regulation of the Caenorhabditis elegans oxidative stress defense protein SKN-1 by glycogen synthase kinase-3. Proceedings of the National Academy of Sciences of the United States of America. 2005;102(45):16275-80.
233. Glover-Cutter KM, Lin S, Blackwell TK. Integration of the unfolded protein and oxidative stress responses through SKN-1/Nrf. PLoS genetics. 2013;9(9):e1003701. Epub 2013/09/27.
234. Sankaranarayanan S, De Angelis D, Rothman JE, Ryan TA. The use of pHluorins for optical measurements of presynaptic activity. Biophysical journal. 2000;79(4):2199-208. Epub 2000/10/12.
235. Chase DL, Pepper JS, Koelle MR. Mechanism of extrasynaptic dopamine signaling in Caenorhabditis elegans. Nature neuroscience. 2004;7(10):1096-103. Epub 2004/09/21.
236. Aprison EZ, Dzitoyeva S, Ruvinsky I. The serotonin circuit that coordinates germline proliferation and egg laying with other reproductive functions in Caenorhabditis elegans. Proceedings Biological sciences. 2022;289(1987):20220913. Epub 2022/12/01.
237. Dag U, Nwabudike I, Kang D, Gomes MA, Kim J, Atanas AA, et al. Dissecting the functional organization of the C. elegans serotonergic system at whole-brain scale. Cell. 2023;186(12):2574-92 e20. Epub 2023/05/17.

238. Collins KM, Bode A, Fernandez RW, Tanis JE, Brewer JC, Creamer MS, et al. Activity of the C. elegans egg-laying behavior circuit is controlled by competing activation and feedback inhibition. eLife. 2016;5. Epub 2016/11/17.
239. Grunder S, Pusch M. Biophysical properties of acid-sensing ion channels (ASICs). Neuropharmacology. 2015;94:9-18. Epub 2015/01/15.
240. Bartoi T, Augustinowski K, Polleichtner G, Grunder S, Ulbrich MH. Acid-sensing ion channel (ASIC) 1a/2a heteromers have a flexible 2:1/1:2 stoichiometry. Proceedings of the National Academy of Sciences of the United States of America. 2014;111(22):8281-6. Epub 2014/05/23.
241. Yang L, Palmer LG. Ion conduction and selectivity in acid-sensing ion channel 1. The Journal of general physiology. 2014;144(3):245-55.
242. Eastwood AL, Goodman MB. Insight into DEG/ENaC channel gating from genetics and structure. Physiology (Bethesda). 2012;27(5):282-90. Epub 2012/10/03.
243. Collier DM, Snyder PM. Extracellular chloride regulates the epithelial sodium channel. The Journal of biological chemistry. 2009;284(43):29320-5.
244. de Bono M, Tobin DM, Davis MW, Avery L, Bargmann CI. Social feeding in Caenorhabditis elegans is induced by neurons that detect aversive stimuli. Nature. 2002;419(6910):899-903. Epub 2002/11/01.
245. Zhang Y, Lu H, Bargmann CI. Pathogenic bacteria induce aversive olfactory learning in Caenorhabditis elegans. Nature. 2005;438(7065):179-84. Epub 2005/11/11.
246. Shtonda BB, Avery L. Dietary choice behavior in Caenorhabditis elegans. The Journal of experimental biology. 2006;209(Pt 1):89-102. Epub 2005/12/16.
247. Olofsson B. The olfactory neuron AWC promotes avoidance of normally palatable food following chronic dietary restriction. The Journal of experimental biology. 2014;217(Pt 10):1790-8. Epub 2014/03/01.
248. Milward K, Busch KE, Murphy RJ, de Bono M, Olofsson B. Neuronal and molecular substrates for optimal foraging in Caenorhabditis elegans. Proceedings of the National Academy of Sciences of the United States of America. 2011;108(51):20672-7. Epub 2011/12/03.
249. Bendesky A, Tsunozaki M, Rockman MV, Kruglyak L, Bargmann CI. Catecholamine receptor polymorphisms affect decision-making in C. elegans. Nature. 2011;472(7343):313-8. Epub 2011/03/18.
250. Meisel JD, Panda O, Mahanti P, Schroeder FC, Kim DH. Chemosensation of bacterial secondary metabolites modulates neuroendocrine signaling and behavior of C. elegans. Cell. 2014;159(2):267-80. Epub 2014/10/11.
251. Hao Y, Yang W, Ren J, Hall Q, Zhang Y, Kaplan JM. Thioredoxin shapes the C. elegans sensory response to Pseudomonas produced nitric oxide. eLife. 2018;7. Epub 2018/07/18.
252. Kimata T, Sasakura H, Ohnishi N, Nishio N, Mori I. Thermotaxis of C. elegans as a model for temperature perception, neural information processing and neural plasticity. Worm. 2012;1(1):31-41. Epub 2012/01/01.
253. Hukema RK, Rademakers S, Jansen G. Gustatory plasticity in C. elegans involves integration of negative cues and NaCl taste mediated by serotonin, dopamine, and glutamate. Learn Mem. 2008;15(11):829-36. Epub 2008/11/06.
254. Krashia P, Nobili A, D'Amelio M. Unifying Hypothesis of Dopamine Neuron Loss in Neurodegenerative Diseases: Focusing on Alzheimer's Disease. Frontiers in molecular neuroscience. 2019;12:123.
255. Masato A, Plotegher N, Boassa D, Bubacco L. Impaired dopamine metabolism in Parkinson's disease pathogenesis. Molecular neurodegeneration. 2019;14(1):35.
256. Simunovic F, Yi M, Wang Y, Macey L, Brown LT, Krichevsky AM, et al. Gene expression profiling of substantia nigra dopamine neurons: further insights into Parkinson's disease pathology. Brain : a journal of neurology. 2009;132(Pt 7):1795-809.
257. Houghton PJ, Howes MJ. Natural products and derivatives affecting neurotransmission relevant to Alzheimer's and Parkinson's disease. Neuro-Signals. 2005;14(1-2):6-22.

258. Austin KW, Ameringer SW, Cloud LJ. An Integrated Review of Psychological Stress in Parkinson's Disease: Biological Mechanisms and Symptom and Health Outcomes. Parkinson's disease. 2016;2016:9869712. Epub 2017/01/07.
259. Rothman SM, Mattson MP. Adverse stress, hippocampal networks, and Alzheimer's disease. Neuromolecular medicine. 2010;12(1):56-70. Epub 2009/11/28.
260. Bangsbo J, Johansen L, Graham T, Saltin B. Lactate and H+ effluxes from human skeletal muscles during intense, dynamic exercise. The Journal of physiology. 1993;462:115-33. Epub 1993/03/01.
261. Guo Y, Zhou IY, Chan ST, Wang Y, Mandeville ET, Igarashi T, et al. pH-sensitive MRI demarcates graded tissue acidification during acute stroke - pH specificity enhancement with magnetization transfer and relaxation-normalized amide proton transfer (APT) MRI. NeuroImage. 2016;141:242-9. Epub 2016/07/23.
262. Ichihara K, Haga N, Abiko Y. Is ischemia-induced pH decrease of dog myocardium respiratory or metabolic acidosis? The American journal of physiology. 1984;246(5 Pt 2):H652-7. Epub 1984/05/01.
263. Engin K, Leeper DB, Cater JR, Thistlethwaite AJ, Tupchong L, McFarlane JD. Extracellular pH distribution in human tumours. International journal of hyperthermia : the official journal of European Society for Hyperthermic Oncology, North American Hyperthermia Group. 1995;11(2):211-6. Epub 1995/03/01.
264. Simmen HP, Blaser J. Analysis of pH and pO2 in abscesses, peritoneal fluid, and drainage fluid in the presence or absence of bacterial infection during and after abdominal surgery. American journal of surgery. 1993;166(1):24-7. Epub 1993/07/01.
265. Johnson D, Allman E, Nehrke K. Regulation of acid-base transporters by reactive oxygen species following mitochondrial fragmentation. American journal of physiology Cell physiology. 2012;302(7):C1045-54.
266. Johnson D, Nehrke K. Mitochondrial fragmentation leads to intracellular acidification in Caenorhabditis elegans and mammalian cells. Molecular biology of the cell. 2010;21(13):2191-201.
267. Benomar S, Lansdon P, Bender AM, Peterson BR, Chandler JR, Ackley BD. The C. elegans CHP1 homolog, pbo-1, functions in innate immunity by regulating the pH of the intestinal lumen. PLoS pathogens. 2020;16(1):e1008134.
268. Peters CH, Ghovanloo MR, Gershome C, Ruben PC. pH Modulation of Voltage-Gated Sodium Channels. Handbook of experimental pharmacology. 2018;246:147-60. Epub 2018/02/21.
269. Rook ML, Musgaard M, MacLean DM. Coupling structure with function in acid-sensing ion channels: challenges in pursuit of proton sensors. The Journal of physiology. 2021;599(2):417-30.
270. Zhang P, Fyfe GK, Grichtchenko, II, Canessa CM. Inhibition of alphabeta epithelial sodium channels by external protons indicates that the second hydrophobic domain contains structural elements for closing the pore. Biophysical journal. 1999;77(6):3043-51. Epub 1999/12/10.
271. Amin MS, Wang HW, Reza E, Whitman SC, Tuana BS, Leenen FH. Distribution of epithelial sodium channels and mineralocorticoid receptors in cardiovascular regulatory centers in rat brain. American journal of physiology Regulatory, integrative and comparative physiology. 2005;289(6):R1787-97. Epub 2005/09/06.
272. Geffeney SL, Cueva JG, Glauser DA, Doll JC, Lee TH, Montoya M, et al. DEG/ENaC but not TRP channels are the major mechanoelectrical transduction channels in a C. elegans nociceptor. Neuron. 2011;71(5):845-57.
273. Taylor HBC, Jeans AF. Friend or Foe? The Varied Faces of Homeostatic Synaptic Plasticity in Neurodegenerative Disease. Frontiers in cellular neuroscience. 2021;15:782768.
274. Liu X, Liu C, Ye J, Zhang S, Wang K, Su R. Distribution of Acid Sensing Ion Channels in Axonal Growth Cones and Presynaptic Membrane of Cultured Hippocampal Neurons. Frontiers in cellular neuroscience. 2020;14:205. Epub 2020/08/01.
275. Hooper PL, Durham HD, Torok Z, Crul T, Vigh L. The central role of heat shock factor 1 in synaptic fidelity and memory consolidation. Cell stress & chaperones. 2016;21(5):745-53. Epub 2016/06/11.
276. Kim SY, Webb AE. Neuronal functions of FOXO/DAF-16. Nutrition and healthy aging. 2017;4(2):113-26. Epub 2017/04/28.
277. Martinez G, Khatiwada S, Costa-Mattioli M, Hetz C. ER Proteostasis Control of Neuronal Physiology and Synaptic Function. Trends in neurosciences. 2018;41(9):610-24. Epub 2018/06/28.

278. Staab TA, Griffen TC, Corcoran C, Evgrafov O, Knowles JA, Sieburth D. The conserved SKN-1/Nrf2 stress response pathway regulates synaptic function in Caenorhabditis elegans. PLoS genetics. 2013;9(3):e1003354. Epub 2013/04/05.
279. Wilson MA, Iser WB, Son TG, Logie A, Cabral-Costa JV, Mattson MP, et al. skn-1 is required for interneuron sensory integration and foraging behavior in Caenorhabditis elegans. PloS one. 2017;12(5):e0176798. Epub 2017/05/02.
280. Lu B, Su Y, Das S, Liu J, Xia J, Ren D. The neuronal channel NALCN contributes resting sodium permeability and is required for normal respiratory rhythm. Cell. 2007;129(2):371-83.
281. Cochet-Bissuel M, Lory P, Monteil A. The sodium leak channel, NALCN, in health and disease. Frontiers in cellular neuroscience. 2014;8:132.
282. Berends AC, Luiten PG, Nyakas C. A review of the neuroprotective properties of the 5-HT1A receptor agonist repinotan HCl (BAYx3702) in ischemic stroke. CNS drug reviews. 2005;11(4):379-402.
283. Eijkelkamp N, Linley JE, Baker MD, Minett MS, Cregg R, Werdehausen R, et al. Neurological perspectives on voltage-gated sodium channels. Brain : a journal of neurology. 2012;135(Pt 9):2585-612.
284. Ortega-Ramirez A, Vega R, Soto E. Acid-Sensing Ion Channels as Potential Therapeutic Targets in Neurodegeneration and Neuroinflammation. Mediators of inflammation. 2017;2017:3728096. Epub 2017/10/24.
285. Duda J, Potschke C, Liss B. Converging roles of ion channels, calcium, metabolic stress, and activity pattern of Substantia nigra dopaminergic neurons in health and Parkinson's disease. Journal of neurochemistry. 2016;139 Suppl 1(Suppl Suppl 1):156-78. Epub 2016/02/13.
286. Doyle KM, Kennedy D, Gorman AM, Gupta S, Healy SJ, Samali A. Unfolded proteins and endoplasmic reticulum stress in neurodegenerative disorders. Journal of cellular and molecular medicine. 2011;15(10):2025-39. Epub 2011/07/05.
287. Rasheed N, Ahmad A, Pandey CP, Chaturvedi RK, Lohani M, Palit G. Differential response of central dopaminergic system in acute and chronic unpredictable stress models in rats. Neurochemical research. 2010;35(1):22-32. Epub 2009/07/02.
288. Mari Y, Katnik C, Cuevas J. ASIC1a channels are activated by endogenous protons during ischemia and contribute to synergistic potentiation of intracellular Ca(2+) overload during ischemia and acidosis. Cell calcium. 2010;48(1):70-82.
289. Aoyama K, Burns DM, Suh SW, Garnier P, Matsumori Y, Shiina H, et al. Acidosis causes endoplasmic reticulum stress and caspase-12-mediated astrocyte death. Journal of cerebral blood flow and metabolism : official journal of the International Society of Cerebral Blood Flow and Metabolism. 2005;25(3):358-70.
290. Swanson RA, Farrell K, Simon RP. Acidosis causes failure of astrocyte glutamate uptake during hypoxia. Journal of cerebral blood flow and metabolism : official journal of the International Society of Cerebral Blood Flow and Metabolism. 1995;15(3):417-24.
291. Kirby J, Ning K, Ferraiuolo L, Heath PR, Ismail A, Kuo SW, et al. Phosphatase and tensin homologue/protein kinase B pathway linked to motor neuron survival in human superoxide dismutase 1-related amyotrophic lateral sclerosis. Brain : a journal of neurology. 2011;134(Pt 2):506-17.
292. Schneider CA, Rasband WS, Eliceiri KW. NIH Image to ImageJ: 25 years of image analysis. Nature methods. 2012;9(7):671-5. Epub 2012/08/30.
293. McWilliam H, Li W, Uludag M, Squizzato S, Park YM, Buso N, et al. Analysis Tool Web Services from the EMBL-EBI. Nucleic acids research. 2013;41(Web Server issue):W597-600. Epub 2013/05/15.

294.Bendesky A, Pitts J, Rockman MV, Chen WC, Tan MW, Kruglyak L, and Bargmann CI. Long-range regulatory polymorphisms affecting a GABA receptor constitute a quantitative trait locus (QTL) for social behavior in Caenorhabditis elegans. PLOS genetics. 2012;8(12):e1003157.

295. L'Etoile ND, Bargmann CI. Olfaction and odor discrimination are mediated by the C. elegans guanylyl cyclase ODR-1. Neuron. 2000;25(3):575-86.

XIII. Appendix

TABLE 1. *C. elegans* strains and lines used in this study.	
Strains/Lines	**Source**
Bristol (N2) isolate	CGC
*unc-119(ed3);*Ex[p_{del-2}DEL-2_{1-27}::DsRed; *unc-119*(+)]	This study (Bombardment)
*unc-119(ed3);*Ex[p_{del-3}DEL-3_{1-45}::DsRed; *unc-119*(+)]	This study (Bombardment)
unc-119(ed3);Ex[p_{del-4}DEL-4_{1-36}::mCherry; *unc-119*(+)]	This study (Bombardment)
HA3 nuls11[osm-10::GFP + *lin-15*(+)]	CGC
NY2078 ynls[flp-8p::GFP]	CGC
BZ555 egls1[p_{dat-1}GFP]	CGC
GR1366 mgls42 [tph-1::GFP + *rol-6(su1006)*]	CGC
CZ631 juls14[acr-2p::GFP + lin-15(+)]	CGC
unc-119(ed3);Ex[p_{del-2}DEL-2_{1-27}::DsRed; p_{flp-8}GFP*;unc-119*(+)]	This study (Cross)
unc-119(ed3);Ex[p_{del-2}DEL-2_{1-27}::DsRed; OSM-10::GFP*;unc-119*(+)]	This study (Cross)
unc-119(ed3);Ex[p_{del-2}DEL-2_{1-27}::DsRed; p_{dat-1}GFP*;unc-119*(+)]	This study (Cross)
unc-119(ed3);Ex[p_{del-3}DEL-3_{1-45}::DsRed; p_{flp-8}GFP*;unc-119*(+)]	This study (Cross)
unc-119(ed3);Ex[p_{del-3}DEL-3_{1-45}::DsRed; OSM-10::GFP*;unc-119*(+)]	This study (Cross)
unc-119(ed3);Ex[p_{del-3}DEL-3_{1-45}::DsRed; p_{dat-1}GFP*;unc-119*(+)]	This study (Cross)
unc-119(ed3);Ex[p_{del-3}DEL-3_{1-45}::DsRed;TPH-1::GFP*;unc-119*(+);*rol-6(su1006)*]	This study (Cross)
unc-119(ed3);Ex[p_{del-4}DEL-4_{1-36}::mCherry; p_{flp-8}GFP*;unc-119*(+)]	This study (Cross)
unc-119(ed3);Ex[p_{del-4}DEL-4_{1-36}::mCherry; OSM-10::GFP*;unc-119*(+)]	This study (Cross)
unc119(ed3);Ex[p_{del4}DEL4_{1-36}::mCherry; p_{dat1}GFP*;unc-119*(+)]	This study (Cross)
unc119(ed3);Ex[p_{del4}DEL4_{1-36}::mCherry; TPH1::GFP*;unc-119*(+);*rol-6(su1006)*]	This study (Cross)
unc-119(ed3);Ex[p_{del-4}DEL-4_{1-36}::mCherry; p_{acr-2}GFP*;unc-119*(+)]	This study (Cross)

T28B8.5 *del-4(tm717)*	SHIGEN
F26A3.6 *del-3(tm5642)*	SHIGEN
unc-119(ed3);Ex[p_{del-2}DEL-2::mCherry; *unc-119*(+)]	This study (Bombardment)
unc-119(ed3);Ex[p_{del-3}DEL-3::DsRed; *unc-119*(+)]	This study (Bombardment)
unc-119(ed3);Ex[p_{del-4}DEL-4::DsRed; *unc-119*(+)]	This study (Bombardment)
unc-119(ed3);Ex[p_{del-4}DEL-4::GFP;*unc-119*(+)]	This study (Bombardment)
N2; Ex [p_{del-4} DEL-4:: DsRed; *rol-6(su1006)*]	This study (Injections)
LX645 dop-1(vs100)	CGC
LX702 dop-2(vs105)	CGC
LX703 dop-3(vs106)	CGC
RB781 pkc-1(ok563)	CGC
VC127 pkc-2 (ok328)	CGC
MJ500 tpa-1 (k501)	CGC
KG532 *kin-2(ce179)*	CGC
K11E8.1 *unc-43(tm1605)*	SHIGEN
del-4(tm717);dop-1(vs100)	This study (Cross)
del-4(tm717);dop-2(vs105)	This study (Cross)
del-4(tm717);dop-3(vs106)	This study (Cross)
del-4(tm717);pkc-1(ok563)	This study (Cross)
del-4(tm717);pkc-2 (ok328)	This study (Cross)
del-4(tm717);tpa-1 (k501)	This study (Cross)
del-4(tm717);kin-2(ce179)	This study (Cross)
del-4(tm717);unc-43(tm1605)	This study (Cross)
TJ375 gpls1 [*hsp-16.2*p::GFP]	CGC
CF1553 muls84 [(pAD76) sod-3p::GFP) + *rol-6(su1006)*]	CGC
CL2166 dvls19 [(pAF15) gst-4p::GFP::NLS)]	CGC
SJ4005 zcls4 [*hsp-4*::GFP]	CGC

PS3551 *hsf-1(sy441)*	CGC
CF1038 *daf-16(mu86)*	CGC
EQ87 [P_{hsf-1} HSF-1::GFP; *rol-6(su1006)]*	Ao-Lin Hsu (University of Michigan, USA)
DAF-16(d/f/h)::GFP	Tibor Vellai (Eötvös Loránd University, Budapest)
LD1008 IdEx9 [skn-1(operon)::GFP + rol-6(su1006)	CGC
LD1 [skn-1b/c::GFP + rol-6(su1006)]	CGC
IR1155 N2; Ex[$P_{let-858}$GCaMP2.0; *rol-6(su1006)*]	Palikaras et al. (Palikaras et al., 2015)
AGD383 uthls202 [aak-2(intron1)::aak-2(aa1-aa321)::Tomato::unc-54 3'UTR + *rol-6(su1006*)]	CGC
del-4(tm717); zcls4[p_{hsp-4}GFP]	This study (Cross)
del-4(tm717); uthls202[aak-2(intron1)::aak-2(aa1-aa321)::Tomato::unc-54 3'UTR ; *rol-6(su1006)]*	This study (Cross)
del-4(tm717);skn-1b/c::GFP	This study (Cross)
IR723 N2; Ex [p_{asic-1}SNB-1::SEpHluorin; *rol-6(su1006)*]	Voglis et al. (Voglis and Tavernarakis, 2008)
del-4(tm717); p_{asic-1}SNB-1::SEpHluorin; *rol-6(su1006)*	This study (Cross)
KP3085 nuls122 [p_{acr-2}::pHluorin:: SNB-1; p_{myo-2}DsRed]	CGC
DG1856 *goa-1(sa734)*	CGC
CB407 *unc-49(e407)*	CGC
unc-119(ed3);Ex[p_{del-4}DEL-4::GFP;p_{del-4}SNB-1::DsRed ;*unc-119*(+)]	This study (Co-bombardment)
EG8244 [*unc-119(ed3)*; oxSi834 [P_{unc-47} GFP::SNB-1::*unc-54* UTR; *unc-119*(+)]	E. Jorgensen (University of UTAH, Salt Lake City)
KP3947 nuls183 [p_{unc129}NLP-21::Venus + p_{myo-2}NLS::GFP]	CGC
del-4(tm717); [*unc-119(ed3)*; oxSi834[P $_{unc-47}$GFP::SNB-::unc-54 UTR; *unc-119*(+)]	This study (Cross)
del-4(tm717); nuIs183 [p_{unc129}NLP-21::Venus; p_{myo-2}NLS::GFP]	This study (Cross)
N2; Ex [p_{dat-1}ASAP-1; *rol-6(su1006)*]	This study (Injections)
del-4(tm717); p_{dat-1}ASAP-1; *rol-6(su1006)*]	This study (Cross)
del-4(tm717); egls1[p_{dat-1}GFP]	This study (Cross)
p_{del-4} DEL-4:: DsRed; egls1 [p_{dat-1}GFP]; *rol-6(su1006)*	This study (Cross)
BR5270 byIs161 [p_{rab-3}F3(delta)K280 + p_{myo-2}mCherry]	CGC

byIs161 [p_{rab-3}F3(delta)K280 + p_{myo-2}mCherry]; egIs1 [p_{dat-1}GFP]	This study (Cross)
del-4(tm717); byIs161 [p_{rab-3}F3(delta)K280 + p_{myo-2}mCherry]; egIs1 [p_{dat-1}GFP]	This study (Cross)
p_{del-4}DEL-4::DsRed; *rol-6(su1006)*; byIs161 [p_{rab-3}F3(delta)K280 + p_{myo-2}mCherry]; egIs1 [p_{dat-1}GFP]	This study (Cross)
UA44 baIn11[p_{dat-1}a-Synuclein; p_{dat-1}GFP]	G. Caldwell (University of Alabama, Tuscaloosa)
del-4(tm717); baIn11[p_{dat-1}::a-Synuclein; p_{dat-1}GFP]	This study (Cross)
p_{del-4}DEL-4:: DsRed; *rol-6(su1006)*; baIn11[p_{dat-1}a-Synuclein; p_{dat-1}GFP]	This study (Cross)
CB1033 *che-2(e1033)*	CGC

Some strains were provided by the Caenorhabditis Genetics Center (CGC), which is funded by NIH Office of Research Infrastructure Programs (P40 OD010440), and others by S. Mitani (National Bioresource Project) in Japan. *C. elegans* strains *del-4(tm717)*, *del-3(tm5642)* and *unc-43(tm1605)* were generated by the International *C. elegans* gene knockout consortium.

Table 2. Oligonucleotides used in this study.

OLIGONUCLEOTIDES	SOURCE	IDENTIFIER
Primer for the *del-4(tm717)* variation (Forward): 5′-AAAAGTGTGGACCCGGATAT-3′	This paper	N/A
Primer for the *del-4(tm717)* variation (Reverse): 5′-AAAAGTGTGGACCCGGATAT-3′	This paper	N/A
Primer for the *del-3(tm5642)* variation (Forward): 5′-ATGTGGCTCCGAGGACTTTTC-3′	This paper	N/A
Primer for the *del-3(tm5642)* variation (Reverse): 5′- GCAATCAGACACCACACCCAGTA-3′	This paper	N/A
Primer for the *dop-1(vs100)* variation (Forward): TGTGCTGAAATGAACGAATGAGAC	This paper	N/A
Primer for the *dop-1(vs100)* variation (Reverse): TCGGATCATTCAAGTCCCGTC	This paper	N/A
Primer for the *dop-2(vs105)* variation (Forward): AACGATTCCTTGCGATTCTGG	This paper	N/A
Primer for the *dop-2(vs105)* variation (Reverse): AACCATAAATCTGTGTGAGCAAAGC	This paper	N/A
Primer for the *dop-3(vs106)* variation (Forward): TGTGGGCACCTCATTCACTGG	This paper	N/A
Primer for the *dop-3(vs106)* variation (Reverse): ACCGCGCTGAACCAAAGTATG	This paper	N/A
Primer for the *pkc-1(ok563)* variation (Forward): TTGAGCGTGCTCGGGTCC	This paper	N/A
Primer for the *pkc-1(ok563)* variation (Reverse): ACCTTCCACGTTTGTTCCGTG	This paper	N/A
Primer for the *pkc-2(ok328)* variation (Forward): ACTTGCGACGTCGAATTTGTAGG	This paper	N/A
Primer for the *pkc-2(ok328)* variation (Reverse): CCATAAGCCCACCAATCCACAG	This paper	N/A

Primer for the *tpa-1(k501)* variation (Forward): CGCCATTGGTGCTAACATGAC	This paper	N/A
Primer for the *tpa-1(k501)* variation (Reverse): CCGACGAGCATTTCATACATCAA	This paper	N/A
Primer for the *kin-2(ce 179)* variation (Forward): AATAGCAGAGGGTCAGTAATTGACTG	This paper	N/A
Primer for the *kin-2(ce179)* variation (Reverse): AGTACGGATAAGCTCTTAGAGAGAAGC	This paper	N/A
Primer for the *unc-43(tm1605)* variation (Forward): TAAACTACTGCCATCAGCGTGG	This paper	N/A
Primer for the *unc-43(tm1605)* variation (Reverse): CCAAATTTTCTCATTCGCGC	This paper	N/A
Primer for *del-4* (exons 1-10) (Forward): 5′-GATGGGTGTATTTTGGACCG-3′	This paper	N/A
Primer for *del-4* (exons 1-10) (Reverse): 5′-TCAAGACACGATTCTCCTGA-3′	This paper	N/A
Primer for *del-2* transcriptional reporter (Forward): 5′-TCTTATGATGCACGGCG-3′	This paper	N/A
Primer for *del-2* transcriptional reporter (Reverse): 5′-GGTACCCGTCCACTATTAGTAAT-3′	This paper	N/A
Primer for *del-3* transcriptional reporter (Forward): 5′-5′-GCATGCTTACATTTGAGGGTTTAG-3′	This paper	N/A
Primer for *del-3* transcriptional reporter (Reverse): 5′-ACCGGTGTTTTCGATTCAGTTTT-3′	This paper	N/A
Primer for *del-4* transcriptional reporter (Forward): 5′-CTGCAGGTCGACACATCATAAATC-3′	This paper	N/A
Primer for *del-4* transcriptional reporter (Reverse): 5′-ACCGGTCCTCAACCATCGAGCATTT-3′	This paper	N/A
Primer for *del-2* translational reporter with mCherry (exons 5-11) (Forward): 5′-CTGCAGGATTTCTCTGTCAAGTGG-3′	This paper	N/A
Primer for *del-2* translational reporter with mCherry (exons 5-11) (Reverse): 5′-ACCGGTCATATTGTCAGGCAAGTT-3′	This paper	N/A
Primer for *del-2* translational reporter with mCherry (exons 2-4) (Forward): 5′-CTGCAGAGTTGATGATGATTAAAGAA-3′	This paper	N/A
Primer for *del-2* translational reporter with mCherry (exons 2-4) (Reverse): 5′-CTGCAGTGAAAATGCTCAAACAAA-3′	This paper	N/A
Primer for del-3 translational reporter (exons 2-7) (Forward): 5′-ACCGGTTGTTCACGATGATCAACTATT-3′	This paper	N/A
Primer for del-3 translational reporter (exons 2-7) (Reverse): 5′- ACCGGTGGTGTGTCTCCTGAAGCTA-3′	This paper	N/A
Primer for del-4 translational reporter with GFP (promoter and CDS) (Forward): 5′-ACGCGTCGACACATCATAAATCTCCACCCAC-3′	This paper	N/A
Primer for del-4 translational reporter with GFP (promoter and CDS) (Reverse): 5′-CGGGGTACCCCATCATTAGAATGAGGCTTTGG-3′	This paper	N/A
Primer for SNB-1 coding gene (Forward): 5′-CGG GGTACCGAATTCGGACGCTCAAGGAGATGCCGGC-3′	This paper	N/A
Primer for SNB-1 coding gene (Reverse): 5′-CGGGGTACCGAATTCTTTTCCTCCAGCCCATAAAACG-3′	This paper	N/A
Primer for *del-4* promoter (Forward): 5′-CTGCAGGTCGACACATCATAAATC-3′	This paper	N/A

Primer for *del-4* promoter (Reverse): 5′-GGATCCCATCTGCAATTTTATTTT-3′	This paper	N/A
Primer for ASAP1 voltage indicator (Forward): 5′-TAGCCGCCACCATGGAGAC-3′	This paper	N/A
Primer for ASAP1 voltage indicator (Reverse): 5′-AGATCTTTCATTAGGTTACCACTTCAAG -3′	This paper	N/A
Primer for *dat-1* promoter (Forward): 5′-CTGCAGATCCATGAAATGGAACTTGA-3′	This paper	N/A
Primer for *dat-1* promoter (Reverse): 5′-GGATCCGGCTAAAAATTGTTGAG-3′	This paper	N/A
Primer for *del-4* cDNA for RTPCR (Forward): 5'-ATGACATGGTTGTTAGTTGCACG-3'	This paper	N/A
Primer for *del-4* cDNA for RTPCR (Reverse): GTGCAAAGTAACCGAATACATCAG	This paper	N/A
Primer for pmp-3 cDNA for RTPCR (Forward): 5′-ATGATAAATCAGCGTCCCGAC-3′	This paper	N/A
Primer for pmp-3 cDNA for RTPCR (Reverse): 5′-TTGCAACGAGAGCAACTGAAC -3′	This paper	N/A
Primer for KSM vector (Forward): 5′-AGATCTGGTTACCACTAAACCAGCC-3′	This paper	N/A
Primer for KSM vector (Reverse): 5′-TGCAGGAATTCGATATCAAGCTTATCGATACC-3′	This paper	N/A
Primer for *del-4* cDNA for expression on *Xenopus* oocytes (Forward): 5′-CTTGATATCGAATTCCTGCAATGGGTGTATTTTGGACCGGC-3′	This paper	N/A
Primer for *del-4* cDNA for expression on *Xenopus* oocytes (Reverse): 5′-GTTTAGTGGTAACCAGATCTTCAATCATTAGAATGAGGCTTTGGTGGAAC-3′	This paper	N/A

Table 3. List of abbreviations used in this study.

Abbreviation	Definition
a.u.	arbitrary units
ACh	Acetylcholine
AD	Alzheimer's Disease
ALS	Amyotrophic Lateral Sclerosis
AMP	Adenosine MonoPhosphate
AMPK	AMP-activated protein Kinase
ANOVA	one-way ANalysis Of Variance
AS	Acidic Stress
ASAP1	Accelerated Sensor of Action Potentials1 (Genetic Voltage Indicator)
ASICs	Acid Sensing sodium Channels
BLAST	Basic Local Alignment Search Tool
BS	Basal Slowing
BSA	Bovine Serum Albumin
BSR	Basal Slowing Response

BSRC	Biomedical Sciences Research Center
CaMKK2	Calcium/CalModulin-dependent protein Kinase Kinase 2
cAMP	cyclic Adenosine MonoPhosphate
cRNA	coplementary RNA
ctrl	control
DCVs	Dense Core Vesicles
DEG	DEGenerin
DEL	DEgenerin Like
DiI	Dioctadecyl tetramethylIndodicarbocyanine-disulphonic acid, lipophilic carbocyanine tracer
ds RNA	double stranded RNA
DsRED	Red fluorescent protein from Discosoma
EGFP	enhanced GFP
ENaC	Epithelial sodium (Na^+) Channel
ER	Endoplasmic Reticulum
ERC	European Research Council
E_{rev}	average reversal potential
ERS	ER Stress
ER^{UPR}	ER Unfolded Protein Response
ESF	European Social Fund
FOXO	FOrkhead boX O4
GABA	Gamma-AminoButyric Acid
GCaMP2.0	Genetically encoded CalciuM indicator 2.0
GFP	Green Fluorescent Protein
HB101	*Eserichia coli* bacterial strain
HEPES	(4-(2-HydroxyEthyl)-1-PiperazineEthanesulfonic acid), a zwitterionic sulfonic acid buffering agent
hr/hrs	hour/hours
HS	Heat Stress
HSF1	Heat Shock transcription Factor 1
HSPs	Heat Shock Proteins
HT115(DE3)	*Eserichia coli* bacterial strain, commonly used for gene knockdown with RNAi
I	current
IC50	half-maximal inhibitory concentration
Imax	maximal current
IQD	interquartile range
IV	Current-voltage relationships
kb	kilobase
KCNQ	voltage-gated potassium channel
L4 stage	Larval stage 4

LTSt	Long-Term Starvation
M13	isotonic buffer solution for *C. elegans*
M9	isotonic buffer solution for *C. elegans*
mCherry	a member of the mFruits family of monomeric red fluorescent proteins
MES	2-(N-Morpholino)EthaneSulfonic acid
mg	milligram
ml	millilitre
mM	millimolar
mRNA	messenger RNA
mV	milliVolt
N2	*C. elegans* wild-type isolate, Bristol variation
NCBI	National Center for Biotechnology Information
NCRR	National Center for Research Resources
ND96	physiological NaCl solution
NEB	New England Biolabs
ng	nanogram
NGM	nematode growth medium
NIH	National Institutes of Health
NLS	Nuclear Localization Signal
NMJ	Neuromuscular Junction
NRF2	Nuclear Factor erythroid 2 - related factor 2
NSRF	National Strategic Reference Framework
O/D	Over Day
O/N	Over Night
OP50	Eserichia coli bacterial strain, common *C. elegans* food source in the laboratory
OS	Oxidative Stress
PCR	Polymerase Chain Reaction
PD	Parkinson’s Disease
PKC	Protein Kinase C
pPD95.77	plasmid vector
pPK719	plasmid DNA carrying the coding sequence of the unc-119 gene
pRF4	plasmid DNA carrying the coding sequence of the mutant collagene rol-6(su1006) causing a dominant "roller" phenotype
RNAi	RNA interference or Post-Transcriptional Gene Silencing
ROS	Reactive Oxygen Speicies
sec	seconds
SEM	Standard Error of the Mean
SEpHluorin	Super-Ecliptic pHluorin, a pH sensitive GFP variant
SGK1	Serum and Glucocorticoid-induced protein Kinase 1
SLC5A11	sodium/SoLute Cotransporter-like 5A11

SVs	Synaptic Vesicles
TRP	Transient Receptor Potential
TVEC	Two-Electrode Voltage Clamp
UTRs	UnTranslated regions
w/v	weight per volume
wt	wild-type
YFP	Yellow Fluorescent Protein
Δ	difference
ΔE_{rev}	reversal potential shift
µg	microgram
µl	microlitre
µm	micrometre
µM	microMolar

Table 4. List of *C. elegans* neurons referred in this study**.**

Neuron Name	Description	Neuronal type	Location	DELs expression
ADEL/R	Anterior DEirids Left/Right	mechanosensory, dopaminergic	head	DEL-3, DEL-4
ADF	Amphid neurons with Dual ciliated endings	sensory (gustatory, oxygen-sensory), serotonergic	head	
ASE	Amphid neurons with Single-ciliated Endings	gustatory, glutamatergic	head	DEL-2, DEL-3, DEL-4
ASH	Amphid neurons with Single-ciliated Endings	polymodal sensory, glutamatergic	head	DEL-2, DEL-4
ASI	Amphid neurons with Single-ciliated Endings	sensory (gustatory, thermosensory), insulin releasing	head	DEL-2 DEL-4
CEPDL/R	Dorsal Left/Right neurons of CEPhalic sensilla	mechanosensory, dopaminergic	head	DEL-2, DEL-3, DEL-4
CEPVL/R	Ventral Left/Right neurons of CEPhalic sensilla	mechanosensory, dopaminergic	head	DEL-3, DEL-4
DA 1-9	Ventral cord "dorsal A" motor neurons	motor, cholinergic	body (ventral nerve cord)	DEL-4
DB 1-7	Ventral cord "dorsal B " motor neurons	motor/proprioceptive, cholinergic	body (ventral nerve cord)	DEL-4
NSML/R	NeuroSecretory Motor neurons Left/Right	motor, sensory (proprioceptive/mechanosensory), serotonergic	pharynx (anterior bulb)	DEL-3, DEL-4
PDE	Posterior DEirid neurons	sensory, dopaminergic	posterior half of the body	DEL-3, DEL-4
PHA	PHAsmid neurons	chemosensory, glutamatergic	tail, right and left lumbar ganglia	DEL-2, DEL-3, DEL-4
PHB	PHasmid neurons	chemosensory, glutamatergic	tail, right and left lumbar ganglia	DEL-2, DEL-3
PHC	PHasmid neurons	thermosensory, glutamatergic	tail, right and left lumbar ganglia	DEL-2, DEL-3
PVM	Posterior Ventral Microtubule neuronal cell	mechanosensory	left side to the posterior half of the body	DEL-4
URX	head neurons with nonciliated dendritic endings	oxygen and minor CO_2 sensory, cholinergic	head	

VA 1-12	Ventral Cord motor neurons	motor, cholinergic	body (ventral nerve cord)	DEL-4
VB 1-11	Ventral Cord motor neurons	motor, proprioceptive	body (ventral nerve cord)	DEL-4
amphid	sensory organ consisting of 12 sensory neurons (ADF, ADL, AFD, ASE, ASG, ASH, ASI, ASJ, ASK, AWA, AWB, AWC) and one socket cell	sensory	head (posterior to the nerve ring)	
phasmid	sensory organ consisting of 3 sensory neurons (PHA, PHB, PQR), one sheath and two socket cells	sensory	tail (lateral sides, behind the rectum)	
deirid	a pair of sensory papillae		lateral cervical region	

Information retrieved form WORMATLAS (https://www.wormatlas.org/neurons/Individual%20Neurons/Neuronframeset.html)

Table 5. List of genetic neuronal markers used in this study.

Neuronal Marker	Expression pattern	Type of Neurons
OSM-10::GFP	ASH, ASI, PHA, PHB	sensory, glutamatergic
p_{flp-8}GFP	ASE, URX, PVM, AUA, AVM	sensory
p_{dat-1}GFP	CEP, ADE, PDE	dopaminergic
TPH-1::GFP	NSM, ADF, HSN, AFD	serotonergic
p_{acr-2}GFP	VA/B, DA/B	motor, cholinergic
p_{unc-47}GFP	RME, AVL, RIS, DVB, VD, DD	motor, GABAergic
p_{unc129}NLP-21::Venus	DA/B, MC	motor, cholinergic

Information retrieved form WORMBASE (https://wormbase.org/)

Table 6. List of *C. elegans* genes referred in this study and their mammalian orthologs.

***C. elegans* Gene**	**Definition of Nematode Gene**	**Human Ortholog**	**Definition of Human Ortholog**
aak-2	AMP-Activated Kinase	PRKAA1 and 2	PRotein Kinase AMP-activated catalytic subunit Alpha 1 and 2
acd-1	ACid-sensitive Degenerin	ASIC4	Acid Sensing Ion Channel subunit family member 4
acr-2	AcetylCholine Receptor	CHRNA3 and 6	CHolinergic Receptor Nicotinic Alpha 3 subunit and alpha 6 subunit
age-1	AGEing alteration	PIK3CB, D and G	PhosphatidylInositol-4,5-bisphosphate 3-Kinase Catalytic subunit Beta, Delta and Gamma
asic-1	Acid-Sensing/Amiloride-Sensitive Ion Channel	SCNN1B, D and G	sodium channel epithelial 1 subunit beta, delta and gamma
cat-2	abnormal CATecholamine distribution	TH	Tyrosine Hydroxylase
che-2	abnormal CHEmotaxis	IFT80	IntraFlagellar Transport 80
daf-16	abnormal DAuer Formation	FOXO4	FOrkhead boX O4
daf-2	abnormal DAuer Formation	IGF1R, INSR and INSRR	insulin-like growth factor 1 receptor, insulin receptor and insulin receptor related receptor
dat-1	DopAmine Transporter	SLC6A2 and 3	solute carrier family 6 member 2 and 3
del-2	DEgenerin Like		
del-3	DEgenerin Like		
del-4	DEgenerin Like	SCNN1G	sodium channel epithelial 1 subunit gamma
dop-1	DOPamine receptor	DRD1	dopamine receptor D1
dop-2	DOPamine receptor	DRD3	dopamine receptor D3
dop-3	DOPamine receptor	DRD3	dopamine receptor D3
flp-8	FMRF-Like Peptide		
goa-1	G protein,O, Alpha subunit	GNAO1	G protein subunit alpha o1
gst-4	Glutathione S-Transferase		
hsf-1	Heat Shock Factor	HSF1 and 2	heat shock transcription factor 1 and 2
hsp-16.2	Heat Shock Protein		
hsp-4	Heat Shock Protein	HSPA5	heat shock protein family A (Hsp70) member 5
kin-1	protein KINase	PRKACA	protein kinase cAMP-activated catalytic subunit alpha
kin-2	protein KINase	PRKAR1B	protein kinase cAMP-dependent type I regulatory subunit beta
let-858	LEThal	CWC22	spliceosome associated protein homolog
lin-15	abnormal cell LINeage		
myo-2	MYOsin heavy chain structural genes	MYH1, 2 and 3	myosin heavy chain 1, 2 and 3
myo-3	MYOsin heavy chain structural genes	MYH1, 2 and 3	myosin heavy chain 1
nlp-21	Neuropeptide-Like Protein		

osm-10	OSMotic avoidance abnormal		
pkc-1	Protein Kinase C	PRKCE	protein kinase C epsilon
pkc-2	Protein Kinase C	PRKCA	protein kinase C alpha and beta
pmp-3	Peroxisomal Membrane Prorein related	ABCD4	ATP binding cassette subfamily D member 4
rab-3	RAB family	RAB3A	member RAS oncogene family
rol-6	ROLler: helically twisted, animals roll when moving	COLQ	collagen like tail subunit of asymmetric acetylcholinesterase
skn-1	SKiNhead	NFE2, NFE2L1, NFE2L2	Erythroid Nuclear Factor 2, NFE2 like bZIP transcription factor 1 and 2
snb-1	SyNaptoBrevin related	VAMP2	vesicle associated membrane protein 2
snt-1	SyNapTotagmin	SYT1	synaptotagmin 1
sod-3	SuperOxide Dismutase	SOD2	superoxide dismutase 2
tpa-1	tetradecanoyl phorbol acetate resistant	PRKCD and PRKCQ	protein kinase C delta and protein kinase C theta
tph-1	TryPtophan Hydroxylase	TPH1 and 2	tryptophan hydroxylase 1 and 2
xbp-1	X-box Binding Protein	XBP1	X-box binding protein 1
unc-119	UNCoordinated	UNC-119	lipid binding chaperone
unc-129	UNCoordinated	GDF10	growth differentiation factor 10
unc-43	UNCoordinated	CAMK2D	(calcium/calmodulin dependent protein kinase II delta
unc-47	UNCoordinated	SLC32A1	solute carrier family 32 member 1
unc-49	UNCoordinated		
unc-54	UNCoordinated	MYH1, 2 and 3	myosin heavy chain 1, 2 and 3

Information retrieved from WORMBASE (https://wormbase.org/)

Table 7. Key Resources Table

REAGENT or RESOURCE	SOURCE	IDENTIFIER
Bacterial and virus strains		
Escherichia coli: OP50	Jonathan Ewbank lab; *Caenorhabditis* Genetics Center (CGC)	WB-STRAIN: WBStrain00041971; WormBase ID: WBStrain00041971
Escherichia coli: HB101 strain: *E. coli* [supE44 hsdS20(rB-mB-) recA13 ara-14 proA2 lacY1 galK2 rpsL20 xyl-5 mtl-1]	*Caenorhabditis* Genetics Center (CGC)	WB-STRAIN: WBStrain00041075; WormBase ID: WBStrain00041075
Escherichia coli: Ht115 (DE3): E. coli [F-, mcrA, mcrB, IN(rrnD-rrnE)1, rnc14::Tn10(DE3 lysogen: lacUV5 promoter -T7 polymerase].	*Caenorhabditis* Genetics Center (CGC)	WB-STRAIN:HT115; WormBase ID: WBStrain00041079

Escherichia coli: Na22	*Caenorhabditis* Genetics Center (CGC)	WB-STRAIN: WBStrain00041948; WormBase ID: WBStrain00041948
Chemicals, peptides, and recombinant proteins		
Levamisole	Sigma-Aldrich	Product No.: PHR1798; CAS: 16595-80-5
Tetramisole hydrochloride	Sigma-Aldrich	Product No.: L9756; CAS: 16595-80-5
Paraquat (N, N'-dimethyl-4,4'-bipyridinium dichloride)	Sigma-Aldrich	Product No.: 36541; CAS: 75365-73-0
Tunicamycin from *Streptomyces sp.*	Sigma-Aldrich	Beilstein No.: 6888090; CAS: 11089-65-9
Dopamine hydrochloride	Sigma-Aldrich	Beilstein No.: 3656720; CAS: 62-31-7
UltraPure Agarose	Invitrogen	Cat.#: 16500500
Ethidium Bromide	Sigma-Aldrich	Cat.#: 1.11615.0010; CAS: 1239-45-8
Nanobeads NIST Traceable Particle Size Standard 100 nm	Polysciences	Cat.#: 64010-15
DiI (dioctadecyl tetramethylindodicarbocyanine-disulphonic acid)	Invitrogen	Cat.#: N22880
Aldicarb	Sigma-Aldrich	Product No. 33386; CAS: 116-06-3
TRIzol reagent	Invitrogen	Cat.#: 15596026
pcDNA3.1 /Puro - CAG - ASAP1 plasmid	Schnitzer et. al., 2014	Addgene plamid#52519; RRID:Addgene_52519
pPD95.77 (L2464)	Fire Lab *C. elegans* Vector Kit – 1995; http://n2t.net/addgene:1495	Addgene plasmid# 1495; RRID:Addgene_1495
pL4440	Fire Lab *C. elegans* Vector Kit – 1999; http://n2t.net/addgene:1654	Addgene plasmid# 1654; RRID:Addgene_1654
pPD96.52 (L2534)	Fire Lab *C. elegans* Vector Kit – 1999; http://n2t.net/addgene:1608	Addgene plasmid#1608; RRID:Addgene_1608
pPK719 (unc-119) rescue	Roger Pocock lab (BRIC, Copenhagen, Denmark); ; http://n2t.net/addgene:38149	Addgene, plasmid #38149; RRID:Addgene_38149
Critical commercial assays		
NucleoSpin Tissue, Mini kit for DNA from cells and tissue	Macherey-Nagel	Cat. # 740952.250
Topo TA Cloning Kit	Invitrogen	Cat.# K457501
iScript™ cDNA Synthesis Kit	Bio-Rad	Cat.#: 1708890
SuperScript™ III First-Strand Synthesis System	Invitrogen	Cat. # 18080051
NEB Q5® Site-Directed Mutagenesis Kit	New England BioLabs	Cat. # E0554S
NEBuilder® HiFi DNA Assembly Master Mix	New England BioLabs	Cat. # E2621L
mMESSAGE mMACHINE™ T7 Transcription Kit	Ambion	Cat.# AM1344

Deposited data		
WormBase	International consortium for *C. elegans* and related nematodes	https://wormbase.org//#012-34-5
Blast: Basic Local Alignment Search Tool - NCBI	NIH: National Library of Medicine – National Center for Biotechnology Information	https://blast.ncbi.nlm.nih.gov/Blast.cgi
WormBook	THE ONLINE REVIEW OF *C. elegans* BIOLOGY	http://wormbook.org/
Experimental models: Organisms/strains		
C. elegans strains, see Table 1		
Xenopus laevis oocytes	EcoCyte Bioscience (Dortmund,Germany)	N/A
Recombinant DNA		
del-2 (exons 5-12) in pL4440 (RNAi)	This paper	N/A
del-3 (exons 2-7) in pL4440 (RNAi)	This paper	N/A
del-4 (exons 1-10) in pL4440 (RNAi)	This paper	N/A
p_{del-2}DsRed transcriptional reporter in the pPD95.77 plasmid vector	This paper	N/A
p_{del-3}DsRed transcriptional reporter in the pPD95.77 plasmid vector	This paper	N/A
p_{del-4}mCherry transcriptional reporter in the pPD95.77 plasmid vector	This paper	N/A
p_{del-2}DEL-2::mCherry translational reporter in pPD95.77	This paper	N/A
p_{del-3}DEL-3::DsRed translational reporter in pPD95.77	This paper	N/A
p_{del-4}DEL-4::GFP translational reporter in pPD95.77	This paper	N/A
p_{del-4}DEL-4::DsRed translational reporter in pPD95.77	This paper	N/A
p_{del-4}SNB-1::DsRed synaptic vesicle marker in pPD95.77	This paper	N/A
p_{dat-1}ASAP-1 voltage sensor in pPD96.52	This paper	N/A
pEK230: *del-4* cDNA in the KSM vector	This paper	N/A
pEK238: *del-4(tm717)* cDNA in the KSM vector	This paper	N/A
Software and algorithms		

ImageJ 1.48V	Schneider et al. (292)	https://imagej.nih.gov/ij/index.html; RRID: SCR_003070
GraphPad Prism 8.0.2	GraphPad Software	https://www.graphpad.com/
Photoshop CS5	Adobe	https://www.adobe.com/gr_en/products/photoshop/landpb.html
Volocity High-Performance 3D imaging software	Volocity	https://www.volocity4d.com/
SnapGene Viewer	SnapGene by Dotmatics	https://www.snapgene.com/snapgene-viewer
CenGen	CeNGEN - THE COMPLETE GENE EXPRESSION MAP OF THE C. ELEGANS NERVOUS SYSTEM	https://www.cengen.org/
Phobius tool	Stockholm Bioinformatics Centre; McWilliam et al. (293)	http://phobius.sbc.su.se/

XIV. Publications

1. Dionysia Petratou, Martha Gjikolaj, Eva Kaulich, William Schafer, and Nektarios Tavernarakis; (2023). A proton-inhibited DEG/ENaC ion channel maintains neuronal ionstasis and promotes neuronal survival under stress. iScience *26*, 107117. 10.1016/j.isci.2023.107117.
2. 2. Dionysia Petratou, Persefoni Fragkiadaki, Eirini Lionaki, and Nektarios Tavernarakis; (2023). Assessing Locomotory rate in response to food for identification of neuronal and muscular defects in C. elegans. Star protocols.

iScience

CellPress
OPEN ACCESS

Article

A proton-inhibited DEG/ENaC ion channel maintains neuronal ionstasis and promotes neuronal survival under stress

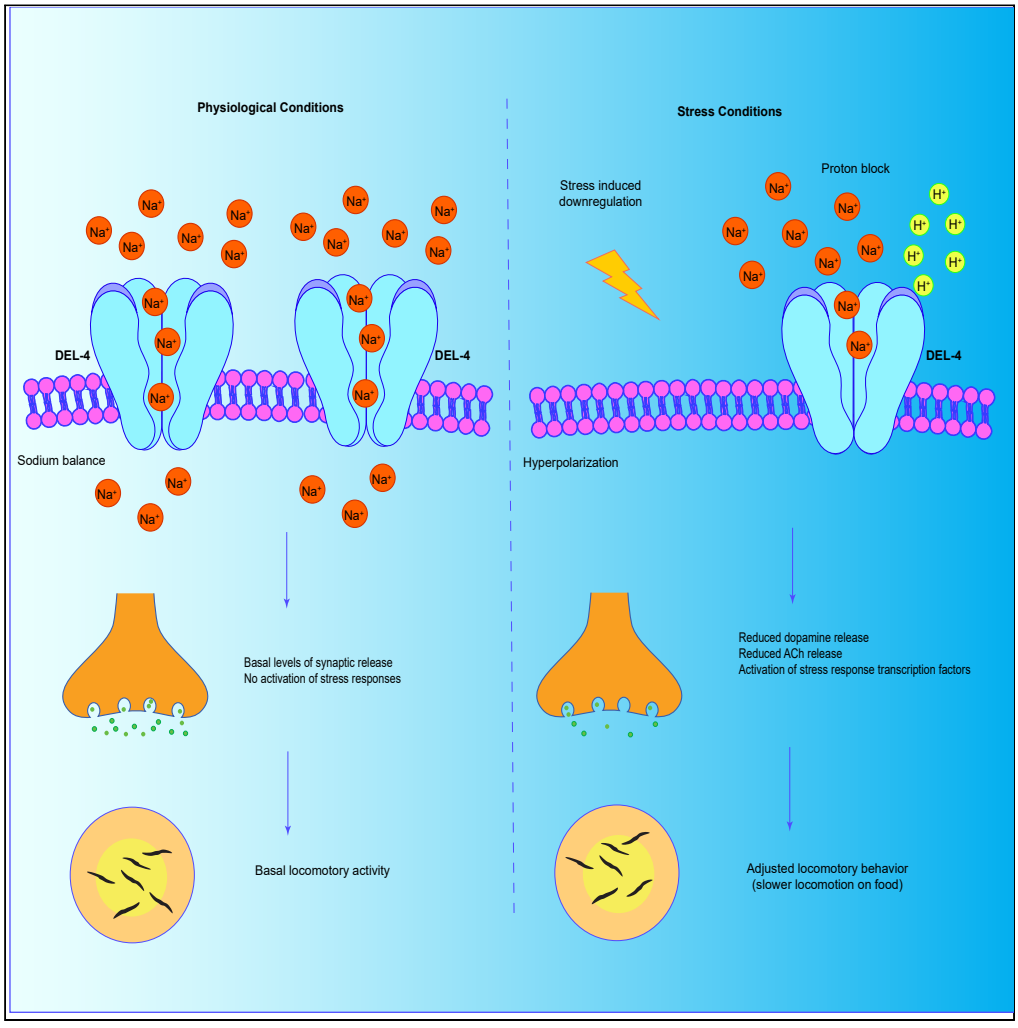

Dionysia Petratou, Martha Gjikolaj, Eva Kaulich, William Schafer, Nektarios Tavernarakis

tavernarakis@imbb.forth.gr

Highlights

The degenerin DEL-4 forms a sodium leak homomeric proton-inhibited channel

DEL-4 regulates neuronal membrane potential and neurotransmission

Heat stress and starvation reduce DEL-4 expression

DEL-4 depletion triggers systemic stress responses and neurodegeneration

Petratou et al., iScience 26, 107117
July 21, 2023
https://doi.org/10.1016/j.isci.2023.107117

iScience

CellPress
OPEN ACCESS

Article

A proton-inhibited DEG/ENaC ion channel maintains neuronal ionstasis and promotes neuronal survival under stress

Dionysia Petratou,[1,2] Martha Gjikolaj,[1,2] Eva Kaulich,[3] William Schafer,[3] and Nektarios Tavernarakis[1,2,4,*]

SUMMARY

The nervous system participates in the initiation and modulation of systemic stress. Ionstasis is of utmost importance for neuronal function. Imbalance in neuronal sodium homeostasis is associated with pathologies of the nervous system. However, the effects of stress on neuronal Na^+ homeostasis, excitability, and survival remain unclear. We report that the DEG/ENaC family member DEL-4 assembles into a proton-inactivated sodium channel. DEL-4 operates at the neuronal membrane and synapse to modulate *Caenorhabditis elegans* locomotion. Heat stress and starvation alter DEL-4 expression, which in turn alters the expression and activity of key stress-response transcription factors and triggers appropriate motor adaptations. Similar to heat stress and starvation, DEL-4 deficiency causes hyperpolarization of dopaminergic neurons and affects neurotransmission. Using humanized models of neurodegenerative diseases in *C. elegans*, we showed that DEL-4 promotes neuronal survival. Our findings provide insights into the molecular mechanisms by which sodium channels promote neuronal function and adaptation under stress.

INTRODUCTION

Physiological stress, perceived by the sensory system, induces cellular stress responses that trigger organismal adaptation. Organisms have adapted to overcome different types of stress that emerge throughout their lives. Organismal homeostasis, behavior, and survival are altered by environmental stresses, such as heat, starvation, hypoxia, and oxidative stress.[1–3] The nervous system is an essential sensor of environmental changes.[4] Stress perception and decision-making for specific behavioral responses occur through adjustments in neuronal activity, plasticity, or signal transduction.[3] Neurons modify their properties and excitation patterns via structural and functional plasticity to convey stressful messages. Functional neuronal plasticity in response to stress is contingent on the regulation of neurotransmitter receptors, transporters, and ion channels. Several studies in mammals have demonstrated the effects of diverse types of stress on neurotransmitter and receptor levels. Gamma-aminobutyric acid (GABA), glutamate, acetylcholine, corticoid, serotonin, and dopamine receptors compose indicative signaling initiators whose expression levels depend on distinct types of stress.[5–9]

Nevertheless, how stressful stimuli are perceived and what molecular modifications modulate excitation and intrinsic neuronal properties are not fully understood. Recent studies have revealed that stress modifies ion channel abundance or activation. In mammals, acute and chronic stress differentially coordinates the expression of voltage-gated potassium channels.[10,11] Activation of AMP-activated protein kinase (AMPK) potentially mediates the effects of acute stress on potassium-conducting channels.[11] In *Drosophila melanogaster*, starvation suppresses KCNQ potassium channel activity via sodium/solute cotransporter-like 5A11.[12] Oxidative stress modulates the expression of calcium-conducting channels.[13,14] Likewise, reactive oxygen species activate the TRP ankyrin1 channel, which acts as an oxidative and nitrative stress sensor.[15] However, the regulation of sodium channels in neuronal cells and their participation in signal transduction in response to stress remain unclear.[16]

Early studies have indicated that neural conduction in the nematode *Caenorhabditis elegans* differs from that in vertebrates.[17] Research on neuronal electrical properties has revealed that several *C. elegans* neurons only generate graded responses. This notion prevailed until the recent discovery that specific

[1]Institute of Molecular Biology and Biotechnology, Foundation for Research and Technology, Heraklion, 70013 Crete, Greece

[2]Department of Basic Sciences, Medical School, University of Crete, Heraklion, 71003 Crete, Greece

[3]Neurobiology Division, MRC Laboratory of Molecular Biology, Cambridge Biomedical Campus, CB2 0QH Cambridge, UK

[4]Lead contact

*Correspondence: tavernarakis@imbb.forth.gr

https://doi.org/10.1016/j.isci.2023.107117

C. elegans sensory neurons may fire action potentials.[18] Nevertheless, the potassium and calcium currents generate both graded and action potentials in *C. elegans*. Classical voltage-gated sodium channels and sodium-dependent potentials have not yet been identified.[19] Despite the lack of voltage-dependent sodium channels, several findings suggest that Na+ currents contribute to neuronal firing in *C. elegans*. Patch-clamp recordings revealed that the absence of extracellular Na+ abolishes action potentials.[20]

Degenerin/epithelial sodium channels (DEG/ENaCs) constitute a large family of voltage-insensitive sodium channels, expressed in the nervous system and epithelial tissues.[21] They have been implicated in several human pathologies, including respiratory syndromes, vascular, cardiac, and neurodegenerative diseases.[22] Few studies have pinpointed their implications in stress responses. In vertebrates, pharmacological inhibition of acid-sensing sodium ion channels (ASICs) (Table S1) reduces stress-associated reactions in behavioral models and exhibits antidepressant-like effects.[23,24] Oxidative stress inhibits the expression of α-ENaC[25,26] and regulates the activation of ASICs.[27,28] SGK1, a Ser-Thr kinase induced by the corticosteroid signaling pathway, modulates the abundance of ENaC and ASIC1 in the plasma membrane.[29–31] Elevation of corticosterone by acute stress causes a protein kinase C (PKC)-dependent increase of ASIC currents in cultured hippocampal neurons.[32,33]

In this study, we sought to delineate the participation of DEG/ENaC family members in stress perception and subsequent integration to modify behavioral responses in animals. We used *C. elegans* as a model organism for its extensively characterized nervous system, exceptional genetic tractability, and significant conservation with mammalian systems. We show that the degenerin-like (DEL) proteins DEL-2, DEL-3, and DEL-4, three members of the degenerin family, are expressed in chemosensory and dopaminergic neurons. DEL-3 and DEL-4 are additionally expressed in serotonergic, with DEL-4 also expressed in cholinergic motor neurons. The dopamine-mediated basal slowing response revealed that DEL-4 affects dopaminergic signaling. Interestingly, we found that DEL-4 forms a proton-blocked homomeric amiloride-sensitive sodium channel. Using reverse genetics, pharmacological analysis, and imaging techniques, we provide evidence that DEL-4 is regulated by specific types of stress and contributes to the adaptation of neuronal signaling to modify the locomotory rate of the animal. Analysis of neurodegenerative disease models revealed the neuroprotective properties of DEL-4. Discerning the neuronal mechanisms that drive the effects of stress on sensory integration and neuronal cohesion will provide valuable insights into how stress advances the progression of neurodegenerative diseases and may provide new pharmaceutical targets.

RESULTS

Localization pattern of degenerins DEL-2, DEL-3, and DEL-4

The degenerin DEG/ENaC subfamily of *C. elegans* comprises approximately 30 members. We focused on the three members, DEL-2, DEL-3, and DEL-4, previously identified in a serial analysis of gene expression to localize in ASE neurons, the primary set of gustatory neurons in *C. elegans*.[34]

To determine the expression patterns of these three degenerins, we generated transcriptional reporters (STAR Methods, Table 2). Epifluorescence imaging revealed that all three DELs were localized to the head, midbody, and tail neurons (Figures 1, S1A and S2). To identify neurons that express DEL-2, DEL-3, and DEL-4, we crossed their transcriptional reporters with several neuron-specific fluorescent markers, specifically for sensory, dopaminergic, serotonergic, and cholinergic motor neurons (Table 1, S2 and S3). We verified the expression of these three channels in ASE neurons, as previously described,[34] using a transcriptional reporter of FLP-8 (Figure 1). Further analysis revealed that DEL-2 localizes in the amphids ASH and ASI (apart from ASE), phasmids PHA and PHB, and dopaminergic neurons CEPDL/R (Figures 1A and S2A). DEL-3 is present in the chemosensory neurons ASE, PHA, PHB, and PHC, in most dopaminergic neurons (CEPDL/R, CEPVL, ADEL, and PDE), and in the serotonergic neurons NSML/R (Figures 1B and S2B). DEL-4 displayed broad expression. It localizes at the chemosensory neurons ASE, ASI, ASH, and PHA, in all dopaminergic neurons (CEPDL/R, CEPVL/R, ADEL/R, and PDE) and the serotonergic neuron NSMR (Figures 1C and S2C). Moreover, DEL-4 subsists in cholinergic motor neurons VA/B, DA/B, and mechanosensory PVM neurons (Figures 1C and S2C). Additionally, we looked at the CenGen data for neurons identified to express DEL-2, DEL-3, and DEL-4. Indeed, some of the neurons that we propose that express DELs coincide with those identified in the CenGen (Key Resources Table - KRT), specifically, the DEL-2 expression in the neurons ASH, ASE, ASI, PHB, and CEP and the DEL-3 expression in the neurons CEP, ADE,

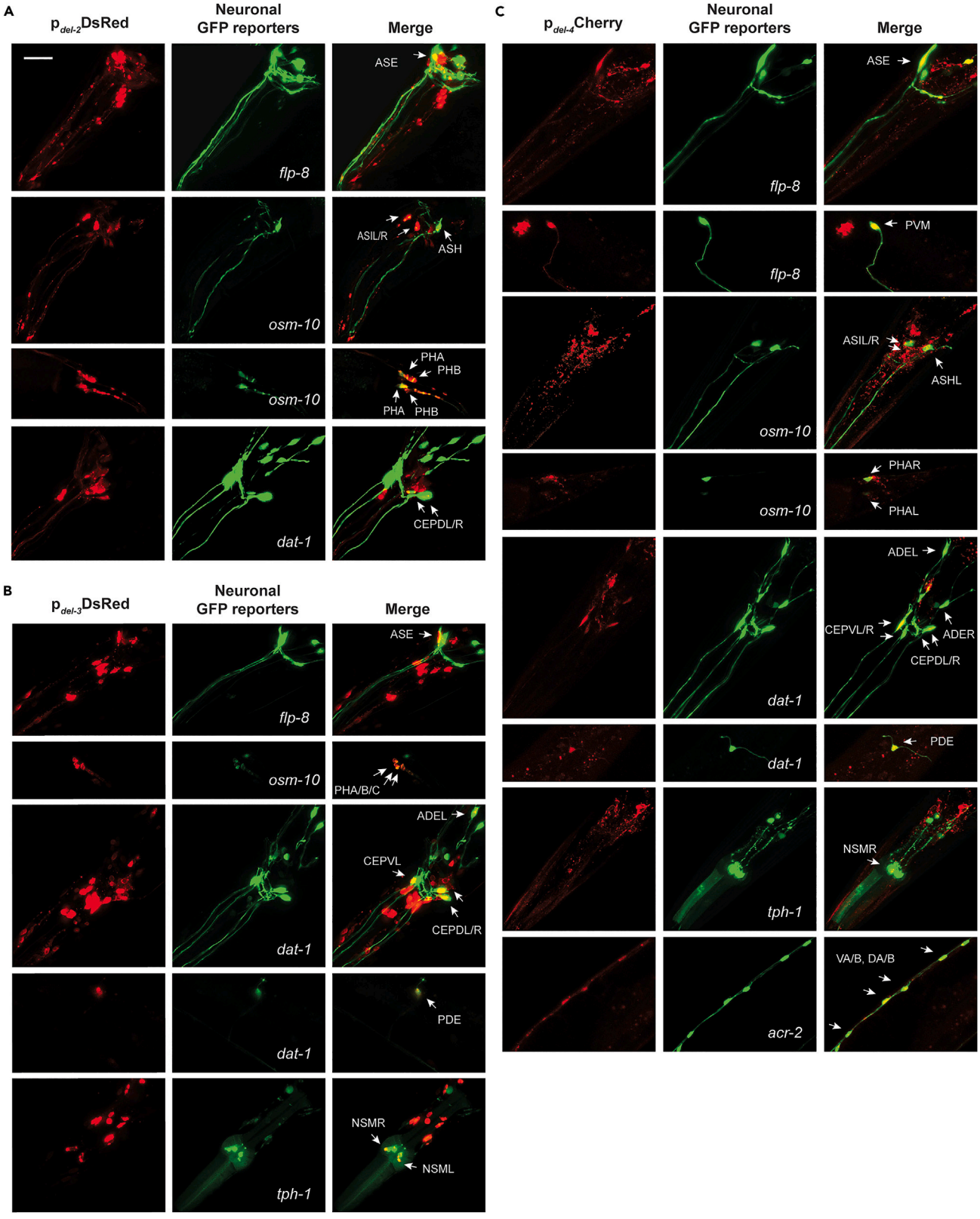
A
p del-2 DsRed
Neuronal GFP reporters
Merge
ASE
flp-8
ASIL/R
ASH
osm-10
PHA
PHB
PHA PHB
osm-10
dat-1
CEPDL/R
B
p del-3 DsRed
Neuronal GFP reporters
Merge
ASE
flp-8
osm-10
PHA/B/C
ADEL
CEPVL
CEPDL/R
dat-1
dat-1
PDE
tph-1
NSML
NSMR
C
p del-4 Cherry
Neuronal GFP reporters
Merge
ASE
flp-8
PVM
flp-8
ASIL/R
ASHL
osm-10
PHAR
PHAL
osm-10
ADEL
CEPVL/R
ADER
CEPDL/R
dat-1
dat-1
PDE
NSMR
tph-1
VA/B, DA/B
acr-2

Figure 1. Neuronal expression of DEL-2, DEL-3, and DEL-4

(A) Expression of DEL-2 in the chemosensory neurons ASE, ASH, ASI, PHA, and PHB and in the set of dopaminergic neurons CEPDL/R in the head (Tables S2 and S3).

(B) Expression of DEL-3 in the chemosensory neurons ASE, PHA, PHB, and PHC, in the dopaminergic neurons CEPDL/R, CEPVL, ADEL, and PDE in the head and midbody, and the serotonergic neurons NSMR/L (Tables S2 and S3).

(C) Identification of DEL-4 expression in the chemosensory neurons ASE, ASI, ASH, and PHA, in the mechanosensory neuron PVM, in all six dopaminergic neurons CEPDL/R, CEPVL/R, ADEL/R in the head, and PDE in the midbody, in the serotonergic neuron NSMR and cholinergic motor neurons VA/B and DA/B (Tables S2 and S3). (A–C) Confocal images at 40x lens (maximum intensity projections) of strains that were generated by crossing *del-2, del-3*, or *del-4* transcriptional reporters (red – left column) with the respective neuronal reporters (green – middle column). Left columns: *del-2*, *del-3*, and *del-4* promoters drive the expression of mCherry or dsRed in the nervous system. Middle columns: transcriptional GFP neuronal reporters are shown in green. Promoters of *flp-8* and *osm-10* drive expression in the sensory neurons ASE, URX, PVM, and ASH, ASI, PHA, and PHB, respectively. The promoter of *dat-1* drives expression of GFP in the dopaminergic neurons (CEPD, CEPV, ADE, and PDE), the *tph-1* promoter in the serotonergic neurons (NSM and ADF), and the *acr-2* promoter in the cholinergic motor neurons (VA/B and DA/B) (Tables S2 and S3). (right columns) The right column of each panel corresponds to merged images. We utilized the merged images of z-stacks to assess colocalization (see also Figure S2). One day adult animals. Arrows indicate neuronal cell somas where mCherry or dsRed is co-expressed with GFP (left is anterior). Scale bar 20 μM. See also Figure S2.

PDE, and NSM. Therefore, we conclude that DEL-2, DEL-3, and DEL-4 show a neuronal localization pattern, which in the case of DEL-4 expands from sensory to motor neurons.

DEL-4 exhibits high similarity to human ENaCs and ASICs (ENaC1b and ASIC1b), as identified by protein BLAST (see Methods section). *In silico* analysis using the tool Phobius of the Stockholm Bioinformatics Center (http://phobius.sbc.su.se/)[35] predicted that DEL-4 shares a topology analogous to that of the rest of the DEG/ENaC family members (Figure S1B, green, yellow, red, and orange boxes). It adopts a characteristic structural model consisting of two transmembrane domains, two small intracellular regions at the N- and C-terminus, and one large extracellular loop. The broader expression pattern of DEL-4 both in sensory and motor neurons together with its similarity to human ENaCs and ASICs led us to focus our study on DEL-4 as a putative regulator of neuronal ionstasis, and further examined its role in regulation of stress response.

DEL-4 downregulation simulates a stress-like state

To investigate the possible effects of stress on DEL-4 ion channel, we measured its expression under various types of stress (Figures 2 and S3). Heat stress and long-term starvation reduced DEL-4 levels (Figures 2A, 2E, S3F and S3G). In contrast, oxidative stress, ER, and acidic pH stress did not affect them (Figures 2B–2E). These finding suggest that heat stress (HS) and long-term starvation can modulate DEL-4-mediated signaling.

Heat shock transcription factor 1 (HSF-1) is the homolog of the mammalian HSF1 and master regulator of heat shock response.[36–38] Interestingly, heat stress in the absence of *hsf-1* further reduces *del-4* expression (Figures 2E–2G). This implies that *del-4* suppression upon HS is not HSF-1 dependent; however, the presence of HSF-1 ameliorates DEL-4 depletion upon HS. Consistently, *in silico* analysis revealed the presence of HSF-1 binding sites in *del-4* promoter region (Figures S1B and S1C). Since heat stress curtailed the abundance of DEL-4 in the neuronal cell membrane, we hypothesized that the null *del-4* mutant (Figure S1D) where DEL-4 is permanently absent would experience sustained stress. Indeed, alleviation of DEL-4 resulted in a statistically significant increase of HSF-1 protein levels throughout the whole-body (Figure 2G) and hypodermis nuclei (Figures 2H, S4A and S4I). HSP-16.2 expression levels, directly regulated by HSF-1, are also increased in *del-4* mutant background (Figures 2I, S4B and S4I). To further verify the activation of HSF-1 in the absence of *del-4*, we tested the thermotolerance of *del-4* mutants and overexpressing animals. As predicted, *del-4* mutants were HS resistant as they survived longer than wild type (wt) after HS, while DEL-4-overexpressing animals were sensitive to thermal stress (Figure 2J). These findings underline the role of DEL-4 in the regulation of heat shock response.

As mentioned previously, long-term starvation depletes DEL-4 protein levels (Figures 2A and 2E). DAF-16, the homolog of mammalian FOXO, is a key transcription factor activated in response to starvation. Upon starvation, DAF-16 translocates to the nucleus to promote metabolic adaptations necessary for resistance to stress.[39] Nonetheless, long-term starvation reduces DAF-16 expression and triggers its translocation back to the cytoplasm in an AGE-1/PI3K-dependent manner.[40] We found that downregulation of *del-4* reduced DAF-16 protein levels in the whole body (Figures 3A and 3K) and decreased the nucleus/cytoplasm ratio of DAF-16 (Figures 3B, 3K, S4C and S4I), mimicking the response to long-term starvation. We also observed a reduction in the expression of a well-established DAF-16-target gene, namely

Table 1. *C. elegans* strains and lines used in this study

REAGENT or RESOURCE	SOURCE	IDENTIFIER
Experimental model: *C. elegans* Strains		
Wild type: Bristol (N2) isolate	*Caenorhabditis* Genetics Center	RRID: WB-STRAIN: WBStrain00000001; WormBase ID: WBStrain00000001
$p_{del\text{-}2}$DsRed: *unc-119(ed3)*;Ex[$p_{del\text{-}2}$DEL-$2_{1\text{-}27}$::DsRed; *unc-119*(+)]	This paper	N/A
$p_{del\text{-}3}$DsRed: *unc-119(ed3)*;Ex[$p_{del\text{-}3}$DEL-$3_{1\text{-}45}$::DsRed; *unc-119*(+)]	This paper	N/A
$p_{del\text{-}4}$Cherry: *unc-119(ed3)*;Ex[$p_{del\text{-}4}$DEL-$4_{1\text{-}36}$::mCherry; *unc-119*(+)]	This paper	N/A
$p_{osm\text{-}10}$GFP: HA3 nuls11[osm-10::GFP + *lin-15*(+)]	*Caenorhabditis* Genetics Center	RRID: WB-STRAIN: WBStrain00008277; WormBase ID: WBStrain00008277
$p_{flp\text{-}8}$GFP: NY2078 ynls78[flp-8p::GFP]	*Caenorhabditis* Genetics Center	RRID: WB-STRAIN:WBStrain00029169; WormBase ID: WBStrain00029169
$p_{dat\text{-}1}$GFP: BZ555 egls1[$p_{dat\text{-}1}$GFP]	*Caenorhabditis* Genetics Center	RRID: WB-STRAIN:WBStrain00004039; WormBase ID: WBStrain00004039
$p_{tph\text{-}1}$GFP: GR1366 mgls42 [tph-1::GFP + *rol-6(su1006)*]	*Caenorhabditis* Genetics Center	RRID: WB-STRAIN:WBStrain00007909; WormBase ID: WBStrain00007909
$p_{acr\text{-}2}$GFP: CZ631 juls14[acr-2p::GFP + lin-15(+)]	*Caenorhabditis* Genetics Center	RRID:WB-STRAIN:WBStrain00005354; WormBase ID: WBStrain00005354
$p_{del\text{-}2}$DsRed; $p_{flp\text{-}8}$GFP: *unc-119(ed3)*;Ex[$p_{del\text{-}2}$ DEL-$2_{1\text{-}27}$::DsRed; $p_{flp\text{-}8}$GFP;*unc-119*(+)]	This paper	N/A
$p_{del\text{-}2}$DsRed; $p_{osm\text{-}10}$GFP: *unc-119(ed3)*;Ex[$p_{del\text{-}2}$ DEL-$2_{1\text{-}27}$::DsRed; OSM-10:: GFP;*unc-119*(+)]	This paper	N/A
$p_{del\text{-}2}$DsRed; $p_{dat\text{-}1}$GFP: *unc-119(ed3)*;Ex[$p_{del\text{-}2}$ DEL-$2_{1\text{-}27}$::DsRed; $p_{dat\text{-}1}$GFP;*unc-119*(+)]	This paper	N/A
$p_{del\text{-}3}$DsRed; $p_{flp\text{-}8}$GFP: *unc-119(ed3)*;Ex[$p_{del\text{-}3}$ DEL-$3_{1\text{-}45}$::DsRed; $p_{flp\text{-}8}$GFP;*unc-119*(+)]	This paper	N/A
$p_{del\text{-}3}$DsRed; $p_{osm\text{-}10}$GFP: *unc-119(ed3)*;Ex[$p_{del\text{-}3}$ DEL-$3_{1\text{-}45}$::DsRed; OSM-10:: GFP;*unc-119*(+)]	This paper	N/A
$p_{del\text{-}3}$DsRed; $p_{dat\text{-}1}$GFP: *unc-119(ed3)*;Ex[$p_{del\text{-}3}$ DEL-$3_{1\text{-}45}$::DsRed; $p_{dat\text{-}1}$GFP;*unc-119*(+)]	This paper	N/A
$p_{del\text{-}3}$DsRed; $p_{tph\text{-}1}$GFP: *unc-119(ed3)*;Ex[$p_{del\text{-}3}$ DEL-$3_{1\text{-}45}$::DsRed;TPH-1::GFP;*unc-119*(+); *rol-6(su1006)*]	This paper	N/A
$p_{del\text{-}4}$Cherry; $p_{flp\text{-}8}$GFP: *unc-119(ed3)*;Ex[$p_{del\text{-}4}$ DEL-$4_{1\text{-}36}$::mCherry; $p_{flp\text{-}8}$GFP;*unc-119*(+)]	This paper	N/A
$p_{del\text{-}4}$Cherry; $p_{osm\text{-}10}$GFP: *unc-119(ed3)*;Ex[$p_{del\text{-}4}$ DEL-$4_{1\text{-}36}$::mCherry; OSM-10::GFP;*unc-119*(+)]	This paper	N/A
$p_{del\text{-}4}$Cherry; $p_{dat\text{-}1}$GFP: *unc119(ed3)*; Ex[p_{del4} $DEL4_{1\text{-}36}$::mCherry; p_{dat1}GFP;*unc-119*(+)]	This paper	N/A
$p_{del\text{-}4}$Cherry; $p_{tph\text{-}1}$GFP: *unc119(ed3)*; Ex[p_{del4} $DEL4_{1\text{-}36}$::mCherry; TPH1::GFP;*unc-119*(+); *rol-6(su1006)*]	This paper	N/A
$p_{del\text{-}4}$Cherry; $p_{acr\text{-}2}$GFP: *unc-119(ed3)*;Ex[$p_{del\text{-}4}$ DEL-$4_{1\text{-}36}$::mCherry; $p_{acr\text{-}2}$GFP; *unc-119*(+)]	This paper	N/A

(*Continued on next page*)

Table 1. *Continued*

REAGENT or RESOURCE	SOURCE	IDENTIFIER
del-4 mutant: T28B8.5 *del-4(tm717)*	National Bioresource Project, Japan	WormBase ID: WBVar00250586
DEL-2::mCherry: *unc-119(ed3)*;Ex[p_{del-2} DEL-2::mCherry; *unc-119*(+)]	This paper	N/A
DEL-3::DsRed: *unc-119(ed3)*;Ex[p_{del-3} DEL-3::DsRed; *unc-119*(+)]	This paper	N/A
DEL-4::DsRed: *unc-119(ed3)*;Ex[p_{del-4} DEL-4::DsRed; *unc-119*(+)]	This paper	N/A
DEL-4::GFP: *unc-119(ed3)*;Ex[p_{del-4} DEL-4::GFP;*unc-119*(+)]	This paper	N/A
DEL-4::DsRed: N2; Ex [p_{del-4} DEL-4::DsRed; *rol-6(su1006)*]	This paper	N/A
dop-1(vs100): LX645 *dop-1(vs100)*	*Caenorhabditis* Genetics Center	RRID:WB-STRAIN:WBStrain00026369; WormBase ID: WBStrain00026369
dop-2(vs105): LX702 *dop-2(vs105)*	*Caenorhabditis* Genetics Center	WB-STRAIN:WBStrain00026373; WormBase ID: WBStrain00026373
dop-3(vs106): LX703 *dop-3(vs106)*	*Caenorhabditis* Genetics Center	RRID:WB-STRAIN:WBStrain00026374; WormBase ID: WBStrain00026374
pkc-1(ok563): RB781 *pkc-1(ok563)*	*Caenorhabditis* Genetics Center	RRID:WB-STRAIN:WBStrain00031494; WormBase ID: WBStrain00031494
pkc-2 (ok328): VC127 *pkc-2 (ok328)*	*Caenorhabditis* Genetics Center	RRID:WB-STRAIN:WBStrain00035524; WormBase ID: WBStrain00035524
tpa-1 (k501): MJ500 *tpa-1 (k501)*	*Caenorhabditis* Genetics Center	RRID:WB-STRAIN:WBStrain00026559; WormBase ID: WBStrain00026559
kin-2(ce179): KG532 *kin-2(ce179)*	*Caenorhabditis* Genetics Center	RRID:WB-STRAIN:WBStrain00023482; WormBase ID: WBStrain00023482
unc-43(tm1605): K11E8.1 *unc-43(tm1605)*	National Bioresource Project, Japan	WormBase ID: WBVar00250586
del-4(tm717);dop-1(vs100)	This paper	N/A
del-4(tm717);dop-2(vs105)	This paper	N/A
del-4(tm717);dop-3(vs106)	This paper	N/A
del-4(tm717);pkc-1(ok563)	This paper	N/A
del-4(tm717);pkc-2 (ok328)	This paper	N/A
del-4(tm717);tpa-1 (k501)	This paper	N/A
del-4(tm717);kin-2(ce179)	This paper	N/A
del-4(tm717);unc-43(tm1605)	This paper	N/A
$p_{hsp-16.2}$GFP: TJ375 gpIs1 [*hsp-16.2*p::GFP]	*Caenorhabditis* Genetics Center	RRID:WB-STRAIN:WBStrain00034895; WormBase ID: WBStrain00034895
p_{sod-3}GFP: CF1553 muIs84 [(pAD76) sod-3p::GFP) + *rol-6(su1006)*]	*Caenorhabditis* Genetics Center	RRID:WB-STRAIN:WBStrain0000486; WormBase ID: WBStrain00004861
p_{gst-4}GFP: CL2166 dvIs19 [(pAF15) gst-4p::GFP::NLS)]	*Caenorhabditis* Genetics Center	RRID:WB-STRAIN:WBStrain00005102; WormBase ID: WBStrain00005102
p_{hsp-4}GFP: SJ4005 zcls4 [*hsp-4*::GFP]	*Caenorhabditis* Genetics Center	RRID:WB-STRAIN:WBStrain00007694; WormBase ID:WBStrain00007694
hsf-1(sy441): PS3551 *hsf-1(sy441)*	*Caenorhabditis* Genetics Center	RRID:WB-STRAIN:WBStrain00007673; WormBase ID:WBStrain00007673
daf-16(mu86): CF1038 *daf-16(mu86)*	*Caenorhabditis* Genetics Center	RRID:WB-STRAIN:WBStrain00007210; WormBase ID: WBStrain00007210

(*Continued on next page*)

Table 1. *Continued*

REAGENT or RESOURCE	SOURCE	IDENTIFIER
p_{hsf-1}HSF-1::GFP: *EQ87* iqIs28 *[pAH71 P*hsf-1::hsf-1::gfp*; pRF4* rol-6 (su1006)*]*	Ao-Lin Hsu (University of Michigan, USA)	N/A
p_{daf-16}DAF-16::GFP: p_{daf-16}DAF-16(d/f/h)::GFP	Tibor Vellai (Eötvös Loránd University, Budapest)	N/A
p_{skn-1}SKN-1::GFP: LD1008 ldEx9 [skn-1(operon)::GFP + rol-6(su1006)	*Caenorhabditis* Genetics Center	RRID:WB-STRAIN:WBStrain00024127; WormBase ID: WBStrain00024127
p_{skn-1}SKN-$1^{B/C}$::GFP: LD1 ldIs7 [skn-1b/c::GFP + rol-6(su1006)]	*Caenorhabditis* Genetics Center	RRID:WB-STRAIN:WBStrain00024125; WormBase ID: WBStrain00024125
$p_{let-858}$GCaMP2.0: IR1155 N2; Ex[$P_{let-858}$GCaMP2.0; *rol-6(su1006)*]	This paper	Palikaras et al., 2015
p_{aak-2}AAK-2::Tomato: AGD383 uthls202 [aak-2(intron1)::aak-2(aa1-aa321)::Tomato:: unc-54 3'UTR + *rol-6(su1006)*]	*Caenorhabditis* Genetics Center	RRID:WB-STRAIN:WBStrain0000009; WormBase ID: WBStrain00000095
del-4(tm717); p_{hsp-4}GFP: *del-4(tm717)*; zcls4[p_{hsp-4}GFP]	This paper	N/A
del-4(tm717); p_{aak-2}AAK-2::Tomato: *del-4(tm717)*; uthls202[aak-2(intron1):: aak-2(aa1-aa321)::Tomato::unc-54 3'UTR ; *rol-6(su1006)]*	This paper	N/A
del-4(tm717);p_{skn-1}SKN-$1^{B/C}$::GFP: *del-4(tm717)*; ldIs7 [skn-1b/c::GFP + rol-6(su1006)]	This paper	N/A
p_{asic-1}SNB-1::SEpHluorin: IR723 N2; Ex [p_{asic-1} SNB-1::SEpHluorin; *rol-6(su1006)*]	Voglis et al.[77]	N/A
del-4(tm717); p_{asic-1}SNB-1::SEpHluorin: *del-4 (tm717)*; N2; Ex [p_{asic-1}SNB-1::SEpHluorin; *rol-6(su1006)*]	This paper	N/A
p_{acr-2}SNB-1::SEpHluorin: KP3085 nuls122 [p_{acr-2}::pHluorin:: SNB-1; p_{myo-2}DsRed]	*Caenorhabditis* Genetics Center	WormBase ID: WBStrain00047338
goa-1(sa734): DG1856 *goa-1(sa734)*	*Caenorhabditis* Genetics Center	RRID: WB-STRAIN:WBStrain00022814
unc-49(e407): CB407 *unc-49(e407)*	*Caenorhabditis* Genetics Center	WormBase ID: WBStrain00004164
DEL-4::GFP;p_{del-4}SNB-1::DsRed: *unc-119(ed3)*;Ex[p_{del-4} DEL-4::GFP;p_{del-4}SNB-1::DsRed ;*unc-119*(+)]	This paper	N/A
GFP::SNB-1: EG8244 [*unc-119(ed3)*; oxSi834 [P_{unc-47} GFP::SNB-1::*unc-54* UTR; *unc-119*(+)]	E. Jorgensen (University of UTAH, Salt Lake City); Nonet et al.[95]	N/A
NLP-21::YFP: KP3947 nuls183 [p_{unc129}NLP-21:: Venus + p_{myo-2}NLS::GFP]	*Caenorhabditis* Genetics Center	RRID:WB-STRAIN:WBStrain00023636; WormBase ID: WBStrain00023636
del-4(tm717); GFP::SNB-1: *del-4(tm717)*; [*unc-119(ed3)*; oxSi834[P_{unc-47}GFP::SNB-::unc-54 UTR; *unc-119*(+)]	This paper	N/A
del-4(tm717); NLP-21::YFP: nuls183 [p_{unc129}NLP-21:: Venus; p_{myo-2}NLS::GFP]	This paper	N/A
p_{dat-1}ASAP-1:N2; Ex [p_{dat-1}ASAP-1; *rol-6(su1006)*]	This paper	N/A
del-4(tm717); p_{dat-1}ASAP-1: *del-4(tm717)*; p_{dat-1} ASAP-1; *rol-6(su1006)*]	This paper	N/A
del-4(tm717); p_{dat-1}GFP: *del-4(tm717)*; egls1[p_{dat-1}GFP]	This paper	N/A
DEL-4::DsRed; p_{dat-1}GFP: p_{del-4} DEL-4:: DsRed; egls1 [p_{dat-1}GFP]; *rol-6(su1006)*	This paper	N/A

(*Continued on next page*)

Table 1. *Continued*

REAGENT or RESOURCE	SOURCE	IDENTIFIER
BR5270: BR5270 byIs161 [p_{rab-3}F3(delta) K280 + p_{myo-2}mCherry]	*Caenorhabditis* Genetics Center	RRID:WB-STRAIN:WBStrain00003901; WormBase ID: WBStrain00003901
BR5270; p_{dat-1}GFP: byIs161 [p_{rab-3}F3(delta) K280 + p_{myo-2}mCherry]; egIs1 [p_{dat-1}GFP]	This paper	N/A
del-4(tm717);BR5270; p_{dat-1}GFP: *del-4(tm717)*; byIs161 [p_{rab-3}F3(delta)K280 + p_{myo-2}mCherry]; egIs1 [p_{dat-1}GFP]	This paper	N/A
DEL-4::DsRed; BR5270; p_{dat-1}GFP: p_{del-4} DEL-4::DsRed; *rol-6(su1006)*; byIs161 [p_{rab-3}F3(delta)K280 + p_{myo-2}mCherry]; egIs1 [p_{dat-1}GFP]	This paper	N/A
UA44: UA44 baIn11[p_{dat-1}a-Synuclein; p_{dat-1}GFP]	Guy Caldwell (University of Alabama, AL, USA); Sanjib Guha et al.[96]	RRID:WB-STRAIN:WBStrain00035179; WormBase ID: WBStrain00035179
del-4(tm717); UA44: *del-4(tm717)*; baIn11 [p_{dat-1}::a-Synuclein; p_{dat-1}GFP]	This paper	N/A
DEL-4:: DsRed; UA44: p_{del-4}DEL-4:: DsRed; *rol-6(su1006)*; baIn11[p_{dat-1}a-Synuclein; p_{dat-1}GFP]	This paper	N/A
che-2 (e1033): CB1033 *che-2 (e1033)*	*Caenorhabditis* Genetics Center	RRID:WB-STRAIN:WBStrain00004231; WormBase ID: WB-STRAIN:WBStrain00004231
dat-1(tm903)	National Bioresource Project, Japan	WormBase ID: WBVar00249925
del-4(tm717) rescue: *del-4(tm717)*; Ex [p_{del-4}DEL-4,p_{myo-2}] (rescue)	This paper	N/A
cat-2(e1112): *CB1112 cat-2(e1112)*	*Caenorhabditis* Genetics Center	RRID:WB-STRAIN:WBStrain00004246; WormBase ID: WBStrain00004246
del-4(tm717); $p_{hsp-16.2}$GFP: *del-4(tm717)*; TJ375 gpIs1 [*hsp-16.2*p::GFP]	This paper	N/A
del-4(tm717); p_{gst-4}GFP: *del-4(tm717)*; dvIs19 [(pAF15) gst-4p::GFP::NLS)]	This paper	N/A
del-4(tm717); p_{sod-3}GFP: *del-4(tm717)*; muIs84 [(pAD76) sod-3p::GFP) + *rol-6(su1006)*]	This paper	N/A
del-4(tm717); $P_{let-858}$GCaMP2.0: *del-4(tm717)*; $P_{let-858}$GCaMP2.0; *rol-6(su1006)*	This paper	N/A

sod-3, upon *del-4* suppression (Figures 3C, 3K, S4D and S4I). L1 larvae required DAF-16 activation and nuclear translocation to enter into starvation-induced diapause and endure starvation.[40,41] Since *del-4* downregulation reduced DAF-16 levels and activity, we hypothesized that arrested L1 survival would be reduced in a *del-4* mutant background. In accordance with our hypothesis, we discovered that *del-4* mutants were more sensitive to long-term starvation compared to wt (Figure 3D), while DEL-4-overexpressing animals were more resistant corroborating the notion that DEL-4 is required for an intact response to prolonged starvation.

To determine whether DEL-4 deficiency triggers other types of metabolic stress responses, we assessed the activation of the ER unfolded protein response (ER^{UPR}) and oxidative stress response in the *del-4* mutant background. We observed that depletion of DEL-4 upregulated *hsp-4*, a well-established target of ER^{UPR} and a homolog of the mammalian BiP (Figures 3E, 3K, S4E and S4I). ER stress triggers cytosolic Ca^{2+} release from the sarco-endoplasmic reticulum which in turn induces Ca^{2+}-calmodulin protein kinase β-dependent AMPK activation (Arias-Del-Val et al., 2019).[42] To determine whether DEL-4 is a mediator of this pathway, we suppressed *del-4* in animals carrying the genetically encoded calcium indicator GCaMP2.0 expressed throughout the body ($p_{let-858}$GCaMP2.0) or an AMPK translational reporter (p_{aak-2}AAK-2::Tomato). In both cases, the reduction or absence of DEL-4 induced a systemic increase in the cytoplasmic calcium and AMPK levels (Figures 3F, 3G, 3K, S4F, S4G and S4I).

Table 2. Oligonucleotides used in this study

REAGENT or RESOURCE	SOURCE	IDENTIFIER
Oligonucleotides		
Primer for the *del-4(tm717)* variation (Forward): 5′-AAAAGTGTGGACCCGGATAT-3′	This paper	N/A
Primer for the *del-4(tm717)* variation (Reverse): 5′-AAAAGTGTGGACCCGGATAT-3′	This paper	N/A
Primer for the *del-3(tm5642)* variation (Forward): 5′-ATGTGGCTCCGAGGACTTTTC-3′	This paper	N/A
Primer for the *del-3(tm5642)* variation (Reverse): 5′- GCAATCAGACACCACACCCAGTA-3′	This paper	N/A
Primer for the *dop-1(vs100)* variation (Forward): TGTGCTGAAATGAACGAATGAGAC	This paper	N/A
Primer for the *dop-1(vs100)* variation (Reverse): TCGGATCATTCAAGTCCCGTC	This paper	N/A
Primer for the *dop-2(vs105)* variation (Forward): AACGATTCCTTGCGATTCTGG	This paper	N/A
Primer for the *dop-2(vs105)* variation (Reverse): AACCATAAATCTGTGTGAGCAAAGC	This paper	N/A
Primer for the *dop-3(vs106)* variation (Forward): TGTGGGCACCTCATTCACTGG	This paper	N/A
Primer for the *dop-3(vs106)* variation (Reverse): ACCGCGCTGAACCAAAGTATG	This paper	N/A
Primer for the *pkc-1(ok563)* variation (Forward): TTGAGCGTGCTCGGGTCC	This paper	N/A
Primer for the *pkc-1(ok563)* variation (Reverse): ACCTTCCACGTTTGTTCCGTG	This paper	N/A
Primer for the *pkc-2(ok328)* variation (Forward): ACTTGCGACGTCGAATTTGTAGG	This paper	N/A
Primer for the *pkc-2(ok328)* variation (Reverse): CCATAAGCCCACCAATCCACAG	This paper	N/A
Primer for the *tpa-1(k501)* variation (Forward): CGCCATTGGTGCTAACATGAC	This paper	N/A
Primer for the *tpa-1(k501)* variation (Reverse): CCGACGAGCATTTCATACATCAA	This paper	N/A
Primer for the *kin-2(ce 179)* variation (Forward): AATAGCAGAGGGTCAGTAATTGACTG	This paper	N/A
Primer for the *kin-2(ce179)* variation (Reverse): AGTACGGATAAGCTCTTAGAGAGAAGC	This paper	N/A
Primer for the *unc-43(tm1605)* variation (Forward): TAAACTACTGCCATCAGCGTGG	This paper	N/A
Primer for the *unc-43(tm1605)* variation (Reverse): CCAAATTTTCTCATTCGCGC	This paper	N/A
Primer for *del-4* (exons 1-10) (Forward): 5′-GATGGGTGTATTTTGGACCG-3′	This paper	N/A
Primer for *del-4* (exons 1-10) (Reverse): 5′-TCAAGACACGATTCTCCTGA-3′	This paper	N/A
Primer for *del-2* transcriptional reporter (Forward): 5′-TCTTATGATGCACGGCG-3′	This paper	N/A
Primer for *del-2* transcriptional reporter (Reverse): 5′-GGTACCCGTCCACTATTAGTAAT-3′	This paper	N/A

(*Continued on next page*)

Table 2. *Continued*

REAGENT or RESOURCE	SOURCE	IDENTIFIER
Primer for *del-3* transcriptional reporter (Forward): 5′-5′-GCATGCTTACATTTGAGGGTTTAG-3′	This paper	N/A
Primer for *del-3* transcriptional reporter (Reverse): 5′-ACCGGTGTTTTCGATTCAGTTTT-3′	This paper	N/A
Primer for *del-4* transcriptional reporter (Forward): 5′-CTGCAGGTCGACACATCATAAATC-3′	This paper	N/A
Primer for *del-4* transcriptional reporter (Reverse): 5′-ACCGGTCCTCAACCATCGAGCATTT-3′	This paper	N/A
Primer for *del-2* translational reporter with mCherry (exons 5-11) (Forward): 5′-CTGCAGGATTTCTCTGTCAAGTGG-3′	This paper	N/A
Primer for *del-2* translational reporter with mCherry (exons 5-11) (Reverse): 5′-ACCGGTCATATTGTCAGGCAAGTT-3′	This paper	N/A
Primer for *del-2* translational reporter with mCherry (exons 2-4) (Forward): 5′-CTGCAGAGTTGATGATGATTAAAGAA-3′	This paper	N/A
Primer for *del-2* translational reporter with mCherry (exons 2-4) (Reverse): 5′-CTGCAGTGAAAATGCTCAAACAAA-3′	This paper	N/A
Primer for del-3 translational reporter (exons 2-7) (Forward): 5′-ACCGGTTGTTCACGATGATCAACTATT-3′	This paper	N/A
Primer for del-3 translational reporter (exons 2-7) (Reverse): 5′- ACCGGTGGTGTGTCTCCTGAAGCTA-3′	This paper	N/A
Primer for del-4 translational reporter with GFP (promoter and CDS) (Forward): 5′-ACGCGTCGACACATCATAAATCTCCACCCAC-3′	This paper	N/A
Primer for del-4 translational reporter with GFP (promoter and CDS) (Reverse): 5′-CGGGGTACCCCATCATTAGAATGAGGCTTTGG-3′	This paper	N/A
Primer for SNB-1 coding gene (Forward): 5′-CGG GGTACCGAA TTCGGACGCTCAAGGAGATGCCGGC-3′	This paper	N/A
Primer for SNB-1 coding gene (Reverse): 5′-CGGGGTACCGAA TTCTTTTCCTCCAGCCCATAAAACG-3′	This paper	N/A
Primer for *del-4* promoter (Forward): 5′-CTGCAGGTCGA CACATCATAAATC-3′	This paper	N/A
Primer for *del-4* promoter (Reverse): 5′-GGATCCCATCTG CAATTTTATTTT-3′	This paper	N/A
Primer for ASAP1 voltage indicator (Forward): 5′-TAGCCG CCACCATGGAGAC-3′	This paper	N/A
Primer for ASAP1 voltage indicator (Reverse): 5′- AGATCTT TCATTAGGTTACCACTTCAAG -3′	This paper	N/A
Primer for *dat-1* promoter (Forward): 5′-CTGCAGATCCAT GAAATGGAACTTGA-3′	This paper	N/A
Primer for *dat-1* promoter (Reverse): 5′-GGATCCGGCTAAAAATTGTTGAG-3′	This paper	N/A
Primer for *del-4* cDNA for RTPCR (Forward): 5′-ATGACATGGTTGTTAGTTGCACG-3′	This paper	N/A
Primer for *del-4* cDNA for RTPCR (Reverse): GTGCAAAGTAACCGAATACATCAG	This paper	N/A
Primer for pmp-3 cDNA for RTPCR (Forward): 5′- ATGATAAATCAGCGTCCCGAC-3′	This paper	N/A
Primer for pmp-3 cDNA for RTPCR (Reverse): 5′- TTGCAACGAGAGCAACTGAAC -3′	This paper	N/A
Primer for KSM vector (Forward): 5′-AGATCTGGTTACCACTAAACCAGCC-3′	This paper	N/A
Primer for KSM vector (Reverse): 5′-TGCAGGAATTCGATATCAAGCTTATCGATACC-3′	This paper	N/A
Primer for *del-4* cDNA for expression on *Xenopus* oocytes (Forward): 5′-CTTGATATCGAATTCCTGCAATGGGTGTATTTTGGACCGGC-3′	This paper	N/A
Primer for *del-4* cDNA for expression on *Xenopus* oocytes (Reverse): 5′-GTTTAGTGGTAACCAGATCTTCAATCATTAGAATGAGGCTTTGGTGGAAC-3′	This paper	N/A

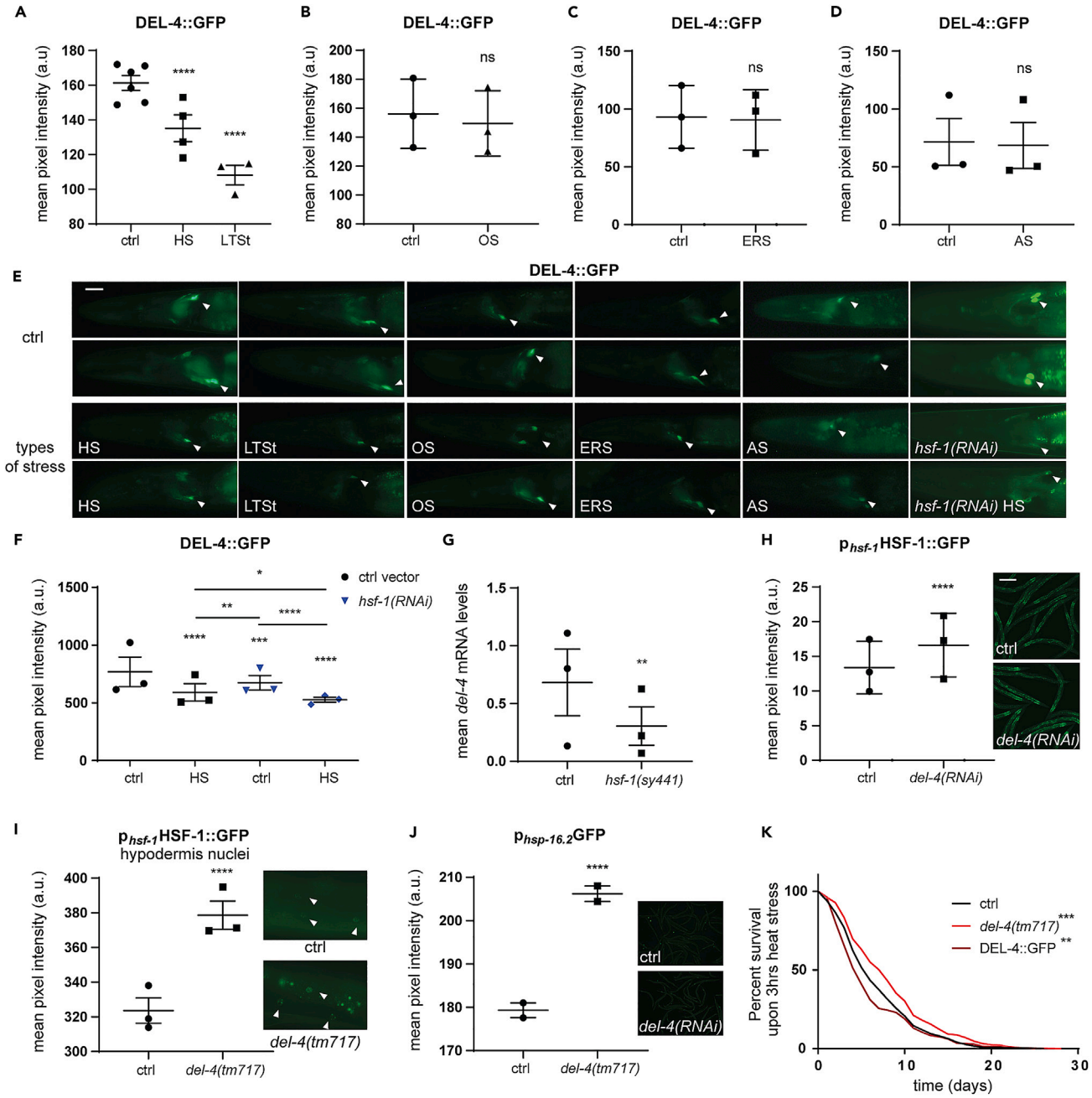

Figure 2. Regulation of DEL-4 expression by specific stress stimuli

(A) Expression levels of DEL-4 diminish upon heat stress and starvation. Imaging of 2-day adult animals, control or treated for 3 h at 37°C and left O/N for recovery or starved for 24 h (STAR Methods).

(B and C) Oxidative stress and ER stress do not alter the expression levels of DEL-4. For oxidative stress induction, we placed animals expressing the DEL-4 translational reporter on OP50 seeded NGM treated with paraquat to a final concentration of 8 mM (STAR Methods). We induced ER stress with tunicamycin, plated on OP50 seeded NGM at a final concentration of 2.5 μg/mL. Animals were placed on NGM with paraquat or tunicamycin at the L4 stage. Imaging was performed on day one of adulthood.

(D) Acidic stress does not affect DEL-4 levels. One-day adult animals were treated for 1 h in a 15 μL drop with M13 brought to pH3.5 with CH3COOHNa.

(E) Representative epifluorescent images of the head region of DEL-4::GFP-expressing animals under control conditions or upon heat stress, long-term starvation, oxidative stress, ER stress, and acidic stress (STAR Methods). We measured the intensity only in the neuronal cell body, which exhibited the highest expression level (arrowhead). Left is anterior. Lens 40x. Scale bar 20 μm.

(F and G) HSF-1 regulates the expression levels of DEL-4. (F) Downregulation of *hsf-1* with RNAi reduces the expression levels of DEL-4::GFP, upon control conditions and HS Imaging of 2-day adult animals, control or treated for 3 h at 37°C and left O/N for recovery (STAR Methods). (G) Reduced *del-4* mRNA

Figure 2. *Continued*

levels in the *hsf-1(sy441)* mutant. We measured with RT-PCR the mean *del-4* mRNA levels, using as template cDNA of 3-day adult wt and *hsf-1* mutant animals. We isolated total mRNA from wt and *hsf-1* mutants, reversely transcribed it into cDNA and used as template for RT-PCR. Dot plot, dots represent the mean *del-4* mRNA levels from independent biological replicates. We performed 3 independent biological replicates and for each biological we performed three technical replicates.

(H–K) *del-4* depletion activates HSF-1. (H) Increased HSF-1expression levels upon *del-4*(RNAi). The levels of HSF-1 were measured from the whole body at day 4 of adulthood. 5x lens, scale bar 20 μm. (I) The *del-4* mutant *(tm717)* displays increased nucleus to cytoplasm ratio of HSF-1 expression levels. HSF-1 levels in hypodermis nuclei are increased in the *del-4* mutant. We overlooked the nuclei located above the gut to avoid intestinal autofluorescence. 40x lens, scale bar 200 μm. (J) Absence of DEL-4 increases the expression levels of the HSF-1 target *hsp-16.2*. Measurements from the whole body of one-day adults. 5x lens, scale bar 20 μm. (K) Survival of wt, *del-4(tm717)* mutants and DEL-4 overexpressing animals after 2.5 h of heat stress applied on day 1 of adulthood. Death events were measured every second day. Mutants of *del-4* display enhanced resistance, while DEL-4-overexpressing animals exhibit reduced resistance to heat stress. For statistical significance, survival curve analysis was performed. (A–D, F–H, I, J) Dot plots, dots represent the number of independent biological replicates, error bars represent SEM Non-significant (ns) p = 0.1234, *p = 0.0332, **p = 0.0021, ***p = 0.0002, ****p < 0.0001. two-way ANOVA analysis. (A–D, F) n represents number of neuronal cell somas. (A) Control: n = 289; HS: n = 205; LTSt: n = 177. All HS and LTSt experiments were performed separately, except for one of the three repeats, but were plotted together for illustration purposes. (B) ctrl: n = 169, OS: n = 161. (C) ctrl: n = 97, ERS: n = 105. OS and ERS experiments were performed separately but plotted together for illustration purposes. (D) ctrl n = 105 and LpH n = 102. (F) ctrl: n = 243, HS: n = 233, hsf-1(RNAi): n = 213, HS and *hsf-1(RNAi)*: n = 286. (A–F) Control (ctrl), heat stress (HS), long-term starvation (LTSt), acidic (AS), oxidative stress (OS), and ER stress (ERS) (Table S1). (H) ctrl n = 219, *del-4(RNAi)* n = 237, n represents the number of individual animals measured (I) ctrl n = 279, HS n = 325, n represents the number of nucleuses (J) ctrl: n = 161, *del-4(tm717)*: n = 96, n represents number of animals. (K) 4 biological replicates, ctrl n = 356, *del-4(tm717)* n = 396, DEL-4::GFP n = 273, n represents number of animals participated in the lifespan assay. See also Figure S3.

SKN-1, the *C. elegans* homolog of mammalian Nrf2, is known for its role in Phase II detoxification genes transcription, thereby contributing to survival and resistance to oxidative stress.[43] We observed that systemic *del-4* knockdown enhanced the expression levels of *skn-1* and its target gene *gst-4* (Figures 3H, 3I, 3K, S4E and S4I). Specifically, SKN-1 increased both systemically and particularly in the ASI nuclei (Figures 3J and 3K). Collectively, these data indicate that DEL-4, acting in neurons, modulates the activation of several metabolic stress responses throughout the body. The question that rises is how this signal is transmitted from neurons to distal tissues and whether it is translated to behavioral adaptation to environmental stress.

DEL-4 modulates dopaminergic signaling

As previously described, DEL-4 is expressed in all dopaminergic neurons. Dopamine signaling is involved in several forms of behavioral plasticity, reward, stress processing, and control of motor output. Therefore, we reasoned that DEL-4 could integrate stress stimuli through dopaminergic signaling. In *C. elegans*, the functionality of the dopamine pathway can be readily assessed by monitoring a specific locomotory response to food availability cues, which is termed basal slowing response (BSR) (Table S1), and consists of a decrease in the animal's locomotory rate upon encountering food.[44] To assess whether DEL-4 modulates dopaminergic signalling, we tested the ability of animals to elicit a BSR in the presence or absence of DEL-4. Interestingly, *del-4* mutant animals exhibit a stronger BSR compared to wt (Figure 4A). In addition, transgenic animals overexpressing DEL-4 display a higher locomotory rate on food, and thus reduced BSR compared to wt (Figure 4A). These results suggest the involvement of DEL-4 in the regulation of dopaminergic signaling.

To examine the possible epistatic interaction of DEL-4 with the intracellular dopaminergic signaling pathway, we performed a BSR assay for the double mutants of *del-4* and each of the dopamine receptor genes (*dop-1*, *dop-2*, or *dop-3*) (Figures 4B and 4E; Tables 1 and S4) or their downstream kinase genes (*pkc-1*, *pkc-2*, *tpa-1*, *unc-43*, or *kin-2*) (Figures 4C–4E; Tables 1 and S4). In most instances, we observed that the BSR of the double mutants was equivalent to that of dopamine receptor or kinase single mutants. The only exceptions were the *del-4(tm717); pkc-2(ok328)* double mutants, which share the same phenotype as the single *del-4(tm717)* mutant. This observation suggests that PKC-2 either lies upstream of DEL-4 or that it functions independently (Figure 4C). These findings indicate that DEL-4 acts upstream of the dopaminergic signaling pathway.

To corroborate the effects of DEL-4 on dopaminergic signaling, we sought to estimate dopamine levels in the synapse of dopaminergic neurons, in the presence or absence of DEL-4. To this end, we used a pH-sensitive version of EGFP, the super ecliptic phluorin (Tables 1 and S1), fused to synaptobrevin, expressed specifically in dopaminergic neurons. We observed reduced basal levels of synaptic release in the absence of DEL-4 (Figure 5A). Moreover, *del-4(tm717)* mutants were resistant to paralysis in a dopamine resistance assay, further suggesting that the amount of dopamine in the synaptic cleft is reduced in the absence of DEL-4 (Figures 5B and S5).

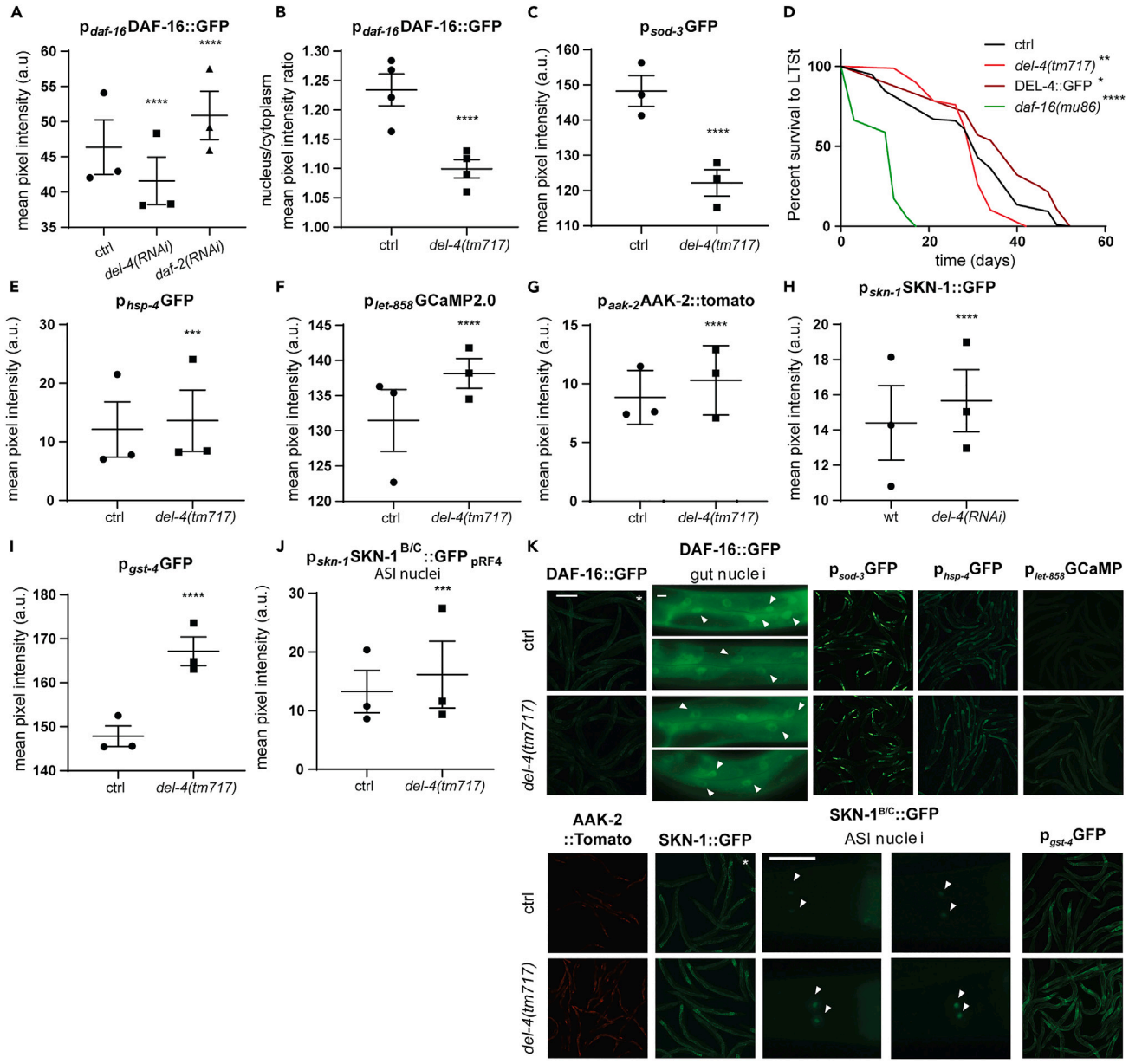

Figure 3. DEL-4 differentially regulates systemic stress responses

(A) Downregulation of *del-4* by RNAi decreases DAF-16 expression levels, measured in the whole body. *daf-2* RNAi was used as a positive control. Four-day adult animals.

(B) The DAF-16 ratio of nucleus to cytoplasm is decreased in the *del-4(tm717)* mutant. We measured the intensity levels of DAF-16 in the nuclei and adjacent cytoplasm of the gut and calculated the ratio. One-day adult animals.

(C) *del-4* elimination lowers the DAF-16 target SOD-3 expression levels. We measured the expression levels of *sod-3* from the whole body of animals expressing the transcriptional reporter p_{sod-3}GFP, under control conditions and in the *del-4(tm717)* mutant.

(D) *del-4(tm717)* mutant animals were sensitive to food deprivation compared to wt while animals overexpressing DEL-4 where more resistant. We measured the survival of wt, *del-4(tm717)* mutants, DEL-4::GFP-overexpressing animals, and *daf-16(mu86)* mutants during starvation. The *daf-16(mu86)* mutant was used as the positive control. Animals were bleached and placed as eggs in 1.5 mL M9. Every second day, 20 μL were retrieved from each genotype, put on OP50 seeded NGM as L1 larvae and allowed for three days to grow. We counted the animals that reached the L4 stage or adulthood (STAR Methods). Survival curve analyses were used for evaluation of statistical significance.

(E) The transcriptional reporter of HSP-4, an ER stress marker, displays elevated fluorescence intensity levels in the *del-4* mutant background compared to control. One-day adult animals.

(F) Cytoplasmic Ca^{2+} levels rise upon *del-4* depletion. Measurement of intracellular Ca^{2+} levels using the genetically encoded calcium indicator GCaMP2.0 driven by the *let-858* promoter for systemic expression.

Figure 3. *Continued*

(G) Increased AAK-2 levels in *del-4(tm717)* mutant animals. We measured the expression levels of AAK-2 from the whole body of animals expressing the translational reporter p_{aak-2}AAK-2::Tomato.

(H and I) DEL-4 downregulation increases systemic expression levels of SKN-1 (four-day adult animals) and its target GST-4 (one-day adult animals).

(J) SKN-1 expression levels of isoforms B and C are elevated in ASI nuclei in the *del-4* mutant background. One-day adults.

(K) Representative images of the designated reporters. Asterisks indicate *del-4(RNAi)* instead of the *del-4* mutant. Images illustrating whole animals were retrieved with a 5x lens and the scale bar corresponds to 20 μm. Images of p_{daf-16}DAF-16::GFP (gut nuclei) and were captured with a 20x lens and those of p_{skn-1}SKN-$1^{B/C}$::GFP in ASI nuclei with a 40x lens. In this case, the scale bar corresponds to 200 μm (left is anterior). (A–C, E–J) Dot plots, dots indicate mean levels of independent biological replicates. two-way ANOVA. Error bars represent SEM Non-significant (ns) p = 0.1234, *p = 0.0332, **p = 0.0021, ***p = 0.0002, ****p < 0.0001. One-way ANOVA. (A)ctrl n = 134, *del-4(RNAi)* n = 149, *daf-2(RNAi)* n = 152, n represents the number of animals. (B) ctrl n = 442, *del-4(tm717)* n = 375, n represents the number of nucleuses. (C) ctrl n = 178, *del-4(tm717)* n = 132, n represents number of animals. (D) ctrl n = 97, *del-4(tm717)* n = 79, DEL-4::GFP n = 28, *daf-16(mu86)* n = 92, n represents number of animals. (E) ctrl n = 120, *del-4(tm717)* n = 112, n represents number of animals. (F) ctrl n = 155, *del-4(tm717)* n = 161, n represents number of animals. (G) ctrl n = 128, *del-4(tm717)* n = 92, n represents number of animals. (H) ctrl n = 301, *del-4(RNAi)* n = 300, n represents number of animals. (I) ctrl n = 165, *del-4(tm717)* n = 162, n represents number of animals. (J) ctrl n = 143, *del-4(tm717)* n = 113, n represents number of ASI nuclei. See also Figure S4.

DEL-4 was present in the VA, VB, DA, and DB cholinergic motor neurons of the ventral nerve cord (Figure 1C). Muscle cells are innervated by cholinergic and GABAergic neurons. Firing through cholinergic neurons promotes muscle contraction, whereas the activation of GABAergic neurons evokes muscle relaxation. Both types of motor neurons express dopamine receptors, which act antagonistically to control *C. elegans* locomotion. The D1-like dopamine receptor, DOP-1, is confined to cholinergic motor neurons, where it stimulates acetylcholine (ACh) release (Table S1). The D2-like dopamine receptor, DOP-3, localizes primarily in GABAergic neurons and, to a much lesser extent, in cholinergic motor neurons. DOP-3 functions by inhibiting ACh release.[45] According to the BSR data (Figure 4B), all three dopamine receptors lie downstream of the effects of DEL-4 on BSR. To study the effect of DEL-4 downregulation on motor output, we estimated the degree of synaptic release initially at the cholinergic and subsequently at GABAergic neuromuscular junctions (NMJ). Interestingly, we saw that DEL-4 depletion results in reduced basal levels of synaptic release at the cholinergic NMJ, compared to wt (Figure 5C). To verify that the decreased cholinergic neurotransmission at the NMJ is due to presynaptic defect, we used a combination of aldicarb and levamisole resistance assays.[46] *del-4* mutants were resistant to the paralytic effects of aldicarb while animals overexpressing DEL-4 were sensitive, compared to wt (Figure 5D). However, DEL-4 depletion or overexpression did not alter the resistance of animals to levamisole (Figure 5E). These results indicate a presynaptic defect at the NMJ upon DEL-4 downregulation, causing a reduction in ACh synaptic release.

Subsequently, we sought to investigate the effects of DEL-4 depletion in GABAergic neurotransmission. DEL-4 is not expressed in GABAergic motor neurons. Therefore, we anticipated that alterations in GABAergic neurotransmission would rely solely on dopaminergic signaling. Notably, *del-4* mutants exhibit increased synaptic vesicle (SV) density in GABAergic motor neurons compared to control (Figures 5F, 5G, and 5J). This result indicates a dopamine-dependent increase in GABAergic motor neuron signaling upon DEL-4 downregulation. The activation of inhibitory motor neurons combined with the reduced cholinergic motor signaling explains the moderate locomotor activity of the *del-4* strain in the BSR.

Apart from neurotransmitters, neurons release neuropeptides that are packaged into dense core vesicles (DCVs) throughout the neuronal cell soma, axons, and dendrites. We determined the number of DCVs in the dorsal neural cord cholinergic motor neurons and did not observe any difference between *del-4* and control animals (Figures 5H, 5I, and 5K). These results suggest that DEL-4 specifically affects signaling through SVs but not through DCVs.

Collectively, the aforementioned findings support the notion that DEL-4 depletion decreases dopaminergic signaling, with an ultimate impact on downstream motor neuron neurotransmission and locomotory behavior. To shed light on the mechanism through which DEL-4 modulates neuronal function, we will investigate the physiological characteristics of a putative DEL-4 channel.

DEL-4 is a proton-gated sodium channel on neuronal cell membrane

To assess whether the subcellular localization of DEL-4 fits the known pattern of transmembrane channels, we labeled animals expressing the DEL-4::GFP with the lipophilic dye DiI. DiI stains the membranes of amphids, phasmids, and chemosensory neurons with nerve endings exposed to the environment (Table S2). Confocal imaging at high magnification revealed the colocalization of DEL-4 with DiI and its membranous localization (Figures 6A and S6A). To further examine DEL-4 site of action on neuronal membrane, we

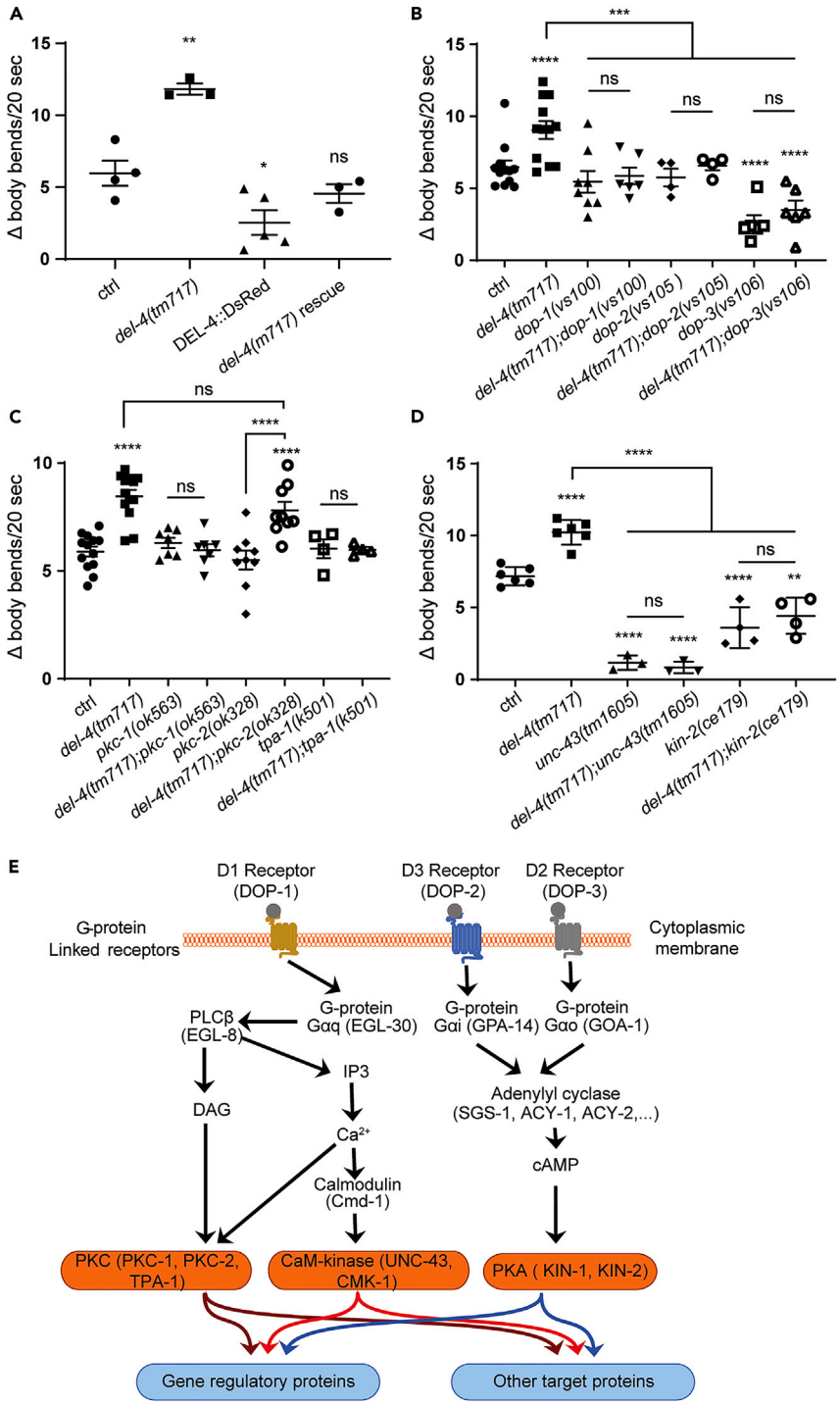

Figure 4. DEL-4 acts upstream in the dopaminergic signaling pathway to modulate *C. elegans* locomotory rate

(A) Basal slowing response (BSR) (STAR Methods and Table S1) of wt, *del-4(tm717)* mutants, DEL-4 overexpressing animals and *del-4(tm717)* rescue animals. *del-4* mutant animals display reduced number of body bends per 20 s on a plate with food compared to wild type and therefore show a strengthened BSR, while the BSR response of DEL-4 overexpressing animals which move faster on a plate with food is reduced. Mutant animals for *del-4* transformed with the endogenous DNA sequence of the *del-4* promoter and CDS (*del-4(tm717)* rescue animals) display the same BSR as the wt (ctrl).

Figure 4. *Continued*

(B) Dopamine receptors lie downstream of DEL-4. BSR of wt, *del-4(tm717)*, *dop-1*(vs*100*), *dop-2*(vs*105*), *dop-3*(vs*106*), *del-4(tm717);dop-1*(vs*100*), *del-4(tm717);dop-2*(vs*105*) and *del-4(tm717);dop-3*(vs*106*) animals (Tables 1 and S4). The phenotype of the double mutants for *del-4* and *dop-1*, *dop-2* or *dop-3* is the same as that of the single mutants of dopamine receptors.

(C) PKC-1 and TPA-1 are downstream of DEL-4, whereas PKC-2 may not contribute to the DEL-4 phenotype. BSR for homologs of mammalian PKC isoforms. BSR of wt, *del-4(tm717)*, *pkc-1(ok563)*, *del-4(tm717);pkc-1(ok563)*, *pkc-2(ok328)*, *del-4(tm717);pkc-2(ok328)*, *tpa-1(k501) and del-4(tm717);tpa-1(k501)* (Tables 1 and S4). Double-deficient mutants of *del-4(tm717);pkc-1(ok563)* and *del-4(tm717);tpa-1(k501)* exhibit the same phenotype as the *pkc-1(ok563)* or *tpa-1(k501)* single mutants, respectively. The BSR of *del-4(tm717);pkc-2(ok328)* double mutants is the same as in the *del-4(tm717)* single mutant.

(D) UNC-43 and KIN-2 lie downstream of DEL-4 in the dopaminergic signaling pathway. BSR of wt, *del-4(tm717)*, *unc-43(tm1605)*, *del-4(tm717);unc-43(tm1605)*, *kin-2(ce179)* and *del-4(tm717);kin-2(ce179)* animals. Double mutants *del-4(tm717);unc-43(tm1605) and del-4(tm717);kin-2(ce179)* present the same phenotype as *unc-43(tm1605)* and *kin-2(ce179)* single mutants, respectively (Tables 1 and S4). UNC-43 is an ortholog of the human calcium/calmodulin-dependent protein kinase II. KIN-2 is a regulator of KIN-1, which is an ortholog of the human cAMP-dependent protein kinase. The *kin-2(ce179)* mutant carries a gain of function mutation.

(E) Schematic representation of the dopamine signaling pathway. Dopamine receptors form G-protein coupled receptors, which upon binding of dopamine activated downstream G-proteins. D1 Receptors activate the IP3/DAG calcium pathway, and D3 and D2 receptors activate the adenylyl cyclase/cAMP signaling pathway. Inside parenthesis: *C. elegans* homologs. (A–D) Dot plots, dots represent the ratio Δ body bends/20s of independent biological replicates. The ratio Δ body bends/20s corresponds to body bends/20s on an empty plate minus body bends/20s on a plate with food. We tested 8–15 animals in every replicate of each BSR experiment. In all experiments, we used one-day-old adult animals. Error bars represent SEM Non-significant (ns) p = 0.1234, *p = 0.0332, **p = 0.0021, ***p = 0.0002, ****p < 0.0001. two-way ANOVA. (A) ctrl n = 36, *del-4(tm717)* n = 34, DEL-4::dsRed n = 42, *del-4(tm717)* rescue n = 45 (B) ctrl n = 116, *del-4(tm717)* n = 112, *dop-1*(vs*100*) n = 74, *del-4(tm717);dop-1*(vs*100*) n = 103, *dop-2*(vs*105*) n = 37, *del-4(tm717);dop-2*(vs*105*) n = 36, *dop-3*(vs*106*) n = 59, *del-4(tm717);dop-3*(vs*106*) n = 58, (C) ctrl n = 117, *del-4(tm717)* n = 117, *pkc-1(ok563)* n = 69, *del-4(tm717);pkc-1(ok563)* n = 66, *pkc-2(ok328)* n = 88, *del-4(tm717);pkc-2(ok328)* n = 84, *tpa-1(k501)* n = 41, *del-4(tm717);tpa-1(k501)* n = 51. (D) ctrl 6 n = 60, *del-4(tm717)* n = 60, *unc-43(tm1605)* n = 30, *del-4(tm717);unc-43(tm1605)* n = 30, *kin-2(ce179)* n = 40, *del-4(tm717);kin-2(ce179)* n = 40. In all cases, n represents the number of animals.

co-expressed DEL-4::GFP with SNB-1::dsRed, a synaptic vesicle marker, under the control of the *del-4* promoter. Despite their partial colocalization, the two reporters showed distinct expression patterns (Figure 6B). DEL-4 has a broader expression pattern, expands throughout cell somas and neuronal processes, and does not exhibit a punctate distribution, similar to SNB-1. Therefore, we conclude that DEL-4 is not exclusively located in synaptic regions.

Channels of the diverse DEG/ENaC family consist of three subunits. In mammals, ENaCs form heterotrimeric channels, whereas ASICs are both heterotrimeric and homotrimeric.[21,47] The subunit composition modifies the biophysical properties of the channel.[48] ENaCs are highly selective for Na^+ and Li^+ ions.[49] ASICs exhibit a weak preference for Na^+ and Li^+, but are also permeable for K^+ and in some cases Ca^{2+} ions.[50] We have previously shown that DEL-4 is a constitutively open channel mediating inward Na^+ current at neutral pH.[51] To further characterize DEL-4 channels' physiological properties, we implemented a two-electrode voltage clamp in *Xenopus laevis* oocytes, ectopically expressing either the wt protein DEL-4 or the protein product of the *del-4* mutant and nuclease-free water-injected oocytes as negative control (Figures 6C, 6D, 6F and S6B). The truncated protein from the *del-4* mutant was translated in frame from the N′ terminus up to a small part of the extracellular loop, comprising the first cytoplasmic domain at the N′ terminus, the first transmembrane domain, and the whole post-M1 domain (Figure S1B). We perfused oocytes with a sodium-rich solution (1XNDN96, see STAR Methods) and recorded the currents produced by stepping the membrane voltage from −150 to +75 mV, from a holding potential of −60 mV (Figure 6C). Amiloride, a common blocker of DEG/ENaC channels, abolished these currents in a dose-dependent manner, with an IC_{50} of 179 μM (Figures 6E, 6G and S6C). The truncated DEL-4 product did not elicit currents similar to the nuclease-free water-injected control (Figures 6D and 6F). The latter suggests that the missing parts of the protein are either responsible for the Na^+ currents or for the trafficking of the protein to the plasma membrane. Next, we investigated ion selectivity by carrying out ion substitution experiments. DEL-4 homomeric channel is permeable to monovalent cations, preferentially to Na^+ (selectivity sequence: $Na^+ = Li^+ > K^+ > Ca^{2+}$) but appears to be Ca^{2+} impermeable, at least in the *Xenopus* oocytes expression system (Figures 6H, 6I and S6D). These results revealed that DEL-4 subunits can form a homomeric channel in *Xenopus* oocytes. This channel localizes to the plasma membrane of neuronal cells, is blocked by amiloride in a dose-dependent manner, and is highly permeable to Na^+ and Li^+.

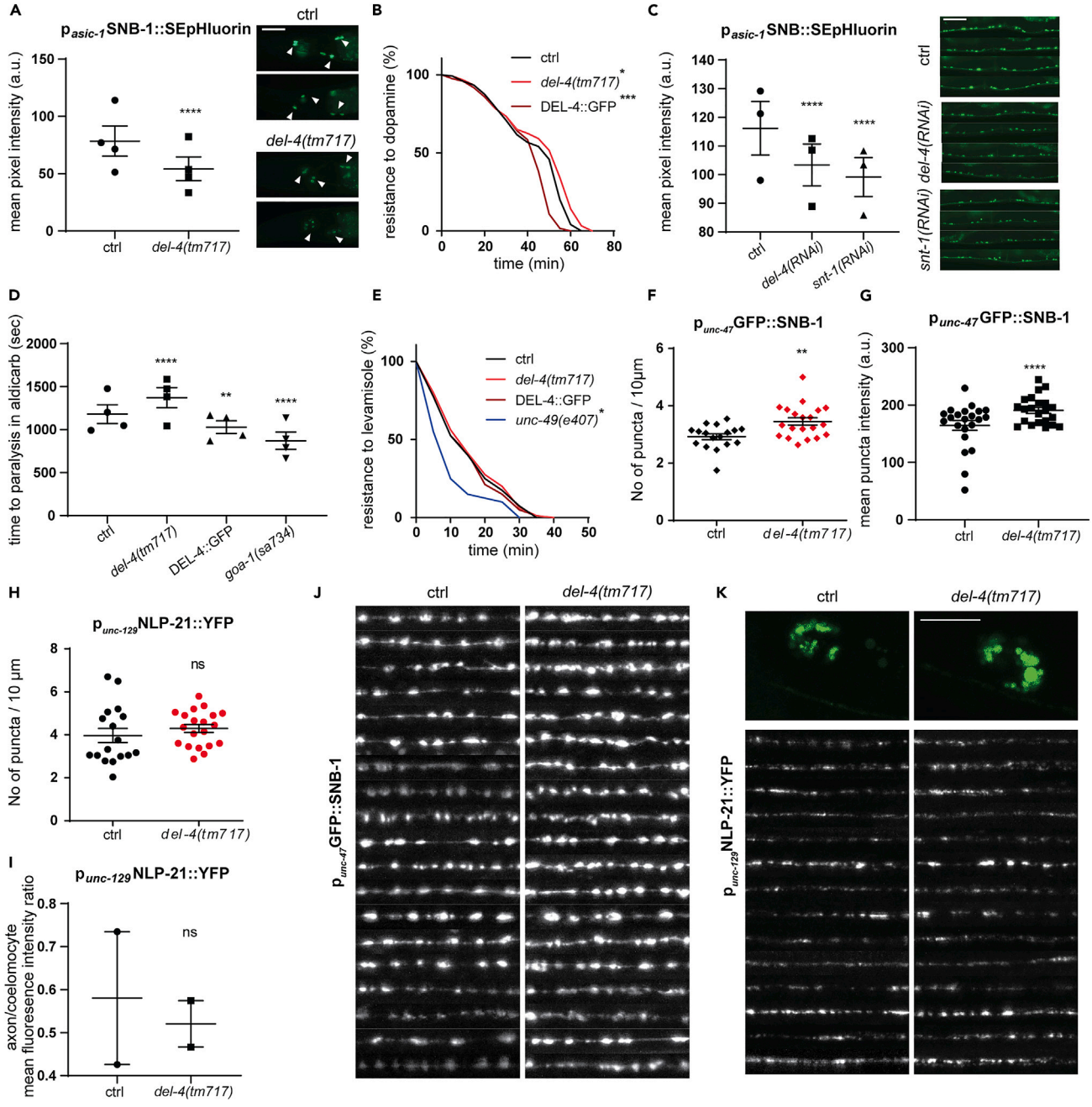

Figure 5. Synaptic vesicle exocytosis of dopaminergic and motor neurons is altered in response to DEL-4 abundance

(A) Basal levels of synaptic release from dopaminergic neurons are reduced in the *del-4(tm717)* mutant background. Left, measurements of Super Ecliptic pHluorin (STAR Methods) expressed in synaptic vesicles of dopamine-releasing neurons in controls and *del-4(tm717)* mutants. (Right) Representative images of p_{asic-1}SNB-1::SEpHluorin from control (top) and *del-4(tm717)* mutants (bottom). Some of the illustrated images came up by merging serial stacks using Adobe Photoshop CS5 (KRT) for illustration purposes only, so that all dopaminergic neurons may be visible in one image. We counted the mean pixel intensity in one-day adults from all cell bodies in the head (indicated with arrowheads). Left is anterior. Lens 40x. Scale bar 20 µM.

(B) Increased resistance of *del-4(tm717)* mutant animals to dopamine. Time course to paralysis of *del-4* mutant and overexpressing animals. We performed the time course assay with one-day adult animals in a 15 µL drop of 40 mM dopamine diluted with M9. Thirty animals per genotype were used in each experiment. Survival curve analysis was performed to estimate the statistical significance. Biological independent replicates were performed by two experimenters (MG and DP) and by one of them blindly. See also Figure S5.

(C) (Left) Reduced synaptic release from cholinergic motor neurons following *del-4* knockdown. We employed the Super Ecliptic pHluorin tagged with SNB-1 driven by the *acr-2* promoter to measure the basal levels of synaptic release in cholinergic motor neurons. The mean pixel intensity of neuronal somas was

Figure 5. *Continued*

calculated. We used *snt-1(RNAi)* as a positive control. (Right) Representative images of cholinergic motor neurons from animals expressing p_{acr-2}SEpHl::SNB-1, upon control (ctrl) (top), *del-4* (middle), or *snt-1* RNAi conditions. Scale bar 20 μm. Lens 20x. One-day adults.

(D) *del-4(tm717)* downregulation increases the resistance to aldicarb-mediated paralysis. We measured the time to paralysis of indicated genotypes at day one of adulthood in 15 μL of 10 mM aldicarb (STAR Methods). Positive control *goa-1(sa734)* (Tables 1 and S4) is an aldicarb hypersensitive strain. Survival curve analysis was performed to estimate statistical significance. Biological independent replicates were performed by two experimenters (MG and DP) and by one of them blindly.

(E) Absence or overexpression of DEL-4 causes the same phenotype as wt in the levamisole resistance assay. Time course to paralysis of the indicated genotypes at day one of adulthood in a 15 μL drop of 400 μM levamisole diluted with M9 (STAR Methods). We used the *unc-49(e407)* mutant strain (Tables 1 and S4) that exhibited sensitivity to levamisole as a positive control. For statistical analysis, survival curve analysis was performed.

(F, G, J) Synaptobrevin 1 positive puncta accumulate at the presynaptic terminals of dorsal cord GABAergic motor neurons in the *del-4(tm717)* mutant. Measurements were performed at day-one adult animals (STAR Methods). (F) Increased number of puncta/10 μm in the *del-4* mutant background. Scatterplot graph of control and *del-4(tm717)* animals showing the number of SNB-1 puncta per 10 μm. We measured the number of puncta per ten μm of GABAergic motor neurons from animals expressing the p_{unc-47}GFP::SNB-1 synaptic vesicle genetic reporter.

(G) Increased intensity of SNB-1 positive puncta in the *del-4(tm717)* mutant. We measured the mean puncta intensity along GABAergic motor neurons of control and *del-4(tm717)* mutants. (H, I, K) DEL-4 absence does not alter the release of dense core vesicles from the dorsal chord cholinergic motor neurons. Measurements were performed at day-one adult animals.

(H) Scatterplot demonstrating the number of NLP-21::YFP puncta per 10 μm of the dorsal neural chord. Cholinergic expression was achieved with the *unc-129* promoter (STAR Methods). Fluorescence of coelomocytes is a result of NLP-21::YFP endocytosis upon release. Control and *del-4(tm717)* mutant animals display the same phenotype.

(I) Quantification of neuropeptide release from cholinergic motor neurons, expressed as the mean pixel intensity ratio of axons to coelomocytes for control and *del-4* mutants. We measured the mean fluorescence intensity from axons of cholinergic motor neurons from animals expressing the neuropeptide NLP-21. We did not observe a statistically significant difference between control and *del-4* mutants.

(J) A panel of 19 images of dorsal neural cords expressing SNB-1::GFP in GABAergic motor neurons driven by the *unc-47* promoter. Left, control. Right, *del-4(tm717)*. Axons were straightened using the straightened function of ImageJ[94] (see KRT). The scale bar is the same as that in (K).

(K) Top, shown in green, representative images of the NLP-21::YFP strain indicating cholinergic motor neurons alongside coelomocytes in control (left) and *del-4(tm717)* (right) animals. Bottom, shown in black and white, panel of fragments of 14 straightened dorsal cord cholinergic motor neurons.

(K and L) Scale bar, 10 μm. Confocal images. Lens 63x. Day one of adulthood. (A, C, D, F–I) Dot plots, dots represent the mean values of biologically independent experiments. Error bars represent SEM ns $p = 0.1234$, *$p = 0.0332$, **$p = 0.0021$, ***$p = 0.0002$, ****$p < 0.0001$. two-way ANOVA analysis. (A) ctrl n = 301, *del-4(tm717)* n = 405, n = number of cell bodies, (B) ctrl n = 120, *del-4(tm717)* n = 120, DEL-4::GFP n = 120, n = number of animals (C) ctrl n = 494, *del-4(RNAi)* n = 618, *snt-1(RNAi)* n = 594, n = number of neuronal cell somas, (D) ctrl n = 21, *del-4(tm717)* n = 26, DEL-4::GFP n = 22, *goa-1(e407)* n = 21, n represents number of animals. (E) ctrl n = 80, *del-4(tm717)* n = 80, DEL-4::GFP n = 80, *unc-49(3407)* n = 20, n = number of animals. (F) ctrl n = 30, *del-4(tm717)* n = 34, n = number of animals (G) ctrl n = 272, *del-4(tm717)* n = 322, n = number of GFP::SNB-1 positive puncta counted from 30 ctrl and 34 *del-4(tm717)* animals, (H) ctrl n = 482, *del-4(tm717)* n = 646, n = number of NLP-21::YFP positive puncta counted from 25 ctrl and 31 *del-4(tm717)* animals, (I) ctrl n = 20, *del-4(tm717)* n = 35.

DEG/ENaC family members create sodium channels that are either constantly activated or gated by mechanical stimuli, peptides, or protons.[52] DEL-4 was previously shown to be a constitutively open channel at neutral pH and significantly inhibited by extracellular acidity[51] (Figure S6B). To further determine the DEL-4 homomeric channel's properties, we perfused DEL-4 expressing *Xenopus* oocytes with solutions of gradually reduced pH, starting from a baseline of pH 7.4. DEL-4-expressing oocytes showed a maximal current at around pH 5 and were inhibited by both high and lower pH, with pH_{50S} of 5.78 and 4.25 (Figures 7A–7C and S6E). Both the truncated control and the water-injected control oocytes did not show this inhibition with decreased pH (Figures S6B, S6F, and S6H). DEL-4 was not permeable to protons, as the ΔE_{rev} did not show statistically significant shift when extracellular proton concentration was increased from neutral pH to pH 4 (Figure S6G). It is likely that the pH_{50S} reflects the physiological range similar to what has been described for all the DEG/ENaC members such as the nematode ACD-5 or the human ENaCs. Their pH responses presumably reflect the environmental contexts, i.e. on the intestinal luminal membrane or epithelia, respectively, where they are expressed.[51,53] Therefore, inhibition of the DEL-4 homomeric channel by protons emerges in the limited range of pH 4.5–5.5, and this function is lost in the *del-4* mutant, which is incompetent to conduct current, in *Xenopus oocytes*.

Blocking a sodium channel in neurons may disrupt ion balance along the plasma membrane, since Na^+ stops entering the cytoplasm. Thus, the cytoplasmic membrane becomes more negatively charged, reducing the likelihood of an action potential. To verify this hypothesis, we used the genetically encoded voltage indicator, ASAP1 (Table S1), expressed in dopaminergic neurons. Changes in the membrane potential cause conformational changes in ASAP1 which lead to an increase in fluorescence upon hyperpolarization and a decrease in depolarization events.[54] As shown previously, DEL-4 is inhibited by extracellular low pH (Figures 7A–7C and S6E). Interestingly, treatment of ASAP1 reporter animals with low pH buffer leads to neuronal hyperpolarization in the presence of DEL-4 (Figures 7D and 7E). Similarly, *del-4* mutant animals displayed elevated levels of ASAP1 fluorescence compared to control animals under neutral pH

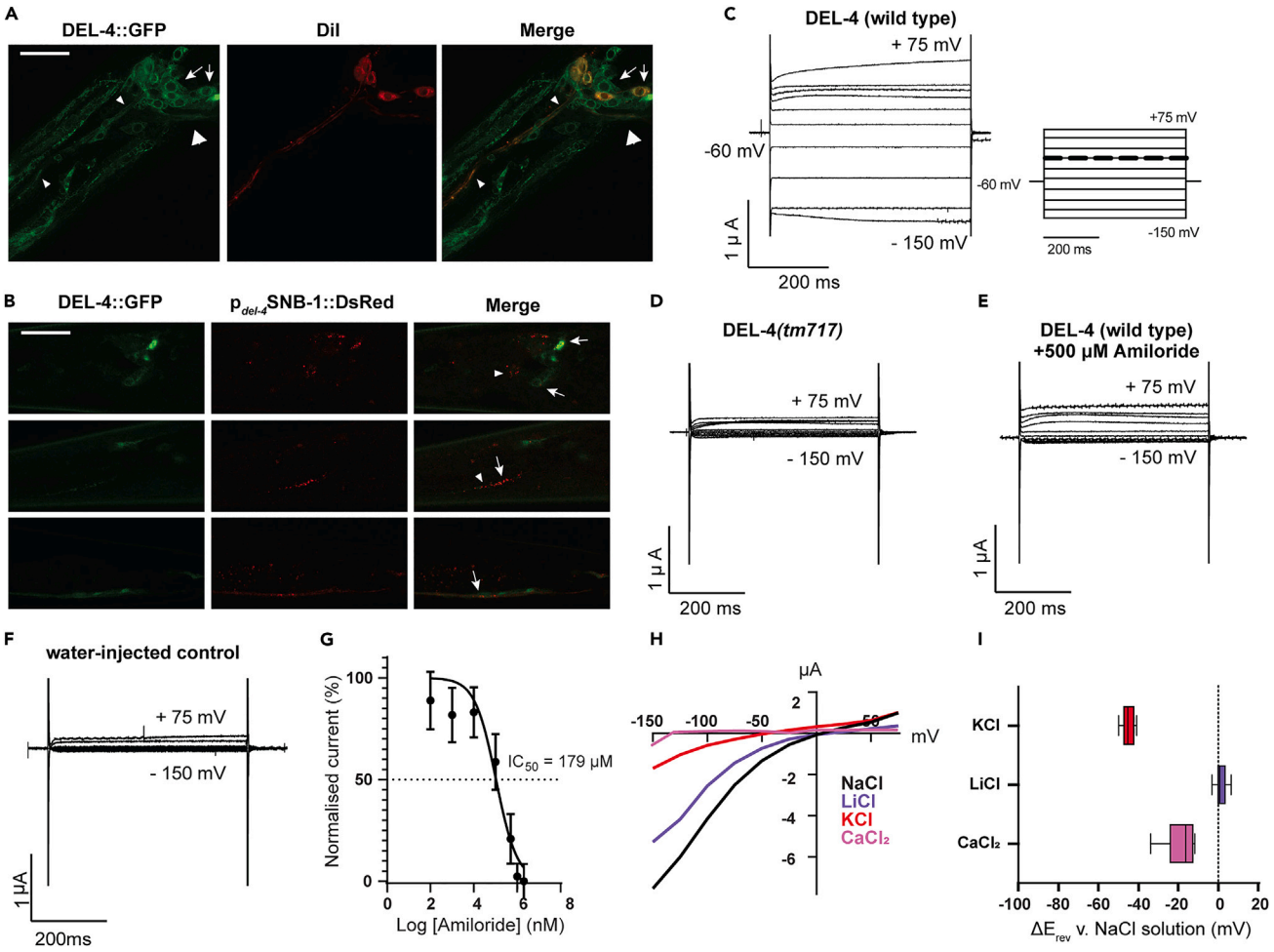

Figure 6. Subcellular localization, ion selectivity, and amiloride sensitivity of the homomeric DEL-4 channel

(A) DEL-4 localizes to the cytoplasmic membrane of neuronal cells. The DEL-4 translational reporter colocalized with DiI staining (KRT) on the surface of neuronal cell bodies and processes. Left: the *del-4* promoter drives the expression of DEL-4 tagged with GFP. Middle: DiI staining in seen in red. Right: merged images. We utilized the merged images of z-stacks to assess colocalization (see Figure S6A). Neuronal cell bodies (arrows), dendrites (small arrowheads) and axons (large arrowhead) are indicated. One-day adult animals. Left is anterior. Scale bar 20 µM. Confocal images (maximum intensity projections) with a 63x lens.

(B) Co-expression of DEL-4::GFP and SNB-1::dsRed driven by the same promoter (*del-4* promoter) revealed only random cases of colocalization. Left, expression of DEL-4 tagged with GFP in neurons driven by the *del-4* promoter (p_{del-4}DEL-4::GFP). Middle, *del-4* promoter drives the expression of *snb-1* (seen in red) in neurons (p_{del-4}SNB-1::dsRed. Right, merged images. Confocal images (Z-stacks). Lens 63x. Arrows indicate random cases of colocalization. Arrowheads indicate sites where DEL-4 and SNB-1 do not colocalize. We utilized merged z stack images to assess colocalization. Left is anterior. Scale bar 20 µm.

(C) DEL-4 subunits assemble into a constitutively open homomeric channel at neutral pH 7.4.

(D and F) Mutant *del-4(tm717)* or water-injected oocytes do not exhibit transient currents at neutral pH.

(E) DEL-4 currents at neutral pH can be blocked with 500 µM amiloride (STAR Methods).

(C–F) Representative transient currents in a *Xenopus* oocyte injected with *del-4* cRNA or *del-4(tm717)* cRNA or nuclease-free water and perfused with a physiological NaCl solution (ND96) at pH 7.4, in the absence (B) or presence (C) of 500 µM amiloride. The voltage steps applied were from −150 to +75 mV from a holding potential of −60 mV.

(G) Blocking of the DEL-4 homomeric channel by amiloride is dose-dependent. The normalized (I/Imax) current of the amiloride dose-response curves for the DEL-4 homomer revealed a half-maximal inhibitory concentration (IC_{50}) of 179 µM (LogIC50 = 4.61) (n = 5), as denoted by the dashed line. Currents were recorded at a holding potential of −60mV, normalized to maximal currents, and best fitted with Hill's equation (nonlinear fit log (inhibitor) vs. normalized response – variable slope) in GraphPad Prism.

(H and I) Representative normalized current-voltage (IV) relationships for *Xenopus* oocytes expressing DEL-4. The raw current for each oocyte and the leak current were subtracted at pH 7.4. We calculated the average ΔE_{rev} of 9 oocytes for each construct of when shifting from a NaCl solution to a KCl, LiCl or $CaCl_2$ solution. The interpolated curves displayed a shift in the reversal potential ΔE_{rev}. Replacement of NaCl with equimolar LiCl did not shift the reversal

Figure 6. *Continued*

potential ($E_{rev(Na/Li)}$ = −1.18 ± 0.93 mV) but replacement with equimolar KCl resulted in a reversal potential shift ($E_{rev(Na/K)}$ = 43.45 ± 1.86 mV) $E_{rev(Na/Ca)}$ 31.24 ± 7.77 mV (N = 10). A negative shift in E_{rev} indicates a preference for Na^+ over the respective ion, and a positive shift indicates a preference for the respective ion over Na^+. Data are presented as median and interquartile range (IQD), calculated using the Tukey method. See also Figure S6.

condition, while acidification did not affect membrane potential of *del-4* mutants (Figures 7D and 7E). Therefore, both extracellular acidification and DEL-4 channel deficiency hyperpolarizes the dopaminergic neurons *in vivo*, in accordance with our *in vitro* data.

DEL-4 participates in low pH sensory detection modulating behavioral responses to stress

Given DEL-4's ability to block Na^+ currents upon extracellular acidification, we wanted to test the behavioral response of control and *del-4* mutant animals upon encountering low pH environment. To this end, we performed a drop test assay, where the backward movement of animals upon contact with a drop of acidic buffer is monitored and quantified. This behavioral response is considered as avoidance to low pH stimulus. We challenged the animals with solutions of pH 2.2, 4.5, or 6.6. We observed that animals lacking DEL-4 were insensitive to pH 4.5, but not 2.2 or 6.6, while wt animals and animals that overexpress DEL-4 responded to all different buffers (Figure 8A). This finding indicates that closure of DEL-4 mediates the behavioral response to low pH stimuli.

Having established that DEL-4's ability to conduct current is affected by pH (Figures 7A–7C, S6B, S6E–S6H), and that blocking of Na^+ influx through DEL-4 leads to neuronal hyperpolarization Figures 7D and 7E), we sought to identify whether heat shock and long-term starvation could affect neuronal membrane potential in the presence or absence of DEL-4. To this end, we utilized again the reporter animals expressing ASAP1 in dopaminergic neurons and subjected them to prolonged starvation, thermal stress, or acidic stress (Figures 8B–8D). We found that all tested types of stress lead to hyperpolarization of dopaminergic neurons when DEL-4 is present. Interestingly, in the absence of DEL-4, neuronal membrane potential is not altered any further, than the state of the unstressed mutant, an effect that is also obvious upon DEL-4 depletion alone (Figures 8B–8D). Since starvation and heat stress limit the expression of DEL-4 (Figures 5A and 5D), while acidic stress blocks the channel's pore (Figures 7A–7C), we propose that different types of stress may hyperpolarize dopaminergic neurons by either reducing DEL-4 levels or by inhibiting conductance of current through DEL-4 channel. These findings put DEL-4 at the epicentre of stress stimuli sensation and integration.

DEL-4 displays neuroprotective effects on neurodegenerative human disease models in *C. elegans*

Several studies have shown that dysregulated dopaminergic signaling has a causative effect on the initiation and progression of neurodegenerative diseases, including Parkinson disease (PD) and Alzheimer disease (AD).[55,56] Both pathologies are complex disorders that depend on environmental and genetic factors. Data from gene expression profiling revealed the deregulation of neurotransmitters and ion channel receptors expression in PD.[57] Low levels of ACh and dopamine in the brain characterize AD and PD, respectively.[58] Moreover, chronic stress exacerbates AD and PD pathology.[59,60] In line with the effects of DEL-4 on neurotransmission and locomotion and the regulation of DEL-4 by stress, we hypothesized that downregulation of DEL-4 would aggravate the phenotype of these two neurodegenerative diseases. We utilized two *C. elegans* disease models, the UA44 as a Parkinson's model and the BR5270 as an Alzheimer disease models. These models express human α-synuclein in dopaminergic neurons, or the pro-aggregation F3ΔK280 tau fragment pan-neuronally.[61,62] In accordance to our hypothesis, we discovered that in both disease models overexpression of DEL-4 curtailed degeneration, whereas DEL-4 downregulation exacerbated this phenotype (Figure 9). In addition, depletion of DEL-4 induced dopaminergic neurodegeneration on day 5 and 7 of adulthood, even in the absence of aggregation prone proteins (Figure 9). Consequently, we propose that disruption of neuronal sodium homeostasis exacerbates neurodegeneration in control and in disease genetic background.

DISCUSSION

In this study, we characterized the contribution of a proton-inhibited DEG/ENaC channel to the perception and sensorimotor integration of specific types of stress. We observed that heat stress and starvation reduced the expression levels of DEL-4, which localizes to the plasma membrane of sensory, dopaminergic, serotonergic, and motor neurons while, vice versa, DEL-4 affects the activation of cellular stress responses throughout the body. Mechanistically, DEL-4 modifies the neuronal excitability pattern and alters synaptic

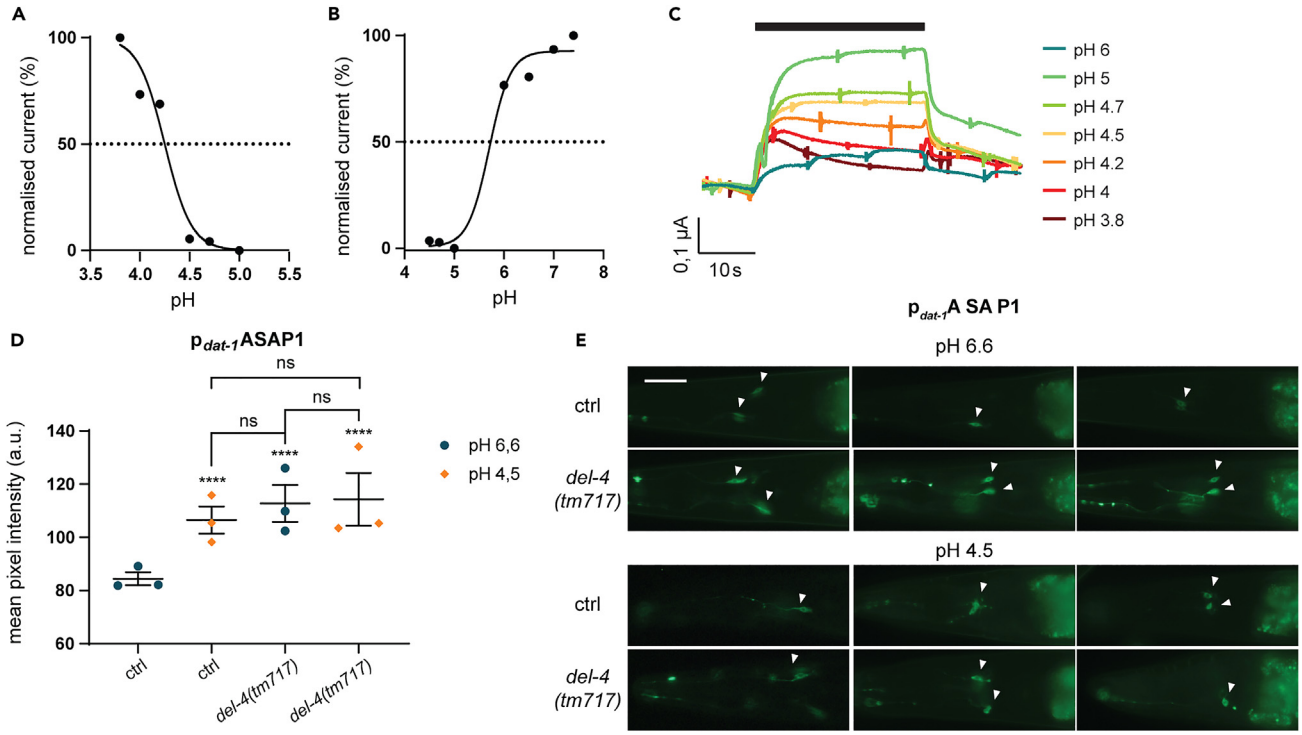

Figure 7. Acidic pH blocks the homomeric DEL-4 channel and hyperpolarizes dopaminergic neurons similar to DEL-4 depletion

(A and B) Extracellular protons inhibit the DEL-4 homomeric channel. Current to pH relationships of heterologously expressed DEL-4 homomeric channel, when perfused with solutions of increasing pH starting from 3.8 until 7.5 (n = 5). The channel is fully open at 100% current and closed at 0% current. Amount of total DEL-4 cRNA (500 ng/µL) injected. Only the mean values are presented. The voltage steps were from −150 to +75 mV from a holding potential of −60 mV. Currents were recorded at a holding potential of −60mV, normalized to maximal currents, and best fitted with Hill's equation in GraphPad Prism.

(C) Representative traces of DEL-4 expressing *Xenopus* oocytes when perfused with ND96 solution at various proton concentrations from a neutral baseline (pH 7.4). Currents were recorded at a holding potential of −60mV, and traces were baseline-subtracted and drift-corrected using Roboocyte2+ (Multichannels) software.

(D) Low pH enhances the intensity of ASAP1 in dopamine-releasing neurons. Quantification of resting membrane potential using a line expressing the genetic voltage indicator ASAP1 in dopaminergic neurons using the dat-1promoter. Control and *del-4(tm717)* mutant animals were imaged on day 2 of adulthood under control conditions and after acidic stress. Absence of DEL-4 and acidification increase ASAP1 fluorescence intensity, thus hyperpolarizing dopaminergic neurons. Mean pixel intensity was measured from cell bodies of dopaminergic neurons. Fluorescence intensity measurements of ASAP1 after 15 min incubation in M13 solution of pH 6.6 (ctrl) or pH 4.5, generated with $CH_3COOHNa$ (pH) (STAR Methods). The incubation time was followed by a recovery time of 10 min in M13 pH 6.6, to recover GFP fluorescence that quenched due to the pH sensitivity of GFP. Error bars represent the SEM ns p = 0.1234, *p = 0.0332, **p = 0.0021, ***p = 0.0002, ****p < 0.0001. two-way ANOVA analysis. Dot plot, dots represent the mean fluorescence of biological replicates. ctrl pH 6.6 n = 263, ctrl pH 4.5 n = 216, *del-4(tm717)* pH 6.6 n = 307, *del-4(tm717)* pH 4.5n = 317. n = number of dopaminergic neuron cell somas.

(E) Representative images of dopaminergic neurons expressing ASAP1 (p_{dat-1}ASAP1) in control and *del-4(tm717)* mutant animals under control or acidic stress conditions. Top, pH 6.6, bottom, pH 4.5. Scale bar 20 µm. Lens 20x. Left is anterior. See also Figure S6.

vesicle release from dopaminergic and motor neurons to adjust the locomotory rate of the animal. Finally, we demonstrated that DEL-4 modulation affects the integrity and viability of dopaminergic neurons. Our data highlight the significance of a DEG/ENaC member in neuronal sodium homeostasis and stabilization of resting membrane potential and provide valuable insight into DEG/ENaC sodium channel regulation upon stress. Our findings are consistent with those of previous studies, indicating that stress regulates mammalian ENaCs and ASICs.[25–29,31] However, our experiments represent the first *in vivo* study to illustrate that specific types of stress affect the abundance of a DEG/ENaC channel on the cytoplasmic membrane of neuronal cells.

Our electrophysiology and imaging results showed that low pH blocks the DEL-4 homomeric channel and hyperpolarizes the dopaminergic neurons. Acidification develops under physiological and pathological conditions, such as exercise,[63] ischemic stroke,[64] cardiac ischemia,[65] tumors,[66] and inflammation.[67] Similarly, in *C. elegans*, oxidative stress and mitochondrial fragmentation leads to cellular acidosis triggered by ROS production.[68,69] Pathogen infection and exercise also induce acidification.[69,70]

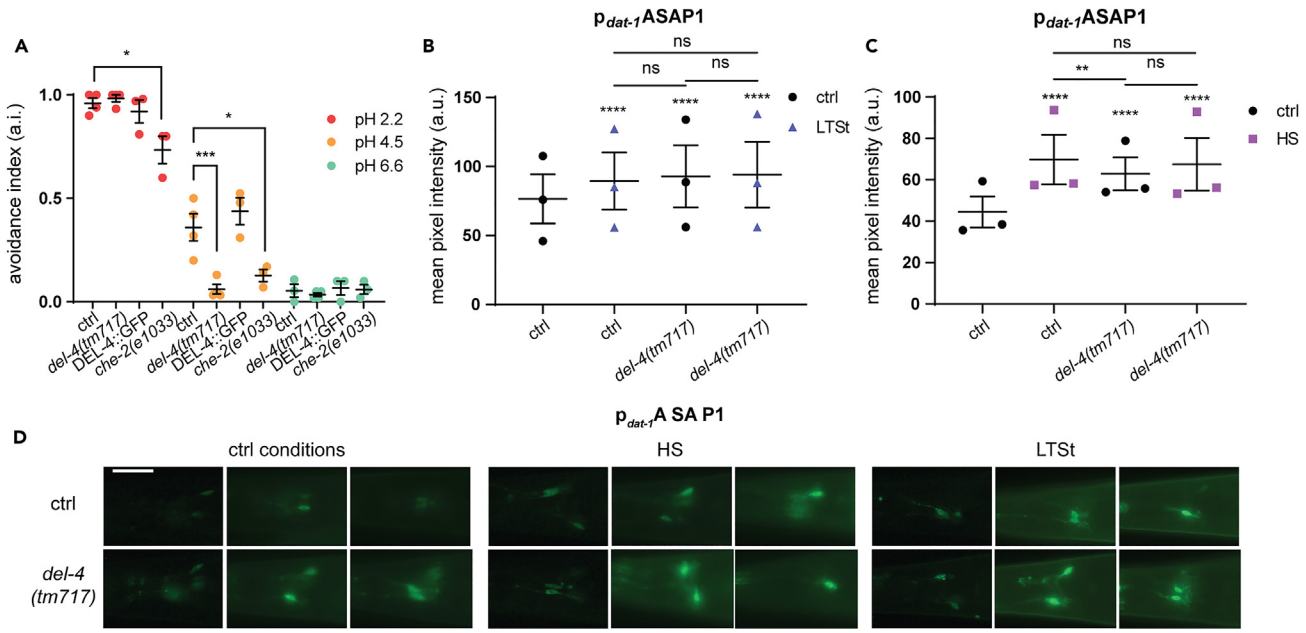

Figure 8. Dopaminergic neurons hyperpolarize upon heat stress and starvation

(A) Graph of avoidance index to M13 solutions of diverse pH values. We measured the responses of wt, *del-4(tm717)*, DEL-4::GFP, and *che-2(e1033)* (Tables 1 and S4) animals in the drop test assay. A drop of M13 buffer was applied with a syringe at the tail of each animal and a backward movement was accounted as avoidance. An avoidance index of 1 represents complete avoidance to the M13 solution, and 0 represents a total lack of avoidance response. The *che-2(e1033)* strain was used as a positive control. Animals were tested on day one of adulthood.

(B and C) Quantification of resting membrane potential using the line expressing ASAP1 in dopaminergic neurons. The voltage indicator ASAP1 was expressed under the *dat-1* promoter. Control and *del-4(tm717)* mutant animals were imaged on day 2 of adulthood under control conditions or after stress (STAR Methods). The absence of DEL-4, LTSt, and HS increases ASAP1 levels, thus hyperpolarizing dopaminergic neurons. The mean pixel intensity was measured from the neuronal cell bodies. (B) Long-term starvation (LTSt) hyperpolarizes dopaminergic neurons, similar to the *del-4(tm717)* mutant. We estimated the intensity levels of ASAP1 in control and *del-4(tm717)* animals after long-term starvation for 24 h on unseeded NGM. (C) The fluorescence of ASAP1 in dopaminergic neurons increases in the *del-4(tm717)* mutant and upon heat stress (HS). We calculated the intensity levels of ASAP1 in dopaminergic neuronal somas from control and *del-4(tm717)* animals after thermal stress for 1 h at 37°C.

(D) Representative images of dopaminergic neurons expressing ASAP1 in control and *del-4(tm717)* mutant animals under control or stress conditions. Scale bar 20 μm. Lens 20x. Left is anterior.Error bars represent SEM ns $p = 0.1234$, *$p = 0.0332$, **$p = 0.0021$, ***$p = 0.0002$, ****$p < 0.0001$. two-way ANOVA analysis. Dot plots, dots represent the mean of independent biological experiments (A) ctrl pH 2.2 n = 79, ctrl pH 4.2 n = 118, ctrl pH 6.6 n = 104, *del-4(tm717)* pH 2.2 n = 107, *del-4(tm717)* pH 4.5 n = 125, *del-4(tm717)* pH 6.6 n = 113, DEL-4::GFP pH 2.2 n = 106, DEL-4::GFP pH 4.5 n = 80, DEL-4::GFP pH 6.6 n = 123, *che-2(e1033)* pH 2.2 n = 108, *che-2(e1033)* pH 4.5 n = 93, *che-2(e1033)* pH 6.6 n = 104. n represents the total number of responses (positive and negative) counted in all experimental repeats. (B) ctrl ctrl n = 197, ctrl LTSt n = 212, del-4(tm717) ctrl n = 189, and del-4(tm717) LTSt n = 260. (C) Three trials, ctrl ctrl n = 177, ctrl HS n = 180, *del-4(tm717)* ctrl n = 213, and *del-4(tm717)* HS n = 186. (B, C) n represents number of dopaminergic neuron cell somas.

The site(s) of proton binding for channel opening in the mammalian ASICs are still relatively poorly understood with several candidate binding sites in the pore-forming and extracellular domains.[71] Among the *C. elegans* DEG/ENaCs, there are two groups of acid-sensitive DEG/ENaCs characterized by being either inhibited or activated by increasing proton concentrations. Three of these acid-sensitive DEG/ENaCs are activated by acidic pH, making them functionally similar to most of the vertebrate ASICs51. By contrast, DEL-4 is part of four acid-inhibited members which also include the degenerin ACD-1, a proton-inhibited glial sodium channel that participates in sensory perception and affects neuronal function.[72] Among mammalian members, low extracellular pH blocks the heteromeric αβ ENaC epithelial channel.[73] Although ENaCs are mainly localized in epithelial tissues, alpha and beta ENaC subunits are abundantly co-expressed in many brain regions.[74] Regarding its *in vivo* function, our results have shown that del-4 mutants are insensitive to solution at pH 4.5 indicating that DEL-4 could be directly involved in acid sensation. Additionally, we have also shown that DEL-4 may play a more modulatory role during neurotransmission. Consequently, DEL-4 could have dual roles depending on where it is expressed. This is similar to what has been suggested for another *C. elegans* DEG/ENaC, DEG-1, which in chemosensory neurons functions in responses to both attractive and repellent cues[72] but in nose nociceptor neurons is required for mechanoreceptor currents.[75] Overall, this work highlights the importance of proton homeostasis in the regulation of sodium channel gating and stress perception.

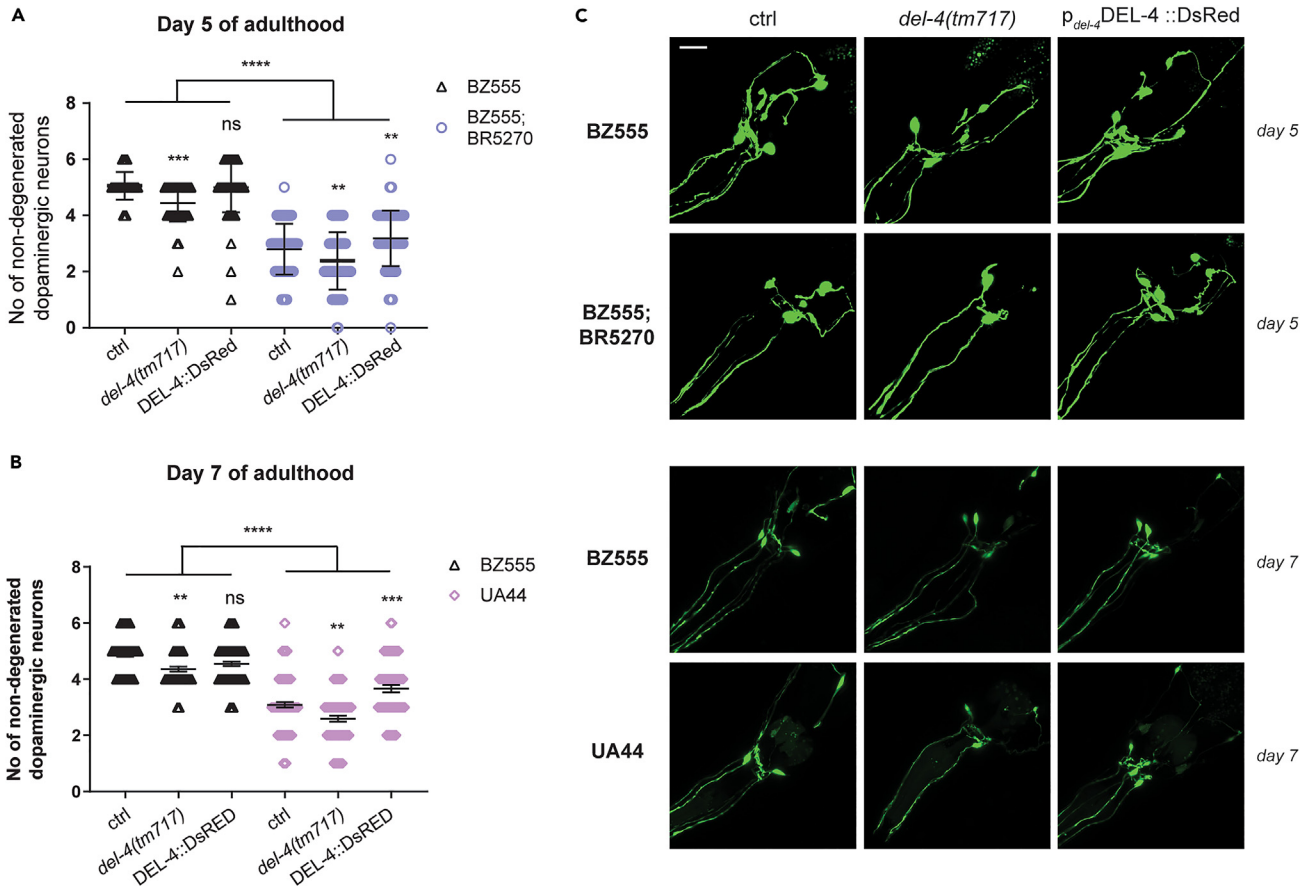

Figure 9. DEL-4 protects against neurodegeneration

(A) Overexpression of DEL-4 promotes survival of dopamine-releasing neurons in the head of *C. elegans* in an Alzheimer disease model. The graph indicates the number of surviving dopaminergic neurons in the head of control and *del-4(tm717)* mutant animals in control (BZ555) and disease conditions (BR5270) (Tables 1 and S4). DEL-4 elimination results in an increased number of degenerated neurons under control conditions and in the tauopathy model. The strain BR5270, which overexpresses the F3 pro-aggregation fragment of the human Tau protein with deleted K280, pan-neuronally, under the rab-3 promoter (p_{rab-3}F3(delta)K280), was used. Measurements were performed on 5-day adult animals.

(B) The *del-4(tm717)* mutant displays increased neurodegeneration under control conditions and in a model of Parkinson disease at day seven of adulthood. Comparison of surviving neurons of control and *del-4(tm717)* mutants under control conditions (BZ555) and in the UA44 model of Parkinson disease. DEL-4-overexpressing animals exhibit reduced degeneration compared to control. The UA44 strain (p_{dat-1}GFP; p_{dat-1}a-syn) expresses human α-synuclein and GFP in dopaminergic neurons. We used UA44 as the synucleinopathy model.(A, B) Error bars represent the SEM ns p = 0.1234, *p = 0.0332, **p = 0.0021, ***p = 0.0002, ****p < 0.0001. One-way ANOVA analysis.

(A–C) Dot plots, dots represent the number of non-degenerated neurons counted per animal.(C) Representative images from the head of control animals (left), *del-4(tm717)* mutants (middle), and DEL-4-overexpressing animals (DEL-4::dsRed) (right). Top, images from the BR5270 strain and the BZ555 control on day five of adulthood. Bottom, images from the UA44 strain and the BZ555 control on day seven of adulthood. Confocal images (maximum intensity projections). Lens 40x. Scale bar 20 μm. Left is anterior. (A–C) Strain BZ555 expresses GFP in dopaminergic neurons (p_{dat-1}GFP). We utilized BZ555 as a control for disease models. (A) BZ555 n = 73, *del-4(tm717)* n = 68, DEL-4::dsRed n = 88, BR5270 n = 158, BR5270;*del-4(tm717)* n = 134, BR5270; DEL-4::dsRed n = 151. (B) BZ555 n = 143, *del-4(tm717)* n = 67, DEL-4::dsRed n = 92, UA44 n = 117, UA44;*del-4(tm717)* n = 83, UA44; DEL-4::dsRed n = 63.

DEL-4 at steady-state conditions behaves as a permanently open channel. Thus, it may participate in neuronal resting membrane potential generation as a Na^+ leak channel. The subcellular localization pattern of DEL-4 supports this notion. DEL-4, unlike other ASICs,[76,77] is distributed throughout the plasma membrane and not specifically at the synapse. In addition, synaptic ASICs are mainly open in response to low pH, whereas DEL-4 would be closed under these conditions. The regulation of the DEL-4 channel by specific types of stress represents a mechanism that controls and alters neuronal excitability in response to environmental stress. DEL-4 modulates transcription factors that affect synaptic activity, neuronal structural maintenance, and survival.[78–82] Vice versa, HSF-1 participates in the regulation of DEL-4, thereby mediating stress signal transmission.

We observe altered neuronal signaling of motor neurons in the absence of DEL-4. We propose that in the case of *del-4* mutant there are two levels of regulation of ACh release from cholinergic motor neurons. First, DEL-4 is expressed in cholinergic motor neurons, therefore its absence could alter (similar to its effect on dopaminergic neurons) the resting membrane potential of cholinergic neurons due to defective ion homeostasis. The second level of regulation of cholinergic motor neurons arises from altered dopaminergic signaling in the *del-4* mutant. In *C. elegans*, the D1-like dopamine receptor, DOP-1, localizes on the cytosolic membrane of cholinergic motor neurons, where it stimulates ACh release. In addition, a deregulation of synaptic homeostasis has been observed in neurological diseases.[83] In *C. elegans*, released dopamine reaches dopamine receptors found on motor neurons through diffusion. We hypothesize that DOP-3 receptor expressed on GABAergic motor neurons is less activated in the *del-4* mutant, therefore increasing GABAergic signaling and further reducing ACh release. Overall, we believe that in the del-4 mutant there is a defected neuronal ionstasis and homeostasis that settle a new equilibrium concerning neuronal activation and synaptic release.

DEL-4 is essential for neural cell homeostasis and survival. The *del-4* mutant showed increased neuronal loss with age compared with the control. In contrast, heightened DEL-4 levels act in a neuroprotective manner in Parkinson and Alzheimer disease models. Conversely, blocking ASIC current attenuates α-synuclein accumulation and protects neurons from degeneration.[84] Mammalian ASICs have also been involved in brain ischemia. Inhibition of ASIC1a attenuates intracellular Ca^{2+} elevation due to cerebral ischemia.[85] Interestingly, acidity has been implicated in the onset and the progression of several features of amyotrophic lateral sclerosis.[86,87] ASIC2 and ASIC3 are upregulated in motor neurons of patients with amyotrophic lateral sclerosis.[88] Our results, concerning the proton-inhibition and the attenuated locomotory rate observed upon DEL-4 downregulation, corroborate the findings that ASICs are implicated in a variety of neurodegenerative diseases, in which acidification is observed.

The difference of DEL-4 to other ASICs is that it constitutes a sodium leak channel at physiological conditions, contrary to most of the mammalian ASICs that open upon acidification. The sodium background channel NALCN, a voltage-independent cation channel, regulates neuronal membrane conductance and coordinates its excitability.[89] Disruption of NALCN results in neuronal hyperpolarization and has been linked with neurodegenerative diseases, such as Alzheimer disease.[90] In view of these findings, the effects of DEL-4 on membrane potential and neurodegeneration are not contrary to a large body of evidence supporting that hyperpolarization is normally protective. In most of these cases, reduced depolarization is mediated by potassium or voltage-gated sodium channels.[91,92]

Several studies have linked chronic stress with the progression of AD and PD. In mammalian AD models, long-term adverse stress worsens cognitive functions and accelerates Aβ deposition.[60] Chronic stress in rodents reduces dopaminergic signaling in distinct brain regions and confines locomotory activity.[93] Research in animal models and humans with PD has revealed that stress worsens mental health and causes locomotion defects.[59] Our findings provide new insights into the molecular mechanisms underlying chronic stress that affects the onset and accelerates the progression of neurodegenerative diseases.

Our electrophysiological analysis indicates that DEL-4 forms a proton-gated homomeric channel. We note that DEL-4 shows extensive sequence similarity with human ENaC1b and ASIC1b. Therefore, it could potentially form either homomeric or heteromeric channels, *in vivo*. Whether the heteromeric channels will share the same electrophysiological properties as the DEL-4 homomeric channel remains to be elucidated. Nevertheless, depletion of DEL-4 is expected to affect all the types of DEL-4 containing channels *in vivo*.

We propose a model in which specific types of stress or acidity reduce or inhibit the DEL-4 channel, inducing hyperpolarization of dopamine neurons and the subsequent perturbation of synaptic release. Concomitantly, cell-non-autonomous modulation of several stress responses affects the excitation patterns of cholinergic and GABAergic motor neurons. This regulation adjusts the motor output of animals to elicit proper behavior in response to stress. Thus, neuronal ionstasis fine-tunes stress response mechanisms and neuroendocrine signaling to control physiological processes, such as locomotion (Figure 10).

Limitations of the study

We have not explored possible interactions of DEL-4 with other degenerin ion channels that could result in the formation of heteromeric sodium channels with distinct electrophysiological properties.

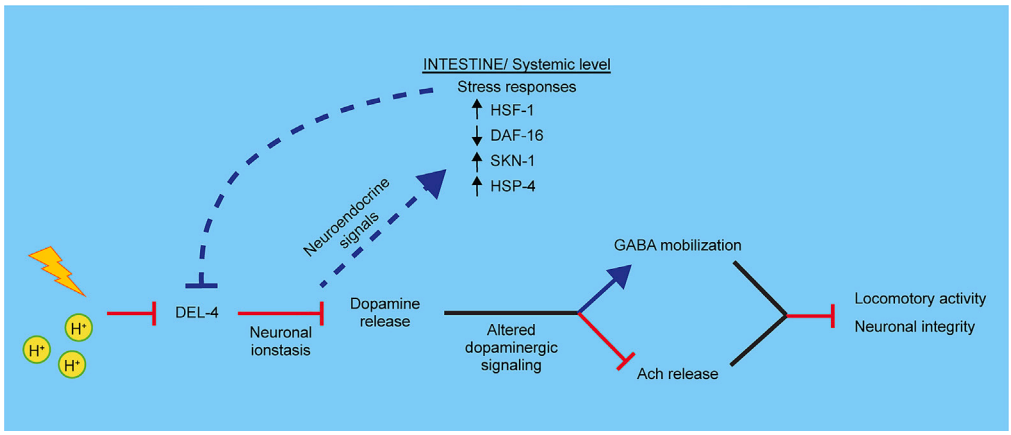

Figure 10. Proposed model

According to our results, we propose that several types of stress regulate the expression or the gating of the DEL-4 channel that acts in mediating stress perception. Consequently, modulation of DEL-4 by stress alters the downstream neuronal signaling through dopaminergic and motor neurons for the animal to adapt its behavioral response. Additionally, the altered neuronal signaling triggers the activation of stress response transcription factors that act through a feedback loop on the DEL-4 channel, to further modulate the stress response.

STAR★METHODS

Detailed methods are provided in the online version of this paper and include the following:

- KEY RESOURCES TABLE
- RESOURCE AVAILABILITY
  - Lead contact
  - Materials availability
  - Data and code availability
- EXPERIMENTAL MODEL AND STUDY PARTICIPANT DETAILS
  - Caenorhabditis elegans
  - Xenopus oocytes
- METHOD DETAILS
  - Generation of *C. elegans* transgenic lines
  - Genetic crosses
  - Molecular cloning
  - Total RNA isolation and qRT-analysis
  - Protein blast
  - RNAi treatment
  - Microscopy
  - Behavioural assays
  - DEL-4 expression and TEVC on Xenopus oocytes
  - Dil staining
  - Stress assays
  - Survival assays
  - Pharmacological assays
- QUANTIFICATION AND STATISTICAL ANALYSIS

SUPPLEMENTAL INFORMATION

Supplemental information can be found online at https://doi.org/10.1016/j.isci.2023.107117.

ACKNOWLEDGMENTS

We especially thank Eirini Lionaki for guidance with experiments and manuscript editing. We thank Angela Pasparaki for technical assistance and all members of our laboratory for useful discussions. Some nematode strains used in this work were provided by the *Caenorhabditis* Genetics Center, which is funded by

the National Center for Research Resources (NCRR) of the National Institutes of Health (NIH, USA), and S. Mitani (National Bioresource Project) in Japan. We thank A. Fire for plasmid vectors. We thank Nikos Kourtis for the construction of *del-4(tm717)* rescue strain. *C. elegans* strains *del-4(tm717)* and *unc-43(tm1605)* were generated by the International *C. elegans* gene knockout consortium. This project was supported by "Flagship Initiative for Neurodegenerative Diseases Research on the Basis of Precision Medicine, in the framework of Hellenic Precision Medicine Research Network for Neurodegenerative Diseases, of the project "Infrastructures for National Research Networks for Precision Medicine and Climate Change" no. 2018ΣΕ01300001 of the GSRT National Public Investments Programme. This project was supported by H2020 FETOPEN project "Dynamic" (EC-GA863203) to N.T. This project was also partially supported by the European Research Council under the grant agreement "ERC-GA695190-MANNA" to N.T. This research was also co-financed by the European Union (European Social Fund - ESF) and Greek national funds through the Operational Program "Education and Lifelong Learning" of the National Strategic Reference Framework (NSRF) 2007-2013 to N.T. Research Funding Program: THALES - Investing in Knowledge Society through the European Social Fund. Project "THALES - BSRC Alexander Fleming" - Development and employment of Minos-based genetic and functional genomic technologies in model organisms (MINOS) - MIS: 376898" to N.T. Additionally, through the Operational Program "Competitiveness, Entrepreneurship, Innovation" of the National Strategic Reference Framework (NSRF) 2014-2020, under the call RESEARCH – CREATE – INNOVATE (project code: T1EDK-01504, "EPHESIAN") to N.T.

AUTHOR CONTRIBUTIONS

Conceptualization, D.P. and N.T.; Methodology, D.P., M.G., E.K., and N.T.; Validation, D.P., M.G., and E.K.; Formal analysis, D.P., M.G., and E.K.; Investigation, D.P., M.G., and E.K.; Resources, W.S. and N.T.; Data curation, D.P., M.G., and E.K.; Writing - original draft, D.P., M.G., and E.K.; Writing - review and editing, D.P., M.G., E.K., W.S., and N.T.; Visualization, D.P., M.G., and E.K.; Supervision, W.S. and N.T.; Project administration, D.P. and N.T.; Funding acquisition, W.S. and N.T.

DECLARATION OF INTERESTS

The authors declare no competing interests.

INCLUSION AND DIVERSITY

We support inclusive, diverse, and equitable conduct of research.

Received: October 25, 2022
Revised: March 28, 2023
Accepted: June 9, 2023
Published: June 14, 2023

REFERENCES

1. Jang, M.S., Toyoshima, Y., Tomioka, M., Kunitomo, H., and Iino, Y. (2019). Multiple sensory neurons mediate starvation-dependent aversive navigation in Caenorhabditis elegans. Proc. Natl. Acad. Sci. USA *116*, 18673–18683.

2. Kim, K.W., and Jin, Y. (2015). Neuronal responses to stress and injury in C. elegans. FEBS Lett. *589*, 1644–1652.

3. Prahlad, V., Cornelius, T., and Morimoto, R.I. (2008). Regulation of the cellular heat shock response in Caenorhabditis elegans by thermosensory neurons. Science *320*, 811–814.

4. Kagias, K., Nehammer, C., and Pocock, R. (2012). Neuronal responses to physiological stress. Front. Genet. *3*, 222.

5. Cattaneo, A., and Riva, M.A. (2016). Stress-induced mechanisms in mental illness: a role for glucocorticoid signalling. J. Steroid Biochem. Mol. Biol. *160*, 169–174.

6. Fogaça, M.V., and Duman, R.S. (2019). Cortical GABAergic dysfunction in stress and depression: new insights for therapeutic interventions. Front. Cell. Neurosci. *13*, 87.

7. Guan, Z.Z. (2008). Cross-talk between oxidative stress and modifications of cholinergic and glutaminergic receptors in the pathogenesis of Alzheimer's disease. Acta Pharmacol. Sin. *29*, 773–780.

8. Juárez Olguín, H., Calderón Guzmán, D., Hernández García, E., and Barragán Mejía, G. (2016). The role of dopamine and its dysfunction as a consequence of oxidative stress. Oxid. Med. Cell. Longev. *2016*, 9730467.

9. Murnane, K.S. (2019). Serotonin 2A receptors are a stress response system: implications for post-traumatic stress disorder. Behav. Pharmacol. *30*, 151–162.

10. Chen, C., Wang, L., Rong, X., Wang, W., and Wang, X. (2015). Effects of fluoxetine on protein expression of potassium ion channels in the brain of chronic mild stress rats. Acta Pharm. Sin. B *5*, 55–61.

11. Zhou, J.J., Gao, Y., Kosten, T.A., Zhao, Z., and Li, D.P. (2017). Acute stress diminishes M-current contributing to elevated activity of hypothalamic-pituitary-adrenal axis. Neuropharmacology *114*, 67–76.

12. Park, J.Y., Dus, M., Kim, S., Abu, F., Kanai, M.I., Rudy, B., and Suh, G.S.B. (2016). Drosophila SLC5A11 mediates hunger by regulating K(+) channel activity. Curr. Biol. *26*, 1965–1974.

13. Nuñez-Villena, F., Becerra, A., Echeverría, C., Briceño, N., Porras, O., Armisén, R., Varela, D., Montorfano, I., Sarmiento, D.,

and Simon, F. (2011). Increased expression of the transient receptor potential melastatin 7 channel is critically involved in lipopolysaccharide-induced reactive oxygen species-mediated neuronal death. Antioxidants Redox Signal. *15*, 2425–2438.

14. Roedding, A.S., Tong, S.Y., Au-Yeung, W., Li, P.P., and Warsh, J.J. (2013). Chronic oxidative stress modulates TRPC3 and TRPM2 channel expression and function in rat primary cortical neurons: relevance to the pathophysiology of bipolar disorder. Brain Res. *1517*, 16–27.

15. Benemei, S., Fusi, C., Trevisan, G., and Geppetti, P. (2014). The TRPA1 channel in migraine mechanism and treatment. Br. J. Pharmacol. *171*, 2552–2567.

16. Wang, S., Yuan, F., and Li, D.P. (2017). M channels and stress response. Oncotarget *8*, 34026–34027.

17. Goodman, M.B., Hall, D.H., Avery, L., and Lockery, S.R. (1998). Active currents regulate sensitivity and dynamic range in C. elegans neurons. Neuron *20*, 763–772.

18. Liu, Q., Kidd, P.B., Dobosiewicz, M., and Bargmann, C.I. (2018). C. elegans AWA olfactory neurons fire calcium-mediated all-or-none action potentials. Cell *175*, 57–70.e17.

19. Bargmann, C.I. (1998). Neurobiology of the Caenorhabditis elegans genome. Science *282*, 2028–2033.

20. Lockery, S.R., and Goodman, M.B. (2009). The quest for action potentials in C. elegans neurons hits a plateau. Nat. Neurosci. *12*, 377–378.

21. Hanukoglu, I., and Hanukoglu, A. (2016). Epithelial sodium channel (ENaC) family: phylogeny, structure-function, tissue distribution, and associated inherited diseases. Gene *579*, 95–132.

22. Qadri, Y.J., Rooj, A.K., and Fuller, C.M. (2012). ENaCs and ASICs as therapeutic targets. Am. J. Physiol. Cell Physiol. *302*, C943–C965.

23. Dwyer, J.M., Rizzo, S.J.S., Neal, S.J., Lin, Q., Jow, F., Arias, R.L., Rosenzweig-Lipson, S., Dunlop, J., and Beyer, C.E. (2009). Acid sensing ion channel (ASIC) inhibitors exhibit anxiolytic-like activity in preclinical pharmacological models. Psychopharmacology (Berl) *203*, 41–52.

24. Zhou, W., Ye, S., Luo, R., Wu, L.M., and Wang, W. (2019). Inhibition of acid-sensing ion channels reduces the hypothalamus–pituitary–adrenal axis activity and ameliorates depression-like behavior in rats. RSC Adv. *9*, 8707–8713.

25. Ilatovskaya, D.V., Pavlov, T.S., Levchenko, V., and Staruschenko, A. (2013). ROS production as a common mechanism of ENaC regulation by EGF, insulin, and IGF-1. Am. J. Physiol. Cell Physiol. *304*, C102–C111.

26. Xu, H., and Chu, S. (2007). ENaC alpha-subunit variants are expressed in lung epithelial cells and are suppressed by oxidative stress. Am. J. Physiol. Lung Cell Mol. Physiol. *293*, L1454–L1462.

27. Andrey, F., Tsintsadze, T., Volkova, T., Lozovaya, N., and Krishtal, O. (2005). Acid sensing ionic channels: modulation by redox reagents. Biochim. Biophys. Acta *1745*, 1–6.

28. Cadiou, H., Studer, M., Jones, N.G., Smith, E.S.J., Ballard, A., McMahon, S.B., and McNaughton, P.A. (2007). Modulation of acid-sensing ion channel activity by nitric oxide. J. Neurosci. *27*, 13251–13260.

29. Arteaga, M.F., Coric, T., Straub, C., and Canessa, C.M. (2008). A brain-specific SGK1 splice isoform regulates expression of ASIC1 in neurons. Proc. Natl. Acad. Sci. USA *105*, 4459–4464.

30. Liu, W., Yuen, E.Y., and Yan, Z. (2010). The stress hormone corticosterone increases synaptic alpha-amino-3-hydroxy-5-methyl-4-isoxazolepropionic acid (AMPA) receptors via serum- and glucocorticoid-inducible kinase (SGK) regulation of the GDI-Rab4 complex. J. Biol. Chem. *285*, 6101–6108.

31. Pearce, D. (2003). SGK1 regulation of epithelial sodium transport. Cell. Physiol. Biochem. *13*, 13–20.

32. Xiong, Z., Liu, Y., Hu, L., Ma, B., Ai, Y., and Xiong, C. (2013). A rapid facilitation of acid-sensing ion channels current by corticosterone in cultured hippocampal neurons. Neurochem. Res. *38*, 1446–1453.

33. Ye, S., Yang, R., Xiong, Q., Yang, Y., Zhou, L., Gong, Y., Li, C., Ding, Z., Ye, G., and Xiong, Z. (2018). Acute stress enhances learning and memory by activating acid-sensing ion channels in rats. Biochem. Biophys. Res. Commun. *498*, 1078–1084.

34. Etchberger, J.F., Lorch, A., Sleumer, M.C., Zapf, R., Jones, S.J., Marra, M.A., Holt, R.A., Moerman, D.G., and Hobert, O. (2007). The molecular signature and cis-regulatory architecture of a C. elegans gustatory neuron. Genes Dev. *21*, 1653–1674.

35. McWilliam, H., Li, W., Uludag, M., Squizzato, S., Park, Y.M., Buso, N., Cowley, A.P., and Lopez, R. (2013). Analysis tool web services from the EMBL-EBI. Nucleic Acids Res. *41*, W597–W600.

36. An, J.H., and Blackwell, T.K. (2003). SKN-1 links C. elegans mesendodermal specification to a conserved oxidative stress response. Genes Dev. *17*, 1882–1893.

37. Murphy, C.T., McCarroll, S.A., Bargmann, C.I., Fraser, A., Kamath, R.S., Ahringer, J., Li, H., and Kenyon, C. (2003). Genes that act downstream of DAF-16 to influence the lifespan of Caenorhabditis elegans. Nature *424*, 277–283.

38. Trinklein, N.D., Murray, J.I., Hartman, S.J., Botstein, D., and Myers, R.M. (2004). The role of heat shock transcription factor 1 in the genome-wide regulation of the mammalian heat shock response. Mol. Biol. Cell *15*, 1254–1261.

39. Hibshman, J.D., Doan, A.E., Moore, B.T., Kaplan, R.E., Hung, A., Webster, A.K., Bhatt, D.P., Chitrakar, R., Hirschey, M.D., and Baugh, L.R. (2017). daf-16/FoxO promotes gluconeogenesis and trehalose synthesis during starvation to support survival. Elife *6*, e30057.

40. Weinkove, D., Halstead, J.R., Gems, D., and Divecha, N. (2006). Long-term starvation and ageing induce AGE-1/PI 3-kinase-dependent translocation of DAF-16/FOXO to the cytoplasm. BMC Biol. *4*, 1.

41. Kaplan, R.E.W., and Baugh, L.R. (2016). L1 arrest, daf-16/FoxO and nonautonomous control of post-embryonic development. Worm *5*, e1175196.

42. Hardie, D.G. (2018). Keeping the home fires burning: AMP-activated protein kinase. J. R. Soc. Interface *15*, 20170774.

43. An, J.H., Vranas, K., Lucke, M., Inoue, H., Hisamoto, N., Matsumoto, K., and Blackwell, T.K. (2005). Regulation of the Caenorhabditis elegans oxidative stress defense protein SKN-1 by glycogen synthase kinase-3. Proc. Natl. Acad. Sci. USA *102*, 16275–16280.

44. Sawin, E.R., Ranganathan, R., and Horvitz, H.R. (2000). C. elegans locomotory rate is modulated by the environment through a dopaminergic pathway and by experience through a serotonergic pathway. Neuron *26*, 619–631.

45. Chase, D.L., Pepper, J.S., and Koelle, M.R. (2004). Mechanism of extrasynaptic dopamine signaling in Caenorhabditis elegans. Nat. Neurosci. *7*, 1096–1103.

46. Mahoney, T.R., Luo, S., and Nonet, M.L. (2006). Analysis of synaptic transmission in Caenorhabditis elegans using an aldicarb-sensitivity assay. Nat. Protoc. *1*, 1772–1777.

47. Gründer, S., and Pusch, M. (2015). Biophysical properties of acid-sensing ion channels (ASICs). Neuropharmacology *94*, 9–18.

48. Bartoi, T., Augustinowski, K., Polleichtner, G., Gründer, S., and Ulbrich, M.H. (2014). Acid-sensing ion channel (ASIC) 1a/2a heteromers have a flexible 2:1/1:2 stoichiometry. Proc. Natl. Acad. Sci. USA *111*, 8281–8286.

49. Canessa, C.M., Schild, L., Buell, G., Thorens, B., Gautschi, I., Horisberger, J.D., and Rossier, B.C. (1994). Amiloride-sensitive epithelial Na+ channel is made of three homologous subunits. Nature *367*, 463–467.

50. Yang, L., and Palmer, L.G. (2014). Ion conduction and selectivity in acid-sensing ion channel 1. J. Gen. Physiol. *144*, 245–255.

51. Kaulich, E., McCubbin, P.T.N., Schafer, W.R., and Walker, D.S. (2023). Physiological insight into the conserved properties of Caenorhabditis elegans acid-sensing degenerin/epithelial sodium channels. J. Physiol. *601*, 1625–1653.

52. Eastwood, A.L., and Goodman, M.B. (2012). Insight into DEG/ENaC channel gating from

genetics and structure. Physiology *27*, 282–290.

53. Collier, D.M., and Snyder, P.M. (2009). Extracellular chloride regulates the epithelial sodium channel. J. Biol. Chem. *284*, 29320–29325.

54. St-Pierre, F., Marshall, J.D., Yang, Y., Gong, Y., Schnitzer, M.J., and Lin, M.Z. (2014). High-fidelity optical reporting of neuronal electrical activity with an ultrafast fluorescent voltage sensor. Nat. Neurosci. *17*, 884–889.

55. Krashia, P., Nobili, A., and D'Amelio, M. (2019). Unifying hypothesis of dopamine neuron loss in neurodegenerative diseases: focusing on alzheimer's disease. Front. Mol. Neurosci. *12*, 123.

56. Masato, A., Plotegher, N., Boassa, D., and Bubacco, L. (2019). Impaired dopamine metabolism in Parkinson's disease pathogenesis. Mol. Neurodegener. *14*, 35.

57. Simunovic, F., Yi, M., Wang, Y., Macey, L., Brown, L.T., Krichevsky, A.M., Andersen, S.L., Stephens, R.M., Benes, F.M., and Sonntag, K.C. (2009). Gene expression profiling of substantia nigra dopamine neurons: further insights into Parkinson's disease pathology. Brain *132*, 1795–1809.

58. Houghton, P.J., and Howes, M.J. (2005). Natural products and derivatives affecting neurotransmission relevant to Alzheimer's and Parkinson's disease. Neurosignals *14*, 6–22.

59. Austin, K.W., Ameringer, S.W., and Cloud, L.J. (2016). An integrated review of psychological stress in Parkinson's disease: biological mechanisms and symptom and health outcomes. Parkinsons Dis. *2016*, 9869712.

60. Rothman, S.M., and Mattson, M.P. (2010). Adverse stress, hippocampal networks, and Alzheimer's disease. NeuroMolecular Med. *12*, 56–70.

61. Cao, S., Gelwix, C.C., Caldwell, K.A., and Caldwell, G.A. (2005). Torsin-mediated protection from cellular stress in the dopaminergic neurons of Caenorhabditis elegans. J. Neurosci. *25*, 3801–3812.

62. Fatouros, C., Pir, G.J., Biernat, J., Koushika, S.P., Mandelkow, E., Mandelkow, E.M., Schmidt, E., and Baumeister, R. (2012). Inhibition of tau aggregation in a novel Caenorhabditis elegans model of tauopathy mitigates proteotoxicity. Hum. Mol. Genet. *21*, 3587–3603.

63. Bangsbo, J., Johansen, L., Graham, T., and Saltin, B. (1993). Lactate and H+ effluxes from human skeletal muscles during intense, dynamic exercise. J. Physiol. *462*, 115–133.

64. Guo, Y., Zhou, I.Y., Chan, S.T., Wang, Y., Mandeville, E.T., Igarashi, T., Lo, E.H., Ji, X., and Sun, P.Z. (2016). pH-sensitive MRI demarcates graded tissue acidification during acute stroke - pH specificity enhancement with magnetization transfer and relaxation-normalized amide proton transfer (APT) MRI. Neuroimage *141*, 242–249.

65. Ichihara, K., Haga, N., and Abiko, Y. (1984). Is ischemia-induced pH decrease of dog myocardium respiratory or metabolic acidosis? Am. J. Physiol. *246*, H652–H657.

66. Engin, K., Leeper, D.B., Cater, J.R., Thistlethwaite, A.J., Tupchong, L., and McFarlane, J.D. (1995). Extracellular pH distribution in human tumours. Int. J. Hyperther. *11*, 211–216.

67. Simmen, H.P., and Blaser, J. (1993). Analysis of pH and pO2 in abscesses, peritoneal fluid, and drainage fluid in the presence or absence of bacterial infection during and after abdominal surgery. Am. J. Surg. *166*, 24–27.

68. Johnson, D., Allman, E., and Nehrke, K. (2012). Regulation of acid-base transporters by reactive oxygen species following mitochondrial fragmentation. Am. J. Physiol. Cell Physiol. *302*, C1045–C1054.

69. Johnson, D., and Nehrke, K. (2010). Mitochondrial fragmentation leads to intracellular acidification in Caenorhabditis elegans and mammalian cells. Mol. Biol. Cell *21*, 2191–2201.

70. Benomar, S., Lansdon, P., Bender, A.M., Peterson, B.R., Chandler, J.R., and Ackley, B.D. (2020). The C. elegans CHP1 homolog, pbo-1, functions in innate immunity by regulating the pH of the intestinal lumen. PLoS Pathog. *16*, e1008134.

71. Rook, M.L., Musgaard, M., and MacLean, D.M. (2021). Coupling structure with function in acid-sensing ion channels: challenges in pursuit of proton sensors. J. Physiol. *599*, 417–430.

72. Wang, Y., Apicella, A., Jr., Lee, S.K., Ezcurra, M., Slone, R.D., Goldmit, M., Schafer, W.R., Shaham, S., Driscoll, M., and Bianchi, L. (2008). A glial DEG/ENaC channel functions with neuronal channel DEG-1 to mediate specific sensory functions in C. elegans. EMBO J. *27*, 2388–2399.

73. Zhang, P., Fyfe, G.K., Grichtchenko, I.I., and Canessa, C.M. (1999). Inhibition of alphabeta epithelial sodium channels by external protons indicates that the second hydrophobic domain contains structural elements for closing the pore. Biophys. J. *77*, 3043–3051.

74. Amin, M.S., Wang, H.W., Reza, E., Whitman, S.C., Tuana, B.S., and Leenen, F.H.H. (2005). Distribution of epithelial sodium channels and mineralocorticoid receptors in cardiovascular regulatory centers in rat brain. Am. J. Physiol. Regul. Integr. Comp. Physiol. *289*, R1787–R1797.

75. Geffeney, S.L., Cueva, J.G., Glauser, D.A., Doll, J.C., Lee, T.H.C., Montoya, M., Karania, S., Garakani, A.M., Pruitt, B.L., and Goodman, M.B. (2011). DEG/ENaC but not TRP channels are the major mechanoelectrical transduction channels in a C. elegans nociceptor. Neuron *71*, 845–857.

76. Liu, X., Liu, C., Ye, J., Zhang, S., Wang, K., and Su, R. (2020). Distribution of acid sensing ion channels in axonal growth cones and presynaptic membrane of cultured hippocampal neurons. Front. Cell. Neurosci. *14*, 205.

77. Voglis, G., and Tavernarakis, N. (2008). A synaptic DEG/ENaC ion channel mediates learning in C. elegans by facilitating dopamine signalling. EMBO J. *27*, 3288–3299.

78. Hooper, P.L., Durham, H.D., Török, Z., Hooper, P.L., Crul, T., and Vígh, L. (2016). The central role of heat shock factor 1 in synaptic fidelity and memory consolidation. Cell Stress Chaperones *21*, 745–753.

79. Kim, S.Y., and Webb, A.E. (2017). Neuronal functions of FOXO/DAF-16. Nutr. Healthy Aging *4*, 113–126.

80. Martínez, G., Khatiwada, S., Costa-Mattioli, M., and Hetz, C. (2018). ER proteostasis control of neuronal physiology and synaptic function. Trends Neurosci. *41*, 610–624.

81. Staab, T.A., Griffen, T.C., Corcoran, C., Evgrafov, O., Knowles, J.A., and Sieburth, D. (2013). The conserved SKN-1/Nrf2 stress response pathway regulates synaptic function in Caenorhabditis elegans. PLoS Genet. *9*, e1003354.

82. Wilson, M.A., Iser, W.B., Son, T.G., Logie, A., Cabral-Costa, J.V., Mattson, M.P., and Camandola, S. (2017). skn-1 is required for interneuron sensory integration and foraging behavior in Caenorhabditis elegans. PLoS One *12*, e0176798.

83. Taylor, H.B.C., and Jeans, A.F. (2021). Friend or foe? The varied faces of homeostatic synaptic plasticity in neurodegenerative disease. Front. Cell. Neurosci. *15*, 782768.

84. Ortega-Ramírez, A., Vega, R., and Soto, E. (2017). Acid-Sensing ion channels as potential therapeutic targets in neurodegeneration and neuroinflammation. Mediat. Inflamm. *2017*, 3728096.

85. Mari, Y., Katnik, C., and Cuevas, J. (2010). ASIC1a channels are activated by endogenous protons during ischemia and contribute to synergistic potentiation of intracellular Ca(2+) overload during ischemia and acidosis. Cell Calcium *48*, 70–82.

86. Aoyama, K., Burns, D.M., Suh, S.W., Garnier, P., Matsumori, Y., Shiina, H., and Swanson, R.A. (2005). Acidosis causes endoplasmic reticulum stress and caspase-12-mediated astrocyte death. J. Cerebr. Blood Flow Metabol. *25*, 358–370.

87. Swanson, R.A., Farrell, K., and Simon, R.P. (1995). Acidosis causes failure of astrocyte glutamate uptake during hypoxia. J. Cerebr. Blood Flow Metabol. *15*, 417–424.

88. Kirby, J., Ning, K., Ferraiuolo, L., Heath, P.R., Ismail, A., Kuo, S.W., Valori, C.F., Cox, L., Sharrack, B., Wharton, S.B., et al. (2011). Phosphatase and tensin homologue/protein kinase B pathway linked to motor

neuron survival in human superoxide dismutase 1-related amyotrophic lateral sclerosis. Brain *134*, 506–517.

89. Lu, B., Su, Y., Das, S., Liu, J., Xia, J., and Ren, D. (2007). The neuronal channel NALCN contributes resting sodium permeability and is required for normal respiratory rhythm. Cell *129*, 371–383.

90. Cochet-Bissuel, M., Lory, P., and Monteil, A. (2014). The sodium leak channel, NALCN, in health and disease. Front. Cell. Neurosci. *8*, 132.

91. Berends, A.C., Luiten, P.G.M., and Nyakas, C. (2005). A review of the neuroprotective properties of the 5-HT1A receptor agonist repinotan HCl (BAYx3702) in ischemic stroke. CNS Drug Rev. *11*, 379–402.

92. Eijkelkamp, N., Linley, J.E., Baker, M.D., Minett, M.S., Cregg, R., Werdehausen, R., Rugiero, F., and Wood, J.N. (2012). Neurological perspectives on voltage-gated sodium channels. Brain *135*, 2585–2612.

93. Rasheed, N., Ahmad, A., Pandey, C.P., Chaturvedi, R.K., Lohani, M., and Palit, G. (2010). Differential response of central dopaminergic system in acute and chronic unpredictable stress models in rats. Neurochem. Res. *35*, 22–32.

94. Schneider, C.A., Rasband, W.S., and Eliceiri, K.W. (2012). NIH Image to ImageJ: 25 years of image analysis. Nat. Methods *9*, 671–675.

95. Nonet, M.L., Holgado, A.M., Brewer, F., Serpe, C.J., Norbeck, B.A., Holleran, J., Wei, L., Hartwieg, E., Jorgensen, E.M., and Alfonso, A. (1999). UNC-11, a Caenorhabditis elegans AP180 homologue, regulates the size and protein composition of synaptic vesicles. Mol. Biol. Cell *10*, 2343–2360.

96. Sanjiib Guha, G.C., and Kapahi, P. (2018). Morphological analysis of dopaminergic neurons with age using Caenorhabditis elegans GFP reporter strains. bio-protocol.

97. Brenner, S. (1974). The genetics of Caenorhabditis elegans. Genetics *77*, 71–94.

98. Fay, D.S. (2013). Classical Genetic Methods (WormBook), pp. 1–58.

99. Mello, C.C., Kramer, J.M., Stinchcomb, D., and Ambros, V. (1991). Efficient gene transfer in C.elegans: extrachromosomal maintenance and integration of transforming sequences. EMBO J. *10*, 3959–3970.

100. Praitis, V., Casey, E., Collar, D., and Austin, J. (2001). Creation of low-copy integrated transgenic lines in Caenorhabditis elegans. Genetics *157*, 1217–1226.

101. Sieburth, D., Madison, J.M., and Kaplan, J.M. (2007). PKC-1 regulates secretion of neuropeptides. Nat. Neurosci. *10*, 49–57.

102. Dittman, J.S., and Kaplan, J.M. (2006). Factors regulating the abundance and localization of synaptobrevin in the plasma membrane. Proc. Natl. Acad. Sci. USA *103*, 11399–11404.

103. Kaulich, E., Carroll, T., Ackley, B.D., Tang, Y.Q., Hardege, I., Nehrke, K., Schafer, W.R., and Walker, D.S. (2022). Distinct roles for two Caenorhabditis elegans acid-sensing ion channels in an ultradian clock. Elife *11*, e75837.

104. Paukert, M., Babini, E., Pusch, M., and Gründer, S. (2004). Identification of the Ca2+ blocking site of acid-sensing ion channel (ASIC) 1: implications for channel gating. J. Gen. Physiol. *124*, 383–394.

105. Hardege, I., Xu, S., Gordon, R.D., Thompson, A.J., Figg, N., Stowasser, M., Murrell-Lagnado, R., and O'Shaughnessy, K.M. (2015). Novel insertion mutation in KCNJ5 channel produces constitutive aldosterone release from H295R cells. Mol. Endocrinol. *29*, 1522–1530.

106. Awayda, M.S., and Subramanyam, M. (1998). Regulation of the epithelial Na+ channel by membrane tension. J. Gen. Physiol. *112*, 97–111.

107. Hedgecock, E.M., Culotti, J.G., Thomson, J.N., and Perkins, L.A. (1985). Axonal guidance mutants of Caenorhabditis elegans identified by filling sensory neurons with fluorescein dyes. Dev. Biol. *111*, 158–170.

108. Morley, J.F., and Morimoto, R.I. (2004). Regulation of longevity in Caenorhabditis elegans by heat shock factor and molecular chaperones. Mol. Biol. Cell *15*, 657–664.

109. You, Y.J., Kim, J., Cobb, M., and Avery, L. (2006). Starvation activates MAP kinase through the muscarinic acetylcholine pathway in Caenorhabditis elegans pharynx. Cell Metabol. *3*, 237–245.

STAR★METHODS

KEY RESOURCES TABLE

REAGENT or RESOURCE	SOURCE	IDENTIFIER
Bacterial and virus strains		
Escherichia coli: OP50	Jonathan Ewbank lab; *Caenorhabditis* Genetics Center (CGC)	WB-STRAIN: WBStrain00041971; WormBase ID: WBStrain00041971
Escherichia coli: HB101 strain: *E. coli* [supE44 hsdS20(rB-mB-) recA13 ara-14 proA2 lacY1 galK2 rpsL20 xyl-5 mtl-1]	*Caenorhabditis* Genetics Center (CGC)	WB-STRAIN: WBStrain00041075; WormBase ID: WBStrain00041075
Escherichia coli: Ht115 (DE3): *E. coli* [F-, mcrA, mcrB, IN(rrnD-rrnE)1, rnc14::Tn10 (DE3 lysogen: lacUV5 promoter -T7 polymerase].	*Caenorhabditis* Genetics Center (CGC)	WB-STRAIN:HT115; WormBase ID: WBStrain00041079
Escherichia coli: Na22	*Caenorhabditis* Genetics Center (CGC)	WB-STRAIN: WBStrain00041948; WormBase ID: WBStrain00041948
Chemicals, peptides, and recombinant proteins		
Levamisole	Sigma-Aldrich	Product No.: PHR1798; CAS: 16595-80-5
Tetramisole hydrochloride	Sigma-Aldrich	Product No.: L9756; CAS: 16595-80-5
Paraquat (N, N′-dimethyl-4,4′-bipyridinium dichloride)	Sigma-Aldrich	Product No.: 36541; CAS: 75365-73-0
Tunicamycin from *Streptomyces sp.*	Sigma-Aldrich	Beilstein No.: 6888090;CAS: 11089-65-9
Dopamine hydrochloride	Sigma-Aldrich	Beilstein No.: 3656720; CAS: 62-31-7
UltraPure Agarose	Invitrogen	Cat.#: 16500500
Ethidium Bromide	Sigma-Aldrich	Cat.#: 1.11615.0010; CAS: 1239-45-8
Nanobeads NIST Traceable Particle Size Standard 100 nm	Polysciences	Cat.#: 64010-15
DiI (dioctadecyl tetramethylindodicarbocyanine-disulphonic acid)	Invitrogen	Cat.#: N22880
Aldicarb	Sigma-Aldrich	Product No. 33386; CAS: 116-06-3
TRIzol reagent	Invitrogen	Cat.#: 15596026
pcDNA3.1 /Puro - CAG - ASAP1 plasmid	Schnitzer et al., 2014[53]	Addgene plamid#52519; RRID:Addgene_52519
pPD95.77 (L2464)	Fire Lab *C. elegans* Vector Kit – 1995; http://n2t.net/addgene:1495	Addgene plasmid# 1495; RRID:Addgene_1495
pL4440	Fire Lab *C. elegans* Vector Kit – 1999; http://n2t.net/addgene:1654	Addgene plasmid# 1654; RRID:Addgene_1654
pPD96.52 (L2534)	Fire Lab *C. elegans* Vector Kit – 1999; http://n2t.net/addgene:1608	Addgene plasmid#1608; RRID:Addgene_1608
pPK719 (unc-119) rescue	Roger Pocock lab (BRIC, Copenhagen, Denmark); http://n2t.net/addgene:38149	Addgene, plasmid #38149; RRID:Addgene_38149
Critical commercial assays		
NucleoSpin Tissue, Mini kit for DNA from cells and tissue	Macherey-Nagel	Cat. # 740952.250
Topo TA Cloning Kit	Invitrogen	Cat.# K457501
iScript™ cDNA Synthesis Kit	Bio-Rad	Cat.#: 1708890
SuperScript™ III First-Strand Synthesis System	Invitrogen	Cat. # 18080051

(*Continued on next page*)

Continued

REAGENT or RESOURCE	SOURCE	IDENTIFIER
NEB Q5® Site-Directed Mutagenesis Kit	New England BioLabs	Cat. # E0554S
NEBuilder® HiFi DNA Assembly Master Mix	New England BioLabs	Cat. # E2621L
mMESSAGE mMACHINE™ T7 Transcription Kit	Ambion	Cat.# AM1344
Deposited data		
WormBase	International consortium for *C. elegans* and related nematodes	https://wormbase.org//#012-34-5
Blast: Basic Local Alignment Search Tool - NCBI	NIH: National Library of Medicine – National Center for Biotechnology Information	https://blast.ncbi.nlm.nih.gov/Blast.cgi
WormBook	THE ONLINE REVIEW OF *C. elegans* BIOLOGY	http://wormbook.org/
Experimental models: Organisms/strains		
C. elegans strains, see Table 1		
Xenopus laevis oocytes	EcoCyte Bioscience (Dortmund, Germany)	N/A
Oligonucleotides		
For primers, see Table 2		
Recombinant DNA		
del-2 (exons 5-12) in pL4440 (RNAi)	This paper	N/A
del-3 (exons 2-7) in pL4440 (RNAi)	This paper	N/A
del-4 (exons 1-10) in pL4440 (RNAi)	This paper	N/A
p_{del-2}DsRed transcriptional reporter in the pPD95.77 plasmid vector	This paper	N/A
p_{del-3}DsRed transcriptional reporter in the pPD95.77 plasmid vector	This paper	N/A
p_{del-4}mCherry transcriptional reporter in the pPD95.77 plasmid vector	This paper	N/A
p_{del-2}DEL-2::mCherry translational reporter in pPD95.77	This paper	N/A
p_{del-3}DEL-3::DsRed translational reporter in pPD95.77	This paper	N/A
p_{del-4}DEL-4::GFP translational reporter in pPD95.77	This paper	N/A
p_{del-4}DEL-4::DsRed translational reporter in pPD95.77	This paper	N/A
p_{del-4}SNB-1::DsRed synaptic vesicle marker in pPD95.77	This paper	N/A
p_{dat-1}ASAP-1 voltage sensor in pPD96.52	This paper	N/A
pEK230: *del-4* cDNA in the KSM vector	This paper	N/A
pEK238: *del-4(tm717)* cDNA in the KSM vector	This paper	N/A
Software and algorithms		
ImageJ 1.48V	Schneider et al.[93]	https://imagej.nih.gov/ij/index.html; RRID: SCR_003070
GraphPad Prism 8.0.2	GraphPad Software	https://www.graphpad.com/
Photoshop CS5	Adobe	https://www.adobe.com/gr_en/products/photoshop/landpb.html
Volocity High-Performance 3D imaging software	Volocity	https://www.volocity4d.com/

(*Continued on next page*)

Continued

REAGENT or RESOURCE	SOURCE	IDENTIFIER
SnapGene Viewer	SnapGene by Dotmatics	https://www.snapgene.com/snapgene-viewer
CenGen	CeNGEN - THE COMPLETE GENE EXPRESSION MAP OF THE C. ELEGANS NERVOUS SYSTEM	https://www.cengen.org/
Phobius tool	Stockholm Bioinformatics Centre; McWilliam et al.[35]	http://phobius.sbc.su.se/

RESOURCE AVAILABILITY

Lead contact

Further information and requests for resources and reagents should be directed to and will be fulfilled by the lead contact, Tavernarakis Nektarios (tavernarakis@imbb.forth.gr).

Materials availability

Plasmids and *C. elegans* lines generated in this study will be available upon request.

Data and code availability

- All data reported in this paper will be shared by the lead contact upon request.
- This paper does not report original code.
- Any additional information required to reanalyse the data reported in this paper is available from the lead contact upon request.

EXPERIMENTAL MODEL AND STUDY PARTICIPANT DETAILS

Caenorhabditis elegans

Nematodes were maintained following standard procedures, as previously described.[97] Stocks were maintained on 5cm NGM plates seeded with OP50 (KRT). Animal rearing temperature was kept at 20°C unless otherwise noted. The OP50 *E. coli* strain was preferably used as a food source except for RNAi experiments, where NGM plates were seeded with HT115 (DE3) bacteria (KRT), carrying the desired RNAi plasmid construct. HB101 *E. coli* bacteria (KRT) were used to form a thin bacterial lawn for the basal slowing response assay.

Isogenic hermaphrodite populations of the same developmental stage were used in all experiments. *C. elegans* has a lifespan of approximately 20 days at 20°C, during which it passes through four larval stages (l1-l4) before reaching adulthood. All experiments were performed during adulthood, with the only exception being the starvation survival assay that monitors animals from the l1 stage until adulthood. Imaging after heat stress and starvation was conducted on day two of adulthood. Animals grown on RNAi plates were imaged on day three or four of adulthood. Animals from the rest of the experiments were imaged on day one of adulthood. The exact day of adulthood that each experiment was performed is also reported in the figure legends.

Males emerge spontaneously in a population (frequency ~0.02 %). A larger male population was obtained following a mild heat sock (3-4 hrs at 35°C or 2s hr at 37°C) of late l4 stage animals.[98] Males were maintained through mating with hermaphrodites. In this study, males were used only for genetic crossing.

Variations *tm717* and *tm5642* were verified by polymerase chain reaction (PCR) using the primers 5′-AAAAGTGTGGACCCGGATAT-3′ and 5′-ACCAAGAGAGGAAGCAGTTCC-3′, 5′-ATGTGGCTCCGAG GACTTTTC-3′ and 5′- GCAATCAGACACCACACCCAGTA-3′ (Table 2). The strains used in this study are listed in Table 1. Strains *unc-119(ed3)*;Ex[$p_{del\text{-}2}$DEL-$2_{1\text{-}27}$::DsRed; *unc-119*(+)], *unc-119(ed3)*;Ex[$p_{del\text{-}3}$DEL-$3_{1\text{-}45}$::DsRed; *unc-119*(+)] and *unc-119(ed3)*;Ex[$p_{del\text{-}4}$DEL-$4_{1\text{-}36}$::mCherry; *unc-119*(+)] are referred in the text as $p_{del\text{-}2}$DsRed, $p_{del\text{-}3}$DsRed and $p_{del\text{-}4}$mCherry, respectively (Table 1).

Xenopus oocytes

Electrophysiology experiments were performed with *Xenopus laevis* oocytes. *Xenopus* oocytes were obtained from EcoCyte Bioscience (Dortmund, Germany) (KRT). They were maintained at 16°C in 1X ND96 solution (96 mM NaCl, 2 mM $MgCl_2$, 2 mM KCl, 1.8 mM $CaCl_2$, pH 7.4).

METHOD DETAILS

Generation of *C. elegans* transgenic lines

Genetic transformation with microinjection

For the generation of transgenic animals, plasmid DNAs were mixed, at a concentration of 50 ng/ml of the plasmid of interest with 50 ng/ml of the pRF4 plasmid bearing the dominant mutation *su1006* of the *rol-6* gene.[99] The dominant mutation *su1006* causes the roller phenotype. The DNA mixtures were microinjected into the gonads of N2 young adult hermaphrodite animals. F1 transgenic progeny were selected based on the roller phenotype to establish independent lines. Translational reporter fusion lines of *del-4* with the DsRed and ASAP1 were generated by injection. The roller phenotype of the line $p_{del\text{-}4}$DEL-4:: DsRed; *rol-6(su1006)* was used for crosses with the strains BZ555, BZ555;BR5270 and UA44.

Biolistic transformation of C. elegans

The second method used to generate transgenic animals was the gold nanoparticle bombardment (biolistic transformation). We used 10 μg of the construct bearing the desired gene and 10 μg of the pPK719 rescue plasmid DNA, carrying the coding sequence of the *unc-119* gene.[100] Transformed animals bearing the *unc-119* rescue construct exhibit wild-type locomotion. DNAs were bombarded on hermaphrodite *unc-119(ed3)* locomotion defective mutant animals of stage L4 or young adulthood, cultured on 9 cm Na22-seeded plates (KRT). The remaining constructs, apart from the two generated with microinjection, including another one translational reporter of *del-4* with DsRed, were introduced into *C. elegans* with biolistic transformation. The $p_{del\text{-}4}$DEL-4::GFP;$p_{del\text{-}4}$SNB-1::DsRed line was generated by co-bombardment of a DNA mixture containing 7 μg $p_{del\text{-}4}$DEL-4::GFP, 7 μg $p_{del\text{-}4}$SNB-1::DsRed and 7 μg *unc-119* rescue plasmid DNA.

Genetic crosses

Generation of males was achieved with a mild heat sock (3-4 hrs at 35°C or 2 hrs at 37°C) of late l4 stage animals.[98] For each mating ~6 hermaphrodites of one genotype were placed in a 3 cm OP50-seeded petri plate with ~18 males. Mating was considered successful when an increased number of male progenies was observed in the plate. Selection of transgenic lines was achieved by exploiting the roller phenotype, by using a UV stereoscope (epifluorescence microscope NIKON SMZ800N) to select fluorescent reporters or by isolating genomic DNA (NucleoSpin Tissue, Mini kit for DNA) (KRT) and performing PCR when selection of genes mutations was needed (see Table 2 for primer sequences).

The following reporters and double mutants were generated by standard genetic crosses (also Tables 1, 2 and S4): *unc-119(ed3)*;Ex[$p_{del\text{-}2}$DEL-$2_{1\text{-}27}$::DsRed; $p_{flp\text{-}8}$GFP;*unc-119*(+)], *unc-119(ed3)*;Ex[$p_{del\text{-}2}$DEL-$2_{1\text{-}27}$::DsRed; OSM-10::GFP;*unc-119*(+)], *unc-119(ed3)*;Ex[$p_{del\text{-}2}$DEL-$2_{1\text{-}27}$::DsRed; $p_{dat\text{-}1}$GFP;*unc-119*(+)], *unc-119(ed3)*;Ex[$p_{del\text{-}3}$DEL-$3_{1\text{-}45}$::DsRed; $p_{flp\text{-}8}$GFP;*unc-119*(+)], *unc-119(ed3)*;Ex[$p_{del\text{-}3}$DEL-$3_{1\text{-}45}$::DsRed; OSM-10::GFP;*unc-119*(+)], *unc-119(ed3)*;Ex[$p_{del\text{-}3}$DEL-$3_{1\text{-}45}$::DsRed; $p_{dat\text{-}1}$GFP;*unc-119*(+)], *unc-119(ed3)*;Ex[$p_{del\text{-}3}$DEL-$3_{1\text{-}45}$::DsRed;TPH-1::GFP;*unc-119*(+);*rol-6(su1006)*], *unc-119(ed3)*;Ex[$p_{del\text{-}4}$DEL-$4_{1\text{-}36}$::mCherry; $p_{flp\text{-}8}$GFP;*unc-119*(+)], *unc-119(ed3)*;Ex[$p_{del\text{-}4}$DEL-$4_{1\text{-}36}$::mCherry; OSM-10::GFP;*unc-119*(+)], *unc119(ed3)*; Ex[p_{del4}DEL$4_{1\text{-}36}$::mCherry; p_{dat1}GFP;*unc-119*(+)], *unc119(ed3)*;Ex[p_{del4}DEL$4_{1\text{-}36}$::mCherry; TPH1::GFP; *unc-119*(+);*rol-6(su1006)*], *unc-119(ed3)*;Ex[$p_{del\text{-}4}$DEL-$4_{1\text{-}36}$::mCherry; $p_{acr\text{-}2}$GFP;*unc-119*(+)], *del-4(tm717)*; zcls4[$p_{hsp\text{-}4}$GFP], *del-4(tm717);* uthls202[aak-2(intron1)::aak-2(aa1-aa321)::Tomato::unc-54 3′UTR ; *rol-6(su 1006)]*, *del-4(tm717)*;skn-1b/c::GFP, *del-4(tm717)*; $p_{asic\text{-}1}$SNB-1::SEpHluorin; *rol-6(su1006)*, *del-4(tm717)*; [*unc-119(ed3)*; oxSi834[P $_{unc\text{-}47}$GFP::SNB-::unc-54 UTR; *unc-119*(+)], *del-4(tm717)*; nuIs183 [p_{unc129}NLP-21::Venus; $p_{myo\text{-}2}$NLS::GFP], *del-4(tm717);* $p_{dat\text{-}1}$ASAP-1; *rol-6(su1006)*], *del-4(tm717)*; egIs1[$p_{dat\text{-}1}$GFP], $p_{del\text{-}4}$ DEL-4:: DsRed; egIs1 [$p_{dat\text{-}1}$GFP]; *rol-6(su1006)*, byIs161 [$p_{rab\text{-}3}$F3(delta)K280 + $p_{myo\text{-}2}$mCherry]; egIs1 [$p_{dat\text{-}1}$GFP], *del-4(tm717)*; byIs161 [$p_{rab\text{-}3}$F3(delta)K280 + $p_{myo\text{-}2}$mCherry]; egIs1 [$p_{dat\text{-}1}$GFP], $p_{del\text{-}4}$DEL-4::DsRed; *rol-6(su1006)*; byIs161 [$p_{rab\text{-}3}$F3(delta)K280 + $p_{myo\text{-}2}$mCherry]; egIs1 [$p_{dat\text{-}1}$GFP], *del-4(tm717)*; baIn11[$p_{dat\text{-}1}$::a-Synuclein; $p_{dat\text{-}1}$GFP], $p_{del\text{-}4}$DEL-4:: DsRed; *rol-6(su1006)*]; baIn11[$p_{dat\text{-}1}$a-Synuclein; $p_{dat\text{-}1}$GFP], *del-4(tm717);dop-1(vs100)*, *del-4(tm717);dop-2(vs105)*, *del-4(tm717);dop-3(vs106)*, *del-4(tm717);pkc-1(ok563)*, *del-4(tm717);pkc-2 (ok328)*, *del-4(tm717);tpa-1 (k501)*, *del-4(tm717);kin-2*

(ce179), del-4(tm717);unc-43(tm1605), del-4(tm717); $p_{hsp-16.2}$::GFP, *del-4(tm717);* dvIs19 [(pAF15) gst-4p::GFP::NLS)], *del-4(tm717);*p_{sod-3}::GFP, *del-4(tm717);* $P_{let-858}$GCaMP2.0; *rol-6(su1006).*

Molecular cloning

All genomic sequences were retrieved from WormBase (www.wormbase.org). To generate a construct for induction of *del-4* RNAi, the *del-4* gene was amplified with PCR from wt genomic DNA isolated from the N2 strain (Nucleospin Tissue kit – see KRT). Subsequently, the PCR product was inserted into the Topo vector (KRT), and subcloned in the pL4440 plasmid vector. Amplified region corresponds to exons 1-10 of the *del-4* gene. The resulting construct was transformed into the Ht115 (DE3) *E. coli* strain (KRT). Ht115 bacteria carrying the empty pL4440 vector were used as a control food in the experiments that use the RNAi technique for gene downregulation. The primers used for the amplification of *del-4* (exons 1-10) were 5′-GATGGGTGTATTTTGGACCG-3′ and 5′-TCAAGACACGATTCTCCTGA-3′ (Table 2).

Conventional cloning procedures were followed for the construction of the translational and transcriptional reporters expressed in *C. elegans*. The promoter region and the first exon of each gene were amplified from wt genomic DNA isolated from the N2 strain, for the generation of p_{del-2}DsRed, p_{del-3}DsRed, and p_{del-4}mCherry transcriptional reporters (KRT). They were inserted in the Topo vector and subcloned in the pPD95.77 plasmid vector (KRT) in frame and at the amino (N) terminus of a pre-existing DsRed or mCherry fluorescent protein. The promoter regions amplified were 1.3 Kb upstream to the start codon of *del-2*, 2 Kb of *del-3*, and 1.5 Kb of *del-4*. The primers used were 5′-TCTTATGATGCACGGCG-3′ and 5′-GGTACCCGTCCACTATTAGTAAT-3′ for del-2, 5′-GCATGCTTACATTTGAGGGTTTAG-3′ and 5′-ACCG GTGTTTTCGATTCAGTTTT-3′ for del-3, 5′-CTGCAGGTCGACACATCATAAATC-3′ and 5′-ACCGGTCC TCAACCATCGAGCATTT-3′ for *del-4* (Table 2). Excision of DNA sequences from the Topo vector was performed with HindIII/XhoI for *del-2* and *del-3*, and with EcoRI for *del-4*.

To generate the p_{del-2}DEL-2::mCherry (KRT) translational reporter construct, we amplified from wt genomic DNA the sequence from the fifth until the eleventh exon, without the stop codon. The primers used were 5′-CTGCAGGATTTCTCTGTCAAGTGG-3′ and 5′-ACCGGTCATATTGTCAGGCAAGTT-3′ (Table 2). The PCR product was inserted into the Topo vector, and an AgeI/PstI was subcloned into the pPD95.77 plasmid vector, in frame with the mCherry coding sequence. Exons two to four were then amplified using the 5′-CTGCAGAGTTGATGATGATTAAAGAA-3′ and 5′-CTGCAGTGAAAATGCTCAAACAAA-3′ primers (Table 2) and subcloned into the Topo vector. A PstI/BglI fragment was then ligated upstream to exon five in pPD95.77 carrying *del-2* (exons 5-11) in frame with mCherry. Finally, the promoter and the first exon of *del-2* were excised from the Topo vector (created previously for the generation of the *del-2* transcriptional reporter) with SphI/PvuII and ligated into pPD95.77 carrying exons 2-11. The translational reporter p_{del-3}-DEL-3::DsRed was generated by amplifying the wild-type genomic region from exon two to exon seven, just before the stop codon, using the primers 5′-ACCGGTTGTTCACGATGATCAACTATT-3′ and 5′-ACC GGTGGTGTGTCTCCTGAAGCTA-3′ (Table 2). The amplified region was inserted into the Topo vector and an AgeI fragment was inserted downstream of exon 1 into pPD95.77 carrying the *del-3* promoter region and the first exon fused with DsRed, created during the construction of the *del-3* transcriptional reporter. For the *del-4* translational reporter p_{del-4}DEL-4::GFP, the promoter and the whole coding region were isolated from genomic wild-type DNA, using the primers 5′-ACGCGTCGACACATCATAAATCTCC ACCCAC-3′ and 5′-CGGGGTACCCCATCATTAGAATGAGGCTTTGG-3′, and inserted into the Topo vector. The promoter and coding regions were isolated using SalI/KpnI and fused with GFP in the pPD95.77 plasmid vector. To create p_{del-4}DEL-4::DsRed, the promoter and coding region of *del-4* were isolated from the GFP-tagged translational reporter construct using SphI/AgeI and inserted into pPD95.77, in frame with the coding sequence of the DsRed gene.

To monitor synaptic vesicle localization, we generated the construct p_{del-4}SNB-1::DsRed (KRT). The SNB-1 coding region and *del-4* promoter were amplified, with 5′-CGG GGTACCGAATTCGGACGCTCAAGGA GATGCCGGC-3′ and 5′-CGGGGTACCGAATTCTTTTCCTCCAGCCCATAAAACG-3′, 5′-CTGCAGGTCGA CACATCATAAATC-3′ and 5′-GGATCCCATCTGCAATTTTATTTT-3′ (Table 2), and inserted into Topo vectors. A KpnI DNA fragment of *snb-1* was excised from Topo and inserted into the pPD95.77 plasmid vector in frame with the DsRed coding sequence. An SphI/KpnI fragment of the *del-4* promoter was then fused upstream to *snb-1* gene. To estimate the resting membrane potential, we generated the construct p_{dat-1} ASAP-1 (KRT). Plasmid pcDNA3.1 /Puro - CAG - ASAP1[54] (plasmid #52519) (KRT) was retrieved from Addgene. We amplified ASAP-1 from plasmid #52519 and the *dat-1* promoter from wt genomic DNA

isolated from the N2 strain, with the primers 5′-TAGCCGCCACCATGGAGAC-3′ and 5′-AGATCTTTCATTA GGTTACCACTTCAAG-3′, 5′-CTGCAGATCCATGAAATGGAACTTGA-3′ and 5′-GGATCCGGCTAAAAA TTGTTGAG-3′. The PCR products were then inserted in Topo vectors. The *myo-3* promoter of pPD96.52 was replaced with a PstI/BamHI fragment containing the *dat-1* promoter. Next, a BamHI/EcoRV fragment containing ASAP1 was inserted downstream of the *dat-1* promoter into pPD96.52.

Total RNA isolation and qRT-analysis

Total RNA extraction from synchronized day-1 or day-2 adult animals was performed using the TRIzol reagent (Invitrogen). For cDNA synthesis the iScript™ cDNA Synthesis Kit (Bio-Rad) was used. Quantitative Real-Time PCR (qRT-PCR) was performed in a Bio-Rad CFX96 Real-Time PCR system and was repeated at least three times. Expression of the housekeeping gene pmp-3 was used as an internal control for normalization. The primers used for measuring pmp-3 mRNA levels were 5′- ATGATAAATCAG CGTCCCGAC-3′ and 5′- TTGCAACGAGAGCAACTGAAC -3′.

Protein blast

Protein BLAST analysis was performed in silico using the protein BLAST tool of the NCBI website (https://blast.ncbi.nlm.nih.gov/Blast.cgi). For this analysis, we retrieved the protein sequences of DEL-2 (isoforms a and b), DEL-3, and DEL-4 from the WORMBASE (https://wormbase.org//#012-34-5).

RNAi treatment

Specific gene downregulation was achieved using the RNA interference technique (RNAi). Animals were fed bacteria expressing double-stranded (ds) RNA, which targets the gene of interest. For the basal slowing assay and for hsf-1 downregulation, animals were synchronized with bleaching solution and eggs were placed on RNAi plates. They were allowed for 2 days at 20°C to grow until the l4 stage. Four to five l4 animals were transferred on new RNAi plates and allowed for 3-4 days to lay progenies. One-day-old adult animals from the second generation grown on RNAi plates were used to measure the basal slowing response. For imaging during *del-4* downregulation, isogenic populations of animals were synchronized with bleaching. Eggs were placed on NGM plates seeded with dsRNA for *del-4* and allowed to hatch and grow until the fourth day of adulthood. Animals were transferred on new RNAi plates every second day. RNAi plates were seeded with 200 μl of O/D culture inoculated with 50 μl O/N culture/ml of the O/D and incubated for 3-4 hrs shaking at 37°C.

Microscopy

Confocal imaging

Confocal images were acquired using an LSM710 Zeiss confocal microscope (Axio-observer Z1). Image z-stacks were captured, and maximum intensity projections were obtained using ZEN 2.3 software (Carl Zeiss, Jena, Germany). Animals were immobilized on a 5% agarose (in M9 solution) pad with a drop of 10 μl Nanobeads (Nanobeads NIST Traceable Particle Size Standard 100 nm, Polysciences) (KRT). The animals used were hermaphrodites on day one of adulthood unless otherwise stated. A 40x lens was used when the images were used for estimating the neuronal pattern of DELs, whereas for the rest of the confocal images, used to estimate colocalization or neurodegeneration, a 63x lens was used.

We followed previously suggested procedures to evaluate dense core and synaptic vesicle release.[62,101] Quantitation of synaptic and dense core vesicle numbers was performed in the dorsal nerve cord, when oriented towards the objective, at the turn of the posterior gonadal arm of young adults (day 1 of adulthood). Maximum intensity projection images were obtained from the dorsal neural cord of $p_{unc-129}$NLP-21::YFP and p_{unc-47}GFP::SNB-1 expressing animals (Table 1). We cross-fertilized *del-4(tm717)* mutants with animals carrying a GFP marker of synaptic vesicles (SVs) expressed under the GABAergic motor neuron-specific, *unc-47* promoter (p_{unc-47}GFP::SNB-1). Genetic tagging of synaptic vesicle-associated proteins or neuropeptides with fluorescent proteins can be used to estimate vesicle and neuropeptide density at presynaptic sites.[102] We quantified SVs at the presynaptic elements of the dorsal nerve cord at the turn of the posterior gonadal arm. We measured the number of puncta per 10 μm and the mean puncta intensity of neurons.

Previous studies assessed the levels of DCVs released via a YFP reporter of NLP-21 neuropeptide expressed under the *unc-129* promoter (KRT).[101] Using this reporter, we determined the relative amount of

DCVs in the dorsal neural cord cholinergic motor neurons. We assessed the release of DCVs by calculating the mean intensity ratio of the axon to coelomocytes, as coelomocytes retrieve the released NLP-21::YFP.[101] We crossed the DCVs reporter strain with the *del-4(tm717)* mutant (Table 1) and performed high-magnification confocal microscopy analysis.

Maximum intensity projections were also retrieved for the posterior coelomocytes of the $p_{unc-129}$NLP-21::YFP strain. The images were analysed using the Volocity Software (Quorum Technologies). We measured the mean fluorescence intensity of cholinergic motor neuron axons from the posterior coelomocytes of NLP-21:: YFP-expressing animals. The number of fluorescent puncta/10 μm was counted and the ratio of axon to coelomocyte mean fluorescence intensity was calculated. Likewise, the mean fluorescence intensity of puncta and the number of puncta per 10 μm were computed in p_{unc-47}GFP::SNB-1 animals.

To monitor neurodegeneration, we cross-fertilized animals overexpressing DEL-4 (p_{del-4}DEL-4::GFP) and *del-4(tm717)* mutants with *C. elegans* Parkinson's and Alzheimer's disease models (Table 1). The UA44 strain was used as the model for Parkinson's disease. It expresses human α-synuclein in dopaminergic neurons, labelled with GFP to monitor degeneration (p_{dat-1}GFP;p_{dat-1}a-synuclein).[61] We assessed neurodegeneration in the Parkinson's disease model at day seven of adulthood. We used the BR5270 strain that pan-neuronally expresses the pro-aggregation F3ΔK280 tau fragment as a tauopathy model.[62] To detect dopaminergic neuronal loss, we crossed the BR5270 strain with animals carrying the p_{dat-1}GFP (BZ555) reporter (Table 1). We measured the degenerated neurons in the tauopathy model at day 5 of adulthood.

Neurodegeneration was assessed based on the morphology of the six dopaminergic neurons in the head (4 CEP and 2 ADE), on days 5 and 7 of adulthood. Estimation of dopaminergic neuron degeneration was performed as previously described.[96] Neurons were considered degenerated when they exhibited either one of the following morphological defects: neuritic blebbing, breaks in neuronal processes or dendrites, absence of neuronal processes, cell body shrinkage, reduced fluorescence or absence. If one or more of the above-mentioned phenotypes were observed, then the neuron was considered degenerated. Fifty to sixty animals were examined per biological replicate for each genotype. The number of degenerated neurons per animal is plotted in graphs for each genotype. Scoring was performed by two investigators (DP and MG) and one of them performed it blindly.

Epifluorescence microscopy

Epifluorescence microscopy was performed using a Zeiss Axio Imager Z2 or EVOS™ FV Auto2 Imaging System (Thermo Fisher Scientific). Mounting of animals on slides was achieved with a 13 μl drop of 30 mM Tetramisole (Tetramisole hydrochloride, Sigma-Aldrich) for imaging with a 5x lens or with 2% agarose pads and 15 μl of 30 mM Tetramisole for imaging with the 20x lens (KRT). Imaging after heat stress and starvation was conducted on day two of adulthood. Animals grown on RNAi plates were imaged on day three or four of adulthood. Animals from the rest of the experiments were imaged on day one of adulthood.

To assess DEL-4 expression levels, we used the DEL-4::GFP translational reporter and measured the intensity of the most brightly fluorescent neuronal cell body in the head of each animal. The HSF-1::GFP expression levels were collected from entire animals and GFP-positive nuclei in the hypodermis. We overlooked the nuclei located above the gut to avoid intestinal autofluorescence. Measurements of SKN-1b/c::GFP were collected from entire animals and ASI neurons. The DAF-16::GFP expression levels were measured from the whole animal and from intestinal cells. We measured the intensity levels of DAF-16 in the nuclei and adjacent cytoplasm of gut cells and calculated the nucleus-to-cytoplasm ratio. The intensity of neuronal cell somas in the head of p_{asic-1}SNB-1::SEpHluorin animals was counted to estimate the basal levels of synaptic release from dopaminergic neurons. Super ecliptic phluorin (SEpHluorin) (Table S1) is a pH-sensitive GFP. When genetically tagged with SNB-1, SEPhluorin is expressed inside synaptic vesicles, where the low pH quenches its fluorescence. Upon vesicle release, SEpHluorin encounters the less acidic environment of the synaptic cleft and recovers its fluorescence, allowing for estimation of synaptic vesicle release. Similarly, the fluorescence intensity from the cell bodies of cholinergic motor neurons was measured in p_{acr-2}SNB-1::SEpHluorin-expressing animals. We acquired visualizations of the ventral cord posterior and anterior to the vulva. To estimate the voltage levels using ASAP1, we counted the intensity from the cell bodies of dopaminergic neurons. Expression levels of phsp-16.2GFP, p_{sod-3}GFP, p_{skn-1}SKN-1::GFP, p_{gst-4}GFP, p_{hsp-4}GFP, $p_{let-858}$GaMP2.0, and p_{aak-2}AAK-2::Tomato were measured from the entire body and expressed as mean pixel intensity in arbitrary units (a.u.).

Imaging with the EVOS™ Imaging System was performed for p_{acr-2}SNB-1::SEpHluorin, the voltage indicator p_{dat-1}ASAP1, and p_{daf-16}DAF-16::GFP in gut nuclei, and the z-stack analysis of the imaging system was used. Analysis of epifluorescence images was performed using Image J 1.48V. For presentation purposes only, the 'straighten' function of ImageJ software was utilized for isolating and straightening animals' heads, bodies, or neuronal processes. The line width in pixels used was 300 for Figures 5D, 7A, S1A, and S6E (ASI nuclei), 400 for Figure 7C, 80 for Figures 7K and 7L, 220 for 8C, 350 for S6E (gut nuclei), and 600 for S6E (hypodermis nuclei).

Behavioural assays

Basal slowing assay

The procedure followed for the basal slowing response was previously described.[44] NGM plates were seeded with HB101 (KRT) in a ring shape, leaving the centre of the plate without food. NGM plates seeded with HB101 bacteria and non-seeded plates were incubated for 16 h (O/N) at 37°C and allowed to cool to room temperature before use. Synchronized well-fed animals on day 1 of adulthood were washed in a 20 μl drop of M9 solution (3 g KH_2PO_4, 6 g Na_2HPO_4, 5 g NaCl, 1 ml 1 M $MgSO_4$, H_2O up to 1 litre) twice. Subsequently, the animals were placed in the unseeded region at the centre of the plate with eyelash hair and allowed to recover for 5 min. The bend number of the anterior body region was counted for each active animal during 20sec. The forward and backward movements were counted. The procedure was performed in the absence or presence of bacteria. Measurements on the seeded plate were performed only for animals that moved on the bacteria. Ten to fifteen hermaphrodite animals were placed on each assay plate, and 8-15 measurements were taken. Each experiment was repeated at least 3 times. To quantify the locomotory response, we calculated for each experiment the ratio of Δ body bends/20sec. Δ body bends/20sec corresponds to the body bends/20sec of each animal on an unseeded plate minus the body bends/20sec on a plate with food.

Population drop-test assay

The population drop test was performed following the standard protocol described in the WormBook (http://wormbook.org/chapters/www_behavior/behavior.html) (KRT), with minor modifications. In brief, 30 animals of each genotype were placed on a 6 cm unseeded NGM agar plate and allowed to rest for 5 min. Drops of M13 buffer (30 mM Tris-HCl pH 7.0, 100 mM NaCl, 10 mM KCl) were delivered with a 0.5 ml syringe at the animal's tail. Glacial acetic acid was used to prepare M13 solutions with pH values of 6.6, 4.5, and 2.2. Backward movement within 4 seconds of drop delivery was considered a positive avoidance response. Each animal was tested with 2-3 drops with an inter-stimulus interval of at least 2 min. We examined well-fed hermaphrodites on day one of adulthood. The avoidance index was calculated as the number of positive responses divided by the total number of trials. An avoidance index of 1 represents complete avoidance to the M13 solution, and 0 represents a total lack of avoidance response.

DEL-4 expression and TEVC on Xenopus oocytes

cDNA generation

C. elegans cDNA was obtained from N2 wild-type and purified using the Invitrogen™ SuperScript™ III First-Strand Synthesis System (KRT). The cDNA inserts were subcloned into the KSM vector under the control of the T7 promoter containing the 3′ and 5′ untranslated regions (UTRs) of the Xenopus beta-globin gene and the poly(A) tail.

Primer generation

The forward primer 5′-AGATCTGGTTACCACTAAACCAGCC-3′ and reverse primer 5′-TGCAGGAATTC GATATCAAGCTTATCGATACC-3′ were used to amplify the KSM vector. Based on the sequence on wormbase.org, the forward primer 5′-CTTGATATCGAATTCCTGCAATGGGTGTATTTTGGACCGGC-3′ and the reverse primer 5′-GTTTAGTGGTAACCAGATCTTCAATCATTAGAATGAGGCTTTGGTGGAAC-3′ were used for amplification of the *del-4* cDNA (based on the sequence in wormbase.org). To generate *del-4(tm717)* deletions, we used the NEB Q5® Site-Directed Mutagenesis Kit (KRT). Plasmids generated were pEK230 (*del-4* cDNA in the KSM vector[51] and pEK238 (*del-4(tm717)* cDNA in the KSM vector). The NEBuilder HiFi DNA Assembly Reaction Protocol was used to assemble the KSM vector and cDNA inserts using NEBuilder® HiFi DNA Assembly Master Mix (KRT) and a vector:insert ratio of 1:2.

mRNA synthesis and microinjection

The linear plasmid was used as the template for *in vitro* RNA synthesis from the T7 promoter using the mMessage T7 kit (Ambion #AM1344) (KRT) to produce 5′-capped RNA (KRT). Oocytes were injected with 25 nl of RNA solution at a total concentration of approximately 500 ng/μl using the Roboinject (MultiChannel Systems). Oocytes were kept at 16°C in 1X ND96 prior to TEVC.

Two-electrode voltage clamp (TEVC)

TVEC was performed 1-2 days post-injection at room temperature using the Robocyte2 (MultiChannel Systems) as previously described.[51,103] *Xenopus* oocytes were clamped at −60 mV using ready-to-use Measuring Heads from MultiChannel Systems filled with 3M KCl. All channels were tested using the Robocyte2 (MultiChannel Systems). Since millimolar concentrations of Ca^{2+} and other divalent ions except Mg^{2+} can block ASIC currents,[104] Ca^{2+}-free buffers were used for substitution experiments of monovalent cations adapted from a previous protocol[105]: 96 mM XCl, 1 mM $MgCl_2$, 5 mM HEPES, pH adjusted to 7.4 with XOH, where X was Na^+, K^+ or Li^+, respectively. To test ion permeability for Ca^{2+}, a previous protocol was used,[72] replacing Na^+ with equimolar Ca^{2+}. If necessary, D-Glucose was used to adjust the osmolarity. Osmolarity was checked and confirmed to be within an error of 210 m.[106] To test pH sensitivity, 1X ND96 solution was used; for solutions with a pH of 5 or lower, MES was used instead of HEPES and adjusted with HCl. I-V relationships for ion selectivity and proton conductance were calculated by subtracting the background leak current in the presence of 500 μM amiloride from the current observed in the absence of amiloride to get the actual current. Actual current I-V curves for each oocyte were fitted to a linear regression line, and the x-intercept was compared between solutions to calculate an average reversal potential (E_{rev}). The reversal potential shift (ΔE_{rev}) was calculated for each oocyte, when shifting between pH solutions or from a NaCl to a KCl, LiCl or $CaCl_2$ solution. To test the responses to pH, channel-expressing *Xenopus* oocytes were perfused with 1X ND96 (using HEPES for buffering pH above 5.5, and MES for pH below 5). The pH was adjusted with HCl and ranged from pH 7.4 (neutral pH of the ND96 solution) to pH 3.8 or pH 4. Background currents measured at pH 7.4 were subtracted from those measured during activation of the channels. For analysis, currents were normalized to maximal currents (I/I_{max}) and best fitted using the Hill's equation (variable slope).

DiI staining

To identify the DEL-4 subcellular localization, we labelled amphid and phasmid neurons with the lipophilic carbocyanine tracer DiI (dioctadecyl tetramethylindodicarbocyanine-disulphonic acid, Invitrogen) (KRT), prepared as described earlier.[107] DiI stains the membranes of amphids, phasmids, and chemosensory neurons with nerve endings exposed to the environment. In brief, one-day-old adult hermaphrodite animals were washed twice with 200 μl M9 free of bacteria and incubated in 200 μl 10 μg/ml DiI diluted in M9. Animals were rotated in a 200 μl tube with DiI for 2-3 hours, washed twice with M9, and then allowed to recover and de-stain for an hour on an OP50-seeded NGM plate before imaging.

Stress assays

Heat stress (HS)

To assess DEL-4 expression levels under the implementation of heat stress, 1-day adult animals expressing DEL-4::GFP were treated for 2 hrs at 37°C. Animals were allowed to recover O/N at 20°C on NGM plates seeded with OP50 and then imaged on day 2 of adulthood. To assess the effect of heat stress on the voltage of dopaminergic neurons, which was measured with ASAP1, 2-day adult hermaphrodite animals were stressed for one hour at 37°C on OP50-seeded plates and then imaged immediately.

Long term starvation (LTSt)

For the starvation assay, one-day-old adult hermaphrodite animals were placed with a platinum pick on unseeded NGM plates. They were allowed to starve for 24 hrs and then imaged on day two of adulthood.

Oxidative stress (OS)

To induce oxidative stress paraquat (N, N′-dimethyl-4,4′-bipyridinium dichloride, Sigma-Aldrich) (KRT) was added on top of OP50-seeded NGM. Paraquat was added to a final concentration of 8 mM diluted in water. Water was placed on the control plates. Plates were allowed to absorb the drug and animals at the L4 stage were placed in plates. Animals were stressed O/N and then imaged on day one of adulthood.

ER stress (ERS)

To induce ER stress tunicamycin (Sigma-Aldrich) (KRT) was plated on OP50-seeded NGM. Tunicamycin was added to a final concentration of 2.5 μg/ml in M9. M9 was placed on control plates. Plates were allowed to absorb the drug or M9 and animals at the L4 stage were placed in the assay plates. Animals were stressed O/N and then imaged on day one of adulthood.

Acidic stress (AS)

To elicit low-pH stress, we used an M13 solution adjusted with CH3COOH at the appropriate pH. Before treatment, one washing step was performed in a 20 μl drop of M13 pH 6.6. For the measurement of DEL-4 expression levels upon acidic stress, one-day adults were incubated for 1 hr within a 20 μl M13 drop of pH 6.6 (control) or pH 3.5 (at low pH stress). To estimate the ASAP1 levels after acidic stress, 2-day adult animals were incubated for 15 min in a 20 μl M13 drop of pH 6.6 (control) or pH 4.5 (low pH stress). After treatment, the animals were incubated in a 20 μl drop of M13 solution pH 6.6 to recover GFP fluorescence that quenches due to the pH sensitivity of GFP.

Survival assays

Survival assay after heat shock

For thermotolerance evaluation, 1-day adult animals were placed on OP50-seeded NGM plates and exposed to 37°C for 2.5 hours. Animals were allowed to recover overnight at 20°C, and on the following day, death events were monitored per day. Animals were scored as dead when they failed to respond to prodding with the platinum wire. Animals were transferred to new plates once every two days to avoid mixing with the progeny.[108]

Starvation survival assay

To analyse survival during starvation, we followed the procedure described previously[109], with a few modifications. After synchronization with the bleaching solution, ~3.500 eggs were incubated in 1.5 ml BSA-coated tubes filled with sterile M9 solution on a rotating carousel (Stuart Scientific SB1 Blood Test Tube Rotator) at 20°C. Twenty-four hours after egg preparation and every second or third day, 20 μl was collected from each tube, plated on OP50-seeded NGM and allowed to grow at 20°C for three days. Three samples (20 μl) were collected from each strain, and the average was calculated. We then counted the animals that reached L4 stage or young adulthood. Day 1 was considered the day after egg preparation and was used as a control and denominator to calculate the percentage of animals that recovered.

Pharmacological assays

Acute aldicarb resistance assay

Aldicarb is a cholinesterase inhibitor that causes paralysis due to acetylcholine (ACh) accumulation at the synaptic cleft. We used aldicarb (100 mM stock in 70% ethanol; Sigma-Aldrich) (KRT), as proposed by Mahoney et al.[46] Animals were collected and washed twice in M9. We differentiated the procedure by placing one-day adult animals in a 15 μl drop of 10 mM aldicarb in M9 instead of using NGM plates with aldicarb. The animals were monitored to identify the moment at which they stopped moving. Seven animals were used per condition in each experiment, with a total of six biological replicates.

Levamisole resistance assay

Levamisole is a nicotinic receptor agonist that paralyzes animals through continuous muscle stimulation. For the levamisole assay, we used 400 μM concentration in M9. Animals were collected with M9 and washed twice. Subsequently, they were placed in a 20 μl drop of 400 μM levamisole (KRT). Locomotion was evaluated by the number of animals not moving in the levamisole drop reported every 5 min until all animals were paralyzed.

Dopamine resistance assay

To monitor dopamine-induced paralysis, 30-40 animals of the selected genotypes and at day one of adulthood were collected with M9 and washed twice. Subsequently, we placed the animals in a 20 μl drop of 40 mM dopamine (Dopamine hydrochloride, Sigma-Aldrich) (KRT), diluted with M9. The number of moving animals was recorded every 5 min of exposure and until all animals were paralyzed. We always used freshly prepared dopamine to avoid oxidization.

QUANTIFICATION AND STATISTICAL ANALYSIS

Sample sizes were not predetermined using statistical methods. Statistical analysis and graphical illustrations were performed using Prism software package (GraphPad Software Inc., San Diego, CA, USA). The results are presented as XY graphs, with error bars representing the standard error of the mean (SEM). Two-way analysis of variance (TWO-WAY ANOVA) was performed for most of the experiments to compare the mean values and evaluate statistical significance. TWO-WAY ANOVA is selected where the mean values of independent biological replicates with pre-calculated SEM are represented in the graph. In the other cases One-way ANOVA is used. The post-hoc analysis to correct for multiple comparisons was performed using the Tukey's multiple comparisons test or the ordinary Two-way ANOVA test for the TWO-WAY ANOVA analysis, while the one-way Tukey's test was used in the One-way ANOVA. For survival analysis the Log-rank (Mantel-Cox) test was used to evaluate statistical significance. All experiments were repeated at least thrice. The number of biological replicates, the sample sizes, the specific type of ANOVA and any further statistical information related to each graph can be found in the Figure legends. The P-values in the graphs are indicated with the following symbols: ns $p=0.1234$, *$p=0.0332$, **$p=0.0021$, ***$p=0.0002$, ****$p<0.0001$.

STAR ✦ Protocols

CellPress

Assessing locomotory rate in response to food for the identification of neuronal and muscular defects in *C. elegans*

Dionysia Petratou[1,2,4], Persefoni Fragkiadaki[3], Eirini Lionaki[1] and Nektarios Tavernarakis[1,2,5,*]

[1]Institute of Molecular Biology and Biotechnology, Foundation for Research and Technology, Heraklion, Crete, GR-70013, Greece

[2]Department of Basic Sciences, Medical School, University of Crete, Heraklion, Crete, GR-71003, Greece

[3]Department of Toxicology, Medical School, University of Crete, Heraklion, Crete, GR-71003, Greece

[4]Technical contact: dipetratou@imbb.forth.gr

[5]Lead contact

*Correspondence: tavernarakis@imbb.forth.gr

Summary

C. elegans is a bacteria-eating soil-dwelling nematode. Typical cultivation of laboratory-reared populations occurs on bacteria-covered solid media, where they move along with sinusoidal undulations. Nematodes decelerate when they encounter food. Dopaminergic and serotonergic neurotransmission regulate this behavior. Here, we describe the procedure for determining food-dependent locomotion rate of fed and fasting nematodes. We detail steps for assay plate preparation, *C. elegans* synchronization, and assessment of locomotion. The behaviors we describe provide information regarding the animal's physiological neuronal and muscular function.

For complete details on the use and execution of this protocol, please refer to Petratou et al.[1] and, Sawin et al.[2].

Graphical abstract

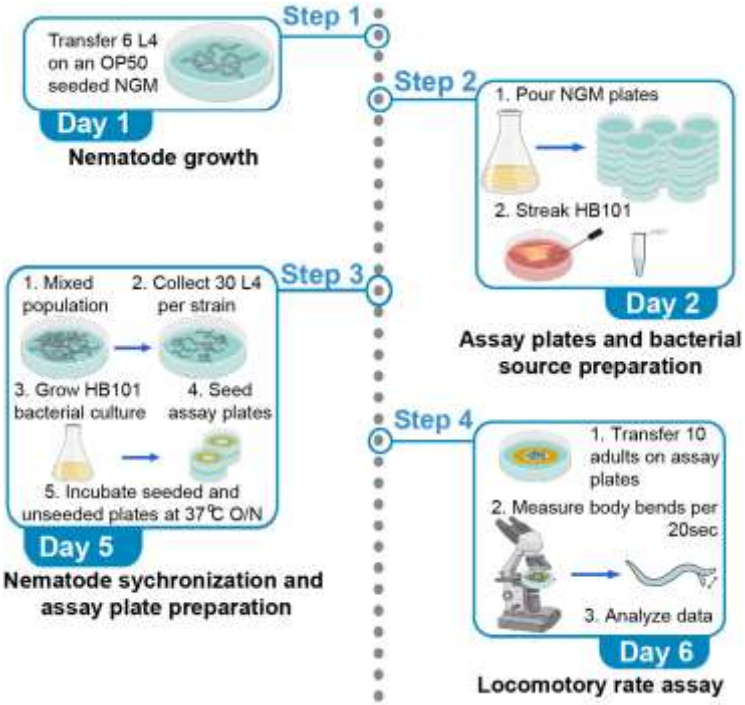

Highlights

- *C. elegans* locomotory rate offers information on neuronal and muscle functionality.
- Locomotory rate assays estimating animal movement in body bends per twenty seconds.
- Protocols for measuring the basal and enhanced slowing responses.
- Quantitative analysis of behavioral results.

Before you begin

C. elegans exhibits a well-defined locomotion pattern of sinusoidal undulations[3,4] when crawling on a solid surface or swimming in a liquid medium. Discrepancies in locomotion wavelength, amplitude, and frequency are symptomatic of abnormalities in certain types of neuronal or muscle cells. In this protocol, we quantitate the locomotory rate of worms as the number of body bends per time unit (twenty seconds). These assays have been previously developed and used in numerous publications[1,2,5-7]. Food presence decelerates the animal and therefore it reduces the number of body bends per time unit, a behavior referred to as basal slowing response (BSR). The dopaminergic system regulates basal slowing response, therefore changes in BSR provide information on dopaminergic neurotransmission. Fasting for 30 minutes before the experiment induces a pronounced deceleration known as enhanced slowing response (ESR). The serotonergic neurotransmission[2] regulates ESR. Finally, measurements acquired exclusively from seeded plates, provide information on neuronal and muscle functionality and may be utilized for screening tests[5]. In this protocol, we outline the three alternative experimental procedures mentioned above and provide an experimental example employing wild-type Bristol N2 animals and the mutant strains *dop-3(vs106)* and *tph-1(mg280)* as control strains defective in dopaminergic and serotonergic signaling, respectively. Employment of more strains proportionally increases preparation time for each step.

Institutional permissions

Experimentation with the nematode *C. elegans* does not require Institutional Animal Care and Use Committee (IACUC) permission.

C. elegans strains maintenance and synchronization

Timing: 5 days

We follow standard nematode maintenance procedures[8]. Maintain animals on OP50-seeded plates (6cm) at 20°C.

1. Place 6 hermaphrodites at the L4 stage on an OP50-seeded plate with a flame-sterilized worm picker, consisting of a platinum wire flattened at the tip and attached on a glass Pasteur pipette. Allow the hermaphrodites to grow and lay eggs for four days. Prepare 1 plate for each strain and incubate them at 20°C **(Troubleshooting 1)**.
2. On day four, use the worm picker to select L4 stage animals from the mixed population. Transfer ~40 L4 stage hermaphrodite animals from each strain on a new OP50-seeded NGM plate to obtain synchronous animals for the assay. The L4 larvae will develop into Day 1 adults within ~18hrs at 20°C, and at this age they will be used in the locomotion assay.

CRITICAL: Avoid using starved animals since starvation affects the locomotory rate.

Alternatives: Another way to obtain Day one adult animals would be, at step one, to allow ~10 adult hermaphrodite animals to lay eggs on OP50-seeded plates for ~6hrs and then remove them with the worm picker. The adults should be on days 1-4 of adulthood, during which period they lay most of their eggs. Incubate them at 20°C for three days until they reach day 1 of adulthood. Another technique for nematode synchronization is bleaching, which is also used for stock decontamination. In this case, a 5% sodium hypochlorite solution (bleaching solution) is used to dissolve the nematode bodies but not their eggshell-protected eggs. For this procedure, apply 2ml M9 on a plate with mixed population of the desired genotype. Collect approximately 1.5ml M9 with floating animals from the plate into a sterile 1.5ml tube. Allow the animals to sink with gravity and remove the supernatant. Add 1.3ml M9, allow the animals to sink with gravity, or spin them down with a microcentrifuge and remove the supernatant to remove bacteria and wash the animals. Repeat twice the washing step. After the second wash, remove the M9 and add 1.3ml bleaching solution. Vortex for 6min for all the animals to dissolve and the eggs to remain. Avoid incubating with bleaching solution for more than 6min because it reduces the embryo's viability. After bleaching, centrifuge the eggs for 30sec at full speed (15.000g), remove the supernatant, and wash with 1.3ml M9. Repeat washing twice more by increasing the centrifugation time by 30sec each time. Dissolve the eggs in 20-50µl M9 and spread them on an OP50-seeded NGM plate. Incubate them at 20°C for three days to reach day one of adulthood [8,9]Using this alternative a big number of animals is obtained and in some cases eggs should be divided to two NGM to avoid starvation.

Preparation of Nematode Growth Medium (NGM) plates

Timing: 2.5hrs

This step describes how to prepare NGM plates for nematode maintenance and assay plates, following the standard procedure previously reported[8,10,11].

3. In a 1L Erlenmeyer flask, weigh 3g NaCl, 2.5g bacto-peptone, 0.2g streptomycin, and 17g agar.
4. Fill the flask with 500mL distilled water, add a magnetic stir bar, and cover its mouth with aluminum foil.

Note: Before autoclaving add only 500ml of water, to avoid overflow of the medium. Afterwards, add sterilized water, as indicated in step 7, up to 1 ml.

5. Autoclave for 30 minutes (min).
6. Allow to cool at 55°C while stirring.

CRITICAL: Cool the medium using a water bath (~10min) or simply air-cooling (~50min) to 60°C so that you can touch the flask for a while without feeling any discomfort.

7. Aseptically add 1ml $MgSO_4$ (1M stock solution), 1ml $CaCl_2$ (1M stock solution), 1ml cholesterol (5mg/ml stock solution), 1ml nystatin (10mg/ml stock solution), 25ml KPO_4 pH 6 (1M stock solution), and sterilized distilled water up to 1L. Mix well by stirring.
8. Dispense the medium into 6cm petri plates with a peristaltic pump. Pour 7ml of the medium per plate.
9. Allow it to solidify ~12hrs at ~22°C and store at 4°C for up to one month.

CRITICAL: Store NGM plates upside down to avoid moisture condensation on the lid. Avoid storing NGM for longer because evaporation raises salt concentration. The salt concentration is vital for the animal's physiology and influences a variety of behavioral responses. Use the same batch of NGM plates for each experimental set. Follow sterile procedures while preparing NGM to avoid contamination.

Seeding of plates for nematode maintenance

Timing: 2-3 days

The following steps describe the preparation of OP50 bacterial culture, utilized as a food source for *C. elegans* maintenance.

10. Streak OP50 bacteria on a 9cm LB plate with a sterile pipette tip and incubate at 37°C for ~12hrs.
11. Pick a single colony with a sterile tip and inoculate 50ml LB. Allow the bacteria to grow by shaking, at 37°C for ~6 hours (hrs), until OP50 OD_{600} = $3x10^8$ – $1x10^9$cfu/ml (OD_{600} 0.9-1.8).
12. Apply 200µl of OP50 at the center of a 6cm petri plate. Spread the culture in a circle using the bottom of a fat vial, but not too close to the plate's edges.

CRITICAL: Avoid growing the bacterial lawn too close to the plate's walls, or the nematodes will crawl out of the medium and dry on the plate wall.

13. Allow the bacterial lawn to grow for ~12hrs at 25°C.

CRITICAL: Maintain aseptic conditions throughout the preparation with a flame.

Note: OP50 is an easily growing bacterial culture. Incubation of 200 µl OP50 on an NGM at 22°C for ~12hrs gives nice bacterial lawns for a wide range of OD_{600} of the liquid culture.

Seeding of assay plates

Timing: 2-3 days

The steps below demonstrate how to prepare an HB101 bacterial culture and seed NGM plates for monitoring the locomotory rate (Troubleshooting 2).

14. Streak HB101 bacteria on a 9cm LB plate and incubate it at 37°C for ~12hrs.
15. Pick a single colony with a sterile pipette tip and inoculate it in 50ml liquid LB, shaking, at 37°C for ~7hrs, until HB101 OD_{600} = $4x10^8$ – $6x10^8$ cfu/ml (OD_{600} 1.3-1.6).
16. On a paper sheet, draw a ring with an inner diameter of ~1cm and an outer of ~3.5cm. Use it as a guide to draw the ring with a marker at the bottom of the assay plates (Figure 1).
17. Spread 100µl HB101 with the bottom of a glass test tube in a ring-shaped manner, leaving the center free of bacteria.

    CRITICAL: Generate bacterial lawns of similar thickness for all biological replicates, as the thickness of the lawn impacts *C. elegans* locomotory rate. Create thin bacterial lawns to limit deceleration due to mechanical hindrance at its thick peripheral area (Figure 2).

18. Prepare one plate for each strain and incubate them 15-17hrs at 37°C along with the same number of unseeded NGM plates, all from the same batch.

CRITICAL: Always seed the assay plates the day before the assay.

Note: HB101 liquid bacterial culture when spread on an NGM plate does not grow easily to a bacterial lawn, compared to OP50, and requires an increased OD_{600} and incubation ~12hrs at 37°C in order to grow a thinner bacterial lawn.

Key resources table

REAGENT or RESOURCE	SOURCE	IDENTIFIER
Bacterial and virus strains		
Escherichia coli: OP50 strain	Jonathan Ewbank lab; *Caenorhabditis* Genetics Center (CGC)	WB-STRAIN: WBStrain00041971; WormBase ID: WBStrain00041971
Escherichia coli: HB101 strain: *E. coli* [supE44 hsdS20(rB-mB-) recA13 ara-14 proA2 lacY1 galK2 rpsL20 xyl-5 mtl-1]	*Caenorhabditis* Genetics Center (CGC)	WB-STRAIN: WBStrain00041075; WormBase ID: WBStrain00041075
Chemicals, peptides, and recombinant proteins		
Agar	Sigma-Aldrich	Cat# 05040

Bacto-peptone	BD, Bacto TM	Cat# 211677
Sodium chloride (NaCl)	EMD Millipore	Cat# 106404
Magnesium sulfate ($MgSO_4$)	Sigma-Aldrich	Cat# M7506
Cholesterol	SERVA Electrophoresis	Cat# 17101.01
Calcium chloride dehydrate ($CaCl_2$ * 2 H_2O)	Sigma-Aldrich	Cat# C5090
di-Potassium hydrogen phosphate (K_2HPO_4)	EMD Millipore	Cat# 137010
Potassium dihydrogen phosphate (KH_2PO_4)	EMD Millipore	Cat# 104873
di-Sodium hydrogen phosphate (Na_2HPO_4)	EMD Millipore	Cat# 106586
Streptomycin	Sigma-Aldrich	Cat# S6501
Nystatin	Sigma-Aldrich	Cat# N3503
Yeast extract	Sigma-Aldrich	Cat# Y0875
Tryptone	Sigma-Aldrich	Cat# T7293
Sodium hydroxide (NaOH)	Sigma-Aldrich	Cat# 106498
Sodium hypochlorite (NaOCl)	Sigma-Aldrich	Cat# 1056142500
Ethanol absolute	VWR BDH Chemicals	CAS# 64-17-5
Experimental models: Organisms/strains		
C. elegans: Strain wild type (N2) Bristol isolate	*Caenorhabditis* Genetics Center	WormBase ID: WBStrain00000001
C. elegans: Strain LX703: *dop-3(vs106)*	*Caenorhabditis* Genetics Center	WormBase ID: WBStrain00026374
C. elegans: Strain MT15434: *tph-1(mg280)*	*Caenorhabditis* Genetics Center	WormBase ID: WBstrain00027519
Software and algorithms		
GraphPad Prism 8.0.2	GraphPad Software Inc., San Diego, USA	https://www.graphpad.com/
Microsoft Excel	Microsoft	https://www.microsoft.com/
Other		
Incubators for stable temperature (20°C & 37°C)	BIOBASE	BJPX – B80II
Shaking incubator with stable temperature (37°C)	Sigma-Aldrich	Eppendorf New Brunswick™, Excella ® 24 Inc Shaker, EPM1352-0014
Dissecting stereomicroscope	Nikon	SZM745
Petri dishes (60 *15 mm)	Sigma-Aldrich	Cat# P5237
Petri dishes (92 *16 mm)	Fisher Scientific	Cat# NC9565080
Peristaltic pump	Wheaton Science Products	WHE-374302
1.5ml microcentrifuge tubes	Sigma-Aldrich	Cat# Z606340

Materials and equipment

NGM medium

Reagent	**Final concentration**	**Amount**
NaCl	50mM	3g
Bacto-peptone	2.5mg/ml	2.5g
Streptomycin	0.2mg/ml	0.2g

Agar	17mg/ml	17g
$MgSO_4$	1mM	1ml
$CaCl_2$	1mM	1ml
Cholesterol	5mg/ml	1ml
Nystatin	10mg/ml	1ml
KPO_4	25mM	25ml
ddH_2O	-	Up to 1L
Total	**-**	**1L**

Note: Mix NaCl, bacto-peptone, streptomycin, and agar in 400-500ml ddH_2O and autoclave. Cool to 55-60°C and add sterilized $MgSO_4$ (stock solution 1M), sterilized $CaCl_2$ (stock solution 1M), cholesterol (stock solution 5mg/ml), nystatin (stock solution 10mg/ml), sterilized KPO_4 (stock solution 1M) and sterilized ddH_2O up to 1L. While still hot pour 7ml per 6cm petri plate using a sterilized peristaltic pump.

M9 buffer

Reagent	**Final concentration**	**Amount**
KH_2PO_4	3mg/ml	3g
Na_2HPO_4	6mg/ml	6g
NaCl	5mg/ml	5g
$MgSO_4$	1mM	1ml
ddH_2O	-	Up to 1L
Total	-	**1L**

Note: Mix all reagents (apart from $MgSO_4$), add ddH_2O up to 1L, and autoclave. Then, add $MgSO_4$. Store at 4°C for up to 2 months.

1 M KPO_4 buffer

Reagent	**Final concentration**	**Amount**
K_2HPO_4	0.32M	57.6g
KH_2PO_4	0.75M	102.2g
ddH_2O	-	1L
Total	**-**	**1L**

Note: Autoclave and store at 22˚C for up to 2 months.

- **1M $MgSO_4$ stock solution*:*** add 24.65g $MgSO_4$(*7 H_2O) and ddH_2O up to 100ml.
  Note: Autoclave and store at 22°C for up to 2 months.
- **1M $CaCl_2$ stock solution:** add 14.7g $CaCl_2$ (*2H_2O) and ddH_2O up to 100ml.
  Note: Autoclave and store at 22°C for up to 2 months.
- **10mg/ml Nystatin stock solution:** add 0.5g Nystatin in 50ml 70% Ethanol.
  Note: Store at 4°C for up to 2 months.
- **5mg/ml Cholesterol stock solution:** add 1g cholesterol in 200ml 100% Ethanol.
  Note: Stir ~12hrs to dissolve. Store at 4°C for up to 5 months.

Bleaching solution

Reagent	**Final concentration**	**Amount**
NaOH (5N)	0.5N	1ml
5% sodium hypochlorite (NaOCl) solution	1%	2ml

ddH_2O	-	7ml
Total	**-**	**10ml**

Note: Always prepare fresh bleaching solution.

LB liquid medium

Reagent	**Final concentration**	**Amount**
NaCl	5mg/ml	5g
Yeast extract	5mg/ml	5g
Tryptone	10mg/ml	10g
ddH_2O	n/a	Up to 1L
Total	**n/a**	**1L**

Note: Autoclave, dispense in 50 ml per 250 ml flask, and store at 22°C for up to 3 weeks.

LB agar plates: Prepare the recipe as in LB liquid.

- Add 15g agar to a final concentration of 15mg/ml.
- Autoclave and air-cool to 55°C – 60°C.
- Pour 17ml medium per 9cm petri plate with a sterilized peristaltic pump.

Note: Store at 4°C for up to one month.

Step-by-step method details

Preparation of materials and animals on the day of the assay

Timing: 40min

This section describes how to prepare assay plates and the nematode strains before the experiment.

1. Remove the assay plates from the 37°C and incubate them at 22°C for at least 30min.

Note: To obtain uniform cooling of all dishes to 22°C, place them on the bench in a single layer and side by side.

CRITICAL: Temperature affects the animal's locomotion. Use plates cooled at 22°C at all times.

2. Label the plates with the designated genotype. Each genotype requires one HB101-seeded and one unseeded NGM plate.
3. Place three 20µl M9 solution droplets on a petri plate lid.
4. With a hair-pick (eyelash glued on a toothpick), collect 15 one-day adult animals in the first droplet of M9 and allow them to wash for 30sec.
5. Transfer the animals in the second droplet with the hair-pick and let them settle for 30sec.
6. Then transfer them to the third droplet with the hair-pick and wash them for ~30sec until they are bacteria-free.

CRITICAL: Wash the nematodes thoroughly to remove all bacteria, as they constitute mechanical and gustatory stimuli for *C. elegans* and affect its locomotory rate (Figure 3).

Note: Use the hair-pick preferably for transferring a small number of nematodes to or from liquid drops, because its thinner, easier to handle and transfers less bacteria with worms than the platinum worm-picker.

Locomotion assay I: Basal slowing response

Timing: 1.5hrs

The locomotion rate of ten to fifteen animals, expressed as body bends per twenty sec, is measured on HB101 seeded and unseeded NGM plate.

7. Transfer the animals with the hair-pick to the unseeded region at the center of the assay plate (Figure 3).
    a. Start with either the unseeded or the HB101-seeded NGM.
8. Cover the plate with its lid and place it under the stereomicroscope for 3min to allow the nematodes to recover and adjust.

Optional: If required, wipe out the moisture from the lid before proceeding.

Alternatives: Instead of manually transferring nematodes in M9 drops, collect the animals with M9 using a P1000 in a 1.5ml tube. Allow the animals to settle for ~1min, remove supernatant, and apply 1ml clean M9. Repeat this washing step twice and then transfer the worms to the center of the assay plate in ~20-50µl M9. Remove the excess M9 from the assay plate with a Kimwipe and let the animals recover for 5min instead of 3min. In this case, a larger number of animals should be used initially as several of them will be lost during washing steps. Utilizing M9 drops enables the use of fewer animals because they all recover in good shape and none is lost or injured as during pipetting. Furthermore, it takes less time for washing but requires experience in handling the hair-pick.

9. Set a timer for 20 seconds, monitor the nematodes, and count and record how many times the head of each animal changes direction (body bends) during that period. Measure the body bends per 20sec for 10 animals (Troubleshooting 3 and 4).

CRITICAL: Avoid tapping the plate and keep the lid on during step 9. Mechanical stimuli such as plate tapping or airflow may affect nematodes' motility.

10. Repeat steps 3-9 for the second assay plate (either the seeded or the unseeded).
11. Repeat for each strain with a seeded and an unseeded NGM. The timing indicated applies to two strains. Time increases by 20-30min for every additional strain.

CRITICAL: Take measurements from different animals and avoid counting the same nematode repeatedly (Troubleshooting 3). Record 10-15 measurements from the seeded (Troubleshooting 4)

and 10-15 measurements from the unseeded plate. Try to preserve the same number of measurements for each strain, as this will facilitate your statistical analysis.
A bend is considered complete when the whole head area, starting from directly behind the pharynx, moves to the opposite direction. Advance one count every time the animal makes a complete bend in the opposite direction (Figure 4). Measure bends during both forward and backward locomotion. When assessing the HB101-seeded plate, do not count animals that dawdles in the thick edge of the bacterial lawn or crawls off food.

Note: Perform the locomotion assay at 20-23°C. However, in the case of increased day-to-day temperature fluctuations prefer a 20°C consistent room temperature, to promote reproducibility.

Locomotion assay II: Enhanced slowing response

Timing: 2hrs

The locomotion rate of ten to fifteen animals, expressed as body bends per twenty seconds, is measured on HB101 seeded and unseeded NGM plates after 30min starvation.

Repeat the same steps as in Locomotion Assay I (Basal slowing response) but with the following modifications:

12. In step 1 (in step-by-step method details), equilibrate at 22°C one more unseeded NGM for each strain.

Note: Equilibration of the unseeded NGM to 22°C is necessary if the NGM plate was not prepared the previous day and was therefore stored at 4°C.

13. In step 2 (in step-by-step method details), label this plate “starvation plate”.
14. After step 6 (in step-by-step method details), transfer the animals with the hair-pick to the “starvation plate” and let them starve for 30min (Troubleshooting 5).
15. Proceed with step 7 (in step-by-step method details).

Locomotion assay III: Locomotion rate on a seeded plate

Timing: 2hrs

The locomotion rate of ten to fifteen animals, expressed as body bends per twenty seconds, is measured on HB101-seeded NGM plates.

Repeat the protocol as in Assay I only for the HB101-seeded plate.

Alternatives: In this assay, the OP50 bacterial strain may replace the HB101. However, a thin bacterial lawn remains a prerequisite. Additionally, in step 9, body bends can be recorded for 9min instead of 20sec. The 9min of counting are separated into 3 blocks of 3min each, with 30min intervals between them. In this case, divide by 9 the number of body bends counted per animal for the 9 minutes to

calculate body bends per minute per animal. Determine the mean body bends per min for each strain by averaging the body bends per min for all 10 nematodes measured for each strain. Calculate the standard deviation for the 10 measurements.

Expected outcomes

In a successful BSR (assay I), we expect wild-type animals to produce 13-17 body bends per 20sec on the seeded plate (same for assay III), and 18-24 body bends per 20 seconds on the unseeded plate. In the ESR (assay II), the bends on the unseeded plate remain the same, but they decrease to 3-6 bends on the seeded one.

We demonstrate an experimental example of the basal and the enhanced slowing response assays (figure 5). The dopaminergic pathway mediates the BSR, whereas the ESR requires the serotonergic pathway. Therefore, we use the *dop-3(vs106)* strain, which is deficient in the D2-like dopamine receptor DOP-3, as control for BSR (Figure 5A and B). In the ESR, we utilize the strain *tph-1(mg280)* as a negative control, which is a mutant for tryptophan hydroxylase, an enzyme required for serotonin biosynthesis (Figure 5C and D). We used the Bristol N2 strain was as wild type. In both cases, the mutant strains demonstrate defective responses compared to control animals. In the BSR wild type animals display a Δ body bends/20sec ($\Delta bbs)^{20}$ slowing index (see "Quantification and statistical analysis" section) of 5.975 ± 0.5315 (SD), while *dop-3(vs106)* mutants have a slowing index of 2 ± 0.483 (Figure 5A). These index values show that the *dop-3* mutants exhibit a substantially lower slowing response on the seeded plate than the wild type. When we display body bends per 20sec instead of the slowing index (Figure 5B) we also observe that the *dop-3(vs106)* mutants move faster on the empty plate than the control. Wild type animals perform 20.23 ± 0.3881 (SEM) mean body bends/20sec on the unseeded plate and 14.25 ± 0.2297 on the seeded, while *dop-3(vs106)* mutants display 22.29 ± 0.3664 on the unseeded plate and 20.50 ± 0.7071 on the seeded. Therefore, *dop-3(vs106)* animals exhibit basal slowing, but to a considerably lesser extent than control animals (Figure 5B).

Concerning the ESR, the N2 strain has a Δbbs^{20} of 13.27 ± 1.478 (SD) and *tph-1(mg280)* has a Δbbs^{20} of 4.683 ± 6.323 (Figure 5C). The mean body bends/20sec of the wild type on the unseeded plate is 18.83 ± 0.4339 and on the seeded 5.3 ± 0.3387 (SEM), while the mean body bends/20sec of the *tph-1(mg280)* mutant on the unseeded plate is 17 ± 0.6146 and on the seeded plate is 13.23 ± 0.5922 (Figure 5D). Therefore, we observe that the *tph-1* mutant displays a severely reduced slowing index. The third alternative is represented by the measurements of the basal slowing response solely on the seeded NGM.

Quantification and statistical analysis

This analysis applies to Assays I and II.

From the collected data (10 observations from the seeded and 10 measurements from the unseeded plate for each strain), calculate the slowing index Δ body bends/20sec (Δbbs^{20}), as analyzed below, and generate a graph. The slowing index Δbbs^{20} corresponds to the difference between the mean body bends/20sec on the unseeded plate minus the mean on the seeded plate.

1. Collect measurements from 10 animals on the seeded and 10 animals on the unseeded plate.

2. Calculate mean body bends per 20sec on the seeded (m^s) and the unseeded plate (m^u) for each genotype. You may use software like Microsoft Excel for all calculations.
3. Calculate Δ body bends/20sec (Δbbs^{20}) according to the following equation:
$$\Delta bbs^{20} = m^u - m^s$$
4. Compute the standard deviation of the mean for each set of ten measurements counted on seeded (SDs) and unseeded plates (SDu) for each strain.
5. Determine the standard deviation for Δ body bends/20sec for each strain (ΔSD^{20}) according to the following equation: $\Delta SD^{20} = \sqrt{(SDs^2 + SDu^2}$)
6. Use software like GraphPad Prism to plot Δ body bends per 20sec (Δbbs^{20}), together with ΔSD^{20} and the number of measurements (10) of all biological replicates in a grouped table (Figure 5).
7. Analyze the data with Two Way ANOVA using Tukey's test to correct for multiple comparisons. Shapiro-Wilk test may be used to asses normality of data distribution.

Alternatives: Instead of Δ body bends, one may plot body bends per 20sec from seeded and unseeded plates in a column table and graph. However, the number of columns doubles this way, which may be confusing when testing a large number of genotypes (Figure 5). This alternative applies better to the "Locomotion assay – Alternative III" analysis.

Limitations

The locomotion of *C. elegans*, similar to most of its behaviors, is influenced by its microenvironment, such as ambient temperature, moisture of plates, food abundance as well as by population maintenance and handling conditions, like population density or starvation of previous generations. Therefore, the locomotion rate assessment assay is sensitive and challenging and necessitates strict quality control. To eliminate data variation always maintain all tested animals under ad libitum conditions for at least three generations. Use fresh NGM plates from the same batch, seeded together with enough amount of OP50 or HB101 bacterial food source. The incubation temperature and moisture should be kept constant avoiding temperature fluctuations. This assay does not apply to animals with the roller phenotype.

Troubleshooting

Problem 1:

Starvation of the animals before the locomotion rate assay (related to step 1, "Before you begin" section).

Potential solution:

Ensure to use fresh OP50-seeded plates. Apply 200-250µl freshly prepared OP50 to seed NGM. At the first step of synchronization, transfer no more than 5-6 L4 animals.

Problem 2:

HB101 forms a too-thin or too-thick bacterial lawn on the assay plate (related to step 17, "Before you begin" section).

Potential solution:

Always prepare new HB101 O/D culture coming from a fresh streaking. At this step, it is important to determine the point at which the HB101 culture density yields a thin bacterial lawn.

Problem 3:

The body bends/ 20sec of some animals are measured more than once (Related to step 9, "Step-by-step" section).

Potential solution:

Following data recording from every animal, one may pick the nematode with the worm-picker and burn it. However, this means that, every time a measurement from an animal is obtained, the lid of the plate should be lift and then placed again on the plate following the burning of the animal. During this process, the nematodes are exposed to mechanical stimuli, emerging from moving or accidentally tapping the plate and by airflow (from breathing or air-conditioning). This procedure might increase nematodes' mobility. Working with fewer animals (e.g. 5) would make it easier to monitor them.

Problem 4:

During body bend measuring many animals stack and stay almost immobile at the dense periphery of the bacterial lawn (Related to step 9, "Step-by-step" section).

Potential solution:

This is a usual behavior of *C. elegans* that cannot be avoided. To limit this phenomenon, make sure to generate a thin bacterial lawn. Additionally, ensure that the recovery time of the 3-5min is applied. A possible solution is to use more animals so that there would be enough animals to count even though there are also many immobile animals. Another alternative would be to wait for some animals until they start moving again.

Problem 5:

Some animals are censored during the 30min starvation due to desiccation on the plate walls. (related to step 14, "Step-by-step" section).

Potential solution:

Typically, 15-20 animals are sufficient to ensure that 10 will survive for the experiment. However, you may increase them to 30-40 to avoid having very few nematodes at the end of the starvation step. Alternatively, you may apply 4M fructose to the plate's periphery. Administer a few drops on the plate's edge and rotate it to create a fructose ring on its perimeter. Add a dye, like Congo Red or Bromophenol Blue, to visualize the ring. Wild-type well-fed animals avoid this osmotic barrier and remain inside the plate, while it does not affect their mobility[12].

Resource availability

Lead contact

Further information and requests for resources and reagents should be directed to and will be fulfilled by the lead contact, Nektarios Tavernarakis (tavernarakis@imbb.forth.gr).

Materials availability

This study did not generate new unique reagents.

Data and code availability

This study did not generate or analyze any dataset or code.

Acknowledgments

The strains used in this protocol were provided by the Caenorhabditis Genetics Center, which is funded by the National Center for Research Resources of the National Institutes of Health. This work was supported by H2020 FETOPEN project "Dynamic"(EC-GA 863203) to NT. This work was also partially supported by the European Research Council under the grant agreement "ERC-GA695190-MANNA" to N.T. Additionally, through the Operational Program "Competitiveness, Entrepreneurship, Innovation" of the National Strategic Reference Framework (NSRF) 2014-2020, under the call RESEARCH – CREATE – INNOVATE (project code: T1EDK-01504, "EPHESIAN") to NT.

Author contributions

Conceptualization, writing – original draft, visualization D.P. and N.T.; writing – review & editing D.P. E.L.; investigation, data curation, visualization D.P., E.L. and P.F.; methodology, validation, formal analysis D.P.; resources, supervision, project administration, funding acquisition, N.T.

Declaration of interests

The authors declare no competing interests.

References

1. Petratou, D., Gjikolaj, M., Kaulich, E., Schafer, W., and Tavernarakis, N. (2023). A proton-inhibited DEG/ENaC ion channel maintains neuronal ionstasis and promotes neuronal survival under stress. iScience *26*, 107117. 10.1016/j.isci.2023.107117.

2. Sawin, E.R., Ranganathan, R., and Horvitz, H.R. (2000). C. elegans locomotory rate is modulated by the environment through a dopaminergic pathway and by experience through a serotonergic pathway. Neuron *26*, 619-631. 10.1016/s0896-6273(00)81199-x.

3. Berri, S., Boyle, J.H., Tassieri, M., Hope, I.A., and Cohen, N. (2009). Forward locomotion of the nematode C. elegans is achieved through modulation of a single gait. HFSP J *3*, 186-193. 10.2976/1.3082260.

4. Padmanabhan, V., Khan, Z.S., Solomon, D.E., Armstrong, A., Rumbaugh, K.P., Vanapalli, S.A., and Blawzdziewicz, J. (2012). Locomotion of C. elegans: a piecewise-harmonic curvature representation of nematode behavior. PLoS One *7*, e40121. 10.1371/journal.pone.0040121.

5. Koelle, M.R., and Horvitz, H.R. (1996). EGL-10 regulates G protein signaling in the C. elegans nervous system and shares a conserved domain with many mammalian proteins. Cell *84*, 115-125. 10.1016/s0092-8674(00)80998-8.

6. Chase, D.L., Pepper, J.S., and Koelle, M.R. (2004). Mechanism of extrasynaptic dopamine signaling in Caenorhabditis elegans. Nat Neurosci *7*, 1096-1103. 10.1038/nn1316.

7. Voglis, G., and Tavernarakis, N. (2008). A synaptic DEG/ENaC ion channel mediates learning in C. elegans by facilitating dopamine signalling. EMBO J *27*, 3288-3299. 10.1038/emboj.2008.252.

8. Stiernagle, T. (2006). Maintenance of C. elegans. WormBook, 1-11. 10.1895/wormbook.1.101.1.

9. Palikaras, K., SenGupta, T., Nilsen, H., and Tavernarakis, N. (2022). Assessment of dopaminergic neuron degeneration in a C. elegans model of Parkinson's disease. STAR Protoc *3*, 101264. 10.1016/j.xpro.2022.101264.

10. Xiao, Y., Zhang, L., and Liu, Y. (2023). Protocol for assessing the healthspan of Caenorhabditis elegans after potential anti-aging drug treatment. STAR Protoc *4*, 102285. 10.1016/j.xpro.2023.102285.

11. Wibisono, P., and Sun, J. (2022). Protocol to measure bacterial intake and gut clearance of Caenorhabditis elegans. STAR Protoc *3*, 101558. 10.1016/j.xpro.2022.101558.

12. Calahorro, F., Alejandre, E., and Ruiz-Rubio, M. (2009). Osmotic avoidance in Caenorhabditis elegans: synaptic function of two genes, orthologues of human NRXN1 and NLGN1, as candidates for autism. J Vis Exp. 10.3791/1616.

Figures & legends

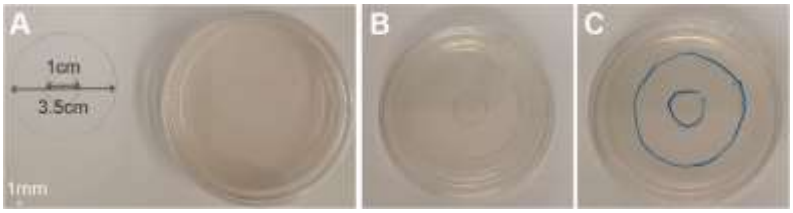

Figure 1: Use a drawn ring as a guide for spreading HB101 bacteria.
Draw the ring on a piece of paper (A) and use it as a guide (B) to copy it at the bottom of the assay plates (C). Scale bar 1mm.

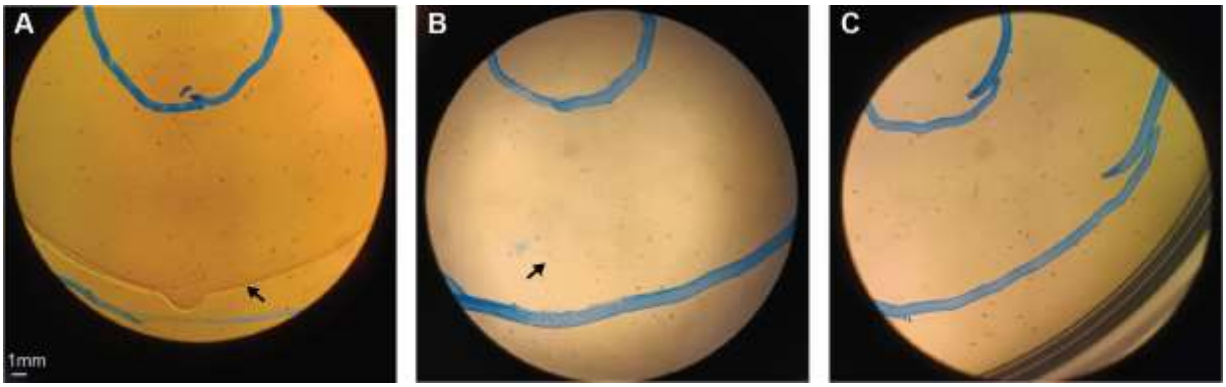

Figure 2: Bacterial lawns of varying thicknesses created by HB101 on assay plates.
Generate thin bacterial lawn on the assay plates as shown in (B) and avoid overly thick (A) or too thin lawns (C). Arrows indicate the thick lawn periphery. In (C) the lawn is so thin that can be hardly observed. Scale bar 1mm.

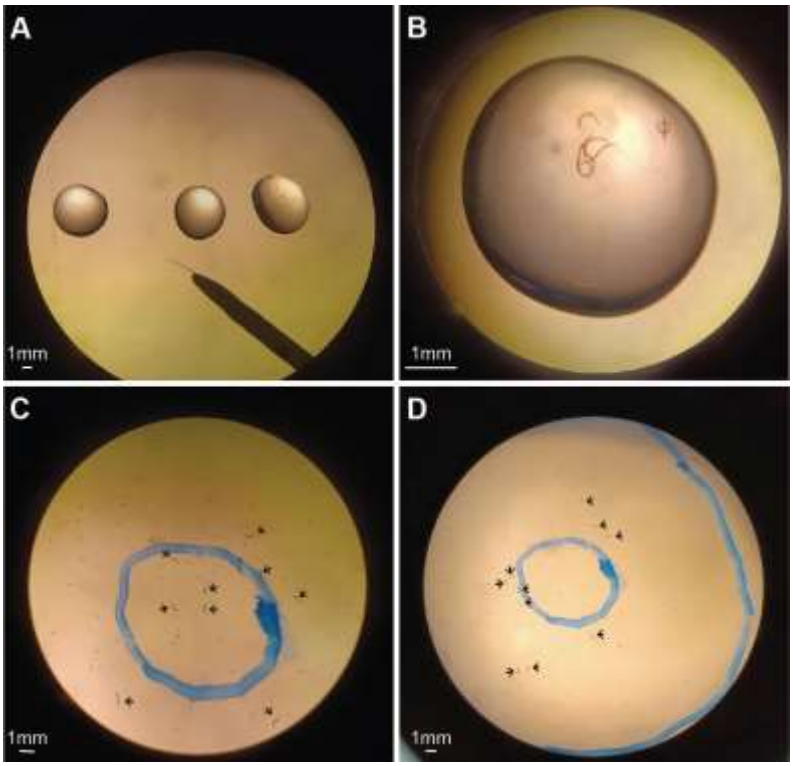

Figure 3: Nematode washing in M9 drops before transferring to the assay plate.
Wash nematodes clean from bacteria in three 20µl M9 drops (A, B) prior to the assay. Following washing, place the animals with the eyelash at the center of the assay plate (C). After three minutes, all nematodes already move onto the bacterial lawn and are ready for counting (D). Arrows point to the nematodes on the assay plate. Scale bars are indicated on each image.

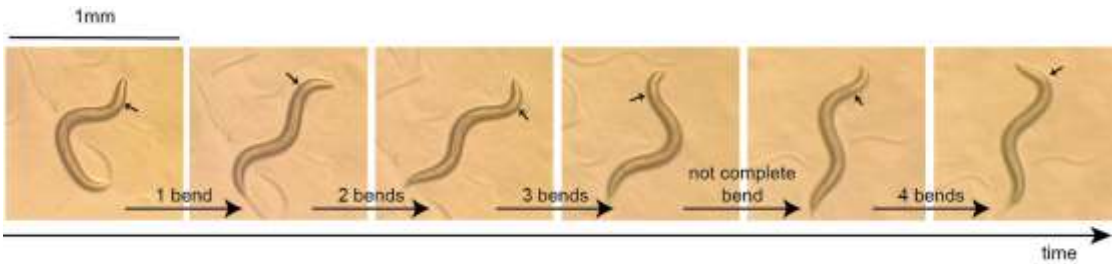

Figure 4: Monitoring nematode's body bends.
Sequential illustrations of the animal's movement. Arrows indicate the region behind the pharynx where the body bends complete. Scale bar 1mm.

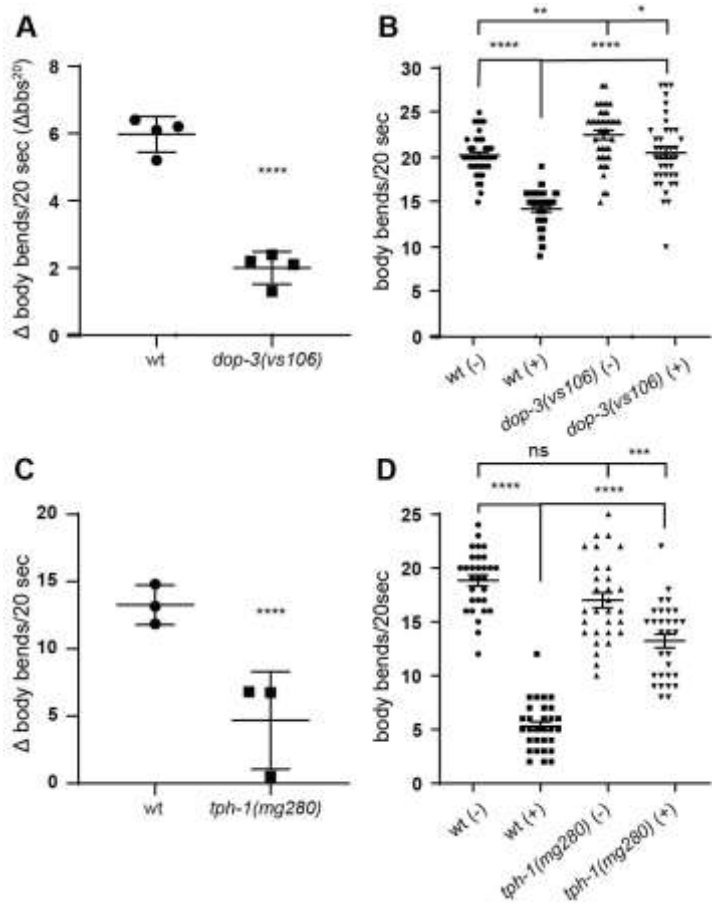

Figure 5: Locomotory rate of control and mutant animals in the basal and enhanced locomotion rate assays.

(A, B) Basal slowing response of wt and *dop-3(vs106)* mutant animals. (A) The basal slowing response expressed as Δ body bends per 20sec. The slowing index of the *dop-3(vs106)* mutants is reduced, pointing to faster movement in the presence of food. (B) The BSR expressed as body bends per 20sec. The mutant animals display increased number of body bends per 20sec on a plate with food compared to wild type and therefore show a reduced BSR.

(C, D) Enhanced slowing response of wt and *tph-1(mg20)* mutants. (C) The enhanced slowing response expressed as Δ body bends per 20sec. Mutant *tph-1(mg280)* animals display reduced slowing index compared to wilt type. (D) The enhanced slowing response expressed as body bends per 20sec. The body bends per 20 seconds of *tph-1(mg280)* mutant animals on a seeded plate are almost the same as on the plate without food.

(A, C) Scatter plots, dots represent the ratio Δ body bends/20sec of independent biological replicates. The ratio Δ body bends/20sec corresponds to body bends/20sec on an empty plate minus body bends/20sec on a plate with food. Error bars represent SD.

(B, D) Scatter plots, dots represent the body bends per 20sec of each animal tested in all biological replicates. Error bars represent SEM. The symbol (-) indicates the absence of HB101 bacterial lawn during the measurement, while the symbol (+) indicates the presence of food.

(A-D) We tested 10 animals in every replicate of each BSR experiment. In all experiments, we used one-day-old adult animals. Non-significant (ns) p=0.1234, *p=0.0332, **p=0.0021, ***p=0.0002, ****p<0.0001. Two-way ANOVA.

(A, B) wt (-) n=40, wt (+) n=40, *dop-3(vs106)* (-) n=40, *dop-3(vs106)* (+) n=40, 4 biological replicates. n represents the number of animals.
(C, D) wt (-) n=30, wt (+) n=30, *tph-1(mg280)* (-) n=30, *tph-1(mg280)* (+) n=30, 3 biological replicates. n represents the number of animals.